UNIVERSITAT DE BARCELONA

A journey towards the identification of novel therapeutical strategies for advanced cholangiocarcinoma with *IDH1* mutations

Queralt Serra Camprubí

A journey towards the identificacion of novel therapeutical strategies for advanced cholangiocarcinoma with *IDH1* mutations

Queralt Serra Camprubí

Universitat de Barcelona
Facultat de Biologia
Programa de Doctorat en Biomedicina

A journey towards the identification of novel therapeutical strategies for advanced cholangiocarcinoma with *IDH1* mutations

Memòria presentada per Queralt Serra Camprubí per optar al grau de doctor/a per la Universitat de Barcelona

Queralt Serra Camprubí
Doctoral Thesis
Barcelona, 2023

Thesis directors: Sandra Peiró and Tian Tian
Thesis tutor: Montserrat Corominas

There will be an answer,

let it be.

The Beatles

Acknowledgements

I fins aquí aquest capítol, UAU! Semblava impossible arribar fins aquí i tocar amb la punteta dels dits el ser doctora. Hi ha hagut una mica de tot aquests últims 5 anys, moments de tots els colors, però "definitely" (Carles i Audald, no se m'enfadeu, sé que "definitivament" serviria però a mi "definitely" em sona molt millor), el PhD m'ha fet però, encara més, m'ha vist créixer. Han estat uns anys de fer passos endavant i d'aprendre moltíssim a tots els nivells, però també de resiliència, d'aprendre a confiar en la feina ben feta i no desesperar. Vaig tornar de Copenhaguen dient que volia fer un doctorat de càncer i immunologia i no us vull fer spoiler, però després de moltes voltes, just allà ha acabat el meu projecte. Aquí comencen els agraïments infinits a totes les persones que m'han acompanyat en aquesta aventura i que m'enduc amb mi per sempre.

La meva entrada al VHIO va ser una mica una carambola. Tot va començar a l'IRB, de fet, en una entrevista per una beca de doctorat per un projecte de recerca bàsica, allà mateix. La Sandra era del panell de selecció i recordo perfectament que després dels 10 minuts d'entrevista, em va demanar fer-me una última pregunta "i si enlloc de recerca bàsica, fos més translacional, com et sentiries?". Vaig pensar que era una pregunta una mica estranya en aquell context però que potser m'estaven intentant caçar per alguna banda. Unes hores més tard, però, ho vaig entendre. Aquella mateixa nit vaig rebre un mail seu dient-me que, si no em donaven la beca, li fes un truc, que ella estaria contenta de tenir-me a l'equip, que acabava de portar el seu grup al VHIO i estava buscant un PhD. Com us podeu imaginar per com han anat les coses, no em van donar la beca i vaig acabar aquí. Jo no li he dit mai, però aquell cop va ser el primer cop que la Sandra em va fer sentir capaç, la determinació amb la que va trucar-me per oferir-me la posició em va captivar i, tot i que fins aquell moment l'epigenètica no m'havia cridat mai l'atenció, vaig decidir acceptar. I sàpigues, Sandra, que si una cosa no has deixat de fer-me sentir mai, és capaç, i per això t'estic immensament agraïda. Gràcies per creure en mi, per donar-me la oportunitat, ser sincera amb mi des del primer dia i dir-me que aprendríem juntes, que tu venies de la ciència bàsica i que tot això era nou per tu també, però que ens en sortiríem, gràcies per treure'm del drama en múltiples ocasions, per ser sempre positiva i treure suc de cada resultat, per treure el cap del despatx amb cara de "quina una en passa ara?" a cada "Sandraaaaaaa" (sé que saps l'entonació jajaja) que jo cridava des del meu lloc, i descollonar-nos després; gràcies per ensenyar-me a pensar i ser crítica i per cada "sé que ho pots fer millor" que post- la fase de "cagar-me en tu" em feia esforçar-me per entregar una feina millor. Vaig disfrutar molt treballant amb tu, i estic molt contenta també d'haver viscut l'època en què eres una més als dinars, cafès i alguna birra, tot ple d'historietes

del tot curioses. Gràcies també per ser suport fins el final, amb trucades o whats, també un cop has estat fora del VHIO, sempre he sentit que m'escoltaves, valoraves la meva opinió i confiaves en mi. Potser algun dia tornem a formar part del mateix equip, who knows? xD Mano a mano amb la Sandra, hi ha hagut el Tian al capdavant d'aquesta aventura. When you arrived as senior postdoc, you meant order and fresh air, you came with new idees and with the will to provide us with day-to-day guidance and support. You tried to make time for all of us and help us with any conceptual and technical problem we had. You taught me cloning, fought with me for a CRISPR/Cas9 knock-in that we never got but made us thrill, and we even set up hand-to-hand a genome wide screening together. At that moment, we had been struggling a bit with moving forward the cholangio project and you actually helped a lot to give it a way through. Then, out of the blue, you found yourself in the position of leading the group, and you actually took it fearlessly and made us always feel safe with all the changes that we faced suddenly, and I am grateful for that. For that, for your hard work to make it work, your guidance and advice. Never forgetting about the brilliant and unforgettable sentences and words that will remain for prosperity, such as "boli de cultivo, no la salir", "tu pongar 3 uL", "calafin", "yo crio", "parjamplo", "ahi está" o "como se puede?" that have made us laugh a lot in our day-to-day in the lab and million julitos.

El primer any, però, no era a la Sandra ni al Tian a qui passava comptes directes, almenys no en el dia a dia. Quan vaig entrar al grup, el projecte de cholangio, que acabaria sent el meu projecte de doctorat, encara no havia arrencat massa, així que mentrestant la Sandra em va posar a ordres de la Pascu. I quina sort la meva. M'ho vaig passar teta Laura, aquell any juntes va ser sens dubte el millor any que he passat al VHIO, cada dia era una aventura i rebel·lar un western era la tasca més emocionant del món. Em vas ensenyar a vibrar amb cada experiment, a lluitar cada un d'ells fins al final, a preguntar-m'ho tot i no deixar res per entendre. Sé que vaig ser llum per tu, ja ho hem parlat altres vegades, però creu-me que vas ser llum per mi també, moltíssima llum, treballar amb tu mano a mano és un dels tresors més grans que m'enduc d'aquesta etapa, no ho canvio per res. Vam tenir discussions científiques eternes, experiments frustrats, westerns per videollamada (que teníem l'Adri ben enfadat perquè deia que parlaves més amb mi que amb ell) i ens vam enroscar a inhibir tots els passos d'una via per entendre com carai explicar els nostres resultats, però sobretot, vam compartir mil riures, molts pitis, converses profundes, un piló de birres, partits de futbol del teu equip, hores venent olis al palo alto i alguna que altra fiesta. Erem un combo del tot còmic i creu-me que tot i que ens comportés moltes bronquillas que fossin la riota de l'Oriol a cultius, escriure al lateral del tub i no al tap és una cosa que passarà a les generacions que em segueixen i que la teva anècdota de la tripsina és la que he explicat a tots els

estudiants que he tingut perquè es mirin les cèl·lules abans de passar-les. No he heretat, però, el teu no anar a l'últim moment, que quasi em deixa sense beca (i sé que ara diràs que vaig tenir la beca de la Caixa gràcies a tu i així és) ni la teva capacitat de fer llibreta amb índexs perfectes (jo encara faig servir els post-its que tant nerviosa et posaven xd). Crec que ens vam fer grans l'una a l'altra pel simple fet que ens adoràvem, o almenys jo ho faig, t'adoro i t'admiro molt, encara ara. Has estat un referent per mi i t'has convertit en una gran amiga, i m'encantaria pensar que ens tindrem sempre. Aquí vull fer un petit apunt, i mencionar també l'Adri i la Jana, que també son com de la família i m'han donat moments fantàstics.

Quan vaig arribar al lab, l'equip també el formaven la Gemma, el Marc i la Jess. La Gemma, treballadora com ella sola, sempre de bòlit amunt i avall per acabar els 5636246 experiments que tenia cada dia, sempre disposada a ajudar i debatre qualsevol experiment, sempre in a una birra i plan i sempre fent pinya. El Marc, con sus nuevas rutinas de deporte, su cocina a baja temperatura y sus canciones de Extremoduro dejadas en formato post-it en mi ordenador, sempre donant vida al labo. Sempre em fa gràcia recordar la digestió del meu primer PDX, que no et vaig deixar aixecar de la cadira del meu costat ni un segon i, pobre, allà vas aguantar contestant totes i cada una de les meves preguntes sense queixar-te (sorry for that xD). I la Jess, la dolça Jess... Crec recordar que la Pascu t'ho deia en els seus agraïments però si és així, em repeteixo, ets la persona més lleial que conec. Tens el teu ordre, les teves manies i els teus protocols sagrats, i això, que no t'ho toquin, tots ho sabem i, de fet, sort en tenim de tenir algú que fiqui una mica d'ordre. Però sempre estàs allà davant de qualsevol crisis, pensant en què ens pots ajudar, sempre disposada a arremangar-te i encarregar-te de tot allò que a nosaltres ens fa bola. Ens cuides com ningú i, a vegades, també ens toques una mica el crostó, però ens ho mereixem, i al final tu i jo som igual de felices després d'haver endreçat. T'havia dit que no sabia com encabir-ho però acabo de canviar d'opinió perquè vull que quedi per escrit el dia que et vaig tancar dins la cambra freda quan em seguies enganxada com una lapa, o el dia que vam haver d'embolicar un pàncrees sencer dins un llençol per no exaltar tota la sala d'espera jajaja. Has estat un suport incondicional Jess i, per això, t'estic molt i molt agraïda. Després va arribar la Carmen, per aportar un aire fresc a l'equip, sempre amb ganes de millorar el com organitzar-nos i gestionar les coses, sempre "mazo" ready per baixar a fer una birra after-work i animar el dinar amb alguna historieta. Eres la siguiente, y solo queda el sprint final, que cuesta, pero se llega y cuando menos te lo esperes el PhD se habrá acabado y llegará esa paz que tanto anhelas, ya lo tienes, mucho ánimo! Després van venir uns quants estudiantitos que m'han anat robant el cor: l'Iker, algú que no passa desapercebut, es fa notar i ens va alegrar la vida mentre hi era; la Nurieta, o la vacuum girl, tant inquieta que

igual que no aguanta una peli fins al final, no es pot estar d'intentar un experiment sempre una vegada més, ambiciosa, decidida i amb un cor que no li cap, estic feliç que seguim en contacte, que seguim compartint vida encara que sigui a través del whats, saps que estic super orgullosa de tu i que confio plenament que arribaràs on et proposis; i finalment, la Mariana...quien me empezó cual polluelo, dudosa, pasando de puntillas, y a quien adoro profundamente. Junto con Núria, empezamos las 3 con ese giro que dio el proyecto hacia la immuno, y lo disfrutamos, creo, y fuimos un gran equipo. Nunca olvidaré el día que entrasteis en cultivos para decirme que Tian os había dicho que el Medip había salido bien y nos fundimos en un abrazo brincando dando vueltas (espero que no nos viera nadie jajaja). Después de esto y, aunque después de darle muchas vueltas, Mariana decidió quedarse y empezar la PhD adventure. Estoy super contenta de que haya sido así, me ha dado un añito más trabajando contigo, en el que nos las hemos visto de todos los colores en este mundo nuevo de la immuno, con Fortessa hasta las 11 de la noche con patatas y cervezas pah ahogar las penes (ahí abajo ya nos conocía todo el mundo jajaja), Cantos obturados en el momento más inesperado y resultados que a veces nos dejaban atónitas. Creo que acabamos siendo una fusión de alto engranaje, y pasamos de asustarnos con una placa de FACs a hacerlas de seis en seis. Ha sido un auténtico placer trabajar contigo, y tu no lo ves, pero no te puedes imaginar la evolución que has hecho hasta hoy, des del día que viniste por primera vez, que después del comentario inolvidable de Tian de una muleta guapa, ya te dije que haríamos un gran equipo. Y así ha sido, no se me ocurre mejor persona para continuar el proyecto. Eres pura dedicación i un ángel, siempre pendiente y cuidando de todo el mundo. Sepas que aún tengo la cerveza que me regalaste para que brindemos fuerte, por esta tesis y por el currazo que nos hemos pegado juntas, que no todo es trabajo y de birras también hemos hecho y chispa, como tú dices, también hemos ido (un día incluso nos cerraron el Julio pah nosotros). Gracias por tanto, guapa. A tots aquests membres, s'hi han incorporat recentment la Sofia, el Joel, la Cheska i la Natalia. I haven´t had the chance to share a lot of time with you since I was on my way out when you started, but you have taken care of me every time I have come to VHIO, asking how I was doing and trying to help, and I am grateful for that. You are going to make a great work and team.

Volia dedicar unes paraules també a l'equip clínic que, al llarg de tot el procés, però sobretot aquest últim any i mig, amb el canvi de format del grup, han fet una feinada i han estat un immens suport perquè aquesta tesis sortís endavant. Sempre pendents a les nostres peticions, bojos perquè no se'ns escapi una sola mostra i sempre intentant tirar endavant projectes que donin opcions als pacients, a qui cuideu com a ningú. La Teresa, incansable i arrolladora, gràcies per acollir-nos com ho vas fer quan la Sandra va marxar i haver estat des de l'inici un pilar imprescindible.

Admiro l'energia i dedicació amb la que lideres l'equip, el teu carisma i professionalitat i ets un autèntic referent. I gràcies, també, Carles i Florian, per ser sempre a peu de canó i fent una feina incessant per aconseguir-nos el que demanàvem, interessant-vos sempre pel què passa allà dalt i fent facilíssim el funcionament d'un equip que crec que és una sort. Recordaré amb especial tendresa els dies que vam compartir a Edinburgh, que va ser realment la primera oportunitat per passar temps junts, i tot i que la jefa ens va fer caminar molt (a tot arreu a peu ajajaja), va ser un viatge molt divertit. I no em volia deixar a l'Àlex, que sempre corre amunt i avall per arribar a tot i agafar sangs en el temps que nosaltres parpellegem. Gràcies a tots, ha estat molt enriquidor tenir-nos.

I fins aquí, l'equip, sense qui no hagués pogut arribar fins aquí. Però del VHIO m'enduc molta més gent que és família i m'han fet passar 5 anys increïbles. Des dels membres de la famosa Guarderia del VHIO, guarderia perquè així ens consideraven els "oldies" com l'Albert o l'Oriol a tots els "jovenets" que començàvem, però confesseu-ho, el primer any us el vam alegrar però bien, i feliços ballàveu els passos de zumba i cul10 a l'almodovar els divendres. També hi havia la Mònica, la Garazi, l'Ale, la Laia, la Fani, i alguns altres de qui ja he parlat més amunt. Quin primer any, que divertit. Ale, gracias por siempre intentar estar, tus bromas y alegría, lo que contigo no se puede salir porque siempre tienes una birra más para (im)poner en la mesa y así no se puede jaja. Laieta, hem tingut un PhD molt paral·lel i sempre ens han coincidit les crisis, així que hem sigut clarament companyes de penes i alegries. Gràcies pels consells científics, i per totes les hores que m'has escoltat sense queixar-te amb les meves ofuscades; gràcies pels, en el seu moment molt habituals ,"comprem una ampolla de vi i anem a casa teva?"que a vegades acabaven en dues i algun sticker icònic; gràcies per saber quan et necessitava i deixar-me un post-it recordant-me les tortugues de Filipines o baixar-me una bossa de patates al Fortessa a les 9 de la nit. Ets la chica de las historietas, cas d'estudi en múltiples ocasions de l'hospital (deuen tenir cultiu de tots els bacteris que en algun moment han poblat el teu cos xD) i algú capaç de marxar a Filipines i tornar amb zero parts del cos sense ferides. Ara, el que no et perdono és el viatge a Lloret a les 12 de la nit eeeh o, bueno, en compensació per obrir-te la butllofa avisant-te del 3456 Nemo xD. Sé que no pots més, però creu-me que queda molt poc d'aquest PhD i el final arriba, compta amb mi pel que necessitis. I aquí em queda fer una altra menció especial a la Fani... Com hem crescut des que ens vam conèixer, quins grans primers dos anys de bogeries, normalitats positives i aquell estil tant particular teu a la pista de ball, seguits per un estiu de surf, excursions del tot còmiques i un Sonar espectacular, però sobretot, que guai haver estat partícip de tot aquest procés que has fet els dos últims anys. Gràcies per escoltar-me sempre, sobretot aquelles hores infinites a cultius

(on at some point ens havíem de callar l'una a l'altra per poder concentrar-nos), caminar passeig de sant joan amunt i avall xerrant fins que no ens notàvem els peus, saps que estic immensament orgullosa de tu i de la teva valentia, d'haver sortit de la teva zona de confort i encarar tots els fantasmes, ets un exemple a seguir i m'encantaria seguir compartint totes aquestes vivències i creixement amb tu. Ets una de les personetes que m'enduc d'aquest doctorat, sense dubte.

I després d'aquell primer any, d'on van sortir tota aquesta trupe que he comentat, va aparèixer el Niko (alias "cuqui", tot i que a ell li sembla repulsiu). Encara que estic segura que tu no hi estaries d'acord, jo crec que lo nostre va ser amistat a primera vista, simplement a tu et va costar una mica més d'acceptar (mira que em va costar convènce't eh jaja). M'ho he passat tant bé amb tu Niko, de veritat. He rigut el que no està escrit, he disfrutat com una nena petita i has tret la millor versió de mi. Enyoraré la nostra complicitat, el buscar-nos per comentar qualsevol cosa i que sempre, tot, acabi en riures. Has estat, sense dubte, el meu partner in crime, el meu salvador de xafar cagarades baixant al metro, el meu confident i l'alentador de moltes bogeries. No tinc pàgines per escriure tots els records i anècdotes que hem compartit plegats, des de l'excursió a Sant Cugat que va acabar en unes olives a Vallvidrera fins a un Sonar inoblidable, passant per un "no te compliques bonita" fent un cafè un dissabte a la tarda. Fa dos anys, tornant del (no) sopar de nadal, vas dir-me que creies que el millor d'aquesta amistat és que podies ser tu mateix tota l'estona i, hi estic d'acord i m'hi sumo. M'has donat confiança sense límits i m'has ensenyat que sent jo mateixa SEMPRE hi guanyo, i tot i que aquest excés de confiança, ens ha portat a algunes discrepàncies, som aquí i, com vaig dir-te una vegada, segueixes sent una de les meves persones preferides. I t'aviso, em sap greu, però he vingut per quedar-me jajaja. La veritat, no m'imagino aquest doctorat sense tu, m'has cuidat moltíssim (que sent tu, és tot un honor jajaj) i t'estic mol agraïda, cuqui! Y en el capítulo Niko, quiero hablar de Thomas, Thomasito para mí. Aunque sé que formo parte de la castaplasta, lo más despreciable del mundo mundial, y hay veces que te irrito x10, yo te aprecio mucho y he aceptado hacer la ruta de los peligros contigo cada vez que abandonamos un sitio, esto hay que valorarlo xD. Compañero de muchas de las aventuras explicadas para el menda anterior, has sido siempre alguien dispuesto a escuchar, ayudar y hacer alguna que otra travesura conmigo, siempre IN a cualquier plan y, sobretodo, a enseñarme cualquier nuevo juego de mesa jijiji. Junto con Niko, habéis sido casa durante esta época y esto me lo llevo conmigo. Os deseo la mayor de las suertes en lo que la vida os depara y espero que me dejéis estar siempre.

I, creadora del títol de grup "aire i amor pur" (un títol reflex de la seva defensa de la ventilació

com a mitjà per poder-nos donar amor durant el COVID), arriba la Cate, o ladyCate, com l'ha batejat el Niko. I us preguntareu perquè? Doncs resulta ser una noia molt conscient del seu estat corporal i amb això, vull dir que té una termoregulació molt fina del seu cos. L'hauríeu d'haver vist a Menorca, tapada amb un vel cual mòmia quan estava al sol, i amb sudadera a l'ombra, tots dos fets separats per una diferència de temps de només 3 segons. Ara, igual que cuida de la seva temperatura, cuida dels altres, i això és el que ha fet la Cate durant aquest PhD, cuidar-me sempre. Hem viscut moments divertidíssims, però sobretot, adoro les nostres birres/cafès per posar ordre, per endinsar-nos en converses profundes i psicoanàlisis m'atreviria a dir que, com a mínim, complicats. I sobretot, agraeixo saber que, com vas dir un dia, hi serem sempre i ens estimarem en totes les isoformes. Gràcies lady, per tutto.

Junto con Niko, Thom i Cate, el grupo de Nikolobirra me ha dado muchísima vida. Lo que empezó con un Pasapalabra de los más entretenido, acabó con un finde en la Pobla de lo más memorable, con el Xuli, el satisfyer llamado Cate, el orgullo de Niko por cerrar el pueblo, y el mareón que os di en el coche con Sara de paquete extra xD. Sara y Juli, gracias por esos momentazos, y por los infinitos Julitos compartidos.

I ara vull parlar de la Paula, que va aparèixer una mica igual que la Cate, seient a la taula del darrera del meu escriptori. Tot va començar per parlar sobre unes beques que podies demanar, després un "què tal el finde?" fins que vam acabar amb unes birres a un banc de Lesseps explicant-nos una mica la vida. I després d'això, hem passat per classificar els tumors de mama amb un croquis de 100 papers tirats al terra del passadís fins a solucionar el món tot degustant uns formatges a la Viblioteca o cuinant una fideuà. Gràcies Pauli, per recordar-me sempre tot el que valc i el que he aconseguit, quan jo me n'he oblidat, per un suport incondicional i un amor tant pur.

I ja vaig acabant amb la gent del VHIO, que m'enrollo com una persiana i comença a ser infumable. Vull acabar amb uns regalets que m'ha fet l'últim any del doctorat, les "Gràcia girls", l'Andrea i l'Alba, que junt amb la Meri, han llegado en tiempo de descuento. La Meri, que us haig de confessar que al principi em feia una mica de por, però m'ha acabat entendrint el cor. Ella era la vigilanta del FACs i jo odiava el FACs, sempre m'oblidava coses i ella m'havia de picar el crostó, és una tia directa i diu les coses com s'han de dir, i jo em cagava. Arrel de la organització del VHIOFinde, on vaig conèixer l'Andrea (d'aquest pendón us en parlo després), vaig començar a passar més temps amb aquesta tal Meri, a jugar a pàdel, fer més birrukis i fins i tot, una raclette,

i m'ha acabat conquistant, os lo digo. Lo nostres va de furgonetes, que entre la del VHIOFinde, que ja pitava 10 segons més tard d'arrencar, i els trajectes amb la seva autocaravana per Barcelona totalment èpics, vam fer el cupo de compartir transports complicats. Gràcies per la pantalla i la cadira, que m'han salvat la vida, l'esquena i la vista per escriure aquesta tesis, i gràcies per preguntar-me, preocupar-te i animar-me. I just fa un moment he mencionat a l'Andrea, Andreita o Andre. I això, creieu-me que no m'ho esperava. Ens havíem creuat alguns cops pel passadís i en alguna birra multitudinària al Julios, però poca cosa més, en 4 anys de doctorat havíem creuat poc més de 3 o 4 paraules jo crec. I com ja t'he dit algun cop, si organitzar el VHIOFinde és el que havia de passar perquè ens trobéssim, doncs ja ha valgut la pena. Carinyosa, dolça, divertida i amb un cap que fa la course navette aproximadament 23 hores i mitja al dia. En els dies bons, a aquesta velocitat fa les bromes i en els dies dolents, les reflexions; així que, imagineu-vos, avorrir-nos no és una opció. Però jo te'ls compro tots i cadascun aquests dies, perquè crec que tot el que ens assemblem fa que t'entengui i que m'entenguis, m'has ajudat moltíssim a donar perspectiva a tot, m'has donat solucions a camins que jo veia sense sortida, treus una millor versió de mi i em cuides moltíssim i espero que em deixis fer-ho a mi també. Gràcies per tot això, yo también te quiero siempre en mi equipo, el de urban, el de birras, el de viajes y el de vida L'Andrea és un dels membres de "Gràcia girls", però tenim un segon membre, l'Albi. Abans de parlar d'ella i totes les coses surrealistes que ens han passat, faig un appeal als agraïments de l'Andrea, on deia que totes tres teníem un petit projecte d'estiu, Bolivía 2023. De llavors fins ara hi ha hagut alguns petits canvis logístics i el destí és Colombia, ho deixo només perquè consti, i l'Albi encara penja d'un fil, però tampoc és sorpresa jiji L'Albi és un personatge donde no los haya, molt fluida i altament hidrofòbica al compromís, la qual cosa fa curtcircuitar als dos primers membres del grup. Al mateix temps, és tendre com ella sola, atenta i generosa. Cuida moltíssim i tot i que no saps mai fins 5 minuts abans si apareixerà, saps segur que si un dia et fa falta, pots comptar amb ella. D'anècdotes, en sobren, des del dia que vam treure una Acciona fora de zona, però per sort ens esperava fora després del pàdel i ens va permetre tornar a 20 per hora per la ronda (tot molt èpic), fins al dia que tu eres al destí correcte en un congrés i jo no, contra tot pronòstic (jajajaj bromiii!). Albi, sé que no està sent el moment més fàcil d'aquest capítol PhD, però poc a poc i dia a dia, això és una muntanya russa i vindran temps millors. I aquí estem mentre et desenrosques, per plorar les penes i brindar les alegries. Junt amb totes elles, les petites iTAG, l'Anna i la Judit, i la Noe, també m'han cuidat molt mentre he estat per allà ultimant l'indesign i aquestes cosillas, i fins i tot l'Anna té una aportació important a la portada de la tesis jaja Venga que ya lo teneeeeis, chiquitinas!

Per acabar, no em vull deixar de donar les gràcies també als Violeta, que han estat el meu salvavides en múltiples ocasions de caos i dubtes; la dolça Flami, compi de agotadores pero divertidos workshops de La Caixa, de debates eternos sobre nuestro querido STING y muchos momentitos de cuidado; l'Andreu, sempre atent; i la Cristina, a qui tinc un carinyo molt especial i estic molt agraïda per la dedicació inacabable. Vull destacar també l'Enrique, que aquest últim any crec que ha passat més hores amb mi que amb el seu grup jajajaj mil gracias por la inmensa ayuda de este último tiempo, por todos los debates científicos y por los ánimos y soporte infinito, nunca olvidaré el día que apareciste a las 10 de la noche post-gym al Fortessa con dos birras, para sacarme del drama xD, inolvidable! Gracies també a la Marta Escorihuela, per posar-ho sempre fàcil. I per últim mencionar el team Summer School (Fonsi, Alex, Iñaki, Andrea i Tian), uno de los grandes recuerdos del PhD, sin duda, i el Comité VHIOFinde 3.0 (Emanuela, Fabio, Laia, Sara, Andrea y, un poco, Meri), que me lo hizo pasar en grande.

I està clar que tot plegat ha estat possible també gràcies a tota aquella gent fora del VHIO que m'ha tret de la bogeria PhD molts dies. Des de l'equipito Sant Nicolau, la Ferrara, la Laia, el Palou, el Pepo, el Marin i l'Olga. Amb qui hem compartit excursions, dinars, algun volley platja i bons vinotxos algunes tardes-vespre entre setmana. El grup de la uni, que han estat uns fixes tots aquests anys, sobretot des que hem anat tornat tots a Barcelona, cosa que no em pot fer més feliç. La Garci, la Lauri i la Hugy, que m'han acompanyat moltíssim amb tot plegat, sent la meva cita setmanal de lovecycle i amb qui hem compartit mil birres, teatres, sopars i fins i tot un esmorzar entre vinyes (regalassu de cumple), gràcies reines! I també d'aquesta colla, doncs el Ciuri (alias cheesecake), que creu que m'he inventat un tipus tumoral per poder fer un PhD, que ha volgut anar a judici per adoptar els meus dits dels peus congelats pel fred suïs ja en dues ocasions i que m'ha donat "tardeos" i nits memorables que m'han fet literalment pixar de riure. I junt amb ell, l'Audald, l'altre membre del Magic Triangle, l'altre prota d'aquests riures memorables, com el dia que vam demanar a Glovo que ens enviessin Alaska. "Que no panda el cunico!", com diu ell, que l'Audald ha fet uns passos de gegant últimament, i n'estic molt orgullosa. Gràcies per estar atent i preocupar-te de com anava tot des de la distància. I, encara que inicialment no fos del grup, vull mencionar l'Alba, la q fa 5 anys només era la novia del Carles però podria dir que sobretot al llarg d'aquesta època de doctorat s'ha convertit en bastant més q això, en la meva parella de submarinisme (encara q sota l'aigua només busca nudis i no em mira mai i si no fos per l'Andreu potser ja hauria mort ofegada...això sí, mai falla ajudant-me a encabir-me com una botifarra dins aquell traje), la meva compi de lovecycle i ioga, i la meva compi de confidències surrealistes. I per tancar el tema uni, només falta la Miri... com m'agrada aquella sensació un o dos

cops l'any de quan arribes i plantes la teva maleta al mig del meu vestíbul. Al cap de 3 dies només penso en deixar de veure-la, però en realitat, sempre l'espero amb il·lusió. Estic feliç que haguem sapigut mantenir l'amistat tot i haver estat sempre lluny i que allò que va començar entre liada i liada a les pràctiques de laboratori de la carrera, hagi perdurat compartint pis a Ribes, habitació a Copenhague i skypes en horaris intempestius Boston-Barcelona. M'agrada ser el teu pit-stop quan passes per casa.

Otro gran grupo que no puedo olvidar son los Nybrolines. La gente flipa cuando les decimos que seguimos encontrándonos 2 o 3 veces al año y a mí esto me llena de orgullo. Somos un equipazo chicos y tened claro, que sois mi grupo vitamina. Lo que las paredes del ST juntaron lo hemos ido cultivando y este es el resultado, vacaciones juntos, fines de año, sidrerías, Distortion… Y como decía Nawi estos días, no solo nos vemos, sinó que seguimos siendo amigos, y eso vale todo el oro del mundo. Especial mención a Anamari y Nach, sólidos como pilares en cada encuentro (ya sé que el resto es porque estáis lejos y lo harías si pudierais) y siempre animando el cotarro y, obviamente, una muy especial a Nawi, que no ha dejado de llamarme y darme soporte en todo el proceso y ha sabido entender qué necesitaba en cada momento. Colombia nos espera amiga, y muchas más aventuras también, te quiero!

No em vull deixar tampoc a la Berta i el Monte, pacients y supportive, escoltant-me en el drama i sent la companyia d'infinits vinotxos tots aquests anys. Gracias también a Jose, mi fiel compi en Reus; Andrea Papu, que aunque lejos siempre tiene las puertas abiertas para recibirme donde sea que este; i l'Alex Subdit, que no s'oblida mai d'avisar-me quan és aquí per anar a fer una birra i que ha fet una aportació molt important a aquesta tesis retornant l'ordinador perdut des de Zurich jajajaja

I ara sí, sé que en teniu el pap ple però prometo que és l'últim paràgraf i aquest va per vosaltres, família. La Rosa i el Sidro, els cosins i tots els peques, que alegreu Pasqua, els reis i qualsevol calçotada a la Pobla i que sé que hi serieu per mi sempre. La Neus, el Gerard i la Marta, que ompliu els dissabtes de dinar a casa els avis. I aquests últims, els avis... M'heu cuidat des de ben petita. La iaia, sempre fent-me el meu dinar preferit quan hi vaig i si no, guardant un tupper sagrat per la neta, comprant-me tot allò que sap que m'agrada i ara ja no et deixo massa, però sempre fent-me pessigolletes i massatges. I l'avi, que el tenim una mica desanimat últimament, però ha estat sempre l'alegria de la casa, incansable, enèrgic, sempre llest per qualsevol enrenou. Diuen que el dia que vaig néixer era calcada a tu, i saps? Potser no físicament, però sí que penso

que una mica ens assemblem. Espero que puguis venir a la tesis, no hi ha cosa que em faria més il·lusió. I finalment, els papis, que haig de dir que han estat sempre un suport incondicional i aquests últims mesos m'han cuidat com una princesa. Gràcies papa per tots els dies que, sense demanar-t'ho, has agafat el cotxe i m'has tornat a Barcelona, per no perdre els nervis el dia de l'ordinador tot i que sé que em volies assassinar i gràcies per escolar-me, junt amb la mama, totes les frustracions dels últims mesos. Gràcies mami, perquè m'has sabut ajudar de la millor manera, ni un diumenge m'ha faltat un tupper per passar la setmana, ara que no sabia ni com trobar temps per fer la compra; gràcies pel recolzament i els infinits ànims que m'has donat i per fer-me sentir sempre capaç. Us estic a tots molt agraïda.

I fins aquí, la turra. Està clar que si una cosa no soc és sintètica i que si una cosa m'agrada és enrollar-me. El que també està clar és que aquest PhD no hagués estat possible sense vosaltres i que us duré sempre amb mi. MIL GRÀCIES!

Abbreviations

2-HG	2-hydroxyglutarate
2D	Two-dimensional
2HGDH	2-HG dehydrogenase
3D	Three-dimensional
5-aza	5-azacytidine
5caC	5-carboxyl-cytosine
5fC	5-formyl-cytosine
5hmC	5-hydroximethyl-cytosine
5mC	5-methyl-cytosine
ACT	Adoptive cell transfer
AITL	Angioimmunoblastic T cell lymphoma
akG	a-ketoglutarate
Alb-Cre	Albumin-Cre
ALT	Alanine aminotransferase
AML	Acute myeloid leukemia
APC	Antigen-presenting cell
ARID1A/B	AT-Rich Interaction Domain 1A/B
ARID2	AT-Rich Interaction Domain 2
AST	Aspartate aminotransferase
ATF2	Activation transcription factor 2
BAP1	BRCA1 Associated Protein 1
BBB	Blood brain barrier
BCAT1/2	Branched-chain amino acid transaminases 1 and 2
BER	Base excision repair
BET	Bromodomain and extraterminal domain
BRAF	B-Raf Proto-Oncogene, Serine/Threonine Kinase
BRCA1/2	BRCA1/2 DNA Repair Associated
CA 19-9	Carbohydrate antigen 19-9
CAF	Cancer-associated fibroblast

CAR	Chimeric antigen receptor
CCA	Cholangiocarcinoma
CCND1	Cyclin D1
CD	Cluster of differentiation
CDKN2A/B	Cyclin dependent kinase inhibitor 2A/B
CEUS	Contrast-enhanced ultrasonography
CNV	Copy number variation
COSMIC	Catalogue of somatic mutations in cancer
CT	Computed tomography
CTCF	CCCTC-binding factor
CTLA-4	Cytotoxic T-Lymphocyte Associated Protein 4
CTNNB1	Catenin Beta 1
DC	Dendritic cell
dCCA	Distal cholangiocarcinoma
DCR	Disease control rate
DDR	DNA Damage Response
DE	Differential expression
DEN	Diethylnitrosamine
dMMR	Deficient Mismatch Repair
DMN	Dimethylnitrosamine
DNA	Deoxyribonucleic acid
DNMT	DNA methyltransferase
DNMTi	DNA methyltransferase inhibitor
DSB	DNA double-strand break
eCCA	Extrahepatic cholangiocarcinoma
ECM	Extracellular matrix
EGF	Epidermal Growth Factor
EGFR	Epidermal Growth Factor Receptor
ELF3	E74 Like ETS Transcription Factor 3
EMT	Epithelial to mesenchymal transition

ERBB1-3	Erb-B2 Receptor Tyrosine Kinase 1-3
ERV	Endogenous retroviruses
f/f	Flox/flox
FDA	U.S. Food and Drug Administration
FFPE	Formalin-fixed paraffin embedding
FGFR1-3	Fibroblast Growth Factor Receptor 1-3
FH	Fumarate hydratase
FOXP3	Forkhead box P3
GBM	Glioblastoma
GEMM	Genetically Engineered Mouse Model
GGT	Gamma-glutamyl transpeptidase
gH2AX	Histone variant H2AX
GOF	Gain-of-function
GSEA	Gene set enrichment analysis
GZMB	Granzyme B
H&E	Hematoxylin and eosin
H3K	Histone H3 lysine
HB-EGF	Heparin Binding Epidermal Growth Factor
HCC	Hepatocellular carcinoma
HepPar1	Hepatocyte Paraffin 1
HER2	Human epidermal growth factor receptor 2
HGF	Hepatocyte growth factor
HLA	Human leukocyte antigen
HOT	Hydroxyacid-oxoacid transhydrogenase
HR	Homologous recombination
HRD	HR repair-deficient
HRP	HR repair-proficient
HSC	Hepatic stellate cells
IC50	Half maximal inhibitory concentration
iCAF	Inflammatory cancer-associated fibroblast

iCCA	Intrahepatic cholangiocarcinoma
ICD-11	International classification of diseases
ICI	Immune checkpoint inhibitor
ICT	Isocitrate
IDH1-3	Isocitrate Dehydrogenase 1-3
IFN	Interferon
IFNsign	Interferon signature
IgG1	Immunoglobulin G1
IHC	Immunohistochemistry
IL	Interleukin
IO	Immuno-oncology
INDEL	Insertion or deletion
IO	Immuno-oncology
IRB	Institutional Review Board
IRF7	Interferon Regulatory Factor 7
ISG15	Interferon Stimulated gene 15
JAK	Janus Kinase
Jmj	Jumonji
Jmj-KDM	Jumonji domain-containing histone lysine-demethylase
KDM	Lysine Demethylase
KRAS	KRAS Proto-Oncogene, GTPase
KRT19	Cytokeratin 19
KTM2A/C/D	Lysine Methyltransferase 2A/C/D
LGG	Low-grade glioma
LOF	Loss-of-function
LOH	Loss-Of-Heterozygosity
LST	Large-Scale Transitions
MAF	Minor allele frequency
MAPK	Mitogen-Activated Protein Kinase
MCL1	Myeloid cell leukemia 1

MDM2	MDM2 Proto-Oncogene
MDS	Myelodysplastic syndromes
MDSC	Myeloid-derived suppressor cell
MHC	Major histocompatibility complex
mIHC	Multiplexing immunohistochemistry
MMR	Mismatch repair
MRI	Magnetic Resonance Imaging
MSI-H	Microsatellite instability-High
MUT	Mutant
MYC	MYC Proto-Oncogene, BHLH Transcription Factor
myCAF	Myofibroblastic cancer-associated fibroblast
NAD(P)	Nicotinamide adenine dinucleotide (phosphate)
NAPRT1	Nicotinate phosphoribosyltransferase
NER	Nucleotide excision repair
NFkB	Nuclear factor-kB
NGS	Next-generation sequencing
NHEJ	Nonhomologous end joining
NK	Natural Killer
NMF	Nonnegative Matrix Factorization
NOD-SCID	Non-obese diabetic/severe combined immunodeficient
NOTCH2-4	Notch Receptor 2-4
NTRK	Neurotrophic tyrosine receptor Kinase
OAS 1-3	2'-5'-Oligoadenylate Synthetase 1-3
ORR	Overall response rate
OS	Overall survival
PALB2	Partner and localizer of BRCA2
PanCK	Pan Cytokeratin
PAR	Poly (ADP-ribose)
PARP1/2	Poly(ADP-ribose) polymerase 1/2
PARPi	PARP inhibitors

PARylation	PARP1/2 poly-ADP-ribosylation
PBMC	Peripheral blood mononuclear cell
PBRM1	Polybromo 1
PCA	Principal component analysis
pCCA	Perihilar cholangiocarcinoma
PD-1	Programmed cell death receptor 1
PD-L1	Programmed cell death ligand 1
PDX	Patient-derived xenograft
PET	Positron emission tomography
PFS	Progression-free survival
PI3K	Phosphatidylinositol-3 kinase
PIK3CA	Phosphatidylinositol-4,5-Bisphosphate 3-Kinase Catalytic Subunit Alpha
PRKCA/B	Protein Kinase C Alpha/Beta
PSC	Primary sclerosing cholangitis
PTEN	Phosphatase And Tensin Homolog
RBMC20	RNA-binding protein RNA binding motif protein 20
RNA-seq	RNA sequencing
RNF213	Ring finger protein 123
RPS	Repair Proficiency Scoring
RT-qPCR	Reverse transcription quantitative real-time polymerase chain reaction
RTK	Receptor Tyrosine Kinase
SAM	S-adenosylmethionine
SD	Standard deviation
SDF1	Stromal-cell derived factor 1
SDH	Succinate dehydrogenase
SMAD4	SMAD Family Member 4
SMARCA2/4	SWI/SNF Related, Matrix Associated, Actin Dependent Regulator of Chromatin, Subfamily A, Member 2/4
SNP	Single nucleotide polymorphism
SNUC	Sinonasal undifferentiated carcinoma

SNV	Single nucleotide variant
SSB	DNA single-strand break
STAT3	Signal transducer and activator of transcription 3
STING	Stimulator of interferon genes
STK11	Serine/Threonine Kinase 11
T-biAb	T cell-engaging bi-specific antibody
TAA	Thioacetamide
TAA	Tumor-associated antigens
TACE	Transarterial chemoembolization
TAI	Telomeric Allele Imbalance
TAM	Tumor-associated macrophage
TAN	Tumor-associated neutrophils
TARE	Transarterial radioembolization
TCA	Tricarboxylic acid cycle
TCB	Tumor cell bispecific antibody
TCGA	The Cancer Genome Atlas Program
TCR	T cell receptor
TDG	Thymine DNA glycosylase
TET	Ten-eleven translocation methylcytosine dioxygenase
TIL	Tumor-infiltrating lymphocyte
TIME	Tumor immune microenvironment
TME	Tumor microenvironment
TMZ	Temozolomide
TNF	Tumor necrosis factor
TP53	Tumor protein P53
Treg	T regulatory cell
TRK	Tropomyosin receptor kinase
VEGF	Vascular Endothelial Growth Factor
WT	Wild-type
YAP	Yes1 Associated Transcriptional Regulator

Index

Summary

The field of cancer treatment has shifted towards personalized medicine, driven by advancements in understanding molecular and genetic abnormalities and identifying specific targets within cancer cells. Precision oncology plays a crucial role, especially in challenging tumor types, such as cholangiocarcinoma (CCA), where chemotherapy has limited efficacy. CCA poses significant challenges in clinical management due to its poor prognosis and lack of effective treatments. Preclinical research is essential to understand CCA better and enhance therapeutic outcomes. While advanced CCA is the most common scenario in clinical practice, most available research models are built with surgically resected primary CCA samples. Thus, there is an urgent need to develop models focused on advanced CCA to improve our understanding of this disease stage and provide representative platforms for testing drug efficacy. *IDH1* mutations are common in intrahepatic CCA, and the targeted inhibitor ivosidenib has shown clinical benefit. However, improved drug efficacy and durable responses are needed. This thesis focuses on developing and characterizing patient-derived xenografts (PDXs) from unresectable metastatic CCA, aiming to identify vulnerabilities for advanced CCA treatment. The PDX models accurately represented the original CCA samples, enabling effective *ex vivo* and *in vivo* drug testing. Assessing the response to PARP inhibitors (PARPi) identified *BRCA2* mutations as potential predictive biomarkers. In contrast, tumors with mutations in *IDH, ARID1A*, and *BAP1* genes showed resistance to PARPi due to a proficient homologous recombination phenotype. To understand the role of *IDH1* mutations in CCA, an unbiased analysis of gene expression and DNA methylation was conducted on *IDH1* wild-type and mutant CCA_PDXs. The results revealed that *IDH1* mutations might shape the immune tumor microenvironment in CCA patients by down-regulating immune signaling-related genes within the tumor cells. Notably, these down-regulated gene sets strongly correlated with promoter methylation, suggesting that DNA methylation-driven suppression of these signatures may contribute to decreased expression. Notably, treating *IDH1* mutant cells with DNA demethylating agents improved T cell functionality of co-cultured lymphocytes. These findings provide insights into the complex interplay between *IDH1* mutations, DNA methylation, and immune-related gene expression in CCA, offering potential therapeutic strategies.

Resum

Recentment, el tractament del càncer s'ha enfocat cap a la medicina personalitzada, una transició impulsada pels avenços en la identificació de dianes específiques en les cèl·lules tumorals. L'oncologia de precisió té un paper crucial, especialment en tipus de tumors molt agressius, com el colangiocarcinoma (CCA), un càncer en què la quimioteràpia té una eficàcia limitada. El CCA és un tumor amb mal pronòstic i sense tractaments efectius. La investigació pre-clínica és essencial per entendre millor el CCA i millorar els resultats terapèutics. Tot i que el CCA avançat és l'escenari més comú en la pràctica clínica, la majoria de models d'investigació disponibles estan construïts amb mostres quirúrgiques de CCA primari. Per tant, és urgent desenvolupar models centrats en el CCA avançat per millorar el coneixement d'aquest estadi de la malaltia i proporcionar plataformes representatives per testar nous fàrmacs. Les mutacions del gen IDH1 són freqüents en el CCA intrahepàtic i l'inhibidor de l'enzim IDH1 mutat, ivosidenib, ha mostrat beneficis clínics. Tanmateix, cal millorar l'eficàcia d'aquest fàrmac per tal d'obtenir respostes duradores. Aquesta tesi es centra a desenvolupar i caracteritzar xenografts derivats de pacient de CCA metastàtic no operable, amb l'objectiu d'identificar vulnerabilitats per al tractament del CCA avançat. Els models generats representen amb precisió les mostres de CCA originals, permetent proves efectives de fàrmacs *ex vivo* i *in vivo*. L'avaluació de la resposta als inhibidors de PARP ha identificat les mutacions del gen BRCA2 com a potencial biomarcador predictiu de resposta a aquests fàrmacs. En canvi, els tumors amb mutacions en els gens IDH, ARID1A i BAP1 han mostrat resistència als inhibidors de PARP, resultats explicats per un fenotip de recombinació homòloga competent. Per entendre el paper de les mutacions d'IDH1 en CCA, s'ha realitzat un anàlisi de l'expressió gènica i la metilació de l'ADN en els models de CCA IDH1 mutats. Els resultats han demostrat que les mutacions IDH1 podrien modular el component immunitari del microambient tumoral mitjançant la regulació a la baixa dels gens relacionats amb la senyalització immunològica en les cèl·lules tumorals. En particular, els promotors d'aquests conjunts de gens presenten una alta metilació, cosa que suggereix una supressió regulada per metilació de l'ADN. En particular, el tractament de cèl·lules IDH1 mutades amb agents demetiladors de l'ADN ha millorat la funcionalitat de les cèl·lules T en co-cultiu. Aquestes troballes proporcionen informació sobre la complexa interacció entre les mutacions IDH1, la metilació de l'ADN i l'expressió gènica relacionada amb el sistema immunitari en CCA, oferint possibles estratègies terapèutiques.

Introduction

1. Cholangiocarcinoma (CCA)

The biliary tract (or biliary system) refers to the organs and ducts that transport, store, and release the bile produced in the liver into the small intestine. The biliary tract includes the gallbladder and the bile ducts inside and outside the liver, also known as the biliary tree [1]. The liver secretes bile into the surrounding small ducts that join to form the common hepatic duct, and the bile is transported through the cystic duct to be ultimately stored in the gallbladder (**Fig I1**). During a meal, the body releases bile into the upper part of the small intestine, called the duodenum. This helps to eliminate waste accumulated in the bile and aids in the digestion of dietary fats and oils by providing bile acids [2].

Cholangiocarcinoma (CCA) encompasses a heterogeneous group of aggressive malignancies arising along the biliary tree [3]. Together with gallbladder cancer, they constitute the group of biliary tract tumors [4]. CCA predominantly arises from the malignant transformation of the epithelial cells lining the bile ducts, termed cholangiocytes; however, tumors may also develop from peribiliary glands and hepatocytes, depending on the underlying liver disease and location [5] (**Table I1**). The common routes of tumor spreading are vascular, lymphatic, intraperitoneal, neural, and intraductal, and the common sites of metastasis are the liver, lymph nodes, and adjacent organs [1].

CCA can be categorized according to the primary anatomic location in the biliary tree as intrahepatic CCA (iCCA), perihilar (pCCA), or distal (dCCA), as agreed by the 11th revision of the International Classification of Diseases (ICD-11) [6] (**Fig I1** and **Table I1**). iCCA arises above the second-order bile ducts within the liver parenchyma and pCCA in the right and/or left hepatic ducts and/or at their junction, and these two can also be collectively referred to as 'extrahepatic' (eCCA); in contrast, dCCA is confined to the common bile duct. pCCA is the most common subtype, accounting for approximately 50–60% of all CCAs, followed by dCCA (20–30%) and iCCA (10–20%) (**Fig I1**) [7].

Based on its macroscopic growth pattern, CCA can also be classified into mass-forming, periductal-infiltrating and intraductal-infiltrating (**Fig I1** and **Table I1**). The mass-forming is the most frequent one and produces a well-delimited, polylobulated mass; the periductal-infiltrating extend lengthwise along the bile duct wall, and the intraductal-infiltrating preferentially grows towards the bile duct lumen [8].

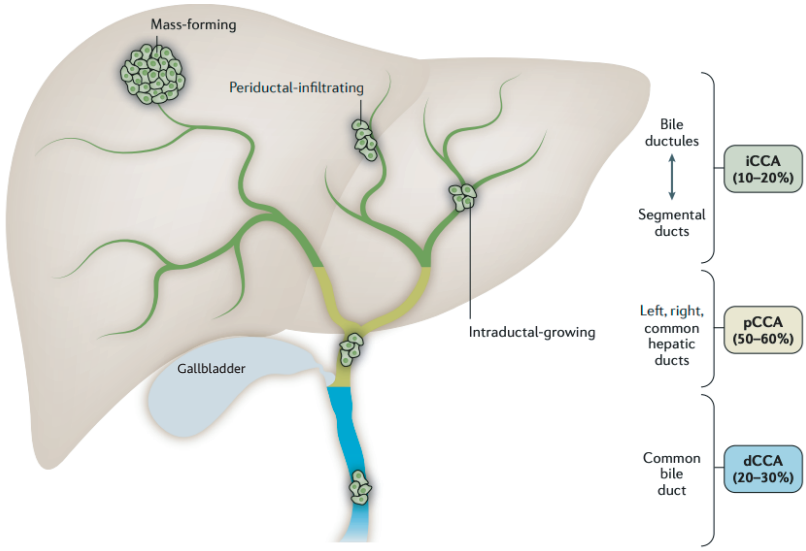

Figure I1. Anatomical classification of cholangiocarcinoma and distinct growth patterns. The three subtypes of CCA, based on anatomical location (iCCA, pCCA, and dCCA) and growth pattern (mass-forming, periductal-infiltrating, and intraductal-growing). Image from [7].

Even though it is considered a rare type of cancer, CCA is the second most common primary hepatic malignancy after hepatocellular carcinoma (HCC) [3], accounting for approximately 15% of all primary liver cancers and about 3% of gastrointestinal tumors [7]. The incidence of CCA highly depends on geographic location and is associated with region-specific risk factors and etiologies (**Table I1**). In Western countries, primary sclerosing cholangitis (PSC) and hepatitis B/C-related liver diseases are the most well-known risk factors, and CCA incidence ranges from 0.35 to 2 cases per 100,000 inhabitants per year [9]. However, these values can be up to 40 times higher in endemic regions of South Korea, China, or Thailand, where cases can be as high as 85 per 100,000 inhabitants annually, owing to chronic liver fluke parasitic infections [7]. Although chronic inflammation of the biliary epithelium is the most common CCA risk, most CCA cases remain sporadic and without any apparent cause.

Often asymptomatic at early stages, CCA is usually diagnosed at an advanced stage, compromising the disease management [3, 7]. While standard-of-care treatment includes tumor resection, only 20-25% of CCA patients are diagnosed sufficiently early to be eligible for surgery. The remaining 75-80% of cases are diagnosed when the disease is already disseminated, with locoregional involvement or/and distant metastatic lesions. Therapeutic

options are limited for advanced metastatic CCA. Moreover, the lack of efficient treatment is associated with a dismal prognosis: patients with advanced CCA have a 5-year survival rate of only 2% and a median survival of 1 year [10].

Table I1. CCA pathogenesis of the different CCA anatomical subtypes

CCA subtype	Location	Histology	Growth pattern	Main risk factors
iCCA	Bile ductules and/or second-order bile ducts within the liver parenchyma	Two histological subtypes: 1. Mucin-producing adenocarcinoma (similar to pCCA/dCCA) 2. A mixed subtype containing areas of non-mucin secreting adenocarcinoma and areas of hepatocytic differentiation	1. Mass-forming 2. Periductal-infiltrating 3. Intraductal-growing	Cirrhosis, viral hepatitis B/C, liver fluke parasitic infections
pCCA/ dCCA	pCCA: right and/or left hepatic ducts and/or their junction dCCA: common bile duct	Mucin-producing adenocarcinomas arising from the lining epithelium and, occasionally, from peribiliary glands	1. Periductal-infiltrating 2. Intraductal-growing	Primary sclerosing cholangitis (PSC), choledochal cyst, and liver fluke (less frequently than iCCA)

Location, histological variants, growth patterns, main related risk factors/etiologies, and prevalent genomic alterations of each CCA subtype are presented.

CCAs can vary significantly in terms of their genetic and epigenetic characteristics, molecular properties, and clinical presentations, even though all originate from the bile duct, as will be addressed in the following sections. This emphasizes the intricacy of the disease and highlights the importance of developing customized treatment strategies [11]. Given the high levels of inter- and intratumoral heterogeneity of CCAs, profiling studies at the molecular level are increasingly critical to comprehend the underlying molecular mechanisms and to facilitate more tailored and effective clinical management options [7].

1.1. Molecular pathogenesis of CCA

The molecular etiology of CCA poses a challenge due to the observed heterogeneity of cancer, wherein numerous genes contribute to distinct signaling pathways [12]. In this section, we will first analyze the genetic factors that play a role in the development of CCAs. We will then explore the signaling pathways involved and, finally, consider the contributions of the tumor microenvironment to this process.

1.1.1. Genetics

Recent molecular profiling studies have delineated the genomic, transcriptomic, and methylation landscapes of CCAs [11]. Compared to other types of cancer, CCA falls in the middle range regarding the number of genomic alterations [13]. Both iCCA and eCCA have a similar number of non-synonymous mutations per tumor, with an average of around

39 and 35, respectively [14]. Importantly, massive sequencing studies also revealed that the most prevalent genetic alterations identified in CCA affect key oncogenic modules such as: "cell cycle regulation, DNA damage, and genomic instability" (*TP53*, *CDKN2A/B*, *CCND1*, *ATM,* and *BRCA1/2*), "epigenetic regulation" (*IDH1/2*, *BAP1*, *PBRM1*, *ARID1A/B*, *ARID2*, *KMT2A/C/D, KDMs SMARCA2/4*), "tyrosine kinase signaling" (*KRAS, ERBB1–3, BRAF, PIK3CA, PTEN, STK11, SMAD4,* and *FGFR1–3*), "immune dysregulation" (JAK–STAT3 signaling), "WNT-CTNNB1 pathway" (*APC*), "Notch and Hippo signaling" (*NOTCH2-4* and *NF2* deletion), together with *FGFR2* and *PRKCA–PRKCB* fusions, and *MYC* and *MDM2* amplifications [12, 14-16] (**Fig I2A**).

Interestingly, not all presented alterations are equally enriched in each CCA subtype [7, 11]. Nakamura et al. highlighted that various genetic mutations have been identified in different subtypes of CCA. For instance, *IDH1/2*, *ARID1A*, *BAP1,* and *FGFR2* fusions are commonly found in iCCA, whereas *ARID1B, ELF3, PRKACA/B*, and *ERBB2/3* alterations are more prevalent in pCCA/dCCA [14, 15] (**Fig I2A**). Moreover, even though *KRAS* mutations are present in all subtypes of CCA, they are most commonly found in eCCA [17]. Several of the listed genomic aberrations (including *IDH1/2, FGFR2, BRAF,* and *ERBB2,* shown as exploded from the pie chart in **Fig I2A**) are clinically actionable targets and have been reported to be present in 25-50% of CCA patients, with this percentage being mainly subjected to the preferred anatomical location of these alterations [14, 18-21] (**Fig I2B**).

To date, the only genomic association with disease etiology has been found in liver fluke-positive CCAs. Tumors that exhibit fluke positivity show a higher prevalence of mutations, and specifically in the *SMAD4* and *TP53* genes, as well as *ERBB2* amplifications. In contrast, *IDH1/2* and *BAP1* mutations are not enriched in these tumors [16].

One interesting finding is the mutual exclusivity of mutations in commonly altered genes found in CCA. For example, mutations in the genes *IDH1/2*, *BAP1*, and *PBRM1* tend to be exclusive of mutations in *KRAS*, *TP53*, and *SMAD4*, respectively [17, 22]. This suggests that different sets of mutations may drive different subtypes of CCA. On the other hand, co-occurring mutations have also been reported, such as *IDH1* with *ARID1A*, *BAP1,* or *PBMR1* [23]. These findings highlight the complex genetic landscape of CCA and the need for personalized approaches to its diagnosis and treatment.

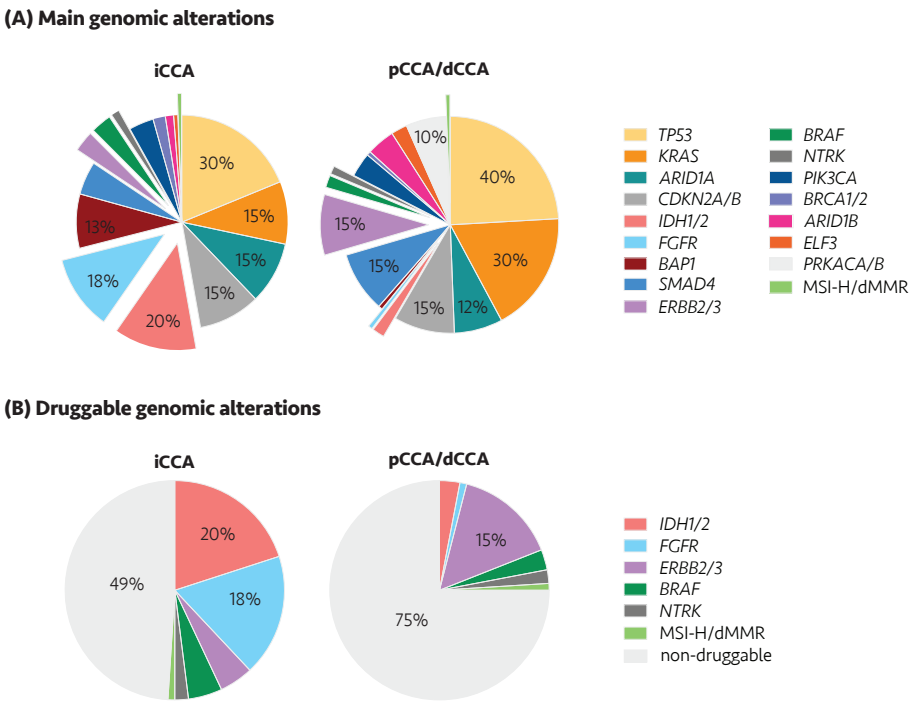

Figure I2. Genomic landscape of CCA. (A) Pie charts exemplifying the main genomic alterations found in the different CCA anatomical subtypes, with indicated percentages of the most prevalent aberrations. pCCA and dCCA, collectively referred to as extrahepatic CCA, are depicted in the same graph, because data reported so far does not differentiate between these two subgroups. The genomic alterations with options of therapeutic actionability are shown as exploded from the pie chart. **(B)** Pie charts indicating the percentage and names of druggable alterations harbored by each CCA subtype. All plots were generated using previously reported data [14, 20, 21]. MSI-H, microsatellite instability-high; dMMR, deficient mismatch repair.

1.1.2. Signaling pathways and molecular networks

The cholangiocyte transformation and subsequent tumor growth is a complex process that is influenced by factors present in the tumor microenvironment (TME) [7]. These factors include pro-inflammatory cytokines and growth factors, which can promote uncontrolled cell proliferation. Moreover, the aberrant expression or activation of cell surface receptors and intracellular signaling pathways play a crucial role in acquiring genetic and epigenetic changes, further driving tumor growth (**Fig I3**). Therefore, a better understanding of the interplay between TME factors and cellular signaling pathways is essential to developing effective therapeutic strategies for treating CCA.

In particular, sustained IL-6/JAK/STAT3 signaling was shown to contribute to CCA cell proliferation by upregulating the anti-apoptotic myeloid cell leukemia 1 (MCL1) [24].

Paracrine factors, such as heparin-binding EGF-like growth factor (HB-EGF), stromal-cell derived factor 1 (SDF1), and vascular endothelial growth factor (VEGF), are secreted by cancer-associated fibroblasts (CAFs). These factors bind to their respective receptor tyrosine kinases (RTK), activating the RAS-MAPK and PI3K-AKT-mTOR pathways. Of note, these pathways are significantly affected by genomic aberrations (*KRAS*, *BRAF*, or *FGFR*) in cases of CCA (see Section 1.1.1). Thus, the dysregulation of growth factor signaling pathways represents a critical oncogenic mechanism in CCA, with the potential to provide actionable therapeutic targets [25].

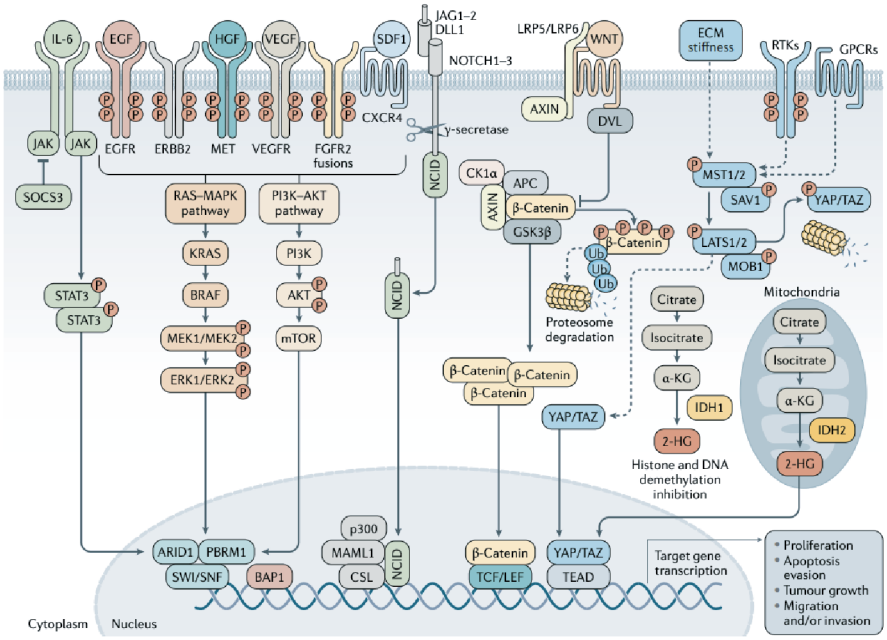

Figure I3. Signaling pathways involved in cholangiocarcinoma development and progression. Representative molecular networks of CCA pathogenesis, showing extracellular ligands that are commonly present in the CCA tumor microenvironment (TME), bound to their respective cell surface receptors and associated downstream signaling pathways. Image from [7].

Developmental pathways, including the Notch and WNT signaling pathways, play a significant role in developing iCCA [26]. The Notch pathway plays a role in the growth and repair of biliary cells, as well as the formation of tubules and fibrosis [27]; overexpression or aberrant activation of Notch signaling was shown to mediate transdifferentiation of hepatocytes into cholangiocytes during carcinogenesis [28] and to promote CCA cell survival via PI3K–AKT signaling [29]. Similarly, the WNT-β-catenin signaling pathway is closely linked to the process of cholangiocyte development and ductular reaction [30]. In addition,

the combination of WNT ligands released by infiltrating inflammatory macrophages [31], and recurrent mutations encoding key components of the pathway [32], can lead to a dysregulation of the signaling pathway. Inhibitors for these pathways are of growing interest, and their efficiency is being investigated in clinical trials [33, 34]. Moreover, increased activity of YAP has been associated with iCCA pathogenesis; YAP protein is an effector protein of the Hippo pathway that regulates organ size, cellular proliferation, and apoptosis [35].

1.1.3. Tumor microenvironment (TME)

The enhanced crosstalk of CCA with the microenvironment has been reported [26]. This crosstalk impacts CCA development, evolution, and invasiveness [25, 36]. Histologically, CCA is characterized by an extensive desmoplastic stroma, a dense fibrous tissue that surrounds and infiltrates the CCA cells [37]. This stroma is composed of various components, including cancer-associated endothelial cells, cancer-associated fibroblasts (CAFs), and a complex group of inflammatory cells [25, 38-41], such as macrophages, neutrophils, natural killer (NK) cells, and T cells. Moreover, extracellular matrix (ECM) proteins such as collagens, laminin, and fibronectin are also present in the stroma of CCA.

CAFs comprise a heterogeneous group of spindle-shaped cells with a mesenchymal origin. They are a key component of the desmoplastic stroma in CCA and are known to promote tumor growth, invasion, and metastasis [25]. CAFs secrete various extracellular matrix proteins and regulatory molecules (such as IL-1β, EGF-like growth factor, and SDF1) to facilitate tumor cell growth and invasion [7]. In addition, CAFs have been shown to promote angiogenesis and suppress anti-tumor immune responses [42]. Recently, a study by Affo et al. combining genetic tracing and single-cell RNA sequencing (scRNA-seq) analysis revealed that hepatic stellate cells (HSC) are the primary source of CAF, and that HSC-derived CAFs are the dominant population interacting with CCA cells [43]. Further, they showed that CAFs in CCAs can be divided into inflammatory and growth factor-enriched (iCAF) and myofibroblastic (myCAF) subpopulations. The myCAF-expressed hyaluronan synthase 2, but not the type I collagen, promotes iCCA, while iCAF-expressed hepatocyte growth factor (HGF) enhances iCCA growth. This study provided evidence that CAF subtype-specific mediators can be therapeutically targeted.

Moreover, recent studies have provided increasing evidence that CCA contains a significant number of immune cells, albeit with highly immunosuppressive properties in most

CCA patients [41]. The tumor immune microenvironment (TIME) of CCA is characterized by the presence of effector tumor-infiltrating lymphocytes (TILs), but it predominantly accumulates suppressive immune cell populations, including programmed cell death ligand-1 $(PD\text{-}L1)^+$ tumor-associated macrophages, myeloid-derived suppressor cells, tumor-associated neutrophils, and Forkhead box P3 $(FOXP3)^+$ Treg cells [44, 45]. Determining the presence of these immune cells in the TME of CCA is critical for understanding the underlying mechanisms of immune evasion and resistance to therapies. Thus, defining and targeting the TIME could provide new approaches for treating CCA in the future. We will detail the state-of-the-art studies regarding the TIME of CCA in Section 4.2.

Thus, CCA's complex and multifactorial molecular etiology is caused in part by mutations in cancer-driver genes and genes involved in signaling pathways, as well as alterations in the TME.

1.2. Clinical manifestations, diagnosis, and treatment

The clinical presentation, diagnosis, and therapeutic intervention of CCA patients are also subjected to anatomical subtypes, as exemplified by **Table I2.** The following sections will address a detailed explanation of each presented aspect.

Table I2. Clinical management of CCA subtypes

CCA subtype	Clinical presentation	Diagnosis	Surgical treatment	Systemic treatment
iCCA	Abdominal pain, weight loss and generalized malaise, but asymptomatic in most of the cases	A combination of: - Blood-based tests of biochemical markers (CA 19-9, hepatic enzymes, etc.) - Imaging techniques, such as contrast-enhanced ultrasonography (CEUS), computed tomography (CT) and Magnetic Resonance Imaging (MRI)	Surgical resection, followed by adjuvant chemotherapy. In specific cases, option of liver transplantation.	(In some cases, locoregional therapy or chemotherapy is effective) 1st line is gemcitabine plus cisplatin, combined with durvalumab 2nd line consists on: - Targeted therapies if a driver alteration is found (*IDH* mutations, *FGFR2* or *NTRK* fusions, *BRAF* mutations, etc.) - FOLFOX if no driver alteration is found
pCCA	Painless jaundice, abdominal pain, weight loss and generalized malaise			1st line is gemcitabine plus cisplatin, combined with durvalumab 2nd line is mainly FOLFOX (due to really few druggable genomic alterations associated with pCCA/dCCA, Fig I2)
dCCA			Pancreatico-duodenectomy	

Summary of the clinical manifestations, the diagnosis approach, and the treatment options of the CCA subtypes.

1.2.1. Clinical manifestations and diagnosis

CCA is often asymptomatic in its early stages. However, as the tumor grows, it can cause numerous clinical manifestations related to biliary tract obstruction (**Table I2**) [1]. In addition to a thorough clinical history and physical examination, the diagnosis of CCA relies on a combination of biochemical marker tests and imaging techniques. The most

commonly used tests are blood-based ones that can determine i) serum levels of carbohydrate antigen 19–9 (CA 19–9) [46], ii) enzyme indicators of hepatic function, including aspartate aminotransferase (AST) and alanine aminotransferase (ALT), and iii) biliary tract-excreted products, like bile salts, alkaline phosphatase or gamma-glutamyl transpeptidase (GGT). These tests help to evaluate liver function and biliary tract obstruction. However, they lack sensitivity and specificity, particularly in early-stage disease [47]. Imaging techniques, such as contrast-enhanced ultrasonography (CEUS), computed tomography (CT), magnetic resonance imaging (MRI), and positron emission tomography (PET) can provide a detailed view of the biliary tree and surrounding tissue, aiding in the detection, localization, and staging of CCA [1, 47]. Overall, a combination of blood-based and imaging tests is usually required for an accurate diagnosis, staging, and evaluation of the treatment response (**Table I2**).

1.2.2. Surgical resection of localized primary CCA

Complete surgical resection remains the cornerstone for the cure for localized CCA (**Table I2** and **Fig I4**). However, only a minority of patients are eligible for surgery, and the risk of tumor relapse remains high [21]. Moreover, the BILCAP trial results have established that adjuvant therapy with capecitabine should be a standard-of-care adjuvant therapy after the surgical resection for CCA [48] (**Table I2** and **Fig I4**).

1.2.3. Management of advanced and metastatic CCA

For patients with unresectable CCA, locoregional therapy or chemotherapies, such as transarterial-chemoembolization (TACE) or radioembolization (TARE), and radiofrequency ablation, have been determined to be safe and reasonably effective [49, 50] (**Fig I4**).

However, systemic chemotherapy is the mainstay of treatment for patients with advanced and metastatic CCA. The standard first-line chemotherapy for advanced CCA patients, and in particular for iCCA patients, involves a combination of gemcitabine and cisplatin (GemCis), which has demonstrated better outcomes than monotherapeutic regimens [51] (**Table I2** and **Fig I4**). This treatment provides a median survival of 1 year. Recent studies have shown promising results for the use of other chemotherapeutic agents, such as the addition of nab-paclitaxel to the GemCis combination, which has demonstrated improved overall survival (OS) and progression-free survival (PFS) in patients with advanced CCA [52].

The TOPAZ-1 trial [53] showed that the combination of the PD-L1 inhibitor durvalumab with the standard-of-care GemCis chemotherapy results in a further improvement in OS, leading to the recent FDA approval of gemcitabine-cisplatin-durvalumab as an additional frontline treatment standard for CCA (**Fig I4**). Similarly, the KEYNOTE-966 trial [54] also demonstrated improved OS by adding the programmed cell death receptor 1 (PD-1) inhibitor pembrolizumab to the GemCis regimen. These findings are significant for patients with advanced CCA, representing an example of immunotherapy success in a biomarker-unselected population.

After progression on first-line, treatment options for advanced CCA are guided by the tumor genomics [55] (**Table I2** and **Fig I4**). As mentioned in Section 1.1.1 and exemplified in Fig I2, it is estimated that approximately 25-45% of patients with CCA harbor actionable genetic alterations, particularly in the iCCA [56]. Based on the encouraging results obtained in the FIGHT-202 and FOENIX-CCA2 trials [57, 58], the FDA has approved pemigatinib and futibatinib for the treatment of patients with previously treated, unresectable locally advanced or metastatic CCA (in the case of futibatinib, iCCA) with an *FGFR2* fusion or other rearrangement. Moreover, based on the ClarIDHy trial [59], the mutant IDH1 inhibitor, ivosidenib, was approved for treating patients with previously treated, locally advanced, or metastatic CCA with *IDH1* mutations. Developing tissue-agnostic drugs for treating CCA is currently a very active area of research. Besides the widely known FGFR and mutant IDH inhibitors, larotrectinib and entrectinib are tumor-agnostic tropomyosin receptor kinase (TRK) inhibitors that are indicated for the treatment of advanced or metastatic solid tumors with neurotrophic tyrosine receptor kinase (NTRK) gene fusions, including 3% of CCA [60, 61]. A recent Rare Oncology Agnostic Research (ROAR) basket clinical trial also demonstrated that the combination of dabrafenib and trametinib showed promising activity in CCA patients with $BRAF^{V600E}$ mutation [62]. Finally, the FDA approved the checkpoint inhibitor pembrolizumab to treat tumors with microsatellite instability high (MSI-H) or deficient mismatch repair proteins (dMMR), including 1-2% of CCA [63] (**Fig I2**).

Recent efforts have also focused on targeting mutations in chromatin regulator genes, such as *ARID1A, BAP1,* and *PBRM1*, as well as in DNA damage repair genes, including *BRCA1/2, ATM,* and *PALB2* [11]. Additionally, some preclinical and early clinical research has shown promise in targeting human epidermal growth factor receptor 2 (HER2)(also referred to as ERBB2) [64] and EGFR receptors [65, 66].

Finally, FOLFOX has been recommended as a second-line chemotherapy option for advanced CCA patients [67], particularly those who do not have an available actionable genomic alteration or for whom genomic analysis is incomplete (**Fig I4**).

A complete diagram guiding the clinical intervention options for CCA treatment explained in this section is depicted below (**Fig I4**).

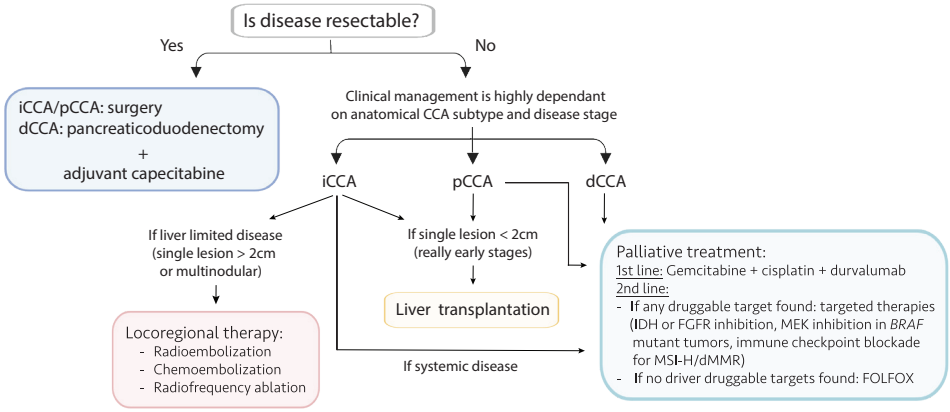

Figure I4. Current clinical management of CCA patients. Flow chart of the presentation and the therapeutic interventions of CCA according to current formal guidelines.

Although there have been significant and encouraging advancements in investigating therapeutic options for advanced and metastatic CCA, the current chemotherapies, targeted therapies, and immunotherapy offer only modest benefits in terms of OS, not managing to significantly increase the current value of ~ 1 year [53, 57-59, 61-63]. This highlights the pressing need for the development of novel therapeutic strategies. To achieve this, there is a critical requirement for developing representative research models for disease study and drug screening.

1.3. CCA research models

To improve clinical management of CCA and develop effective treatments, conducting preclinical research using CCA representative models to enhance our knowledge of CCA pathogenesis is crucial. A recently-published Consensus Statement [68] provides clear guidelines for *in vitro* and *in vivo* CCA preclinical models (**Fig I5**). The statement highlights the significance of these models in replicating the natural history of various CCA subtypes, capturing their molecular heterogeneity, and considering the impact of clinical and therapeutic interventions.

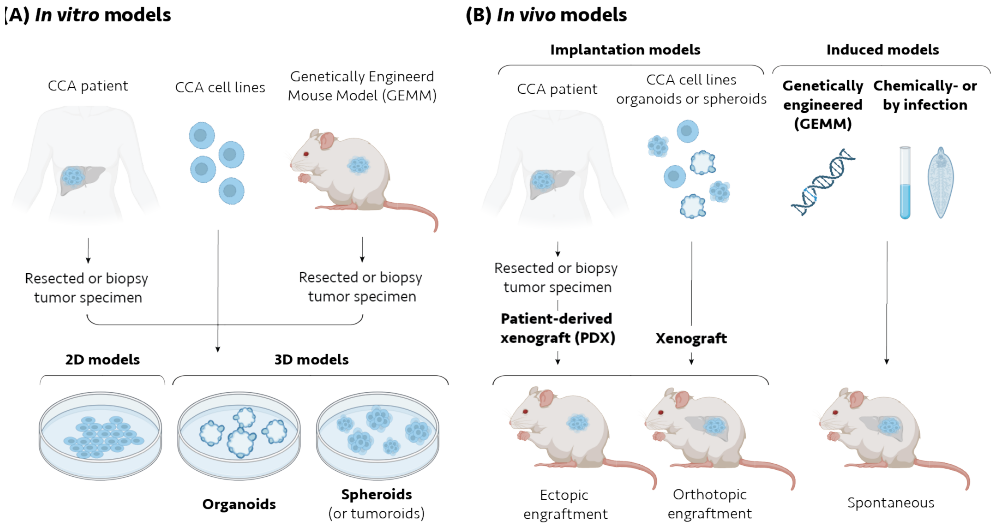

Figure I5. A panel of experimental models for CCA preclinical studies. (A) *In vitro* models, including 2D and 3D culture (as organoids or spheroids) of CCA cell lines or CCA primary cells derived from a CCA patient or a genetically engineered mouse model (GEMM). **(B)** *In vivo* models, including (i) ectopic and orthotopic implantation models, obtained by engrafting either CCA primary cells from a CCA patient or CCA cell lines, organoids, or spheroids, (ii) genetically engineered mouse model (GEMM), and chemically- or infestation-induced models. Adapted from [68]. Image created with BioRender.com. PDX, patient-derived xenograft.

1.3.1. *In vitro* 2D and 3D models

Historically, researchers have relied on *in vitro* immortalized CCA cell lines derived from human CCA specimens to study CCA [69-71]. However, these *in vitro* two-dimension (2D) cell models do not accurately represent the original tumors in numerous manners. For instance, continuous passaging *in vitro* can change the genetic composition [72]. Using primary cultures of CCA cells from tumor tissue are a potential solution, but tumor cells have limited growth potential under this condition [73, 74]. More importantly, tumor cells grown in a 2D monoculture do not accurately replicate the distinct traits of biliary tumors, such as the three-dimension (3D) architecture, cell-to-cell and cell-to-matrix interactions, cellular heterogeneity, and the effect of the TME on cancer progression [7] (**Fig I5**).

To overcome these limitations, researchers have developed multicellular 3D models, such as spheroids and organoids [75-77]. Tissue samples taken through surgery or a needle biopsy can be used to establish spheroids or organoids that accurately reflect the patient's tumor, both histopathologically and genomically (**Fig I5**). These *in vitro* 3D models are reliable systems for drug testing and personalized medicine [76, 78]. However, as they also lack

the TME, artificial co-culturing with stromal or immune cells is needed to evaluate these interactions.

1.3.2. *In vivo* models

In vivo models have also been developed for CCA that exhibit a high degree of similarity to human disease and may offer a more comprehensive understanding of the disease's pathobiology and treatment efficacy. In mice, there are three main categories of models used to induce CCA: i) chemical- and/or infection-induced CCA models, ii) genetically engineered mouse CCA models (GEMM), and iii) CCA cell or tissue implantation models [79, 80] (**Fig I5**).

- Chemical- and/or infection-induced CCA models

Chemical- and/or infection-induced rodent models recapitulate tumor initiation and progression. In these models, tumor development is prompted by the toxic effect of DNA damage inducers or viral infections associated with CCA etiology. Several studies have demonstrated CCA formation after the administration of diethylnitrosamine (DEN) in mice [81, 82], furan or thioacetamide (TAA) in rats [83-85], and dimethylnitrosamine (DMN) in hamsters [86]. Moreover, combining some of these compounds with inflammatory injury by a viral infection of *Opisthorchis viverrini* has also been shown to drive CCA development in mice and hamsters [87]. These models facilitate the recognition of potential risk factors and causes of disease, as well as the evaluation of the onset of tumorigenesis.

- GEMM CCA models

GEMM CCA models are advanced animal models designed to harbor the most frequent genetic, epigenetic, or signaling pathway aberrations commonly seen in human CCAs. These models are intended to trigger tumorigenesis in experimental animals by reproducing the most common genetic events found in human tumors. Therefore, they can accurately mimic the progression of CCAs from preneoplastic and early stages to advanced tumor stages, including metastasis [68, 88]. Importantly, one of the most commonly used techniques for activating or inactivating gene expression *in vivo* is the "Cre-lox" system. This method allows precise control over when and where genes are turned on or off. The most representative *in vivo* CCA models based on genetically engineered mice are presented below (**Table I3**).

Table I3. The most representative GEMM CCA models

Animal model	Gene alteration	Tumor type	Refs
Alb–Cre, *SMAD4*$^{f/f}$, *PTEN*$^{f/f}$	Liver specific inactivation of *SMAD4* and *PTEN*	Multifocal iCCA	[89]
Alb–Cre, *KRAS*$^{LSL-G12D/+}$, *PTEN*$^{f/f}$	Liver specific activation of *KRAS* and inactivation of *PTEN*	iCCA with abundant stroma	[90]
Alb–Cre, *KRAS*$^{LSL-G12D}$, *IDH2*$^{LSL-R172}$	Liver specific activation of *KRAS* and *IDH2*	Multifocal iCCA	[91]
Alb-Cre, *NOTCH1*ICD	Liver specific expression of *NOTCH*	Transplantable CCA	[92]
Alb-Cre, *TRP53*$^{f/f}$, *NOTCH1*ICD	Liver specific inactivation of *TRP53* and expression of *NOTCH*	iCCA with fibrous and inflammatory TME	[93]
Alb–Cre, *KRAS*$^{LSL-G12D/+}$, *TRP53*$^{f/f}$	Liver specific activation of *KRAS* and inactivation of *TRP53*	Multistage iCCA	[94, 95]
Pdx1-Cre, *PIK3CA*$^{LSL-H1047R/+}$	Liver specific activation of *PIK3CA*	eCCA	[96]

Summary for GEMM animal models of CCA, their genomic modification, and the resulting CCA type. F/f, flox/flox (flanking/flanked by LoxP, leading to allele deletion upon Cre-mediated recombination); LSL, Lox-Stop-Lox (null allele until Cre-mediated recombination deletes the Stop cassette).

- CCA cells or tissue implantation models

Subcutaneous and orthotopic liver engraftments of CCA cells into mice represent excellent models for exploring cancer-related mechanisms, identifying novel therapeutic strategies, and predicting drug responses [97]. Currently, two main types of grafts are being investigated. Allograft, known as the syngeneic model, refers to the transplantation of murine CCA cells into immunocompetent mice, and xenograft, defined as the transplantation of human CCA tissue or cells into an immunodeficient mice [79].

Syngeneic models allow for the transplantation of mouse CCA cells into a host with a fully functioning immune system. One important syngeneic model for CCA research was reported by Rizvi et al. [98]. In this study, seven primary murine CCA cell lines (SB1-7) were derived from murine CCA tumors. Of note, these murine CCA tumors were found in C57BL/6 mice upon transduction of constitutively active Akt and YAP in the biliary epithelium [98, 99]. The derived murine CCA cell lines can then be transplanted into immunocompetent C57BL/6 mice to generate allografted tumors, which is ideal for studying tumor–stroma interactions and testing immunotherapy-based strategies.

Xenograft models can be created by injecting established CCA cell lines or implanting surgically-derived human CCA tissue, also known as patient-derived xenografts or PDXs. However, it should be noted that while CCA cell line engraftment is homogenous, reproducible, and technically easy, it does not represent the high heterogeneity observed in patient CCA samples [68]. In contrast, PDX models can maintain most of the features found in the original human tumors, including genetic and histologic traits [100-102]. Importantly, these models can accurately recapitulate CCA intra- and inter-tumor heterogeneity, which allows for a better understanding of the diverse nature of CCA disease within the human

population [101-106]. It is worth noting that the treatment responses observed in PDX models are in agreement with those seen in patients [107-109]. To date, only a few collections of PDX models of CCA have been reported (**Table I4**), with most of these models derived from surgically resected primary tumors. Further PDX models focused on unresectable advanced metastatic CCA are not fully developed yet, as shown by the low number of PDX models derived from metastatic CCA (**Table I4**).

Table I4. Collections of PDX models of CCA reported to date

Publication	Implanted samples			Grown as PDX		
	Total	Primary	Metastatic	Total	Primary	Metastatic
Ojima et. al. 2010 [103]	55	55	0	19	19	**0**
Cavalloni et. al. 2016 [104]	17	17	0	1	1	**0**
Garcia et. al. 2018[110]	5	4	1	5	4	**1**
Vaeteewoottacharn et. al. 2019 [105]	16	16	0	12	12	**0**
Leiting et. al. 2020 [101]	87	79	8	47	42	**5**
Jian et. al. 2020 [102]	44	44	0	34	34	**0**
Y.Wang et. al. 2021 [106]		ND		7	7	**0**

A review of the CCA PDX collections reported to date is presented, specifying the total amount of implanted samples and engrafted PDXs. PDX models derived from primary CCA tumor tissues and those from metastatic lesions are separated. ND, non-determined.

2. IDH mutations

Various types of cancers have been found to have genetic alterations in genes related to metabolism [111]. This includes eight genes encoding four different metabolic enzymes, fumarate hydratase (FH), succinate dehydrogenase (SDH), and isocitrate dehydrogenase 1 and 2 (IDH1 and IDH2) [112]. Interestingly, recurrent mutations in the *IDH1* gene were first identified in a whole-exome sequencing study of 22 glioblastomas [113]. Subsequent studies revealed that mutations in *IDH1/2* (collectively referred to as *IDH*) are prevalent in various tumor types [114], and placed *IDH1* as one of the most commonly mutated metabolic genes in cancer [115].

2.1. Prevalence and prognostic values of *IDH1/2* mutations in cancers

IDH1 and *IDH2* mutations have been identified at a high frequency in a plethora of human cancers originating from different tissues [116]. Initially, *IDH1* and *IDH2* mutations were identified as driver mutations in glioblastoma and acute myeloid leukemia (AML) through two independent cancer genome sequencing projects [113, 117]. Subsequent studies have revealed that *IDH1* and *IDH2* mutations are prevalent in various types of cancer, including low-grade glioma and secondary glioblastoma (70-80%) [118], AML (25%) [119, 120], CCA (15-20%) [23], chondrosarcoma (50%) [121], sinonasal undifferentiated

carcinoma (SNUC; 80%) [122, 123] and angioimmunoblastic T-cell lymphoma (AITL; 25%) [124], among others (**Fig I6**). This highlights the crucial roles of *IDH1* and *IDH2* mutations in the pathogenesis of these cancers.

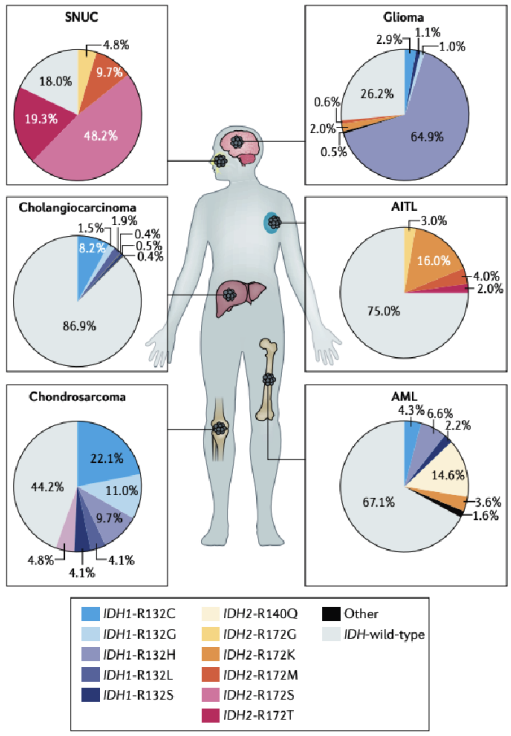

Figure I6. Prevalence and function of *IDH* mutations in cancers. *IDH1* and *IDH2* genes are mutated at varying frequencies in several cancers, including angioimmunoblastic T cell lymphoma (AITL), acute myeloid leukemia (AML), CCA, chondrosarcoma, low-grade gliomas, and sinonasal undifferentiated carcinoma (SNUC), among others. The prevalence of various *IDH* mutations in each cancer type is indicated in the pie charts, and the types of *IDH* mutations are specified in the legend. Image from [114].

The prognostic significance of *IDH1/2* mutations can vary depending on the type and location of the tumor. *IDH1* is the most frequently mutated gene in glioma, including glioblastoma, an aggressive form of the disease [114] (**Fig I6**). Patients with IDH^{mut} gliomas tend to have a better prognosis than those with IDH^{wt} ones [125, 126]. In contrast, mutations of *IDH1/2* do not appear to serve as a favorable prognostic biomarker for AML [127-129] or chondrosarcoma [130]. Several studies have assessed the prognostic implications of *IDH* mutations in CCA and revealed conflicting survival outcomes. A systematic literature review has shown no statistically significant association between *IDH1/2* mutations and OS, PFS, or time to progression [23].

2.2. Mutant IDH enzymes in cancers

Given their high prevalence in various cancer types, *IDH1/2* mutations are thought to play a significant role in the development of these cancers. In the following section, we will first discuss the physiological function of the wild-type IDH enzymes, followed by an explanation of how mutations in *IDH1/2* genes can result in the acquisition of neomorphic enzymatic activity. Finally, we will explore how mutant IDH1/2 enzymes are involved in carcinogenesis and cancer progression.

2.2.1. IDH enzymes and their physiological functions

IDH enzymes play a crucial role in various metabolic processes, including the Krebs cycle (also known as the tricarboxylic acid cycle, TCA), glutamine metabolism, lipogenesis, and redox regulation [131] (**Fig I7**). In humans, five genes (*IDH1, IDH2, IDH3A, IDH3B*, and *IDH3G*) encode for IDH, producing three catalytic isozymes, namely IDH1, IDH2, and IDH3. While IDH1 and IDH2 share significant structural similarities and function as homodimers, IDH3 is active as a heterotetramer composed of two α, one β, and one γ subunit [132]. In the cytosol and mitochondria of cells, these enzymes catalyze the oxidative decarboxylation of isocitrate (ICT) to produce α-ketoglutarate (αKG) and carbon dioxide (CO_2) while reducing the cofactors nicotinamide adenine dinucleotide (phosphate) ($NAD(P)^+$) to NAD(P)H [133] (**Fig I7**). However, the three IDH isoenzymes also differ in subcellular localization, cofactor requirement, allosteric regulation, and catalytic mechanism, which results in overlapping but non-redundant roles in the cellular metabolism [134]. IDH1 is located in the cytoplasm and peroxisomes, whereas IDH2 and IDH3 are located in the mitochondrial matrix as part of the TCA cycle. The catalytic sites of IDH1 and IDH2 require substrate isocitrate and $NADP^+$ cofactor for their activity, and they both undergo a conformation change to form the catalytically active enzyme. IDH3 uses NAD^+ as its electron acceptor, leading to the generation of NADH [135] (**Fig I7**).

IDH enzymes share a common function through the main product of their catalytic reaction, αKG, which promotes the activity of a large group of phylogenetically conserved αKG-dependent dioxygenases [134] (**Fig I7**). In humans, there are more than 60 αKG-dependent dioxygenases that regulate various cellular processes, such as protein hydroxylation [136], carnitine biosynthesis for lipid transportation [137], and chromatin modifications, including histone and DNA demethylation [138-140].

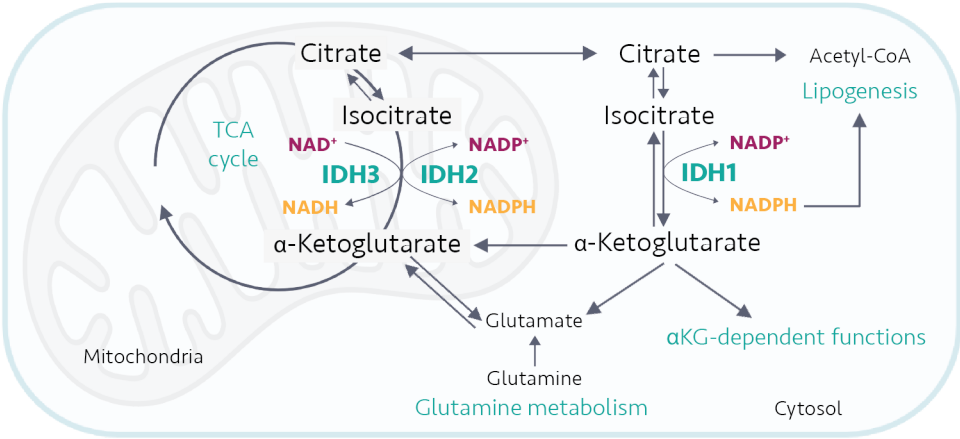

Figure I7. Subcellular localization and chemical reactions catalyzed by IDH enzymes. IDH enzymes produce α-ketoglutarate (αKG) as a result of the oxidative decarboxylation of isocitrate using $NAD(P)^+$. Intermediates involved in this reaction ultimately participate in the TCA cycle, glutamine metabolism, fatty acid synthesis (or lipogenesis), and αKG-dependent reactions, such as protein and nucleic acid hydroxylation. Image created with BioRender.com.

Histone proteins are frequently methylated at the lysine and arginine residues. These modifications, together with other types of chemical modifications on the histone tails, are involved in the modulation of chromatin accessibility and structure, which in turn affects the gene expression [141]. The most extensively studied histone methylation marks include histone H3 lysine 4 (H3K4), H3K9, H3K27, and H3K36 [142]. The Jumonji (Jmj) catalytic domain-containing N-methyl-lysine/arginine demethylases are a diverse family of αKG-dependent dioxygenases that play a critical role in regulating gene expression patterns through the removal of the methyl group from histones [139].

DNA methylation is an essential epigenetic mechanism that plays a fundamental role in gene regulation [143]. DNA methyltransferases (DNMTs) catalyze the transfer of a methyl group from S-adenosylmethionine (SAM) to the fifth carbon of a cytosine residue on DNA, primarily at CpG sites. The process of DNA methylation involves the covalent modification of DNA, which results in the formation of 5-methylcytosine (5mC) [144]. In contrast, the ten-eleven translocation methylcytosine dioxygenase (TET) family of enzymes facilitates the process of DNA demethylation. These αKG-dependent TET enzymes hydroxylate 5mC to produce 5-formylcytosine (5fC) and 5-carboxylcytosine (5caC) [140] (**Fig I8**). This multi-step demethylation process is crucial for the gene regulation [145].

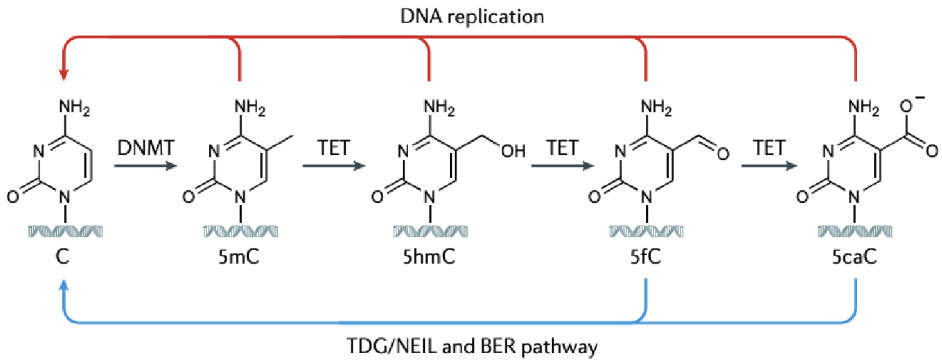

Figure I8. Processing of DNA methylation and demethylation. DNA methyltransferases (DNMTs) catalyze the methylation of cytosine (C) to produce 5-methyl-cytosine (5mC). Sequential oxidation by Ten–Eleven Translocation (TET) enzymes can produce 5-hydroxymethyl-cytosine (5hmC), 5-formyl-cytosine (5fC), and 5-carboxyl cytosine (5caC). 5fC and 5hmC can be actively removed through the actions of thymine DNA glycosylase (TDG)/NEIL and base excision repair (BER) machineries, restoring unmodified cytosine (blue arrows). Modified cytosine can also be removed passively through dilution during DNA replication (red arrows). Figure from [145].

2.2.2. The neomorphic function of mutant IDH1/2 enzymes

Most missense hotspot mutations observed in *IDH1* and *IDH2* are somatic and heterozygous and catalytically affect active sites of IDH enzymes. These mutations involve single amino acid substitutions, mainly affecting either arginine 132 residue (R132) in IDH1, the analogous residue arginine 172 (R172) of IDH2, or arginine 140 (R140) in IDH2 [134, 146].

The α-carboxyl and β-carboxyl groups of isocitrate form hydrogen bonds with the wild-type R132 residue in IDH1, as well as R140 and R172 in IDH2. However, when these residues are mutated, the strong and positively charged hotspot arginine residue is replaced with amino acids with a lower polarity, such as histidine (H), cysteine (C), leucine (L), or glycine (G) for R132 in IDH1, glutamine (Q) for R140 in IDH2, and G, lysine (K), serine (S), or threonine (T) for R172 in IDH2 (**Fig I6**). These replacements hinder the formation of the hydrogen bonds, reducing the enzyme affinities to isocitrate while increasing their affinity to NADPH [114]. Consequently, these mutations prevent the normal function of IDH1/2 in converting isocitrate to αkG and cause a conformational change, leading to the acquisition of a neomorphic enzymatic capacity. This capacity involves the reduction of αKG into the "oncometabolite" D-2-hydroxyglutarate (D-2HG), a process that consumes NADPH and generates $NADP^+$ [147, 148] (**Fig I9**). Of note, D-2HG has two

enantiomers, R-2HG and S-2HG, due to a chiral center at its second carbon atom. Under physiological conditions, both enantiomers are metabolic by-products generated by enzymes such as hydroxyacid-oxoacid transhydrogenase (HOT) or malate dehydrogenase. However, intracellular concentrations of D-2HG are typically maintained in the micromolar range by 2HG dehydrogenase (2HGDH), which converts D-2HG back to αKG. In contrast, the expression of mutant IDH1/2 enzymes can lead to increased levels of R-2HG, ranging from 1 to 30 mM in cells and their immediate surroundings [149].

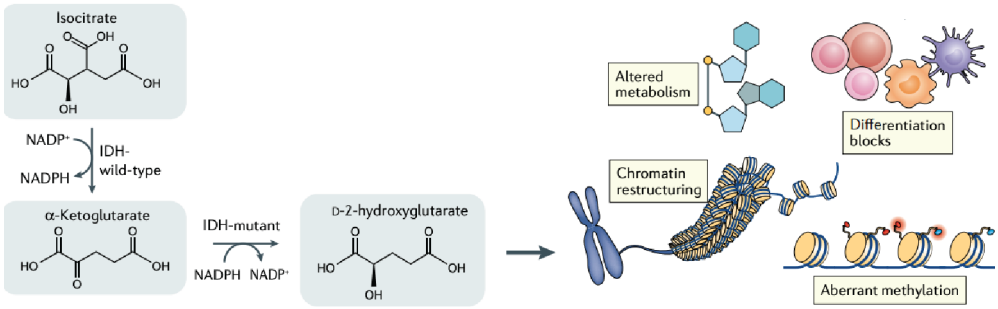

Figure I9. The function of mutant IDH enzymes in cancer. Both IDH1 (cytosol) and IDH2 (mitochondria) normally catalyze the oxidative decarboxylation of isocitrate to α-ketoglutarate; however, the hotspot mutations at R132 in IDH1 and R140 or R172 in IDH2 lead to neomorphic enzymatic activity that results in overproduction of D-2-hydroxyglutarate (D-2HG). This oncometabolite broadly affects cellular functions, including altered metabolism, aberrant DNA and histone methylation, and chromatin restructuring, blocking normal differentiation patterns. Image adapted from [114].

Mutant IDH enzymes cause a metabolic shift that impacts various processes they are involved in under physiological conditions, including the synthesis of fatty acids and the metabolism of glutamine (**Fig I7**). Moreover, R-2HG is structurally similar to αKG. For this reason, R-2HG can competitively inhibit the activity of αKG-dependent enzymes, particularly dioxygenases [150] (**Fig I7**). The inhibition of these enzymes can lead to alterations in various cellular pathways, including epigenetic regulation, chromatin structure, cell differentiation, and metabolism [151] (**Fig I9**).

The following section will address a detailed explanation of the effects of R-2HG and the altered levels of metabolic intermediates resulting from the neomorphic production of this oncometabolite by mutant IDH enzymes.

2.2.3. Role of mutant IDH in cancers

IDH mutations are considered driver events in tumorigenesis and are believed to have

dynamic and evolving roles in the tumor initiation and progression [114]. The current understanding of the pathogenic role of *IDH* mutations and the mutant IDH enzymes they produce have been extensively studied in glioma and AML. These studies have shed light on the underlying mechanisms of these diseases and have provided valuable insights into potential treatment options. Therefore, we will discuss the key findings obtained from these tumor types, focusing on three main areas: cell proliferation and differentiation, metabolism, and epigenetic regulation (**Fig I10**).

- Cell proliferation and differentiation

Several *in vitro* transformation assays have examined the impact of ectopic expression of mutant IDH in various primary and immortalized cells. Although the effect of mutant IDH on cell proliferation remains controversial [152-155], there is more consistent evidence indicating that mutant IDH impedes cell differentiation [91, 156, 157]. As a result, mutant IDH promotes the aberrant self-renewal of stem-like progenitor cells, creating a cellular state more permissive to malignant transformation. Nevertheless, it is worth noting that studies involving mice with controlled IDH^{mut} knock-in alleles in neural progenitors, hematopoietic or hepatic cells have shown that mutant IDH enzymes alone are insufficient to induce malignant transformation *in vivo*, suggesting that additional genetic events are required for this process [91, 158, 159]. Accordingly, the ectopic expression of mutant IDH1 enzyme in mouse liver is insufficient to induce CCA [91, 160]. However, co-expression of the mutant IDH1 (R132C) with the mutant KRAS (G12D) leads to the development of iCCA with high penetrance. Of note, in iCCA patients, mutations of *IDH1* and *KRAS* are mutually exclusive [17, 22]. Therefore, new mouse models that reflect these clinical observations are needed to understand better the role of mutant IDH in CCA carcinogenesis and progression.

- Metabolism

IDH proteins are critical metabolic enzymes, and the mutation of these proteins can lead to metabolic alteration in cancer cells. The neomorphic activity of mutant IDH1 reduces the availability of αKG and NADPH in $IDH1^{mut}$ glioma cells (**Fig I9** and **Fig I10**), which alters the levels of various metabolites, such as amino acids, glutathione metabolites, and TCA cycle intermediates [161].

In both IDH^{mut} glioma and AML, oncometabolite R-2HG produced by mutant IDH enzymes directly inhibits and epigenetically downregulates the αKG-dependent branched-chain amino acid transaminases 1 and 2 (BCAT1/2), which are responsible for the reversible

transamination of branched-chain α-ketoacids to the branched-chain amino acids such as valine, leucine, and isoleucine [162, 163] (**Fig I10**). This explains the altered amount of some amino acids found in *IDH*^{mut} cells. Moreover, mutant IDH enzymes have been shown to affect glutathione metabolism, which play a crucial role in protecting cells from reactive oxygen species (ROS) [164, 165] (**Fig I10**). This is because *IDH1*^{mut} cells consume rather than produce NADPH, which is needed to synthesize glutathione. The decreased glutathione level can lead to increased oxidative stress in glioma cells [166]. Accordingly, a metabolomic profiling study of 33 gliomas showed that levels of glutamine, glutamate, and αKG were substantially lower in *IDH*^{mut} as compared to *IDH*^{wt} tumors [167]. Another example of metabolism reprogramming found in *IDH*^{mut} glioma is the downregulation of the rate-limiting NAD^+ synthesis pathway enzyme nicotinate phosphoribosyltransferase (NAPRT1) [71, 168]. Therefore, *IDH*^{mut} cells adapt to a low NAD^+ pool, which becomes a targetable vulnerability in glioma.

The impact of *IDH* mutations on the metabolism of CCA is not well understood. However, *IDH* mutations have been suggested to cause disturbances in the citrate cycle, glutathione, and purine metabolism in iCCA [169] (**Fig I10**).

- Epigenetic regulation

IDH mutations are consistently associated with a hypermethylated phenotype across all *IDH*^{mut} cancers [12, 15, 170, 171] [157, 172]. The hypermethylated state is characterized by changes in DNA and histone demethylation.

First, mutant IDH enzymes produce R-2HG, which blocks the activity of TET enzymes by competing with αKG, an essential cofactor for TET demethylases (**Fig I10**). TET enzymes are responsible for converting 5mC to 5hmC, and their inhibition can result in a hypermethylated phenotype with high levels of 5mC, mainly within CpG islands (**Fig I8**) [15, 173-175]. Another mechanism contributing to hypermethylation is the inhibition of αKG-dependent Jmj domain-containing histone lysine-demethylases (Jmj-KDMs) by R-2HG [150] (**Fig I10**). The accumulation of histone methylation marks, such as H3K4me3 (associated with active transcription), H3K9me3, and H3K27me3 (linked to repressed chromatin), is frequently reported in the *IDH*^{mut} cancers [142, 156, 172].

The interplay between DNA and histone hypermethylation contributes to a repressed transcriptional landscape that limits epigenetic plasticity and leads to cellular differentiation blocks, contributing to the oncogenesis of *IDH*^{mut} AML, glioma, and CCA [91, 156, 157]. In

addition to affecting differentiation, epigenetic dysregulation of metabolic genes, [163, 168] [176], genes involved in DNA repair [177-180], and genes involved in immune response [181-183] are also found in *IDH*^{mut} cells (**Fig I10**).

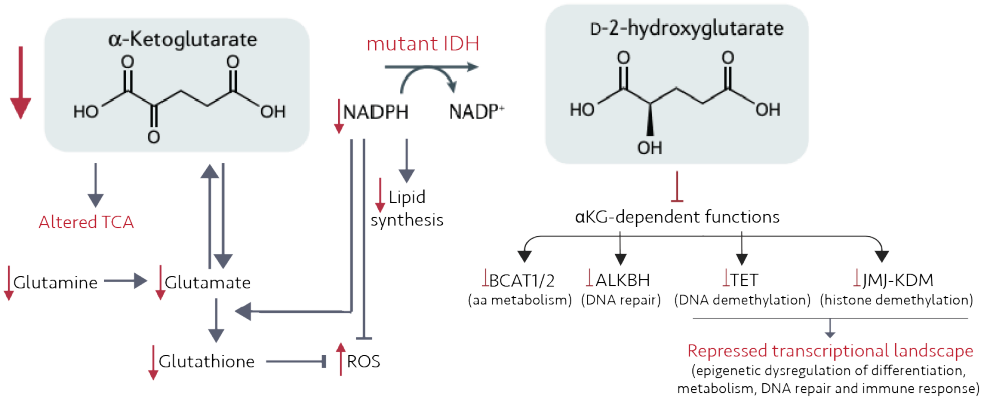

Figure I10. Schematic chart of mutant IDH roles in cancer.

Recent studies have shed light on the impact of *IDH* mutations on chromatin topology. Specifically, DNA hypermethylation induced by mutant IDH enzymes at CCCTC-binding factor (CTCF)-binding sites, which are responsible for preventing enhancer-promoter interactions, can lead to reduced binding of CTCF to DNA, thus compromising insulator function. As a result, a constitutive enhancer can aberrantly interact with the regulatory elements of an oncogene to induce and/or sustain its expression [184]. This newly discovered phenomenon adds an extra layer of transcriptional regulation through chromatin rewiring in *IDH*^{mut} cancers.

2.3. Development of mutant IDH1/2 inhibitors

IDH mutations are expressed exclusively in tumor cells, are prevalent in various types of cancer, and occur early in tumorigenesis. These features make *IDH* mutations appealing therapeutic targets. Consequently, designing small molecular inhibitors of mutant IDH enzymes has become an active area of research [114, 134]. The unique structural features of mutant IDH enzymes have eased the discovery of small-molecule inhibitors [185] that bind to the mutant IDH enzymes allosterically, thereby preventing the conformational switch required for the catalytic activity and stabilizing the mutant enzyme in an open inactive configuration.

Several mutant IDH inhibitors have been developed and tested in clinical settings (**Table I5**). These molecules showed favorable safety profiles and a robust reduction of R-2HG in both preclinical and clinical evaluations [59, 186-188]. However, the efficacy of these molecules found in preclinical models and cancer patients varies significantly among tumor types, with excellent treatment outcomes for hematological malignancies [189-191], moderate outcomes for CCAs [59], and minimal responses for gliomas and chondrosarcomas [188, 192-195].

Table I5. Mutant IDH inhibitors developed to date

Drug	Target	Clinical development status	Refs
Ivosidenib (AG-120)	Mutant IDH1	FDA approved for *IDH1*^{mut}: - relapsed or refractory AML, - locally advanced or metastatic CCA who have been previously treated, and - newly diagnosed adult AML patients (in combination with azacytidine or in monotherapy). Phase I clinical trials for *IDH1*^{mut} glioma or chondrosarcoma	[59, 191, 196-199]
Enasidenib (AG-221)	Mutant IDH2	FDA approved for *IDH2*^{mut} relapsed or refractory AML. Phase I/II clinical trials for *IDH2*^{mut} solid tumors.	[190, 200]
Vorasidenib (AG-881)	Mutant IDH1/2	Phase III clinical evaluation for *IDH1/2*^{mut} gliomas (INDIGO trial).	[188, 201]
BAY-1436032	Mutant IDH1	Phase I clinical trials for both advanced *IDH1*^{mut} solid tumors (glioma and iCCA) and AML	[192, 202, 203]
IDH305	Mutant IDH1	Phase I clinical trial for all *IDH1*^{mut} advanced tumors. It presents improved blood-brain barrier (BBB) penetration.	[204, 205]
DS-1001b	Mutant IDH1	Phase I clinical trial for *IDH1*^{mut} gliomas. It presents improved BBB penetration.	[194, 206]
Olutasidenib (FT-2102)	Mutant IDH1	FDA approved for *IDH1*^{mut} relapsed or refractory AML. Phase I/II clinical trials for advanced *IDH1*^{mut} solid tumors (glioma, chondrosarcoma, iCCA), alone or in combinatorial regimens.	[207-209]
LY3410738	Mutant IDH1/2	Phase I clinical trials for advanced *IDH1/2*^{mut} solid tumors (glioma, chondrosarcoma, iCCA) and AML. LY3410738 is regarded as "second-generation" inhibitor owing to its covalent mode of action and to its potency against secondary *IDH* mutations acquired at resistance to other mutant IDH inhibitors.	[210-212]

List of the mutant IDH inhibitors reported to date, their target molecule, and current clinical development stage.

Enasidenib, an inhibitor of mutant IDH2, decreases methylation and induces cell differentiation in both *in vitro* and *in vivo* models of AML [200]. It also reduced stem cell marker expression in advanced AML patients [191], associated with prolonged survival in preclinical models and a median OS of 9.3 months for relapsed/refractory AML patients. For those who attained complete remission (19.3%), the median OS was 19.7 months. As a result, the FDA has approved enasidenib for treating patients with *IDH2*^{mut} relapsed/ refractory AML [190]. Similarly, ivosidenib, an inhibitor of mutant IDH1, has also been approved by the FDA as a frontline treatment for advanced *IDH1*^{mut} AML patients with a median OS of 8.8 months and an overall response rate of 21.6% [191].

The phase III ClarIDHy trial has yielded positive results, leading to FDA approval of ivosidenib for patients with locally advanced or metastatic *IDH1*^{mut} CCA who have received prior treatment. In this trial, ivosidenib demonstrated good tolerance and improved PFS compared to placebo (median PFS of 2.7 months vs. 1.4 months, respectively). However,

it did not significantly improve the median OS of patients with chemotherapy-refractory *IDH1*^{mut} CCA [59].

3. DNA damage repair in CCA

Cells constantly face stresses that can damage their DNA, including endogenous factors, such as DNA replication, and exogenous factors, such as exposure to ultraviolet radiation [213]. To repair DNA damage and preserve genomic integrity, cells have an arsenal of repair proteins that engage the appropriate repair pathway. However, if the damage is irreparable, these proteins can induce cell cycle arrest and/or apoptosis. The collection of pathways that detect and repair DNA damage is referred to as the DNA damage response (DDR) [214]. Genes that encode the proteins involved in DDR are frequently mutated in cancer, leading to genomic instability, as discussed below.

3.1. DNA damage repair and cancer

Mutations in genes encoding enzymes involved in the DDR contribute to the ability of tumors to grow, metastasize, and respond to DNA-damaging treatments, such as chemotherapy or radiotherapy [215]. They have been identified in cancer cells and the germ lines of individuals with a hereditary predisposition to cancer [216]. Indeed, genome instability caused by DDR deficiencies is a hallmark of cancer [217]. However, the inherent genome instability of rapidly proliferating tumors also provides us with therapeutic opportunities to target DDR pathways and, thus, to specifically kill cancer cells. In the upcoming section, we will explain the common DDR pathways and discuss the potential of targeting DDR pathways in cancer treatment.

3.1.1. DNA damage repair pathways

The process of DDR begins with identifying the damaged area and activating the appropriate DNA repair pathways. The extent and nature of the damage determine which DNA repair mechanism and downstream signaling are used (**Fig I11**) [214].

During DNA replication, the wrong nucleotide can be incorporated, resulting in two mismatched bases. In this situation, the mismatch repair (MMR) pathway is activated (**Fig I11**).

The most common type of DNA damage is the lesion affecting only one strand of the DNA double helix, resulting in single-strand breaks (SSBs). SSBs are often recognized and repaired by the base excision repair (BER) or nucleotide excision repair (NER) pathways. Of note, these pathways rely on the enzymes Poly(ADP-ribose) polymerase 1 (PARP1) or PARP2 to recognize SSBs and catalyze the formation of poly (ADP-ribose) (PAR) chains. These chains allow for the recruitment of DDR factors to re-ligate the break (**Fig I11**).

DNA double-strand breaks (DSBs) are relatively more challenging to repair and pose a greater risk to the genome's integrity. Human cells have two main pathways for fixing DSBs. The first is the non-homologous end joining (NHEJ) pathway, which is responsible for repairing the majority of DSBs by re-ligating the broken ends. However, NHEJ is often considered "error-prone" because it does not use a homologous template for repair. Homologous recombination (HR) is the alternative pathway for repairing DSBs and is active during the S and G2 phases of the cell cycle. HR is also involved in replication forks that have stalled or collapsed. Unlike NHEJ, HR uses a homologous DNA molecule, typically the sister chromatid, as a template for the repair, thereby providing high-fidelity repair mechanisms [214, 215, 218] (**Fig I11**).

3.1.2. Targeting DDR pathways to treat cancer patients

In response to DNA damage, these main DDR routes operate under a complex dynamic network of overlapping signaling pathways that communicate with each other. Frequent occurrences of compromised DDR processes, resulting from defects in DDR genes, have been observed in tumor cells. Such defects create an ideal environment for the rapid accumulation of genetic aberrations, particularly in the context of high-rate cell division. Ultimately, this leads to genomic instability that can thrust cancer initiation and progression. The loss of a repair pathway can create a vulnerability that can be therapeutically exploited and enhance the efficacy of anticancer treatments. For instance, cancer cells may become highly reliant on an alternative repair pathway, which can be targeted by DDR-directed therapies (**Fig I11**). The most promising therapies developed to date primarily focus on DSBs, the most lethal type of DNA damage to cells [214], using the concept of synthetic lethality; here, the idea is that, in addition to the functional genetic defect in a DDR gene of one repair pathway, pharmacological inhibition of the compensatory DDR mechanism could be used to create an unmeasurable amount of genomic instability, mitotic catastrophe, and cell death.

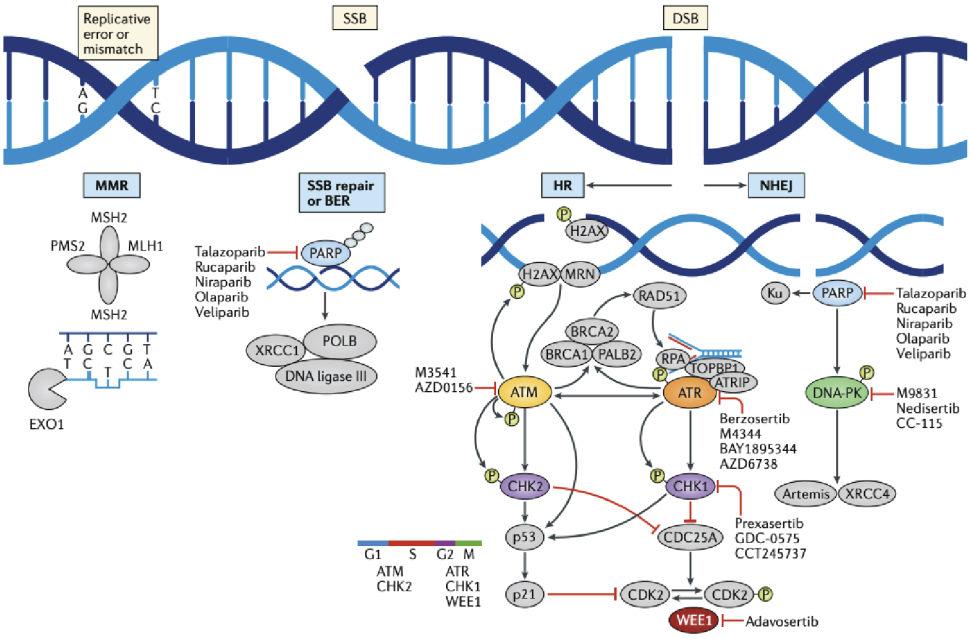

Figure I11. DNA damage response pathways. DDR pathways targeted in the clinic (MMR, BER, HR, and NHEJ) and their corresponding damage triggers (mismatch, SSB, or DSB). The DDR components targeted by the newly developed drugs are also indicated in color. Image from [214].

PARP inhibitors (PARPi) were the first class of drugs to be clinically approved for targeting DDR deficiency: they target essential components of the SSB and NHEJ repair pathways, the PARP proteins (**Fig I11**). PARPi exert their cytotoxic effects through two mechanisms: (1) they inhibit the enzymatic activity of PARP1/2 by blocking the cofactor NAD^+ binding site, and (2) they "trap" PARP1/2, preventing its release from the DNA-damaged site and leading to cell death in HR repair-deficient (HRD) cells, such as those with mutations in the central HR effectors BRCA1/2 (**Fig I12**) [219]. SSB and NHEJ repair become compensatory pathways to cope with DNA damage within an HRD cellular background; therebey, their pharmacological inhibition by PARPi constitutes an example of the already introduced synthetic lethality. Several PARPi have been developed, including olaparib, niraparib, rucaparib, talazoparib, and veliparib. These drugs differ mainly in their PARP trapping capacity [220]. While PARPi were initially approved for use in *BRCA1/2*^{mut} ovarian cancers, they have since been used in other types of cancers, such as breast cancer, pancreatic cancer, and prostate cancer [221].

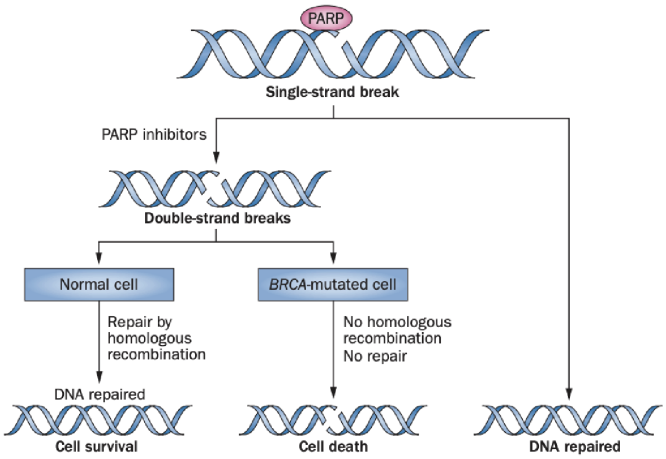

Figure I12. Synthetic lethality of PARPi in Homologous Recombination (HR) deficient tumors. PARP proteins bind to SSB in DNA and recruit other enzymes to repair the DNA damaged site. After inhibition of PARP activity, the DNA damage results in DSBs that cannot be adequately repaired in HRD tumors, such as tumors with *BRCA*^{mut}. This eventually leads to chromosomal instability, cell cycle arrest, and apoptosis. As DDR processes remain intact in noncancerous cells, PARPi are hypothesized to kill cancer cells selectively while sparing normal tissue. Image from [222].

Although *BRCA1/2* mutations are considered the iconic predictors of PARPi sensitivity, a substantial number of patients without these mutations benefit from PARPi monotherapy [223, 224]. To expand the potential benefit of PARPi beyond *BRCA* mutations, multiple studies have been conducted to identify additional molecular traits leading to HR deficiency. This led to the development of the concept of BRCAness, which reflects an HR deficiency phenotype in *BRCA* wild-type tumors [214]. To accurately predict the response to PARPi, diagnostic tests that measure complex "genomic scars" have been designed. In these tests, a genomic instability score can be calculated based on the combination of loss of heterozygosity (LOH), telomeric allelic imbalance (TAI), and large-scale state transitions (LST). While these genetic-based tests are effective in selecting eligible patients, they have limitations. They lack specificity in HR-altered tumors that have restored the HR function because they cannot capture the real-time functional status of the HR pathway. To address this limitation, a functional assay that measures the formation of RAD51 (the last effector of the HR pathway) foci in formalin-fixed paraffin-embedded tumor samples, has been established. This assay can serve as a surrogate for HR activity and has been shown to predict clinical PARPi response and resistance [225, 226]. Therefore, it has become a promising tool for routine practice in combination with genetic studies to select patients who may benefit from PARPi [215].

3.2. DNA damage repair in CCA

Around 25-30% of CCA cases harbor mutations in DDR genes, especially those DDR genes required for functional HR pathways (**Table I6**). As introduced in Section 3.1.2, tumors harboring HR gene mutations can be targeted using agents such as PARPi. Of note, preclinical studies suggest that CCAs with mutations in *ARID1A*, *BAP1,* and *ATM* are susceptible to PARPi [227]. Currently, no PARPi has been approved by the FDA for CCA treatment, but several are being investigated in clinical trials [218].

Table I6. Genes involved in homologous recombination found mutated in CCA

Gene	% in CCA	DDR role	Evidence for PARPi sensitivity	Refs
ARID1A	10-15 %	Chromatin remodeling in NHEJ and HR	Cell lines: ARID1A^{loss} shows PARPi sensitivity. Clinical: retrospective data from a clinical trial suggest that ARID1A^{loss} may result in PARPi resistance in breast and ovarian cancer.	[228-230]
ATM	3 %	Upstream in HR pathway, it phosphorylates and activates downstream HR effectors	Cell lines: ATM^{loss} colorectal lines are PARPi sensitive. Animal model: ATM^{loss} in prostate and pancreatic cancers is sensitive to the combination of PARPi and ATRi, but no effect is reported with PARPi alone. Clinical: phase III trial of olaparib plus paclitaxel in advanced gastric cancer did not show improved median OS in the olaparib arm for patients ATM null.	[231-234]
BAP1	8-10%	In HR repair, it regulates and recruits key downstream effectors, such as BRCA1 and RAD51	Cell lines: BAP1 null pancreatic cell lines were resistant to PARPi. No association could be drawn between *BAP1* mutational status and PARPi sensitivity in malignant pleural mesothelioma (MPM). Clinical: rucaparib in patients with BAP1^{loss} recurrent mesothelioma had early signs of efficacy. CCA case report: a patient with refractory metastatic CCA with novel *BAP1* mutation had a good, prolonged response to Olaparib.	[235-238]
BRCA1/2	2-4%	BRCA1 promotes HR over NHEJ by recruiting effectors BRCA2 and RAD51	Clinical: highly robust evidence in phase III trials with PARPi for prostate, breast, ovarian and pancreatic tumors that led to FDA approval. Very limited data in CCA, one multicenter retrospective study that reported clinical benefit upon PARPi treatment in 3 out of 4 cases of *BRCA1/2*^{mut} CCA previously treated with platinum, obtaining a 3-fold increased OS compared to standard-of-care treatment.	[239]

Genes involved in the HR pathway, their relative mutational frequencies in CCA (extracted from the COSMIC/TCGA database), and a summary of evidence to support PARPi sensitivity when mutated.

3.3. Potential role of *IDH* mutations in DNA damage repair in CCA

Numerous authors have proposed a direct connection between *IDH* mutations and DNA damage repair. To define the specific role of *IDH* mutations in DDR pathways, we have conducted a literature review to compile publications that explore this area.

Indeed, most of these studies suggest that R-2HG has a negative impact on DDR, especially the HR pathway, implying that tumors with *IDH* mutations are associated with the BRCAness phenotype (**Table I7**). These studies found that *IDH*^{mut} tumors respond better to various DNA-damaging agents due to compromised DSB repair, specifically through HR.

Four studies that tested PARPi efficacy reported positive outcomes in preclinical research models [178, 179, 240-242].

Table I7. Publications supporting a detrimental effect of *IDH* mutations on DDR.

Tumor	Research model	*IDH* mutation mechanism	DDR effect	Refs
Glioma	Cell lines, infected with *IDH1*^{wt} or *IDH1*^{R132H}	R-2HG competitive inhibition of αKG-dependent alkB homolog (ALKBH)2/3 DNA repair enzymes	Decreased repair of alkylating DNA adducts generated by chemotherapeutic agents and, consequently, increased sensitivity to these agents.	[243-245]
AML	Mouse model with conditional knock-in *IDH1*^{R132H} in cells of the myeloid lineage	Downregulation of ATM via R-2HG competitive inhibition of αKG-dependent histone demethylases leading to H3K9/H3K27/H3K36 hypermethylation.	Decreased DNA damage repair capacity and increased sensitivity to daunorubicin and irradiation (IR).	[177]
Glioma	Cell lines, infected with *IDH1*^{wt} or *IDH1*$^{R132H/R132C}$	NAD^+ deprivation (detailed in section 2.2.4)	Impaired PARP1-mediated Base Excision Repair (BER) leading to increased sensitivity to temozolomide (TMZ) alone and in combination with PARPi.	[246]
Glioma, AML, CCA	Cell lines from glioma, CCA, fibrosarcoma, colon and kidney cancers, with endogenous, overexpressed or knock-in *IDH1/2*^{mut}. Primary glioma and AML cells	R-2HG competitive inhibition of αKG-dependent KDM4B, resulting in aberrant H3K9 hypermethylation at loci surrounding DNA breaks and impeding recruitment of HR machinery	Impaired HR, accompanied by a selective **sensitivity to PARPi**	[178, 179]
AML	Primary human cells with endogenous *IDH1/2*^{mut}	Downregulation of ATM driven by R-2HG	Increased DNA damage and **sensitivity to PARPi,** IR and daunorubicin	[240]
Glioma, CCA	Cell lines with endogenous and exogenous *IDH1*^{R132H}, and mouse model obtained by intracranial injection of virus carrying PDGFA, shTP53 and *IDH1*^{R132H}	NA	Increased DNA damage, decreased DSB repair capacity and **improved sensitivity to PARPi,** radiation, and their combination	[241]
AML	PDXs	The authors propose the same mechanism as in Sulkowski et al., 2020	**Increased sensitivity to PARPi**	[242]

List of publications advocating a negative impact on DDR of *IDH* mutations, including the tumor type studied, the research model used, and the *IDH* mutation mechanism of action for the subsequent effect on DDR. Abbreviation: NA, non-assessed.

The primary mechanism proposed to explain PARPi sensitivity in *IDH*^{mut} tumors is the competitive inhibition of the αkG-dependent lysine demethylase KDM4B by R-2HG, resulting in aberrant hypermethylation of H3K9 at loci surrounding DNA breaks [179]. This masks a local H3K9 trimethylation signal that is critical for the proper recruitment of TIP60 and ATM, two key HR factors (**Fig I13**). Alternatively, epigenetically repressed ATM expression has also been reported [240].

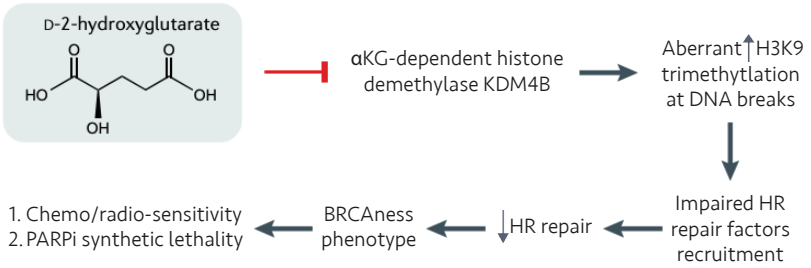

Figure I13. Proposed mechanism of 2-HG-induced BRCAness phenotype and subsequent PARPi synthetic lethality. Flow chart based on [178, 179].

However, other studies have demonstrated opposite effects (**Table I8**). In fact, several studies also pointed out an association between *IDH* mutations and improved DDR machinery (**Table I8**).

Table I8. Publications supporting a beneficial effect of *IDH* mutations on DDR.

Tumor type	Research model	*IDH* mutation mechanism	DDR effect	Refs
Glioma	Cell lines, infected with *IDH1*^{wt} or *IDH1*^{R132H}	NA	Increased RAD51-mediated HR and, as a result, enhanced resistance to TMZ	[247]
Glioma	Mouse model with *IDH1*^{R132H}, in the context of *ATRX* and *TP53* loss	R-2HG inhibition of histone demethylation, leading to enrichment of the activation mark H3K4me3 in genomic regions associated with DDR.	Increased signaling of several DDR pathways, mainly MMR and DSB repair via HR, conferring *in vitro* and *in vivo* radioresistance	[180]
Chondro-sarcoma	Cell lines with endogenous *IDH1/2*^{mut}	NA	Intact HR and PARPi sensitivity irrespective of *IDH* mutation	[248]

List of publications advocating a positive impact on DDR of *IDH* mutations, including the tumor type studied, the research model used, and the *IDH* mutation mechanism of action for the subsequent effect on DDR. Abbreviation: NA, non-assessed.

Of note, most of these studies have been conducted using glioma and AML preclinical models. Whether mutant IDH enzymes have an impact on the HR pathway in CCA is still unknown. Olaparib is currently being tested, alone as well as in combination with AZD6738 (an ATR inhibitor) or durvalumab, in patients with *IDH1/2*^{mut} solid tumors, including advanced glioma and CCA [NCT03212274, NCT03878095, NCT03991832] [249].

4. The immunology of CCA

Tumor immunology studies the interactions between the immune system and tumor cells. It has been well-recognized for over a century that the immune system plays a crucial role in tumor development and progression [250]. The immune system can detect and eliminate most tumors, but some can evade detection. Immune evasion is now considered one of the eight hallmarks of cancer [217]. In 2018, the Nobel Prize was awarded jointly to James P. Allison and Tasuku Honjo for discovering the immune checkpoint proteins cytotoxic T-lymphocyte-associated antigen-4 (CTLA-4) and PD-1, which are used by cancer cells to evade the immune system [251], highlighting the importance of this feature of tumors.

In this section, we will begin by covering the basic principles of tumor immunology. We will then delve into the latest developments in immunology research related to CCA. Lastly, we will explore the possible impact of *IDH* mutations on immune-oncology.

4.1. T cells at the center stage of the tumor immunology

4.1.1. Cancer cells can be recognized by T cells

Cancer immunosurveillance is primarily carried out by lymphocytes, including T, B, and natural killer T (NKT) cells. However, T cells are particularly important in mediating the immune response against cancer cells [252], and these cells have become a primary focus of cancer immunotherapy research.

T lymphocytes can recognize, through their T cell receptors (TCR), specific peptides bound to the major histocompatibility complex (MHC), also known as human leukocyte antigen (HLA), on the surface of target cells [253]. The peptides that T cells recognize are known as "epitopes," while their parent proteins are "antigens." In the context of cancer, these proteins are also known as tumor antigens.

T cells can be divided into two major classes based on the expression of the cluster of differentiation (CD) markers CD8 and CD4. These two types of T cells have different effector functions and recognize cognate epitopes in different ways [254]. $CD8^+$ effector T cells specialize in killing cells that they specifically recognize; they bind to peptides from digested cytoplasmic proteins and are presented on the cell surface through HLA-I molecules. In contrast, $CD4^+$ helper T cells activate other immune cells and recognize peptides from

extracellular proteins presented on the cell surface of antigen-presenting cells (APCs) via HLA-II molecules. This mechanism allows cancer cells to be effectively killed in an antigen-specific manner by $CD8^+$ T cells, since almost all nucleated cells express HLA-I. Therefore, T cells, and specifically $CD8^+$ T cells, are crucial to cancer immunosurveillance.

4.1.2. Cancer immunity cycle

The process of developing an immune response against cancer, which leads to effectively killing tumor cells, is known as the cancer immunity cycle (**Fig I14**) [255].

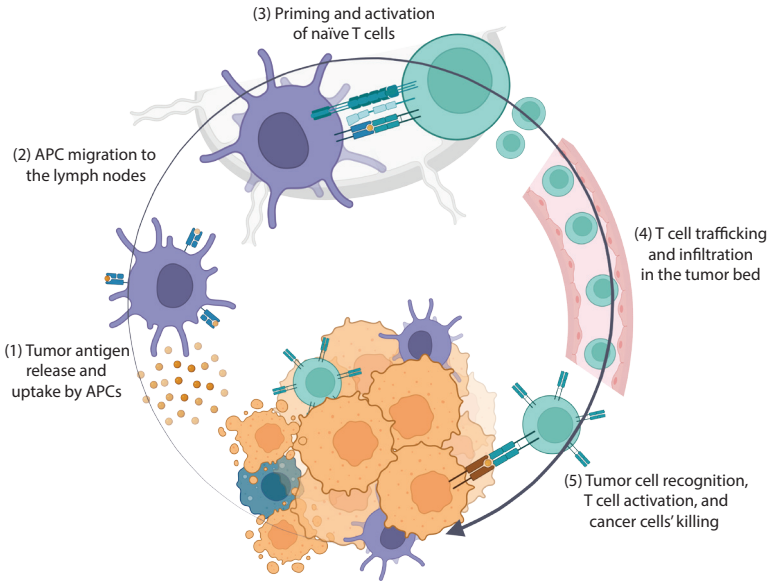

Figure I14. Cancer immunity cycle. (1) The first step involves the release of tumor antigens captured by APCs and subsequently processed and cross-presented on HLA-I. **(2)** Next, these APCs migrate to lymph nodes, **(3)** where they interact with naïve T cells, resulting in their priming and activation. The stimulated T cells proliferate and differentiate into effector T cells that recognize tumor-specific antigens. **(4)** Effector T cells leave the lymph nodes and migrate to the tumor, where they infiltrate into the tumor bed if given the appropriate conditions. **(5)** T cells specifically recognize their cognate tumor antigen presented on the HLA-I molecule of tumor cells, become activated, and kill the tumor cells. This leads to the release of additional tumor antigens that increase the breadth and depth of the response in subsequent rounds of the cycle. Adapted from [255]. Image created with BioRender.com.

The cancer immunity cycle involves several immune cell types, not only T cells. The cycle begins with the release of tumor antigens by tumor cells that are captured and processed by APCs, mainly dendritic cells (DCs) (**Fig I14**, step1). The APCs then migrate to lymph nodes (**Fig I14**, step2), where they interact with naïve T cells, resulting in the priming and activation of effector T cells that will be trained to respond to cancer-specific antigens (**Fig I14**, step3).

In this process, DCs that have internalized tumor antigens cross-present such peptides on HLA-I molecules to prime naïve $CD8^+$ T cells [256]. Moreover, efficient priming of T cells requires the presentation of tumor antigens to be accompanied by co-stimulatory signals exerted by the same APCs. After being primed and activated, T cells subsequently traffic through the blood vessels to the tumor bed (**Fig I14**, step4). If the tumor microenvironment conditions are favorable, such as with appropriate tumor vascularity, the abundance of specific T cell homing chemokines/cytokines, and adequate growth factor signals, T cells infiltrate the tumor and mediate tumor cell killing after specifically recognizing their cognate antigen presented on tumor cells via the highly specific HLA-TCR interaction. Importantly, for full T-cell activation, three signals must happen in sequence (**Fig I4**, step5, and **Fig I15**): signal 1) binding of tumor antigen by T cells through HLA-TCR interaction; signal 2) co-stimulation through the binding of costimulatory molecules; and finally, signal 3) cytokine secretion that directly prompts T cell differentiation, expansion, and cytotoxic capacity, ultimately leading to killing of the tumor cells [257, 258]. Through this process, additional tumor antigens can be released, known as antigen spreading, which increases the breadth and depth of the response in subsequent rounds of the cycle (**Fig I4**).

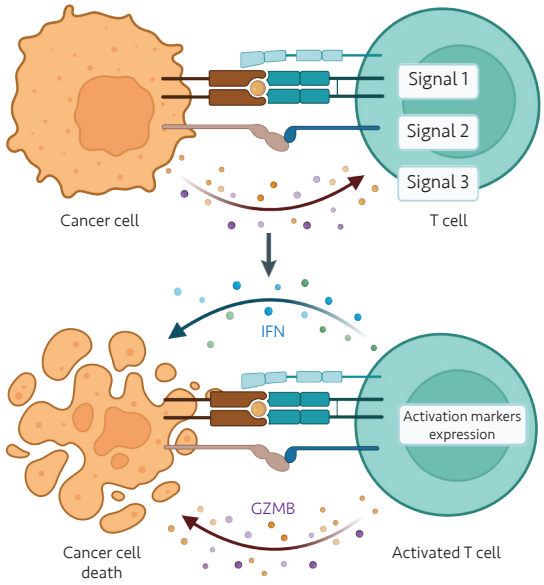

Figure I15. Antigen-specific full T-cell activation. Signal 1 involves the recognition and binding of the tumor antigen by T cells through HLA-TCR interaction; signal 2 follows with a co-stimulation signal through the binding of costimulatory molecules, and finally, signal 3 encompasses the instructive cytokine milieu. The sequential presence of these three signals stimulates T cell activation, expansion, and cytotoxicity, by increasing the expression of specific markers and secreting cytotoxic factors, such as granzyme B (GZMB) and interferons (IFN).

4.1.3. Consequences of cancer immunity cycle dysfunction

Dysregulation of the cancer immunity cycle can lead to the formation of a tumor mass and can be influenced by various factors that facilitate the evasion of tumor cells from the surveillance of immune cells, including factors that affect the effectiveness of T cell priming, infiltration, and effector function [255]. Moreover, T cell homing and function can be impaired by the production of soluble factors that modulate the TME, the transcriptional downregulation of the antigen-presenting machinery or the immune signaling cascade, as well as the local expression of inhibitory molecules by tumor cells [259].

Communication between cells within a tumor affects the behavior of T cells and determines the range of "immune phenotypes" at the tumor site. This, in turn, affects the effectiveness of anti-tumor T cell responses, with higher infiltration of tumor lymphocytes indicating a better prognosis [260]. A consensus has been recently achieved in the scientific community for classifying tumors based on their immune profile [261, 262]. The method calculates the immunoscore of each tumor by quantifying the densities of $CD3^+$ and $CD8^+$ T cells within the tumoral area and its invasive margin and, accordingly, assigns each tumor into one of these four categories [263] (**Fig I16**):

(1) Inflamed, hot tumors (high immunoscore), with a high degree of T cells and cytotoxic T cell infiltration and activation.

(2) Non-inflamed, cold tumors (low immunoscore), with the absence of T cells in the tumor or at the tumor edges. The host immune system cannot effectively mount a T cell–mediated immune response.

(3) Altered tumors (intermediate immunoscore), can follow two distinct patterns:

- **Immunosuppressed** show poor, albeit not absent, T cell and cytotoxic T cell infiltration, but with signs of impaired activation and capacity to expand.
- **Excluded** present no T cell infiltration within the tumor site and accumulated T cells at tumor borders (invasive margin).

Representative images of the aforementioned categorization, with the associated immunoscores for each immune phenotype and the principal characteristics, are depicted below (**Fig I16**).

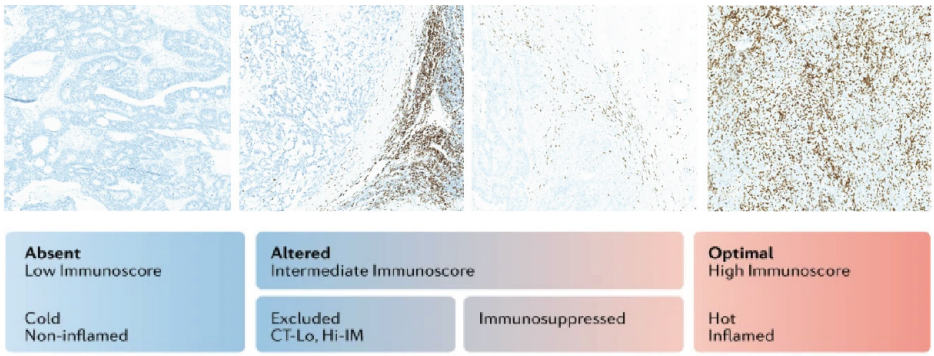

Figure I16. An illustrative example of hot, altered, and cold immune tumors. Brown staining represents $CD3^+$ T cells, and blue counterstaining provides tissue background staining. The level and spatial distribution of T cell infiltration differentiates four distinct solid tumor phenotypes: hot (or inflamed); altered, which can be excluded or immunosuppressed; and cold (or non-inflamed). These tumor phenotypes are characterized by high, intermediate, and low immunoscore, respectively. Of note, in altered-excluded tumors, T cell infiltrates are low at the tumor center and high at the invasive margin. Altered-immunosuppressed tumors display instead a more uniform pattern of (low) T cell infiltration. CT, the center of the tumor; Hi, high; IM, invasive margin; Lo, low. Adapted from [263].

4.1.4. Immuno-oncology treatment

The field of oncology research has been revolutionized by immune-oncology treatments, which have seen remarkable success in clinical settings [255, 264]. Traditionally, cancer treatments have focused on attacking cancer cells directly. However, immune-oncology therapies take a different approach by using drugs that target the patient´s immune system, allowing it to recognize and attack cancer cells more effectively. There are different modalities of cancer immunotherapies (**Fig I17**), most of which rely on T cells and their capacity for antigen-directed cytotoxicity [265]. Thus, immunotherapies can be divided into two groups, depending on if they aim to 1) reinvigorate the naturally occurring anti-tumor immune response (i.e., interleukin-2 [IL-2], immune checkpoint inhibitors and co-stimulatory agonists, bi-specific antibodies or adoptive cell transfer (ACT) with tumor infiltrating lymphocytes (TILs)), or 2) generate *de novo* T cell responses (i.e., ACT with chimeric antigen receptor (CAR) or TCR-engineered T cells and vaccines).

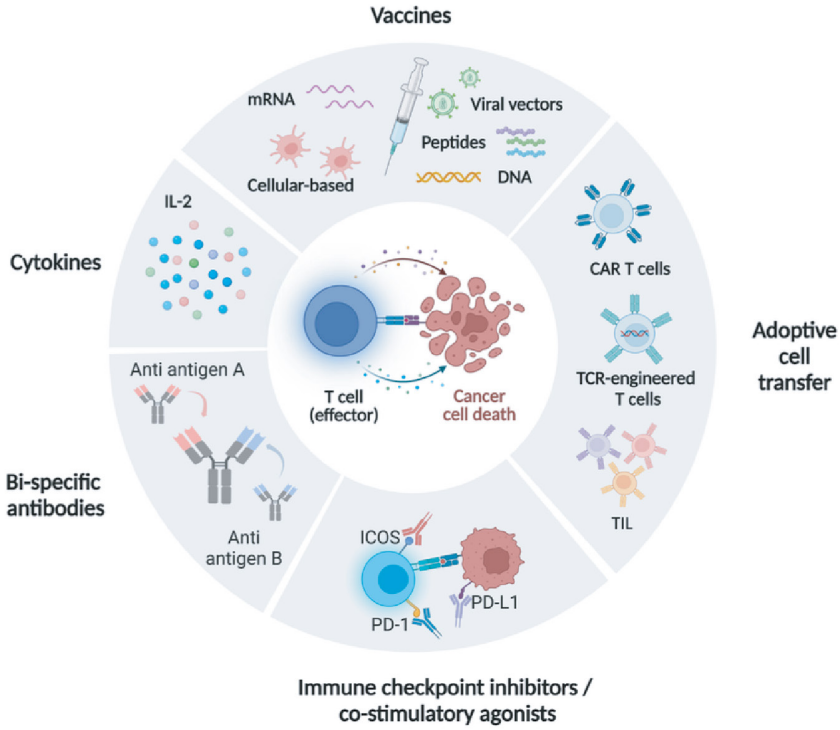

Figure I17 Cancer immunotherapies. Schematic overview of the different modalities of cancer immunotherapies developed to mobilize the immune system to kill cancer cells. Most of these strategies are focused on T lymphocytes and their ability of antigen-directed cytotoxicity and can either aim at reinvigorating naturally occurring tumor-reactive T cells or generating *de novo* T cell responses. Image created with BioRender.com.

One common approach is the use of immune checkpoint inhibitors (ICIs), which block immune checkpoints used by cancer cells to evade the immune system. Briefly, upon TCR engagement, T cells become activated, proliferate and start expressing inhibitory molecules to attenuate T cell activation and prevent an unduly prolonged T cell response that could potentially damage healthy cells (signals 1 and 2, respectively, in **Fig I15**). The continuous expression of these inhibitory molecules leads T cells into a dysfunctional state [266]. These molecules are known as immune checkpoint receptors, and tumors strategically modulate their expression to shut down surrounding T cells and impede immune surveillance. ICIs are designed to interrupt these inhibitory signals of T cell activation to reinvigorate the anti-tumor immune response. Since many immune checkpoints are initiated by ligand-receptor interactions, they can be blocked by antibodies. This is the case of the two most widely therapeutically exploited checkpoints, CTLA-4 and PD-1 [265].

Another approach is adoptive cell therapy (ACT), which involves the isolation and *ex vivo* expansion of T cells up to high numbers, followed by their infusion back into the patients [267]. The efficacy of this therapy relies on the ability of the infused T cell product to recognize and kill cancer cells specifically. This therapy has the advantage of releasing T cells from the immunosuppressive TME [268]. Nevertheless, the highly personalized character of the technique (T cell products are prepared for each individual), hinders its broad applicability. ACT can be performed using autologous infiltrating T cells (TILs), TCR-engineered T cells (i.e., autologous T cells genetically modified to express a specific TCR capable of recognizing the tumor), and CAR-engineered T cells (i.e., autologous T cells genetically modified to express a synthetic chimeric antigen receptor (CAR) able to recognize the tumor in an HLA-independent manner) [267].

Finally, tumor cell bispecific antibodies (TCBs) are a type of immunotherapy that utilizes engineered antibodies with dual specificity that can simultaneously bind to tumor cells and immune cells, constituting a bridge between the two cell populations and facilitating tumor cell killing by redirected immune cells [269]. Thus far, the cancer immunotherapy field has been dominated by T cell-engaging bi-specific antibodies (T-biAbs), focused on activating the T cells [270]. The majority of T-biAbs use an anti-CD3 antibody fragment as a T cell engaging arm, which triggers the activation of the signaling cascade of the TCR complex and mediates the formation of an immunologic synapse, thereby promoting tumor cell lysis [270]. This represents an advantage over ICIs, since it circumvents the HLA restriction of the TCR [269].

4.2. Immunology of CCA

4.2.1. Immuno-oncology in CCA

The approval of ICIs for solid tumors with dMMR brought the first approved immunotherapy for CCA [63, 271]. The deficiency in MMR proteins and its phenotype of MSI-H result in the accumulation of numerous somatic mutations in tumors, making them more immunogenic and leading to improved responses to the immunotherapy [272]. However, dMMR and MSI-H are rare in biliary cancers, occurring in fewer than 3% of CCAs [273]. Despite this, dMMR and MSI-H CCAs demonstrate substantially higher response rates to immune checkpoint inhibition. In a cohort of patients with solid tumors harboring

MSI-H or dMMR and treated with pembrolizumab as monotherapy, nine of 22 patients with CCA (40.9%) experienced durable objective responses, with a striking median OS of 24.3 months [63]. Based on this robust efficacy, MSI or MMR status testing is recommended in patients with advanced CCA.

Notably, the TOPAZ-1 and KEYNOTE-966 trials have demonstrated some success in using ICIs to treat advanced CCA, even in first-line treatment settings and in patients without a specific biomarker [53, 54]. In these trials, the standard-of-care first-line chemotherapy regimen of GemCis was combined with durvalumab (anti-PD-L1) or pembrolizumab (anti-PD-1). Of note, while there was a reported clinical benefit, it is worth noting that the durvalumab- or pembrolizumab-treated groups only showed a modest increase in the median OS as compared to the placebo group (12.8 vs. 11.5 months, and 12.7 vs. 10.9 months, respectively). This suggests that further improvement of the therapeutic effects of these drugs will be required. As such, studies are now focusing on understanding the complex interactions between the CCA tumor cells and the immune microenvironment to develop more effective immune-oncology strategies.

4.2.2. The immune microenvironment of CCA

Although CCA has a low tumor mutational burden, it contains a substantial number of immune cells [41, 274]. However, studies suggested that communication between CCA cells and the TME seems to create and maintain an immunosuppressive environment in most CCA patients [275, 276]. For example, CCA is enriched in suppressive PD-L1$^+$ tumor-associated macrophages (TAMs), while tumor cells show little to no expression of PD-L1 [277]. In addition, TAMs seem to work in close collaboration with CAFs to recruit myeloid-derived suppressor cells (MDSCs), further promoting an immunosuppression phenotype [277]. Tumor-associated neutrophils (TANs) are another immune cell population abundant in CCAs. In eCCAs, TANs have a negative correlation with CD8$^+$ T cells and a positive association with FOXP3$^+$ Treg cells, which is associated with poor outcomes [278]. Similarly, iCCA has a high FOXP3$^+$:CD8$^+$ ratio that is correlated with poor survival [279]. Taken together, these findings highlight the immunosuppressive phenotype in CCA.

The heterogeneity of CCAs is not limited to the genetic and epigenetic levels but also extends to immune phenotypes [280-284], with marked differences in the number, composition, and state of infiltrating immune cells [280, 281, 284]. Several studies have

identified molecular subtypes based on immune profiles, suggesting that these variances might reflect the intrinsic heterogeneity in tumor cell biology, prognostic values, and therapy outcomes [280-284]. Job and colleagues combined gene expression data from the tumor and TME compartments and quantified cell population abundances by immunohistochemistry of 566 iCCA samples. Their analyses identified four TME-based molecular subtypes: I1 (immune desert), I2 (immune activation), I3 (myeloid-enrich), and I4 (mesenchymal-like) [280]. These immune phenotypes correlate levels of immune infiltration with activation of immune-checkpoint-related pathways and patient outcome, providing an immune-based approach for patient stratification and identifying potentially actionable targets for immunotherapy. Similarly, Chen and colleagues established a direct correlation between immune cell infiltration, the proximity of tumor-immune cell interactions, transcriptomic regulation of IFN signatures, and gene promoter DNA methylation [285]. Nonetheless, a deeper comprehension of the intricate TME of CCA is necessary to better classify the patients according to their immune profiles, to assist in determining the most suitable immunotherapy treatment, and to design new immune-oncology treatments.

4.3. *IDH* mutations involvement in tumor immunology

Recent studies suggest that mutant IDH1 plays a crucial role in shaping the tumor immune landscape, which opens up new possibilities for immune-based therapies that target mutant IDH1 [183, 284, 286]. Strikingly, an extensive analysis of human pan-cancer transcriptomic data found a notable association between *IDH1* mutations and gene signatures that suggest reduced leukocyte levels [286]. This correlation was further supported by transcriptomic analysis of human iCCA tumors [280, 284, 287], and it was validated at the protein level through quantitative histologic analysis [288]. However, a study examining immunohistochemical data of 96 human CCAs did not establish a correlation between *IDH1* mutation status and immunological features, and that was also the case in work done by Job et al. [280], indicating the need for more research to determine the immune phenotypes linked to mutant IDH1 [289].

In glioma, $IDH1^{mut}$ tumors are characterized as immunologically "cold" tumors as compared to $IDH1^{wt}$, with a prominent reduction of $CD8^+$ T cell number and a T cell compartment with lower expression of gene signatures reflecting T cell cytotoxicity, interferon response, and cellular stress programs [183, 290-294]. Mechanistically, DNA

hypermethylation leading to epigenetic silencing of certain immune-related factors has been suggested as a potential explanation for the observed immunosuppressed phenotype [181, 182, 291, 295]. Alternatively, T cell mitochondrial respiration impairment or macrophage-altered metabolism have been attributed to paracrine effects of secreted R-2HG uptaken by these immune cell populations [293, 296]

Collectively, the evidence indicates that *IDH* mutations might play a crucial role in tumor immunology, which could result in a wide range of therapeutic immune-oncology options for this particular group of patients.

Objectives

Cholangiocarcinoma (CCA) is a rare aggressive cancer with limited therapeutic options and a dismal prognosis. Although advanced CCA is the most common scenario in the clinic, most available research models are built upon primary CCA surgeries. Thus, there is an urgent need to develop models focused on advanced CCA to improve the biological knowledge of this tumor stage and make representative drug efficacy testing platforms available.

Recent advances in tumor genomic profiling have uncovered *IDH1* mutations as the most common alteration in intrahepatic CCA (iCCA). This discovery has created an opportunity for innovative therapeutic strategies to target the mutant enzyme generated by these mutations. Ivosidenib, a targeted inhibitor of mutant IDH1 enzyme, showed a meaningful clinical benefit for CCA patients, which led to its FDA approval for *IDH1*^{mut} advanced CCA that has progressed to chemotherapy. However, the increase in median progression-free survival (PFS) was modest, indicating the need for new strategies to improve drug efficacy and achieve more durable responses. Additionally, several studies suggest that preclinical models of glioma and AML with *IDH* mutations harbor a deficient homologous recombination (HRD) phenotype and, thus, an increased sensitivity to poly (ADP-ribose) polymerase inhibition (PARPi). However, it is noteworthy that, while the mechanism of action for *IDH* mutations has been deeply studied in other tumor types, their role(s) in CCA oncogenesis and progression are not fully understood.

Therefore, the **overall goal** of this thesis is:

To create accurate research models for unresectable metastatic CCA and use them to understand the cancer-causing abilities of *IDH1* mutation at this disease stage. This will help identify ways to improve treatment for advanced CCA.

The **specific objectives** are:

1. Generate and characterize a patient-derived xenograft (PDX) collection from biopsies of patients with advanced metastatic CCA.

2. Evaluate PARP inhibition efficacy in advanced CCA_PDXs and identify biomarkers of response to the studied treatment.

3. Study the role of *IDH1* mutation in CCA by an in-depth transcriptomic and DNA methylation characterization of *IDH1*^{mut} CCA_PDXs.

4. Propose and validate novel therapeutic strategies for *IDH1*^{mut} CCA patients based on identified vulnerabilities from objective 3.

Materials and methods

Human specimens

CCA metastatic lesions (~1–2 cm long, ~1–2 mm diameter) were obtained by ultrasound-guided core needle biopsy, and one primary tumor sample was obtained during surgery. All procedures were performed in the Vall d'Hebron Hospital with informed written consent from patients. The studies were conducted in accordance with the Declaration of Helsinki. Human samples were handled and processed following the institutional guidelines under protocols approved by the Institutional Review Boards (IRBs) at the Vall d'Hebron Hospital prior to tissue acquisition. Each tumor biopsy specimen was divided into two parts: i) formalin-fixed paraffin embedding (FFPE) and ii) subcutaneous implantation into NOD.CB-17-Prkdc scid/Rj mice (Janvier Labs, RRID:MGI:3760616) for CCA_PDX generation. CCA diagnosis on biopsied samples was confirmed by histopathologic assessment.

Generation of CCA_PDXs

Tumor pieces (15- to 60-mm^3) from patient metastatic lesions (except one from the primary tumor) were obtained from biopsy and immediately subcutaneously implanted into 6-week-old female NOD.CB-17-Prkdc scid/Rj mice (Janvier Labs, RRID:MGI:3760616). Animals were housed in air-filtered flow cabinets with a 12:12 light/dark cycle, and food and water were provided *ad libitum*. Upon growth of the engrafted tumors, a tumor piece was implanted into a new recipient mouse for the model perpetuation. Flash-frozen and FFPE samples were taken for genotyping and histological studies in each passage. The presented collection of CCA_PDX is a part of the EuroPDX consortium (http://www.europdx.eu). All animal procedures were approved by the Ethical Committee for the Use of Experimental Animals at the Vall d'Hebron Institute of Research (VHIR) and by the Catalan Government.

Immunohistochemistry (IHC) and image analysis

CCA_PDX and patient tumors were fixed immediately after excision in 4% buffered formalin solution for a maximum of 24 h at room temperature before being dehydrated, paraffin-embedded, and cut into sections of 3-µm thickness. The following primary monoclonal antibodies were used for IHC staining: anti-KRT19 (Atlas Antibodies Cat# HPA002465, RRID:AB_1079179), anti-HepPar1 (Novus Cat# NBP3-08970, RRID:AB_2909615), anti-ARID1A (Sigma-Aldrich Cat# HPA005456, RRID:AB_1078205), anti-BAP1 (Abcam Cat# ab255611 [EPR22826-65]), anti-Ki67 (Roche Cat# 05278384001, RRID:AB_2631262), anti-cleaved caspase3 (Asp175) (Cell Signaling Technology Cat# 9661, RRID:AB_2341188) and secondary anti-rabbit (Jackson ImmunoResearch Labs Cat# 711-035-152, RRID:AB_10015282) and anti-mouse (Thermo Fisher Scientific Cat# G-21040, RRID:AB_2536527), and UltraMap anti-Rabbit antibody (HRP) (Roche Cat# 05269717001, PRID:AB_2924783). For KRT19, HepPar1 and BAP1 IHC, tissue

sections were heated to 60°C, deparaffinized with xylene (Panreac Cat# 131769.1612), and hydrated with three steps of incubation with ethanol (from 100%, 96%, and 70%). For antigen retrieval, samples were boiled for 7 min in citrate buffer (Merck Cat# 1064480500) at pH 6 for KRT19 staining or at pH 9 for HepPar1 staining; while the procedure was performed for 20 min in Tris-EDTA-0.05% Tween (10mM Tris Base, 1mM EDTA solution) at pH 9 for BAP1. Endogenous peroxidase was blocked by incubating the samples with 3% peroxide hydrogen (#108597, Merck Millipore) diluted in 1× phosphate-buffered saline (PBS) for 10 min. Slides were permeabilized for 15 min in PBS with 1%Tween (A4974,0500, Panreac) and blocked with 3% BSA in 1× PBS for 1 h; samples were then incubated overnight at 4ºC, with the primary antibody anti-KRT19 (Atlas Antibodies Cat# HPA002465, RRID:AB_1079179) diluted 1:200, with anti-HepPar1 (Novus Cat# NBP3-08970, RRID:AB_2909615) diluted 1:500, or with anti-BAP1 (AbCam Cat# ab255611 [EPR22826-65]) diluted 1:100, in blocking buffer and then incubated at room temperature for 1 h with anti-rabbit or anti-mouse secondary antibody (ThermoFisher Scientific Cat# G-21040, RRID:AB_2536527) at a 1:250 dilution. Samples were stained with DAB substrate chromogen (#K3468, Agilent) for 1–10 min and counterstained with Harris hematoxylin (#109254; Sigma) for 2 min, followed by dehydration with ethanol and xylene, and finally mounted in DPX (#06522, Sigma). Positive and negative controls were run along the tested slides for each marker. For ARID1A, Ki67 and cleaved caspase3 staining, slides were heated in the instrument at 75ºC for 8 min and deparaffinized with EZ prep solution (Ventana Medical System, Cat# 950-102 2L). Antigen retrieval was performed at 95ºC for 64 min using the Cell Conditioning 1 buffer (CC1; Ventana Medical System, Cat# 950-124 2L). Subsequent incubation of 8 min with CM inhibitor (ChromoMap DAP kit) was used for peroxidase blockade. For primary antibodies anti-ARID1A (Sigma-Aldrich Cat# HPA005456, RRID:AB_1078205) (1:200), anti-Ki67 (pre-diluted) (Roche Cat# 05278384001, RRID:AB_2631262) and anti-cleaved caspase3 (Cell Signaling Technology Cat# 9661, RRID:AB_2341188) (1:100), slides were first incubated at 37ºC for 32, 24, or 60 min, respectively, and for a further 8 min with UltraMap anti-Rabbit antibody (HRP) (Roche Cat# 05269717001, PRID:AB_2924783). As a detection system, CM ChromoMap DAB kit (Roche Diagnostics, Cat# 760-159) was used according to the manufacturer's instructions, followed by counterstaining with hematoxylin II (Ventana Medical System, Cat# 760-2021) for 8-12 min and bluing reagent (Ventana Medical System, Cat# 760-2037) for 4 min, dehydration, and mounting processes. Slides were scanned in the NanoZoomer 2.0-HT slide scanner (Hamamatsu Photonics) and visualized in the NDP.view2 software (Hamamatsu Photonics) or QuPath [383] [383].

Genomic profiling

Molecular profiling was performed using FFPE tumor tissue obtained from patient biopsies and corresponding PDXs. For patient samples, DNA was analyzed using FoundationOne CDx®

hybrid-capture NGS service platform, an assay designed to detect substitutions, insertions, deletions, and rearrangements in a total of 324 genes, including genes known to be somatically altered in solid tumors that are validated targets for therapy (either approved or in clinical trials) and unambiguous drivers of oncogenesis based on current knowledge. For PDX samples, an in-house NGS panel was used for genomic characterization. Four 8-μm tissue sections from all PDXs, with more than 20% tumor area, were obtained, and DNA extraction was performed with the automated system Maxwell16 FFPE plus LEV DNA purification kit (Promega, Cat# TM349). DNA quality and concentration were measured by Qubit and analyzed by NGS with a custom 435-gene hybrid capture-based panel (VHIO-300 panel, see **Table M1**). Sequencing reads were aligned (BWA v0.7.17, Samtools v1.9) against a custom reference containing all chromosomes from hg19 mm10 reference genomes. Reads aligned to chromosomes from the mm10 genome were removed, and reads aligned to the hg19 genome were further analyzed. Picard (v1.139) was used to remove duplicates. Base recalibration, insertion and deletion (indel) realignment (GATK v3.7.0), and variant calling (VarScan2 v2.4.3, Mutect2 v4.1.0.0) were performed. Variants from both callers are reported. A minimum of 7 reads supporting the variant allele were required to call a mutation. The technique's sensitivity is 5% Minor allele frequency (MAF) for single nucleotide variants (SNVs) and 10% MAF for INDELs. Copy number variations (CNVs) were calculated with CNVkit (v0.9.6.dev0) using an in-house 2N pool as the standard sample. For somatic variant analysis, frequent single nucleotide polymorphisms (SNPs) in the population were filtered based on the gnomAD database (allele frequency ≤ 0.0001). Variants were manually curated, and identified variants were classified using publicly available databases: COSMIC (RRID: SCR_002260), cBioPortal (RRID: SCR_014555), ClinVar (RRID: SCR_006169), VarSome, and OncoKB (RRID: SCR_014782).

Table M1: genomic alterations and fusions included in the VHIO-300 panel

Genomic alterations:

ABL1	*CYLD*	*H3F3C*	*MYCN*	*RBM10*
ABL2	*DAXX*	*HGF*	*MYD88*	*RECQL4*
ACVR1B	*DCUN1D1*	*HIST1H1C*	*MYH9*	*REL*
AKAP9	*DDR2*	*HIST1H2BD*	*MYOD1*	*RET*
AKT1	*DICER1*	*HIST1H3B*	*NBN*	*RFWD2*
AKT2	*DIS3*	*HNF1A*	*NCOR1*	*RHEB*
AKT3	*DNMT1*	*HRAS*	*NF1*	*RHOA*
ALK	*DNMT3A*	*HSD3B1*	*NF2*	*RICTOR*
ALOX12B	*DNMT3B*	*HSP90AA1*	*NFE2L2*	*RIT1*
AMER1	*DOT1L*	*ICOSLG*	*NFKBIA*	*RNF43*
APC	*E2F3*	*IDH1*	*NKX2-1*	*RNPC3*
AR	*EED*	*IDH2*	*NKX3-1*	*ROS1*
ARAF	*EGFL7*	*IFNGR1*	*NOTCH1*	*RPS6KA4*
ARFRP1	*EGFR*	*IGF1*	*NOTCH2*	*RPS6KB2*
ARID1A	*EIF1AX*	*IGF1R*	*NOTCH3*	*RPTOR*
ARID1B	*EP300*	*IGF2*	*NOTCH4*	*RSPO2*
ARID2	*EPCAM*	*IKBKE*	*NPM1*	*RUNX1*
ARID5B	*EPHA3*	*IKZF1*	*NRAS*	*RUNX1T1*
ASXL1	*EPHA5*	*IL10*	*NSD1*	*RYBP*
ASXL2	*EPHA7*	*IL7R*	*NTRK1*	*SDHA*
ATM	*EPHB1*	*INHBA*	*NTRK2*	*SDHAF2*
ATR	*ERBB2*	*INPP4A*	*NTRK3*	*SDHB*
ATRX	*ERBB3*	*INPP4B*	*NUP93*	*SDHC*
AURKA	*ERBB4*	*INSR*	*PAK1*	*SDHD*
AURKB	*ERCC2*	*IRAK4*	*PAK3*	*SETD2*
AXIN1	*ERCC3*	*IRF2*	*PAK7*	*SF3B1*
AXIN2	*ERCC4*	*IRF4*	*PALB2*	*SH2D1A*
AXL	*ERCC5*	*IRS1*	*PARK2*	*SHH*
B2M	*ERG*	*IRS2*	*PARP1*	*SHQ1*
BAP1	*ERRFI1*	*JAK1*	*PAX5*	*SLIT2*
BARD1	*ESR1*	*JAK2*	*PBRM1*	*SMAD2*
BBC3	*ETV1*	*JAK3*	*PDCD1*	*SMAD3*
BCL2	*ETV6*	*JUN*	*PDCD1LG2*	*SMAD4*
BCL2L1	*EXOSC10*	*KAT6A*	*PDGFRA*	*SMARCA4*
BCL2L11	*EZH2*	*KDM5A*	*PDGFRB*	*SMARCB1*
BCL2L2	*FAM175A*	*KDM5C*	*PDK1*	*SMARCD1*
BCL6	*FAM46C*	*KDM6A*	*PDPK1*	*SMO*
BCOR	*FANCA*	*KDR*	*PHOX2B*	*SNCAIP*
BCORL1	*FANCC*	*KEAP1*	*PIK3C2B*	*SOCS1*
BLM	*FANCD2*	*KEL*	*PIK3C2G*	*SOX10*
BMPR1A	*FANCE*	*KIT*	*PIK3C3*	*SOX17*
BRAF	*FANCF*	*KLF4*	*PIK3CA*	*SOX2*
BRCA1	*FANCG*	*KLHL6*	*PIK3CB*	*SOX9*
BRCA2	*FANCL*	*KMT2A*	*PIK3CD*	*SPEN*
BRD4	*FANCM*	*KMT2C*	*PIK3CG*	*SPOP*
BRIP1	*FAS*	*KMT2D*	*PIK3R1*	*SPTA1*
BTG1	*FAT1*	*KRAS*	*PIK3R2*	*SRC*
BTK	*FBXW7*	*LATS1*	*PIK3R3*	*STAG2*
C11ORF30	*FGF10*	*LATS2*	*PIM1*	*STAT3*
CARD11	*FGF14*	*LIFR*	*PLCG2*	*STAT4*

CASP8	*FGF19*	*LMO1*	*PLK2*	*STK11*
CBFB	*FGF23*	*LRP1B*	*PMAIP1*	*STK40*
CBL	*FGF3*	*LYN*	*PMS1*	*SUFU*
CCND1	*FGF4*	*LZTR1*	*PMS2*	*SUZ12*
CCND2	*FGF6*	*MAD2L2*	*PNRC1*	*SYK*
CCND3	*FGFR1*	*MAGI2*	*POLD1*	*TAF1*
CCNE1	*FGFR2*	*MALT1*	*POLE*	*TBX3*
CD274	*FGFR3*	*MAP2K1*	*POLR3A*	*TERT*
CD276	*FGFR4*	*MAP2K2*	*POLR3B*	*TET1*
CD79A	*FH*	*MAP2K4*	*PPP2R1A*	*TET2*
CD79B	*FLCN*	*MAP3K1*	*PPP2R2A*	*TGFBR1*
CDC73	*FLT1*	*MAP3K13*	*PRDM1*	*TGFBR2*
CDH1	*FLT3*	*MAP3K5*	*PREX2*	*TMEM127*
CDK12	*FLT4*	*MAPK1*	*PRKAR1A*	*TMPRSS2*
CDK4	*FOXA1*	*MAPK7*	*PRKCI*	*TNFAIP3*
CDK6	*FOXL2*	*MAX*	*PRKDC*	*TNFRSF14*
CDK8	*FOXP1*	*MCL1*	*PRSS8*	*TOP1*
CDKN1A	*FRS2*	*MDC1*	*PTCH1*	*TOP2A*
CDKN1B	*FUBP1*	*MDM2*	*PTEN*	*TP53*
CDKN2A	*GABRA6*	*MDM4*	*PTPN11*	*TP63*
CDKN2B	*GATA1*	*MED12*	*PTPRD*	*TRAF7*
CDKN2C	*GATA2*	*MEF2B*	*PTPRS*	*TSC1*
CEBPA	*GATA3*	*MEN1*	*PTPRT*	*TSC2*
CHD2	*GATA4*	*MET*	*QKI*	*TSHR*
CHD4	*GATA6*	*MITF*	*RAC1*	*U2AF1*
CHEK1	*GID4*	*MLH1*	*RAD50*	*VEGFA*
CHEK2	*GLI1*	*MLH3*	*RAD51*	*VHL*
CIC	*GNA11*	*MPL*	*RAD51B*	*VTCN1*
CREBBP	*GNA13*	*MRE11A*	*RAD51C*	*WISP3*
CRKL	*GNAQ*	*MSH2*	*RAD51D*	*WT1*
CRLF2	*GNAS*	*MSH3*	*RAD52*	*XIAP*
CSF1R	*GPR124*	*MSH6*	*RAD54L*	*XPO1*
CTCF	*GREM1*	*MTOR*	*RAF1*	*YAP1*
CTLA4	*GRIN2A*	*MUTYH*	*RANBP2*	*YES1*
CTNNA1	*GRM3*	*MYC*	*RARA*	*ZBTB2*
CTNNB1	*GSK3B*	*MYCL*	*RASA1*	*ZNF217*
CUL3	*H3F3A*	*MYCL1*	*RB1*	*ZNF703*

Gene fusions:

Chromosome	Gene	Intron number
2	*ALK*	NM_004304: intron_19
5	*CD74*	NM_013230: intron_6
7	*EGFR*	NM_005228: intron_7
2	*EML4*	NM_019063: intron_6
2	*EML4*	NM_019063: intron_13
8	*FGFR1*	NM_001174067: introns_16_17
10	*FGFR2*	NM_000141: intron_17
4	*FGFR3*	NM_000142: intron_17
5	*NPM1*	NM_002520: intron_5
1	*NTRK1*	NM_002529: intron 9
10	*RET*	NM_020975: intron_11
6	*ROS1*	NM_002944: intron_33
4	*TACC3*	NM_006342: intron_9

CCA tumoroid *ex vivo* 3D cultures

CCA patient-derived tumor cells were isolated from CCA_PDX through a combination of mechanic disruption and enzymatic disaggregation following a described protocol [100]. Briefly, PDX tumors with a volume of less than 500 mm^3 were freshly collected in DMEM/F12/HEPES (L0093-500, Biowest) after surgical resection, minced using sterile scalpels, and dissociated for a maximum of 90 min in DMEM/F12/HEPES supplemented with 0.3 mg/ml collagenase (C9891, Sigma-Aldrich), 0.1 mg/ml hyaluronidase (H3506, Sigma-Aldrich), 2% BSA (VWRC0332, VWR), 5 µg/ml insulin (I1882, Sigma-Aldrich) and 50 µg/ml gentamycin (15750-037, Gibco). After centrifugation, pellets were further dissociated using 0.05% trypsin (HYCLSH30236.02, VWR), 5 mg/ml Dispase (7923, STEMCELL Technologies) and 1 mg/ml DNase (D4263, Sigma-Aldrich). Red blood cells were eliminated by washing the cell pellet with 1× Red Blood Cell (RBC) Lysis Buffer solution (00-4333-57, eBioscience). Cells were then resuspended in DMEM/F12/HEPES supplemented with 2% of fetal bovine serum (10270106, Gibco), 1% penicillin/streptomycin (15140122, Gibco), 10 µg/ml of ROCK inhibitor (S1049, Selleck Chemicals) and 5 µg/ml insulin. For drug efficacy tests, cells were seeded at 4×10^4 cells/well on Matrigel precoated 48-well plates (130187, Thermo Scientific) or at 2×10^4 cells/well in a Matrigel pre-coated Corning 96 Well White Polystyrene Microplate (CLS3610, Corning). On the following day, cells were treated with either vehicle (DMSO) or the corresponding drug and cultured at 37ºC in 5% of CO_2. Medium and treatments were refreshed every 2-3 days.

Cell viability measurement

Cell viability was evaluated at 4 different timepoints for growth kinetics on days 1, 4, 7, and 10. For each measurement, the culture medium was first replaced by cold PBS-EDTA 1 mM and incubated for 1h at 4ºC to melt Matrigel; cell pellets were then obtained by centrifugation at 450 g for 5 min at 4ºC. The supernatant was removed, and pellets were resuspended with 50 µl of PBS with 1mM EDTA and transferred to a Corning 96-Well White Polystyrene Microplate. Cell viability was quantified using CellTiter-Glo Luminescent Cell Viability Assay (Promega; G7570), according to the manufacturer's instruction. Luminescence was measured with infinite M2000 Pro (Tecan®) and i-control 1.11 software. For drug efficacy experiments, cells were treated *ex vivo* with the indicated compounds for 7 days, and cell viability was measured by CellTiter-Glo. As cells were already seeded in the final readout plate (Corning 96-Well White Polystyrene Microplate, CLS3610, Corning), Matrigel was melted by direct on-plate incubation with 50 µl PBS with1 mM EDTA for 1h at 4ºC. Cell viability was evaluated as described above.

Immunofluorescence staining

For immunofluorescence staining, cells were seeded on a Matrigel pre-coated 8-well Nunc

Lab-Tek Chamber Slide™ system (C7182, Thermo Scientific) at 4×10^4 cells/well. After a 72–144-h incubation, cells were fixed with 4% paraformaldehyde (30525-89-4, Santa Cruz Biotechnology) for 15 min, washed with 1% BSA in PBS for 5 min, and permeabilized with 1% Triton X-100 for 20 min at room temperature. After 1 h of blocking in 5% BSA-PBS, cells were incubated at room temperature for 2 hours with the primary antibody anti-KRT19 (Atlas Antibodies Cat# HPA002465, RRID:AB_1079179) or anti-HepPar1 (Novus Cat# NBP3-08970, RRID:AB_2909615) diluted 1:200 in blocking buffer. Cells were then incubated for 1 h with a secondary anti-rabbit antibody (Jackson ImmunoResearch Labs Cat# 711-035-152, RRID:AB_10015282) diluted at 1:400 in blocking buffer, washed twice with 1% BSA PBS, and incubated with DAPI (D9542, Sigma Aldrich) in PBS for 5 min. Slides were then mounted with Fluoromount-G (0100-01, SouthernBiotech). Slides were stored at 4ºC until analysis. Images were acquired with a Nikon confocal microscope C2+ equipped with an LU-N4S laser unit, using the NIS-Elements software.

Drug efficacy studies *in vivo*

Upon xenograft growth (50–150 mm^3), CCA_PDX-bearing mice were randomized and treated with indicated molecules. NEO2734 was provided by Epigene Therapeutics Inc. and dissolved in PEG300 (81162-1L, Sigma-Aldrich). Olaparib (AZD2281) was purchased from MedChemExpress (cat. no. HY-10162) and dissolved in 10% DMSO (v/v) and 10% Kleptose [HP-β-CD] (346102, Roquette) (w/v). Pamiparib was provided by BeiGene and dissolved in sterilized 0.5% methylcellulose (M0262, Sigma-Aldrich). Niraparib (MK-4827) (cat. no. HY-10619) and pemigatinib (INCB054828) (cat. no. HY-109099) were purchased from MedChemExpress. Each treatment regimen is indicated in the figures. Tumor growth was measured 3× per week with a caliper; researchers were blinded to the treatment effect. Mice weights were recorded 3× per week. Tumor volumes were calculated using the formula: $V = (length\times width^2)/2$. According to institutional guidelines, mice were euthanized using CO^2 inhalation once tumors reached 1-1.5 cm^3 or in case of severe weight loss. At the endpoint, tumors were harvested and formaldehyde-fixed and flash-frozen for posterior immunohistochemical and proteomic analyses, respectively.

2-Hydroxyglutarate (2HG) analysis

Single-cell suspensions from CCA cell lines or CCA_PDXs pelleted upon disaggregation were lysed in SDS lysis buffer (2% SDS, 50 mM Tris-HCl pH [7.5], 10% glycerol) and stored at –20 ºC for further metabolite analysis. Medium was collected from cell supernatants, centrifuged to get rid of cell debris and frozen until further evaluation. 2HG analysis was performed based on a previously reported method [384]. Briefly, 25 µl of the cell extract or the collected medium were mixed with 30 µl of succinic acid-d4 (0.1 µg/ml), used as internal standard, with 100 µL of the

derivatization mixture containing o-benzyl hydroxylamine (1M) and N(3-dimethylaminopropyl)-N'-ethylcarbodiimide hydrochloride (1M). Derivatization was performed at room temperature during 1 h. Subsequently, a liquid–liquid extraction with water and ethyl acetate was performed, and the organic extract was evaporated until dry (N2 stream, 40 ºC, <15 psi). Extracts were reconstituted in 300 µl of water: methanol (1:1, v:v) and 3 µl were injected into the LC-MS/MS system. 2HG was determined in the Selected Reaction Monitoring mode by selecting the transition 359 → 236 for 2HG and 333 → 210 for the internal standard. Quantification was performed by external calibration.

Western Blots

Both flash-frozen tumor pieces from *in vivo* studies and harvested CCA cells were lysed in SDS lysis buffer (2% SDS, 50 mM Tris-HCl pH [7.5], 10% glycerol), homogenized and quantified with the DC Protein Array kit (Lowry method; Bio-Rad). Western blots were performed according to standard procedures. Briefly, samples were mixed with 5× loading buffer (250 mM Tris-HCl pH 6.8, 10% SDS, 0.02% bromophenol blue, 50% glycerol, 20% β-mercaptoethanol) and boiled at 95ºC for 5 min. Proteins were analyzed by sodium dodecyl sulfate polyacrylamide gel electrophoresis (SDS-PAGE) using different percentages of polyacrylamide concentrations, ranging from 7.5% to 15%. Gels were run in Tris-glycine-SDS (TGS) buffer (25 mM Tris-OH pH 8.3, 192 mM glycine and 5% SDS), and proteins were transferred to a nitrocellulose membrane (Amersham Protran 0.45 nitrocellulose, GE Healthcare) in transfer buffer (50 mM Tris-OH, 396 mM glycine, 0.1% SDS, and 20% methanol) for 60 to 120 min, depending on the molecular weight of the protein. Membranes were stained with Ponceau S (0.5% Ponceau S and 1% acetic acid) and blocked with 5% non-fat milk or bovine serum albumin (BSA) in TBS-T buffer (25 mM Tris-HCl pH 7.5, 137 mM NaCl, and 0.1% Tween) for 1 h. Primary antibodies were added in fresh blocking solution and incubated overnight at 4 ºC. After three washes of 10 min with TBS-T, membranes were incubated with horseradish peroxidase (HRP)-combined secondary antibodies in fresh blocking solution for 1 h at room temperature. After a new round of washes, membranes were developed by incubation with a substrate for HRP-enhanced chemiluminescence (ECL) and protein bands were visualized in AmershamTM Imager 600 (GE Life Sciences). To detect low-quantity (or otherwise difficult-to-detect) proteins, more sensitive ECL was used.

Antibodies used were: poly/mono-ADP ribose (E6F6A) (Cell Signaling Technology Cat# 83732, RRID:AB_2749858), STING (D2P2F) (Cell Signaling Technology Cat# 13647, RRID:AB_2732796), α-tubulin (Sigma-Aldrich Cat# T9026, RRID:AB_477593), vinculin [EPR8185] (Abcam Cat# ab129002, RRID:AB_11144129) and the secondary antibodies peroxidase-AffiniPure donkey anti-rabbit IgG (H+L) (Jackson ImmunoResearch Labs Cat# 711-035-152, RRID:AB_10015282) and goat anti-mouse IgG (H+L) cross-adsorbed, HRP (Thermo

Fisher Scientific Cat# G-21040, RRID:AB_2536527).

All antibodies were used at 1:1000 concentration in 5% BSA (Poly/Mono-ADP Ribose and STING) or 5% milk (Tubulin and Vinculin). Secondary antibodies were used at 1:2000 for the two former primaries and 1:5000 for the latter; all of them in 5% milk. Quantification of protein levels was done with ImageJ (National Institutes of Health).

RAD51 assay

Three-micrometer FFPE sections from CCA patients and PDXs were used for the analysis of RAD51 foci (as a functional readout of HRD) and γH2AX foci (as a biomarker of endogenous double-stranded DNA damage); each biomarker was counterstained with geminin (as a marker of the S/G2 cell cycle phase) and 4′,6-diamidino-2-phenylindole (DAPI), as previously described [225]. The following primary antibodies were used for immunofluorescence: rabbit anti-RAD51 (Abcam Cat# ab133534, RRID:AB_2722613, 1:1000), mouse anti-γH2AX (Millipore Cat# 05-636, RRID:AB_309864, 1:200), mouse anti-geminin (Leica Biosystems Cat# NCL-L-Geminin, RRID:AB_563738, 1:60), and rabbit anti-geminin (Proteintech Cat# 10802-1-AP, RRID:AB_2110945, 1:400). Goat anti-rabbit Alexa fluor 568 (Thermo Fisher Scientific Cat# A-11036, RRID:AB_10563566), goat anti-mouse Alexa Fluor 488 (Thermo Fisher Scientific Cat# A-28175, RRID:AB_2536161), donkey anti-mouse Alexa Fluor 568 (Thermo Fisher Scientific Cat# A-10037, RRID:AB_2534013) and goat anti-rabbit Alexa Fluor 488 (Thermo Fisher Scientific Cat# A-11070, RRID:AB_2534114) (1:500) were used as secondary antibodies. Scoring was carried out blindly using live images and a 60× immersion oil lens in a Nikon (Amsterdam, Netherlands) Ti-Eclipse microscope. The mean score from two observers is provided for each sample. At least 40 geminin-positive cells were analyzed per sample, and the γH2AX score was used as a quality check to ensure the presence of enough endogenous DNA damage to evaluate HR functionality (cut-off, 25% geminin-positive cells with γH2AX foci). The RAD51 score was considered low or high based on the predefined cut-off of 10% geminin-positive cells with ≥5 RAD51 nuclear foci.

RNA-seq profiling and analysis

Total RNA was isolated from CCA adherent cells or CCA_PDXs by using miRNeasy Mini Kit (50) (Qiagen, Cat# 217004) following the manufacturer's protocol. Extractions of two independent biological replicas were performed. The total RNA quality and quantity were determined using Qubit® RNA HS Assay (Thermo Fisher Scientific) and RNA 6000 Nano Assay on a Bioanalyzer 2100 (Agilent). The RNASeq libraries were prepared following the TruSeq®Stranded mRNA LT Sample Prep Kit protocol (Illumina) according to the manufacturer's recommendations. Briefly, total RNA (500 ng) was enriched for the polyA mRNA fraction and fragmented by divalent metal

cations at high temperatures. To achieve the directionality, the second strand cDNA synthesis was performed in the presence of dUTP. The blunt-ended double-stranded cDNA was 3' adenylated and Illumina platform-compatible adaptors with unique dual indexes and unique molecular identifiers (Integrated DNA Technologies) were ligated. The ligation product was enriched with 15 PCR cycles, and the final library was validated on an Agilent 2100 Bioanalyzer with the DNA 7500 assay (Agilent). The RNASeq libraries were sequenced on NovaSeq 6000 (Illumina) with a read length of 2×100 bp following the manufacturer's protocol for dual indexing. Image analysis, base calling, and quality scoring of the run were processed using the manufacturer's software, Real-Time Analysis (RTA v3.4.4), followed by the generation of FASTQ sequence files.

RNA-seq reads were first mapped against the mouse genome mm10 using Hisat2 to eliminate possible mice contamination. The unmapped fraction of the reads was then re-aligned to the human reference genome (GRCh38), and counts per gene were obtained using featureCounts with the latest GENCODE version as reference (GENCODE v34). RNA expression was analyzed by dimensionality reduction (PCA) and unsupervised hierarchical clustering. To remove noise from the data, low-expressed genes (i.e., with fewer than 0.25 counts per million [CPM] reads) were filtered out. PCA was performed on the variance-stabilized read counts of the remaining 20,295 expressed genes using the *factoextra* R package. After removing batch effects using voom-limma, clustering of the samples was obtained by NMF (non-negative matrix factorization) deconvolution of the expression residuals using the *NMF* R package. Differential gene expression analysis between *IDH1*^{mut} and *IDH1*^{wt} CCA_PDXs was performed using the R package DESeq2 with default parameters. Genes with adjusted p-value < 0.05 were considered significant. Gene set enrichment analysis (GSEA) was performed with the *fgsea* R package, and the HALLMARK database was used as a query. The *pheatmap* R package was used to create all the heatmaps and the *ComplexHeatmap* one to generate Upset Plots. ImmPort database was used to retrieve the list of immune-related genes. "IFNsign score" was calculated by scaling and averaging the expression of "IFNsign" genes [330] in each sample.

Quantitative RT-PCR (qRT-PCR)

Total RNA from CCA adherent cells or CCA_PDXs was isolated, as explained before. RNA was eluted in RNase-free water and quantified using NanoDrop™ 2000 spectrophotometer (ThermoFisher Scientific). cDNA was prepared using qScript™ cDNA SuperMix 100 Assays (Quantabio, Cat# 95048-100) following the manufacturer's instructions. Quantitative determination of RNA levels was performed in triplicate in a final volume of 10 µl with 15–100 ng of cDNA, forward and reverse primers (Sigma; 100-500 nM each), and 1× PerfeCTa® SYBR® Green FastMix (Quantabio; Cat# 95073-01). Thermocycling parameters used were: 95 °C 30 s; 40 cycles 95 °C 5 s, 60 °C 15 s, 72ºC 10 s; melting curve. Values were normalized to the

expression of a housekeeping gene (*HPRT*). Primer sequences used are listed below (**Table M2**).

Table M2: Primer sequences used for qRT-PCR analysis

Gene name	Direction	Sequence (5' → 3')
STING1	Forward	CCAGAGCACACTCTCCGGTA
	Reverse	CGCATTTGGGAGGGAGTAGTA
OAS1	Forward	TGTCCAAGGTGGTAAAGGGTG
	Reverse	CCGGCGATTTAACTGATCCTG
OAS2	Forward	AGGTGGCTCCTATGGACGG
	Reverse	TTTATCGAGGATGTCACGTTGG
OAS3	Forward	GAAGGAGTTCGTAGAGAAGGCG
	Reverse	CCCTTGACAGTTTTCAGCACC
ISG15	Forward	CGCAGATCACCCAGAAGATCG
	Reverse	TTCGTCGCATTTGTCCACCA
IRF7	Forward	GCTGGACGTGACCATCATGTA
	Reverse	GGGCCGTATAGGAACGTGC
TNF	Forward	GAGGCCAAGCCCTGGTATG
	Reverse	CGGGCCGATTGATCTCAGC
CD274	Forward	TGGCATTTGCTGAACGCATTT
	Reverse	TGCAGCCAGGTCTAATTGTTTT
HPRT	Forward	CTGGCGTCGTGATTAGTGAT
	Reverse	GGCTACAATGTGATGGCCT

DNA Methylation profiling and analysis

Genomic DNA from CCA_PDXs was isolated using the DNeasy Blood & Tissue kit (50969506, Qiagen). Genomic DNA (1 μg) was converted using the EZ DNA Methylation Gold Kit (Zymo Research, Cat# D5006) following the manufacturer's instructions. Infinium MethylationEPIC BeadChip arrays (Illumina, Cat# 20087706) were used to analyze DNA methylation, following the manufacturer's instructions. This platform allows to interrogate, at single-nucleotide resolution, approximately 850,000 methylation sites per sample, covering 99% of the reference sequence (RefSeq) genes. Raw files (IDAT files) were provided by the Josep Carreras Research Institute Genomics Unit (Barcelona). IDAT files were then used to obtain DNA methylation beta values through the R package *minfi* (v1.40.0) after performing quality control of samples and probes (removing those with $p > 0.01$). The function GRatioSet.quantile was used for normalization. Sexual chromosomes, SNPs, and cross-hybridized probes were removed. EPIC Illumina annotation was used to assign gene ID to each probe.

Differentially methylated positions (DMPs) or CpGs were extracted using the function topTable from the limma package (v3.50.3), adjusting by the Benjamini-Hochberg method. CpGs with $p < 0.01$ were selected and further filtered with log2 fold change (logFC +/- 0.15).

NMF deconvolution of the top 20000 most variable CpG sites was performed using the *NMF* R package. EPIC array probes were classified as promoter, enhancer, gene body, or other, using annotations provided in the EPIC 850K array manifest b5 (version 1.0 b5, downloaded from:

https://emea.support.illumina.com/downloads/infinium-methylationepic-v1-0-product-files.html). Probes with a value of "Promoter_Associated" in the column 'Regulatory_Feature_Group' were assigned as promoter probes, those with any value in the column 'Phantom5_Enhancers' were assigned as enhancer probes, and probes with a value including "Body" or "1stExon" in the column 'UCSC_RefGene_Group' were assigned as gene body probes. Probes that fell into multiple groups were classified as promoter first, then enhancer probes. The *methylRRA* function of methylGSA (https://bioconductor.org/packages/release/bioc/html/methylGSA.html) was used to perform gene set enrichment analysis (GSEA) of the differentially methylated CpGs on the Hallmark database. Probes were assigned to a gene based on the contents of the EPIC array manifest b5 column 'UCSC_RefGene_Name'. Additionally, promoter and enhancer only associated probes that did not have any gene annotation in the manifest column 'UCSC_RefGene_Name' were then assigned a 'nearest gene' annotation using the function *matchGenes* with the TxDb.Hsapiens.UCSC.hg19.knownGene library from *bumphunter* R package.

The *densityHeatmap* function from the ComplexHeatmap R package was used to create the density heatmaps of our samples based on beta values from positions in the promoters of immune-related genes (i.e., chemokines, cytokines or cytokine receptors from ImmPort database).

Multiplexing immunohistochemistry (mIHC)

Tumor samples were analyzed by Next Generation IHC (NGI), as described in [385], using the Immune-Panel to assess key immune effector cells such as total lymphocytes ($CD3^+$), cytotoxic T cells ($CD8^+$), regulatory T cells ($FOXP3^+$) and monocytes/macrophages ($CD163^+$). Ki67 staining was included to inform about the percentage of the cell populations that are proliferating. The NGI protocol consists of iterative cycles of staining/destaining on the same tissue section and uses the combination of Ventana Discovery Ultra (Roche Diagnostics), Nanozoomer slide scanner (Hamamatsu), and Visiopharm image analysis software. Briefly, an alcohol-soluble chromogen (DISCOVERY AEC KIT (#760-258, Roche-Ventana)) was used to allow the destaining of the samples. After each automated IHC, samples were mounted in an aqueous medium and digitalized (cycle 1). Subsequently, the section was destained in alcohol and submitted to the staining cycle, including all the immune markers, followed by a Pan Cytokeratin (PanCK) staining for tumor area definition. Lymphocyte's expression was evaluated by image analysis as density (number of cells/mm^2), and proliferation was defined as the percentage of Ki67 positive cells within the total amount of positive cells for each population. $CD4^+$ cells were considered all $CD3^+CD8^-$ cells. PanCK staining was used for location analyses, dividing the ROI into three different ROIs: the tumor area (tumoral area), the stroma within 30 µm from the tumor (proximal area), and the stroma >30 µm from the tumor (distal area). Positive controls were included in each slide. Antibodies and protocols used in this study are listed in **Table M3**.

Table M3: Antibodies and Ventana Discovery Ultra protocols used for mIHC

ANTIBODY	COMPANY	REF	ANTIGEN RETRIEVAL	PRIMARY ANTIBODY	SECONDARY ANTIBODY	CHROMOGEN
FOXP3	ABCAM	AB99963	CC1 92' 95º	1h	HRP RB 20'	AECPLUS. 150UL
CD8/144B	DAKO	M7103	CC2 8' 100º CC1 40' 95º	32' 37º 1/100	HRP MS 8'	AECPLUS. 200UL
CD3(2GV6)	ROCHE	790-4341	CC2 8' 100º CC1 40' 95º	40' 36º	HRP RB 8'	AECPLUS. 200UL
CD163	ROCHE	760-4437	CC2 8' 100º CC1 64' 95º	48' 37º	HRP MS 8'	AECPLUS. 200UL
KI67	ROCHE	790-4286	CC2 8' CC1 64' 95º	52' 37ºC	HRP RB 8'	AECPLUS. 200UL
PanCK (AE1/AE3)	PALEX	PDM072	CC2 8' 100º CC1 40' 95º	24' 36º	HRP MS 8'	AECPLUS. 200UL

Cell Lines and culture conditions

CCA cell lines used were: HuCCT1 (RRID:CVCL_0324), HuH28 (RRID:CVCL_2955), Snu1079 (RRID:CVCL_5008) and RBE (RRID:CVCL_4896). All of them were cultured in Roswell Park Memorial Institute RPMI 1640 medium (Biowest Cat# L0501-500) supplemented with 1% penicillin/streptomycin (Gibco Cat# 15140122), 2 mM L-glutamine (Biowest Cat# X0550-100), and 10% FBS (Gibco Cat# 10270106) at 37ºC in 5% CO_2.

The lack of mycoplasma contamination was tested regularly using standard PCR with the primers:

F: 5′-GGCGAATGGGTGAGTAACACG-3′

R: 5′-CGGATAACGCTTGCGACCTATG-3′

Drug treatments

Cells were treated for different times with different concentrations (as indicated in each specific figure) of different drugs: 5-azacytidine (MedChemExpress Cat# HY-10586), decitabine (MedChemExpress Cat# HY-A0004) and ivosidenib (MedChemExpress Cat# HY-18767). Drugs were refreshed daily. Cells were harvested for RNA, protein, DNA, or FACS analysis or re-seeded for co-culture, following the procedures specified in each method description. Also, the two IDH1mutant cell lines (Snu1079 and RBE) were subjected to a constant pressure of ivosidenib treatment (5 μM) for the T-cell cytotoxicity assays.

Dot blot of 5-mC and 5-hmC

DNA from CCA cell lines in basal or corresponding treated conditions was extracted and quantified, as explained before. Genomic DNA (gDNA) was used for 5mC (1300 ng of genomic DNA) and diluted with 65 μl of H_2O. Then, 65 μl of the 2× denaturing solution (0.8 M NaOH, 20 mM EDTA) was added to samples, and the mixes were incubated at 95 ºC for 10 min. Samples

were immediately incubated on ice and mixed with 130 µl of cold (4ºC) 2× neutralizing buffer (2 M ammonium acetate pH 7) for 10 min. Two-fold serial DNA dilutions were prepared in a 96-multiwell plate on ice and then spotted onto a positively charged nylon membrane (RPN1210B, GE Healthcare) in an assembled Bio-Dot apparatus (1706545, Bio-Rad). NaOH (0.4 M) was used to fix DNA samples to the membrane. Blotted membrane was washed with 2× SSC buffer (0.3 M NaCl, 30 mM sodium citrate) for 5 min, dried on a Whatman cellulose filter paper for 10 min, UV crosslinked (energy 120.000 µJ/cm^2) for 1 min, and blocked with PBS, 5% non-fat milk and 0.1% Tween-20 blocking solution for 1 h at room temperature. Membranes were then incubated with the primary antibody at a specified dilution: 1:1000 anti-5mc (#16233D3, Calbiochem). For 5mC detection, membranes were incubated with primary antibody overnight at 4ºC. Membranes were then washed 2× with PBS and incubated with 1:5000 anti-rabbit and 1:2000 anti-mouse, HRP-conjugated secondary antibodies, respectively, for 1 h at room temperature. After extensive washes with PBS, membranes were developed with SuperSignal West Pico Chemiluminescent Substrate (#34580, ThermoFisher Scientific) and exposed in AmershamTM Imager 600 (GE Life Sciences). In addition, membranes were also stained with methylene blue for 5-10 min at room temperature as loading controls.

PBMC isolation

PBMCs were isolated from fresh buffy coats obtained from healthy donors through the Blood and Issue Bank of Catalonia (BST). Blood was diluted 1:3 with 1× phosphate-buffered saline (PBS) and transferred to a 50 ml falcon tube with Ficoll-Paque PLUS (GE Healthcare Cat# 70-1440-02) at a 1:3 ratio, following the manufacturer's instructions. After obtaining the buffy coat, red blood cells (RBC) were lysed with 1× RBC lysis buffer (Invitrogen Cat# 00-4333-57) for 4 min. Obtained PBMCs were counted and frozen with Cryostor CS10 (Stemcell Technologies Cat# 07959) at −80 °C for *in vitro* and *in vivo* experiments.

T cell cytotoxicity assays with HER2-TCB

CCA cell lines treated as above before were seeded in triplicate in 96-well flat bottom plates (0.01 × 10^6 cells/well) (Thermo Fisher Scientific Cat# 130188). The following day, effector PBMCs were added to each well at the indicated ratio (1:1) in PBMC medium (RPMI 1640 (Biowest Cat# L0501-500), 10% heat-inactivated FBS (Gibco Cat# 10270106), 1% L-glutamine (Biowest Cat# X0550-100), 1% HEPES (Gibco Cat#15630080), 1% MEM non-essential amino acid solution (Gibco Cat#11140), and 1% penicillin–streptomycin (Gibco Cat# 15140122)), together with 100 pM of HER2-TCB. For each treatment condition, a control with PBMCs but without HER2-TCB was included. Ivosidenib treatment, but not decitabine treatment, was maintained in the co-culture. The plates were incubated for 72 h. At the endpoint, cells were harvested with

trypsin 0.05%–EDTA (VWR Cat# SH30236.02) and resuspended in fluorescence-activated cell sorting (FACS) buffer of 1× PBS, 2.5 mM EDTA, 1% bovine serum albumin (BSA) (Panreac Cat# A6588), 5% horse serum (Gibco Cat# 26050) in polypropylene V-bottom 96-well plates (Greiner Bio-One Cat# 651201). After 20 min, samples were centrifuged, stained with specified antibodies, and acquired on LSR Fortessa, using BD FACSDiva software (BD Biosciences).

Flow cytometry

Cells were harvested and resuspended in fluorescence-activated cell sorting (FACS) buffer (1× PBS, 2.5 mM EDTA, 1% bovine serum albumin (BSA) (Panreac Cat# A6588), 5% horse serum (Gibco Cat# 26050). Twenty minutes later, samples were centrifuged, and cells were incubated for 30 minutes with the specified antibody on ice in the dark. After a wash with 1× PBS and Zombie Aqua staining (BioLegend Cat# 423101) at 1:1000, samples were acquired on LSR Fortessa. The following antibodies were used: hCD3 (#300408, RRID:AB_314062), hCD8 (#344712, RRID:AB_2044008), hCD4 (#317434, RRID:AB_2562134), hCD25 (#302610, RRID:AB_314280), and hGranzyme B (# 515403, RRID:AB_2114575), all from Biolegend, at 1:300 dilution.

In the case of HER2 staining, cells were incubated in FACS buffer for 30 min with trastuzumab (Herceptin, Roche Cat#180288-69-1) at 2.5 μg/ml. After two washes with 1× PBS, a secondary conjugated antibody Anti-human Alexa-488 (Invitrogen Cat #A11013) was incubated with the cells at a concentration of 1:500 for 30 min. Cells were then washed with 1× PBS and resuspended in Zombie Aqua viability marker, and acquired on LSR Fortessa. The gating strategy for HER2 expression analysis is shown in Fig R32.

Granzyme B intracellular staining was performed following a slightly different protocol. First, cells were incubated with zombie aqua for 25 min at 1:500 concentration at room temperature (RT). Then, cells were washed and stained with the desired extracellular antibodies, as previously explained. After a wash with 1× PBS, cells were fixed with 200 μl of fresh prepared (1 part of concentrate with 3 parts of diluent) fixation/permeabilization working solution (Invitrogen Cat#00-5523-00) for 25 min on ice in the dark. The supernatant was removed after a centrifugation, and cells were permeabilized with 1x permeabilization buffer for 25 min on ice in the dark. After removing the supernatant, cells were stained with Granzyme B antibody in 1× permeabilization buffer at 1:300 concentration for 1h at RT, washed with 1× PBS, and acquired on LSR Fortessa. Flow cytometry data were analyzed with FlowJo software (BD Life Sciences). The gating strategy for T-cell activation and cytotoxicity marker analysis and median fluorescence intensity (MFI) measurements are shown in Fig R33.

Statistical analysis

Chi² tests were used to search for associations between PDX engraftment and categorical clinical features of the patients; Mann–Whitney U-tests were used for detecting various clinical features. These tests were performed using Python 3.6.12 (RRID:SCR_001658) and the Scipy 1.5.2 package. For transcriptomic and DNA methylation landscapes analysis, if multiple tests were carried out on the same data, p-values were corrected for multiple testing by Bonferroni correction or as stated in the figure legends. To assess the significance of overlaps, Fisher's exact test was performed in R with the *stats* package. Unless otherwise stated, statistical tests were performed with GraphPad Prism Version 9.4.1 (RRID:SCR_002798) with methods indicated in the figure legends.

Data availability statement

Next-generation panel sequencing data have been deposited in the NCBI BioProject (https://www.ncbi.nlm.nih.gov/bioproject) under BioProject number PRJNA763182. Data generated in this study that were published are available within the specific article.

Results

1. Generation and characterization of a collection of advanced metastatic CCA_PDXs

1.1. PDX models generated from biopsies of patients with unresectable metastatic CCA

We generated PDX models from biopsy specimens collected over five years (2016 to 2020) from 49 patients with a confirmed diagnosis of metastatic CCA. Patient specimens were subcutaneously implanted into immune-deficient (non-obese diabetic/severe combined immunodeficient; NOD-SCID) mice freshly after the biopsy procedure to generate CCA_PDX lines (P0 PDX). The establishment of CCA_PDX models was determined to be successful based on whether they: i) could be readily and serially transplanted into subsequent passages; ii) recapitulated the histopathologic characteristics of the initial biopsy sample; and iii) reliably retained the main genomic alterations of the latter (**Fig R1A**).

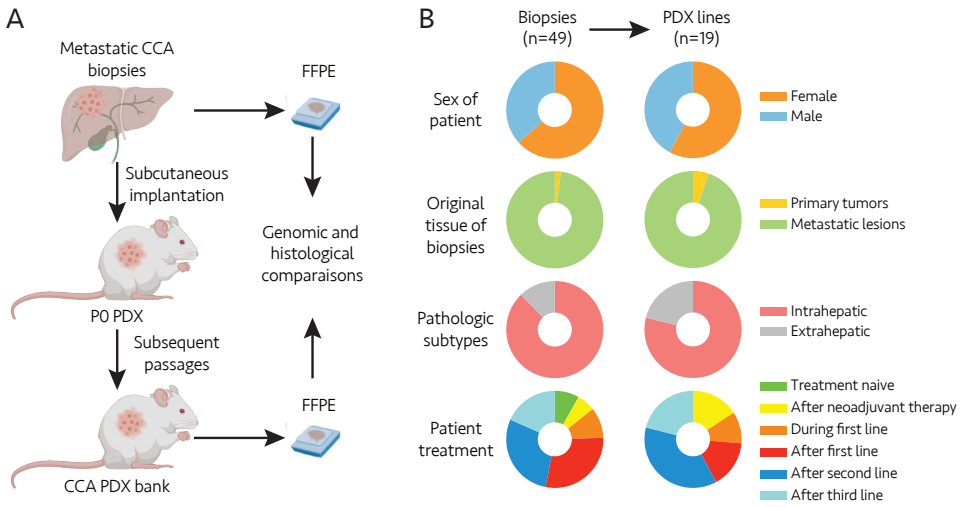

Figure R1. Generation of CCA_PDX models. (A) Schematic illustration of the process of establishing and maintaining CCA_PDXs. Successfully established CCA_PDXs are compared to their foundation biopsy counterparts in histological and genomic analyses. **(B)** Pie charts showing the stratification of all biopsies (n=49) and successfully established CCA_PDXs (n=19) based on patient sex, tissue origin of biopsies, pathologic subtypes, and patient treatment received prior to biopsy.

Of the 49 implanted samples, 19 gave rise to CCA_PDX models (success rate, 38.8%), with a median latency (e.g., time from implantation in mice to tumor growth) of 4.7 months. Of note, specimens from the 48 patients with the unresectable disease (98%) were obtained

by ultrasound-guided biopsy of metastatic lesions, and 1 specimen (2%) was obtained by biopsy of the primary tumor during surgery. Forty-three patients (87.8%) were diagnosed with intrahepatic CCA, and 6 (12.2%) with extrahepatic CCA. Notably, 45 of the 49 patients (91.8%) had already received at least one line of platinum-based chemotherapy, neoadjuvant chemotherapy, and/or targeted therapy; only 4 (8.2%) were treatment naïve (**Fig R1B** and **Table R1**).

Table R1. Characteristics of metastatic CCA patients, biopsies, and PDXs

		Biopsies Total (n= 49)	Unsuccessful engraftment (n=30)	Successful engraftment (n=19)	p value
		n (%)	n (%)	n (%)	
Sex of patient					*0,7516*
•	Female	31 (63.3)	20 (66.7)	11 (57.9)	
•	Male	18 (36.7)	10 (33.3)	8 (42.1)	
Median patient age at biopsy (years) [interquartile range]		59 [49 – 70.5]	61 [40 – 70.8]	57 [48 - 71]	*0.262*
Original tissue of biopsies					*0.8160*
•	Primary tumors	1 (2.0)	0 (0)	1 (5.3)	
•	Metastatic lesions	48 (98.0)	30 (100)	18 (94.7)	
CCA pathologic subtypes					*0.2939*
•	Intrahepatic	43 (87.8)	28 (93.3)	15 (78.9)	
•	Extrahepatic	6 (12.2)	2 (6.7)	4 (21.1)	
Patient treatment					*0.0777*
•	Treatment naive	4 (8.2)	4 (13.3)	0 (0)	
•	After adjuvant treatment (gemcitabine +capecitabine)	3 (6.1)	0 (0)	3 (15.8)	
•	During first line (gemcitabine + platinum)	5 (10.2)	3 (10.0)	2 (10.5)	
•	After first line (gemcitabine + platinum)	14 (28.6)	11 (36.7)	3 (15.8)	
•	After second line (chemotherapy or targeted therapy)	14 (28.6)	7 (23.3)	7 (36.8)	
•	After third line	9 (18.4)	5 (16.7)	4 (21.1)	

Notably, these 19 CCA_PDXs proportionally represented the original 49 patients regarding patient sex, original tissue, pathologic subtypes, and treatment received (**Fig R1B**), suggesting that none of these factors was associated with the success/failure of PDX generation. This was confirmed by further statistical analyses (**Table R1**); none of the analyzed features revealed any statistically significant effect on the engraftment outcome of the samples.

Thus, using biopsy specimens from patients with previously treated and unresectable metastatic CCA, we successfully generated a panel of 19 PDXs that could be serially transplanted and maintained.

1.2. The CCA_PDX characteristics match those of the original biopsy tissues.

Together with the capacity to be readily transplantable into subsequent passages, CCA_PDX models were required to consistently retain the traits of the initial patient samples to be established as a new line of the CCA PDX bank. We first investigated whether the histopathologic characteristics of the original biopsies were preserved in the CCA_PDXs. Histopathologic analyses of hematoxylin and eosin (H&E) stained tissue showed features in the PDXs consistent with the CCA entity and similar to the original specimens (**Fig R2**). Moreover, as the majority of our CCA_PDX collection was generated using biopsy samples from liver metastatic lesions (17 out of 19 PDX), we also used cytokeratin 19 protein (KRT19) and hepatocyte paraffin 1 (HepPar1) as biomarkers to distinguish CCA (which is $KRT19^{+}/HepPar1^{-}$) from hepatocellular carcinoma (HCC) (which is $KRT19^{-}/HepPar1^{+}$) [68, 297]. Immunohistochemistry (IHC) analysis revealed that all CCA_PDXs and their original biopsy specimens were $KRT19^{+}/HepPar1^{-}$, further confirming the CCA identity (**Fig R2**). As expected, the HCC biopsy sample used as a control was $KRT19^{-}/HepPar1^{+}$. It is important to mention that, while just three different CCA_PDX models and their biopsy counterparts are presented here, this analysis was extensively performed in all samples, and that the histopathologic match between patient and PDX was validated for all CCA_PDX models in two different passages.

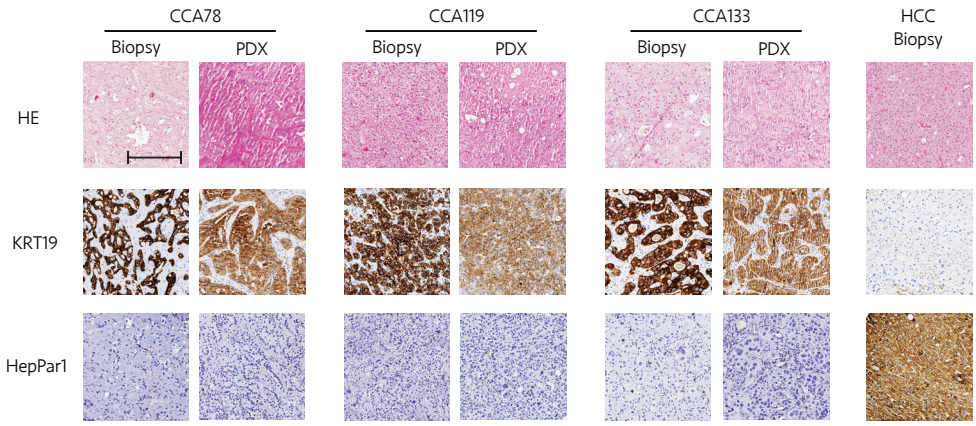

Figure R2. CCA_PDXs maintain the histologic features of the original biopsy specimens. Comparative histologic and immunohistochemical images of tumors of CCA_PDXs compared to each original biopsy specimen. Top row, H&E staining; middle row, immunohistochemical staining of KRT19 (CCA marker); and bottom row, immunohistochemical staining of HepPar1 (HCC). Representative ex-

amples of 19 CCA_PDXs are shown; an HCC biopsy sample was used as a control. CCA_PDX samples were collected at passage 1 (PDX133) or passage 2 (PDX78 and PDX119). Scale bar, 250 μm.

Next, to verify whether the CCA_PDXs faithfully recapitulated the genomic features of each corresponding original biopsy specimen, the genomic DNA samples from fifteen original biopsy samples and their corresponding CCA_PDXs were sequenced (by Foundation Medicine for the biopsies, and in-house next-generation sequencing (NGS) with a custom 435-gene hybrid capture-based panel for the CCA_PDXs). Notably, we found that the CCA_PDX models maintained most of the somatic mutations identified in the corresponding original biopsy specimens (**Fig R3A** and **3B**). Many of these identified somatic mutations were in genes involved in epigenetic regulation (e.g., *IDH1, IDH2, BAP1, ARID1A/B*), DNA damage, and cell cycle control (e.g., *BRCA2, TP53*), or signaling pathways (e.g., *BRAF, PIK3CA*), in line with previous reports attempting to define the genomic profile of CCA entity [12, 14, 15, 298]. Analysis of copy number variation (CNV) revealed a high similarity between CCA_PDXs and their paired original biopsy samples (**Fig R3C**). We also detected amplification of putative oncogene *MDM2* and homozygous deletions of *CDKN2A*, which have been associated with the CCA pathology [14]. Finally, we analyzed the *FGFR2* fusion status, as *FGFR2* fusion genes have been observed in 15-20% of CCA patient samples [298, 299]. We found three types of predicted *FGFR2* fusions in four original biopsy samples as well as in the corresponding CCA_PDXs (**Fig R3A** and **3D**). The identified fusions involve the 5′-part of the *FGFR2* gene, which encodes for an intact tyrosine domain, fused in-frame with 3′-part of the gene encoding the transcription factor activating transcription factor 2 (ATF2) (CCA67), the RNA-binding protein RNA binding motif protein 20 (RBMC20) (CCA75 and CCA75.2), and the ring finger protein 123 (RNF213) (CCA118). Therefore, in both the histopathologic and genomic analyses, the CCA_PDXs faithfully recapitulated the key features of their original biopsy specimens.

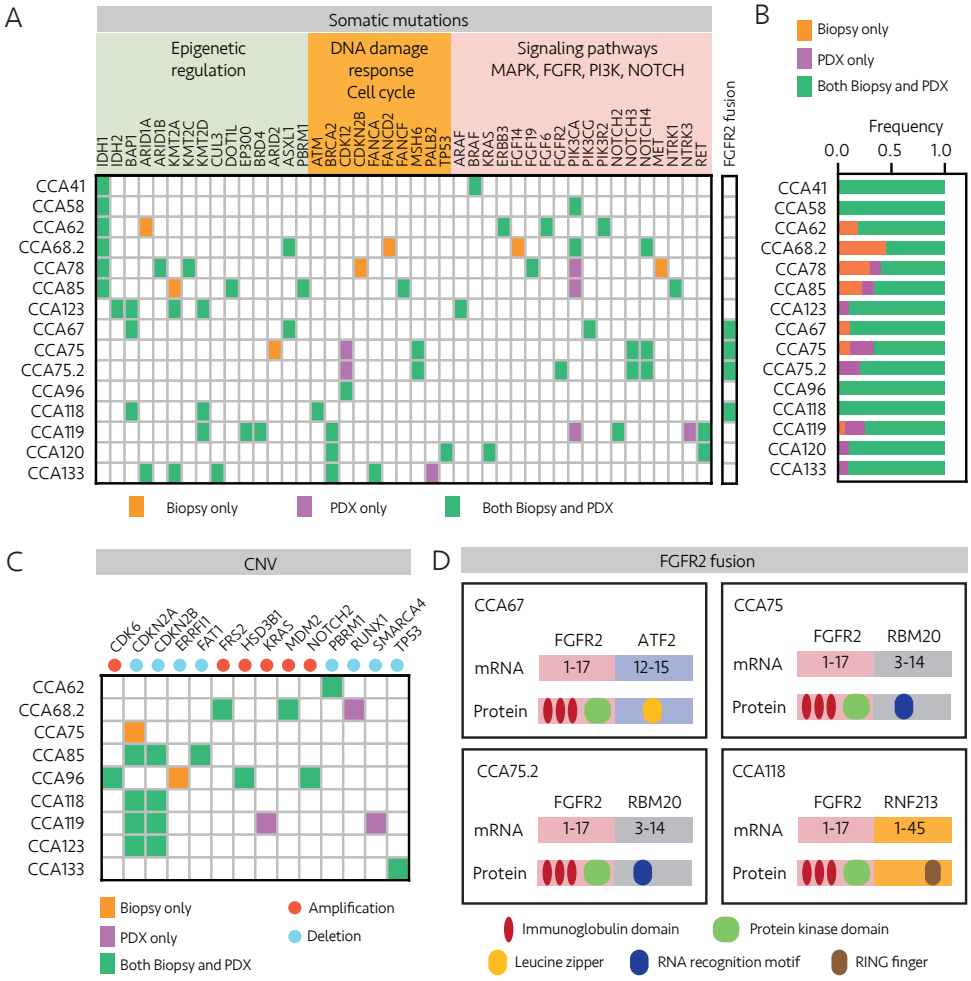

Figure R3. CCA_PDXs maintain the genomic features of the original biopsy specimens. (A) Comparison of somatic mutations and FGFR2 fusions identified in CCA_PDXs tumors and their parental biopsy specimens. Genes harboring mutations were classified into three categories: epigenetic regulation, DNA damage response/cell cycle control, and signaling pathways. CCA_PDX samples were collected at passage 1 (PDX41, PDX123, PDX96, PDX118, and PDX133) or passage 2 (PDX58, PDX62, PDX68.2, PDX78, PDX85, PDX67, PDX75, PDX75.2, PDX119, and PDX120). **(B)** Frequencies of mutations identified as biopsy-specific, PDX-specific, or common somatic mutations. **(C)** Comparison of copy number variations (CNV) identified in CCA_PDXs tumors and the original biopsy samples. **(D)** Diagrams of FGFR2 gene fusions identified in four paired biopsy–PDX samples. Fusion mRNAs (including FGFR2) and their fusion partners are indicated, as well as the predicted protein products of the fusions with their functional domains. Numbers represent the exon of the corresponding genes.

1.3. Short-term *ex vivo* 3D culture of CCA_PDX-derived cells for evaluating drug efficacy.

Although PDX models are valuable for preclinical studies, expanding these models *in vivo* for drug efficacy evaluation is costly and time-consuming. Several studies have demonstrated that tumor cells derived from PDXs can be maintained in *ex vivo* 3D culture systems and used for "pre–*in vivo*" drug screens [100, 300-302]. Importantly, the drug responses obtained from these *ex vivo* culture systems are highly predictive of those from their *in vivo* PDX counterparts. We therefore aimed to establish and optimize a short-term *ex vivo* 3D culture protocol for tumor cells derived from our CCA_PDXs (**Fig R4A**). Briefly, single-cell suspensions were obtained from CCA_PDXs and seeded out on a Matrigel pre-coated dish; after 24 hours, tumoroids began to form at the interface between the culture medium and Matrigel (see Materials and methods). These tumoroids could be grown in culture for at least 10 days (**Fig R4B**), and they maintained CCA histopathologic features and marker expression (e.g., KRT19^{+}/HepPar1^{-}) (**Fig R4C**).

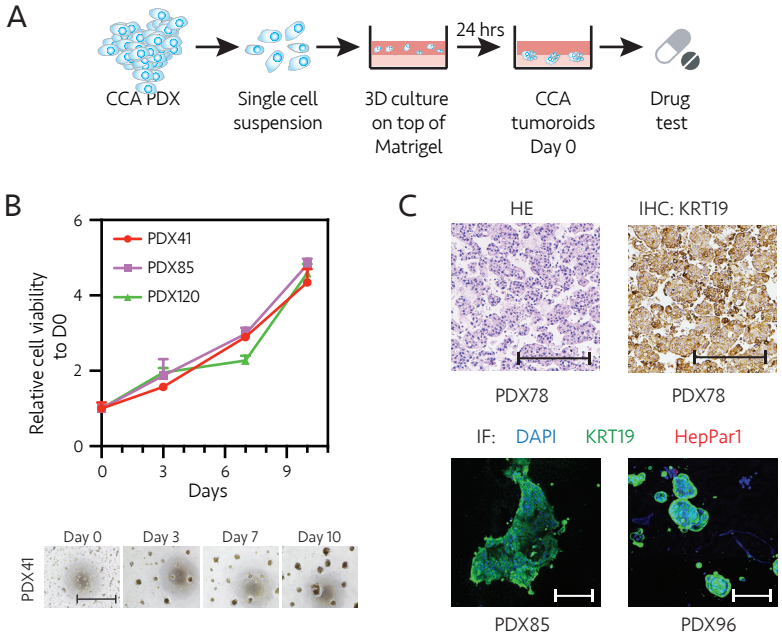

Figure R4. Tumoroids derived from CCA_PDXs proliferate in culture for at least 10 days and maintain CCA histopathological features. (A) Schematic illustration of the process of *ex vivo* 3D culture of tumoroids derived from CCA_PDX. **(B)** Top row: cell proliferation of CCA_PDX-derived tumoroids was determined using CellTiter-Glo assays. Data were normalized to cell viability measured

on day 0 (D0) and are mean ± s.d. from three independent replicates. Bottom row: representative bright-field images of cells derived from PDX41 and cultured *ex vivo*. Images are from days 0, 3, 7, and 10. Scale bar, 1 mm. **(C)** Histopathologic characterization of tumoroids generated using CCA_PDX-derived cells cultured *ex vivo* for 10 days. Top row: H&E staining (left); immunohistochemistry for the CCA marker KRT19 (right); bottom row: CCA marker KRT19 and the hepatocellular carcinoma marker HepPar1; representative images are shown. Scale bars, 250 μm (top row), 50 μm (bottom row).

To test whether this system can be used as a platform for preclinical drug efficacy evaluation, we first focused on a novel bromodomain and extraterminal domain (BET) inhibitor, NEO2734. BET inhibitors have demonstrated efficient anti-tumor activities in both hematopoietic and solid tumors, including CCA [110, 303-306]. NEO2734 is a novel potent BET-CBP/p300 dual inhibitor, and its antitumoral activity has been shown using *in vitro* cell lines, *ex vivo* organoids, and *in vivo* PDX of multiple cancer types [307-309]. We found that NEO2734 showed significant anti-proliferative effects in tumoroids derived from different CCA_PDXs, with an average half maximal inhibitory concentration (IC_{50}) of 685.3 nM (**Fig R5A**), indicating its potential application for CCA treatment. Next, we verified whether results obtained in CCA tumoroids were predictive of the drug response in CCA_PDXs *in vivo*. For this, PDX78 was first expanded in NOD-SCID mice and then treated with vehicle or NEO2734. In agreement with the results obtained *ex vivo*, NEO2734 significantly inhibited the PDX78 tumor growth *in vivo* (**Fig R5B**).

Furthermore, we also tested whether the CCA tumoroids can recapitulate drug responses observed in CCA patients. We used two CCA_PDX models derived from a patient with *FGFR2* fusion. The PDX75 was developed before FGFR inhibitor treatment, and the PDX75.2 after therapy with progressive disease (**Fig R5C**). We found that tumoroids derived from PDX75 were more sensitive to FGFR inhibitor pemigatinib treatment than those derived from PDX75.2 (**Fig R5D**). Of note, in PDX75.2 and the corresponding patient biopsy samples, we could identify *FGFR2* V564L mutation, which has been associated with acquired resistance to FGFR inhibitor in CCA [310-312].

Thus, we have established a short-term, *ex vivo* 3D culture system for tumor cells derived from CCA_PDXs; this CCA tumoroid culture system can be used for rapid drug efficacy tests. Notably, the results obtained from this system agreed with those observed in CCA_PDXs and CCA patients.

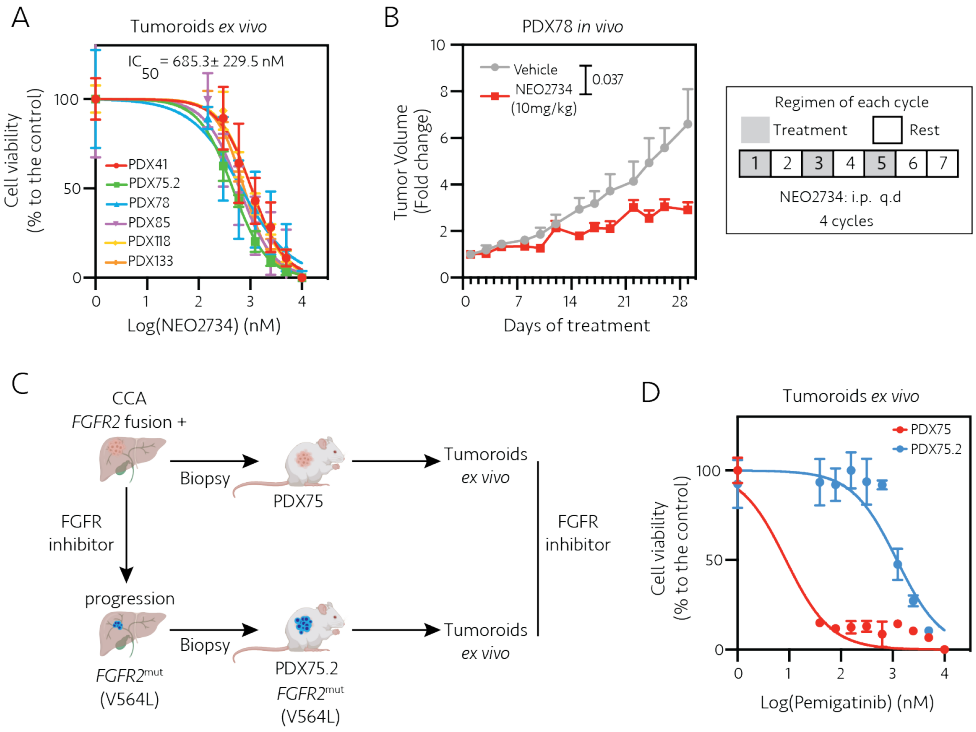

Figure R5. *Ex vivo* 3D culture of tumors derived from CCA_PDXs can be used to evaluate drug efficacy and predict *in vivo* CCA_PDXs and CCA patient drug responses. (A) NEO2734 dose-response curves for a panel of CCA_PDX-derived tumoroids cultured *ex vivo*. Cell viability was determined using a Cell Titer-Glo assay on day 7 (the initiation of treatment was considered as day 1). Data are mean ± s.d. from independent biological replicates (PDX41, n=5; PDX75.2, n=2; PDX78, n=6; PDX85, n=6; PDX118, n=3; PDX113, n=3). **(B)** Effects of NEO2734 evaluated *in vivo* using PDX78. Mice implanted with PDX78 were treated intraperitoneally three times per week for four weeks with either vehicle (n=6) or NEO2734 (10 mg kg–1) (n=6). Each tumor volume was normalized to its volume measured on day 1 of treatment (D1). Data are mean ± s.e.m. (multiple t-tests); the P-value was from data of day 29. **(C)** Schematic illustration of the process of establishing two PDX models from a CCA patient with *FGFR2* fusion (prior to FGFR inhibitor treatment and in progression) and using tumoroids derived from the paired PDXs to test the efficacy of FGFR inhibitor. **(D)** FGFR inhibitor pemigatinib dose-response curves for PDX75- and PDX75.2-derived tumoroids cultured *ex vivo*. Cell viability was determined using a Cell Titer-Glo assay on day 7 (the initiation of treatment was considered as day 1). Data are mean ± s.d. from independent biological replicates (PDX75, n=3; PDX75.2, n=3).

2. Evaluation of the PARP inhibition efficacy in CCA

2.1. PARP inhibitor treatment inhibits the growth of *BRCA2*^{mut} CCA_PDX, but not those harboring *IDH1*, *ARID1A* or *BAP1* mutations

Pathogenic mutations of *IDH1*/2, *ARID1A*/*B*, *BAP1*, and *BRCA1/2* have been found in many types of solid tumors [313], including 30-50% of patients with CCA [14, 15, 169, 298, 299]. Thus, efforts have been made to discover the vulnerability of cancer cells harboring these mutations and to design novel therapeutic strategies accordingly. Notably, the oncometabolite 2-HG produced by mutant IDH1/2 enzymes, and loss of function of ARID1A, BAP1, or BRCA2 have been previously claimed to impair the homologous recombination (HR) pathway, rendering cancer cells sensitive to PARP inhibitor (PARPi) treatment [178, 179, 228, 238, 314, 315]. However, preclinical evidence supporting the employment of PARPi in advanced CCA with these mutations is still missing. Among our 19 established CCA_PDX models, thirteen have confirmed pathogenic mutations of *IDH1* (n=7), *IDH2* (n=1), *ARID1A* (n=1), *BAP1* (n=3), or *BRCA2* (n=1), and 1 with *ARID1A* deletion (PDX84). Of note, we confirmed that all *IDH1/2*^{mut} CCA_PDXs produced significantly higher levels of 2-HG compared to those CCA_PDXs with the wild-type form of *IDH1/2* (*IDH1/2*^{wt}) (average 22.82 μg mL^{-1} for *IDH1/2*^{mut}, versus average 0.06 μg mL^{-1} for *IDH*^{wt}) (**Fig R6A**).

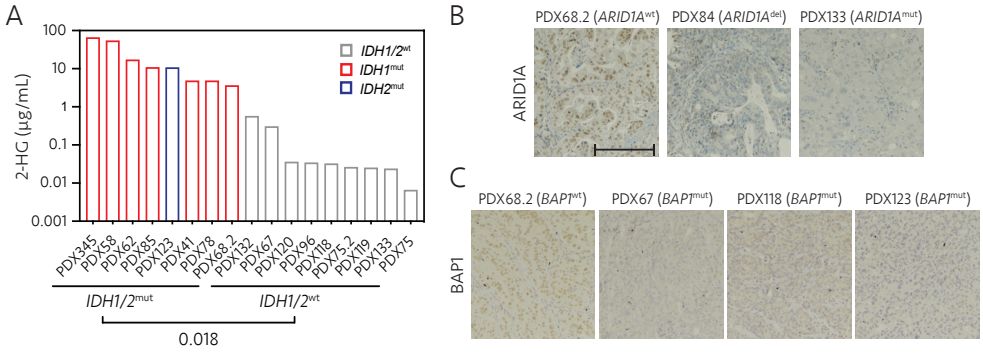

Figure R6. Phenotypic characterization of *IDH1/2*^{mut}, *ARID1A*^{mut} and *BAP1*^{mut} CCA_PDXs. (A) Quantification of 2-HG by LS-MS in *IDH1/2*^{mut} CCA_PDXs (n = 8) and *IDH1*^{wt} CCA_PDXs (n = 9). Unpaired t-tests were used for statistical analysis. **(B)** Representative images of immunohistochemical staining for ARID1A in *ARID1A* altered PDXs (PDX84 and PDX133, with an *ARID1A* deletion (del) and truncating mutation, respectively). **(C)** Representative images of immunohistochemical staining for BAP1 in *BAP1*^{mut} PDXs (PDX67, -118, and -123). PDX68.2, wild type for both *ARID1A* and *BAP1*, was used as a positive control in both cases. Scale bar, 250 μm.

We also checked if *ARID1A* and *BAP1* mutations indeed generated a loss of the corresponding protein (**Fig R6B** and **C**, respectively). ARID1A and BAP1 expression was absent in the tumoral cells of the samples harboring genomic alterations in these genes. The positive staining in these samples corresponds to mouse stromal cells infiltrating the tumoral compartment. Thus, our models are suitable for checking PARPi efficacy.

We then tested the effects of each of three PARPi (i.e., olaparib, pamiparib, and niraparib) using the established *ex vivo* 3D culture system of tumor cells derived from CCA_PDXs harboring genomic alterations in *IDH1*, *ARID1A*, *BAP1,* or *BRCA*2. Of note, these PARPi are either approved by the FDA or are currently being evaluated in multiple clinical trials [316]. As controls, we also included cells derived from CCA_PDXs harboring none of these mutations (wild-type CCA_PDXs). We found that, among all tumoroid models tested, only those derived from *BRCA2*^{mut} CCA_PDX (PDX119, black line) were sensitive to olaparib and pamiparib treatments (**Fig R7A** and **B).** In contrast, neither tumoroids derived from wild-type CCA_PDXs nor those derived from CCA_PDXs harboring *IDH1, ARID1A*, or *BAP1* alterations were found to be sensitive to any of the three PARPi treatments (IC50 >10 μM) (**Fig R7A** and **B**).

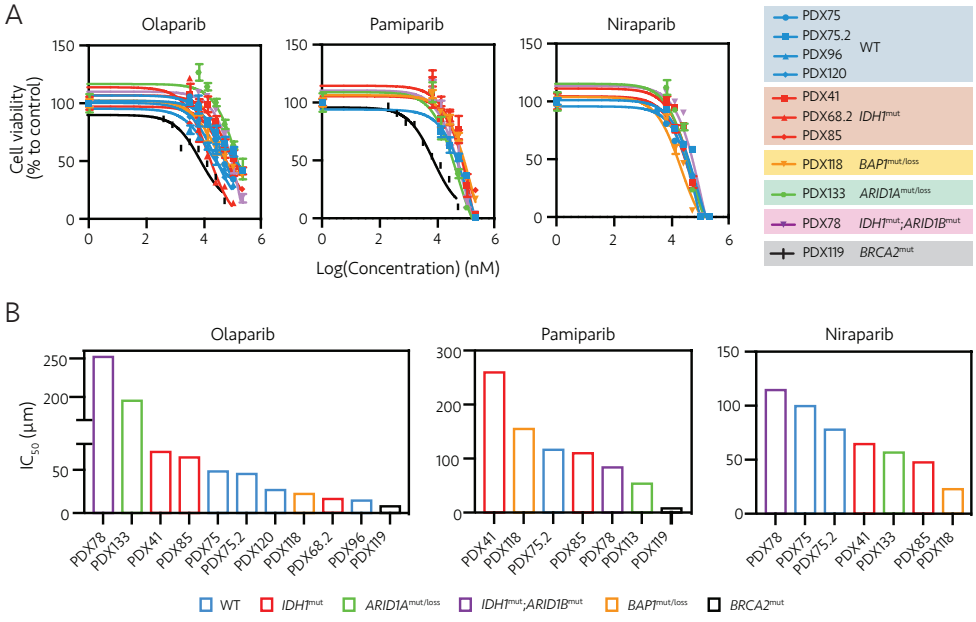

Figure R7. PARPi inhibits the growth *ex vivo* of CCA_PDXs with a *BRCA2* mutation, but not of those with *IDH1*^{mut}, *ARID1A*^{mut}, or *BAP1*^{mut}. (A) Dose-response curves of olaparib (left), pamiparib (middle), or niraparib (right) for a panel of tumoroids derived from CCA_PDXs. Cell viability was de-

termined using a Cell Titer-Glo assay seven days after the treatment initiation. Data are mean ± s.d. from independent biological replicates. For olaparib treatment: PDX41, n=8; PDX68.2, n=2; PDX78, n=6; PDX85, n=11; PDX75, n=2; PDX75.2, n=4; PDX96, n=2; PDX118, n=3; PDX120, n=2; PDX133, n=3; and PDX119, n=3. For pamiparib treatment, PDX41, n=6; PDX78, n=6; PDX85, n=9; PDX75.2, n=2; PDX118, n=3; PDX133, n=3; PDX119, n=3. For niraparib treatment: PDX41, n=3; PDX78, n=3; PDX85, n=6; PDX75, n=2; PDX75.2, n=2; PDX118, n=3; PDX133, n=3. **(B)** Half-maximal inhibitory concentration (IC50) of olaparib (left), pamiparib (middle), and niraparib (right) in tumoroids derived from CCA_PDXs.

Importantly, and in line with these findings, olaparib or pamiparib treatment did not affect the *in vivo* growth of PDX85 (*IDH1*^{mut}, R132C) (**Fig R8A**).

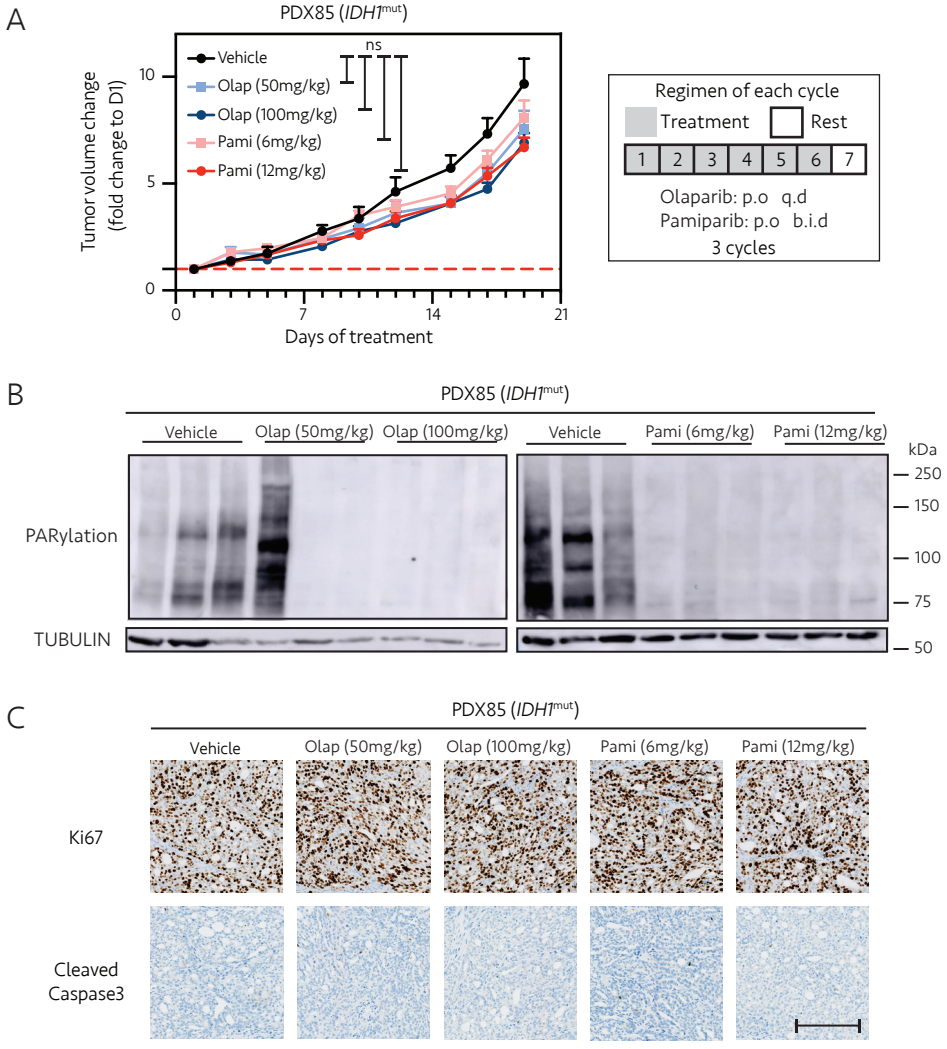

Figure R8. PARP inhibition does not affect the *in vivo* growth of *IDH1*^{mut} PDX85. (A) Effects of olaparib and pamiparib evaluated *in vivo* using PDX85 (*IDH1*^{mut}). Mice implanted with PDX85 were

treated orally six times per week with either vehicle (n=8) or olaparib (at a low or high dose, of 50 or 100 mg kg–1, respectively) (each n=10) or pamiparib (at a low or high dose, of 6 or 12 mg kg–1, respectively) (each n = 8). Each tumor volume was normalized to its volume on D1. Data are mean ± s.e.m. (two-way ANOVA multiple comparisons with Tukey´s correction); the indicated P value reflects data from D20. **(B)** Western blot analysis of the effect of olaparib and pamiparib *in vivo* treatment of PDX85 on PARylation. TUBULIN is used as a loading control. **(C)** Representative images of immunohistochemical staining for a cell proliferation marker (Ki67) and apoptosis marker cleaved caspase 3 in PDX85 cells treated *in vivo* with olaparib and pamiparib.mined using a Cell Titer-Glo assay seven days after the treatment initiation. Data are mean ± s.d. from independent biological replicates. For olaparib treatment: PDX41, n=8; PDX68.2, n=2; PDX78, n=6; PDX85, n=11; PDX75, n=2; PDX75.2, n=4; PDX96, n=2; PDX118, n=3; PDX120, n=2; PDX133, n=3; and PDX119, n=3. For pamiparib treatment, PDX41, n=6; PDX78, n=6; PDX85, n=9; PDX75.2, n=2; PDX118, n=3; PDX133, n=3; PDX119, n=3. For niraparib treatment: PDX41, n=3; PDX78, n=3; PDX85, n=6; PDX75, n=2; PDX75.2, n=2; PDX118, n=3; PDX133, n=3.

One of the main antitumoral mechanisms displayed by PARPi is the blocking of PARP1/2 poly-ADP-ribosylation (PARylation) reactions, impeding this post-translation modification on target proteins and, in consequence, the signal for the recruitment of DNA repair factors to the damaged site [317]. We found that PARylation decreased upon *in vivo* treatment with PARPi (**Fig R8B**), excluding thus the possibility of a suboptimal delivery of the drug to the tumor site and a compromised inhibitor activity in our *in vivo* experimental setting. Further immunohistochemistry (IHC) analysis for the cell proliferation marker Ki67 and the apoptosis marker cleaved-caspase 3 revealed that PARPi treatment did not alter *IDH1*^{mut} tumor cell proliferation or apoptosis *in vivo* (**Fig R8C**).

To strengthen the results, PARPi efficacy *in vivo* was also validated in two other *IDH1*^{mut} models, PDX78 (*IDH1*^{mut}, R132L; *ARID1B*^{mut}) and PDX41 (*IDH1*^{mut}, R132C), and an *ARID1A*^{mut} model, PDX133 (harboring a frameshift insertion in *ARID1A*) (**Fig R9**). We found that PARPi was not able to alter tumor growth in any of these models, confirming the results observed in the *ex vivo* setting.

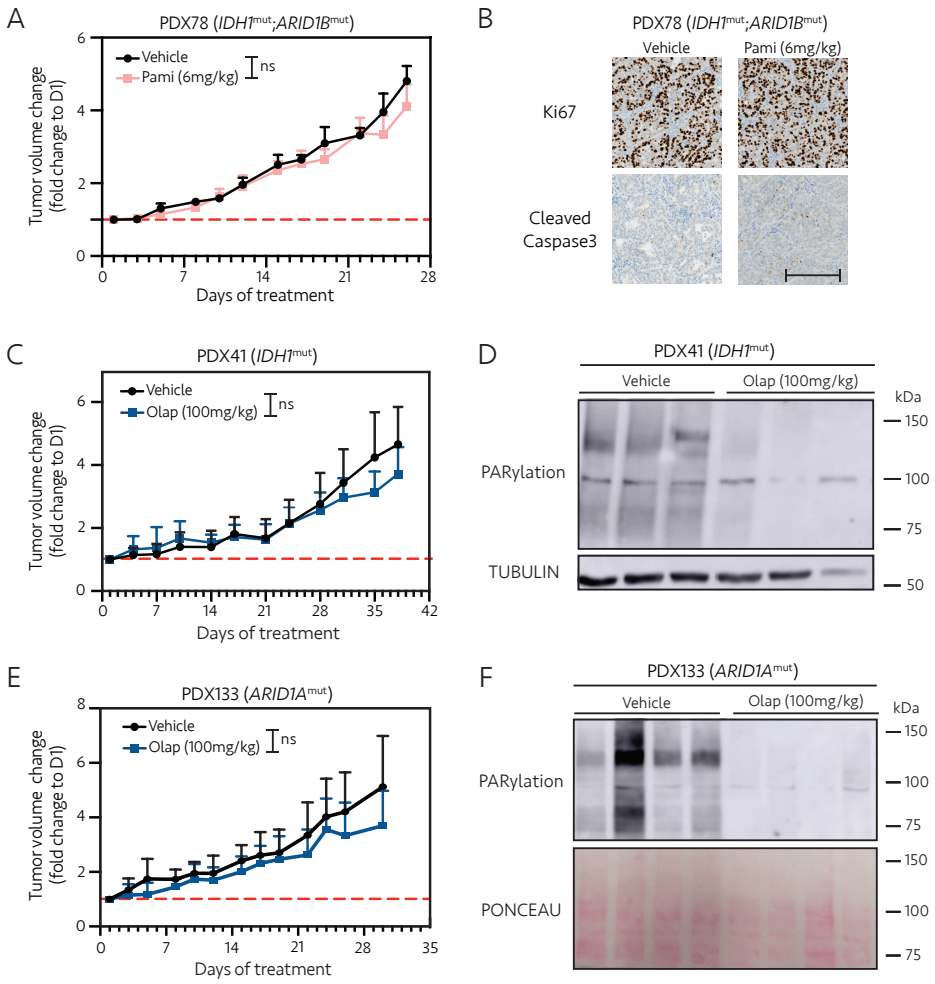

Figure R9. Absence of PARP inhibitor *in vivo* efficacy in *IDH1*^{mut}*ARID1B*^{mut} PDX78, *IDH1*^{mut} PDX41, and *ARID1A*^{mut} PDX133. (A) Effects of pamiparib evaluated *in vivo* using PDX 78 (*IDH1*^{mut}*ARID1B*^{mut}). Mice implanted with PDX78 were treated orally with either vehicle (n=5) or pamiparib (6 mg kg–1) (n=5) six times per week. Each tumor volume was normalized to its volume measured on day 1 of treatment (D1). Data are mean ± s.e.m. (multiple t-tests); the indicated P value was from day 27. **(B)** Representative images of immunohistochemical staining for a cell proliferation marker (Ki67) and apoptosis marker cleaved caspase 3 in PDX78 cells treated *in vivo* with pamiparib. **(C)** Effects of olaparib evaluated *in vivo* using PDX41 (*IDH1*^{mut}). Mice implanted with PDX41 were treated orally with either vehicle (n=10) or olaparib (100 mg kg–1) (n=10) six times per week. Each tumor volume was normalized to its volume measured on day 1 of treatment (D1). Data are mean ± s.e.m. (multiple t-tests); the indicated P value was from day 40. **(D)** Western blot analysis of the effect of olaparib *in vivo* treatment of PDX41 on PARylation. TUBULIN is used as a loading control. **(E)** Effects of olaparib evaluated *in vivo* using PDX133 (*ARID1A*^{mut}). Mice implanted with PDX133 were treated orally with either vehicle (n=8) or olaparib (100 mg kg–1) (n=8) six times per week. Each tumor volume was normalized to its volume measured on day 1 of treatment (D1). Data are mean ± s.e.m. (multiple t-tests); the indicated P value was from day 30. **(F)** Western blot analysis of the effect of olaparib *in vivo* treatment of PDX133 on PARylation. Ponceau S staining is used as a loading control.

In contrast, olaparib treatment significantly inhibited the tumor growth of PDX119 (*BRCA2*^{mut}, G3076R) (**Fig R10**), consistently confirming our *ex vivo* data (**Fig R7**). Of note, this observation agrees with the demonstrated synthetic lethality of PARPi in *BRCA2*^{mut} breast, prostate, and ovarian cancers [318-320].

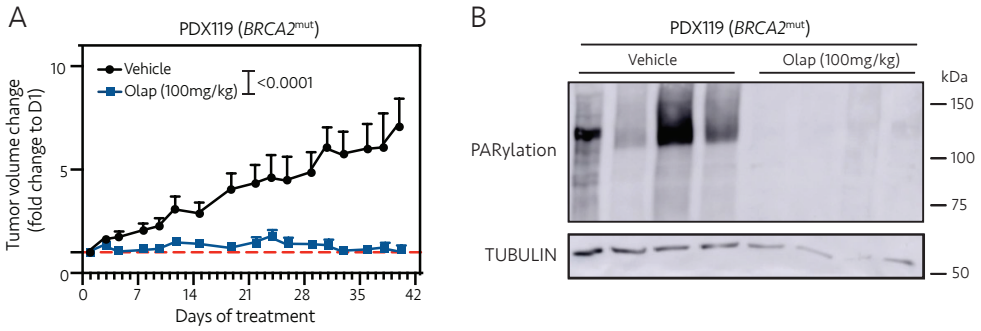

Figure R10. PARPi inhibits the growth of the CCA_PDX with a *BRCA2* mutation. (A) Effects of olaparib evaluated *in vivo* using PDX119 (*BRCA2*^{mut}). Mice implanted with PDX119 were treated orally with either vehicle (n=5) or olaparib (100 mg kg–1) (n=5) six times per week. Each tumor volume was normalized to its volume measured on day 1 of treatment (D1). Data are mean ± s.e.m. (multiple t-tests); the indicated P value was from day 40. **(B)** Western blot analysis of the effect of olaparib and pamiparib *in vivo* treatment of PDX119 on PARylation. TUBULIN is used as a loading control.

Moreover, a 73-year-old male patient with metastatic CCA with a pathogenic *BRCA2* mutation (D2723H) was identified by next-generation sequencing (FoundationOne Panel). This patient was initially diagnosed with localized extrahepatic CCA (T2N2M0), and had received surgical resection (R0) and adjuvant chemotherapy with capecitabine. Unfortunately, multiple metastatic lesions were found after the adjuvant chemotherapy, mainly localized in the celio-mesenteric lymph nodes. He then received cisplatin/gemcitabine, carboplatin/gemcitabine, and durvalumab/tremelimumab (as part of the IMMUNO-BIL clinical trial, NCT03704480) treatments. Because pathogenic *BRCA2* mutation (D2723H) was identified in the tumor samples, he was compassionately treated with olaparib at a dose of 300 mg PO twice daily, continuously. After 10 weeks of treatment, computed tomography (CT) scans showed regressions of several target lesions (**Fig R11**).

Thus, our results showed that PARPi treatments are effective in advanced CCA patient-derived preclinical models with *BRCA2* mutations, but not those harboring *IDH1, ARID1A*, or *BAP1* alterations. In agreement, olaparib showed clinical activity in a CCA patient with a pathogenic *BRCA2* mutation.

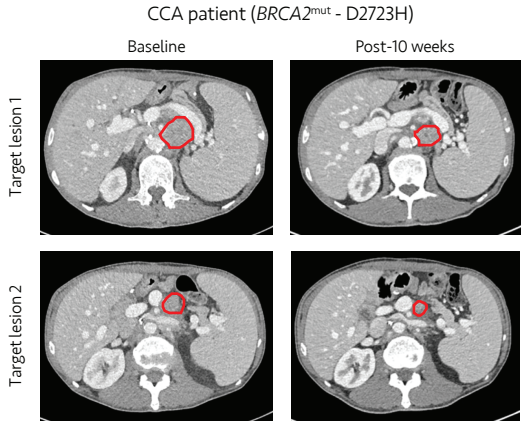

Figure R11. PARPi inhibits the growth of a CCA patient with a *BRCA2* mutation. CT scan images of a 73-year-old male metastatic CCA patient with a pathogenic *BRCA2* mutation at baseline and after 10 weeks of olaparib treatment. Target lesion 1 (adjacent to the splenic vein) and target lesion 2 (mesenteric) were outlined in red lines.

2.2. RAD51 scoring predicts that *IDH1*^{mut}, *ARID1A*^{mut}, and *BAP1*^{mut} CCA patients may not benefit from PARP inhibitor treatment

The rationale for using PARPi to treat *IDH1/2*^{mut}, *ARID1A*^{mut}, *BAP1*^{mut}, or *BRCA2*^{mut} tumors is based on the reported findings that cells harboring these mutations are defective for HR [178, 179, 228, 238, 314, 315]. As we only observed the expected antitumoral effects of PARPi in *BRCA2*^{mut} CCA_PDX, and as this effect was not found in tumoroids or CCA_PDXs with *IDH*, *ARID1A*, or *BAP1* mutations, we next sought to examine the HR status of these CCA_PDXs to determine whether they are HR proficient (HRP) or HR deficient (HRD). We used a recently developed RAD51 assay to estimate HR status in routine formalin-fixed paraffin-embedded (FFPE) tumor samples [225, 226]. This assay analyzes nuclear immunofluorescence staining of the DNA repair protein RAD51 (RAD51), geminin, and DAPI. Tumors were considered HRP if more than 10% of geminin^{+} tumor cells had more than five RAD51^{+} foci (**Fig R12A**). Otherwise, the tumor was scored as HRD. Moreover, immunofluorescence of the phosphorylation of the Ser-139 residue of the histone variant H2AX (γH2AX) was also scored on a consecutive slide to evaluate the basal DNA damage level of the tumor. Of note, the RAD51 assay has been applied in multiple clinical trials and PDX models, and tumors with HRD profiles scored by this assay showed responses to PARP inhibitors with high sensitivity and specificity [321-324].

Using this assay, we found that 17 out of 18 tested CCA_PDXs showed RAD51 scores

above 10% (**Fig R12B**), which is compatible with an HRP profile. Only PDX119 and its original patient samples, with a biallelic pathogenic *BRCA2* mutation showed, as expected, a RAD51 score below 10%, compatible with an HRD profile (**Fig R12B** and **Fig R13).** All samples showed significant DNA damage (γH2AX score median, 59%; IQR, 52%-74%). Importantly, *IDH1/2*^{mut}, *ARID1A/B*^{mut}, and *BAP1*^{mut} CCA_PDXs scored as HRP, similar to the wild-type CCA_PDXs (**Fig R12B**). In line with these findings, we also found that the RAD51 scores increased in the PDX85 (*IDH1*^{mut}) tumors treated with olaparib or pamiparib *in vivo* (**Fig R12C**), indicating that the HR repair pathway is not significantly impaired in these tumors.

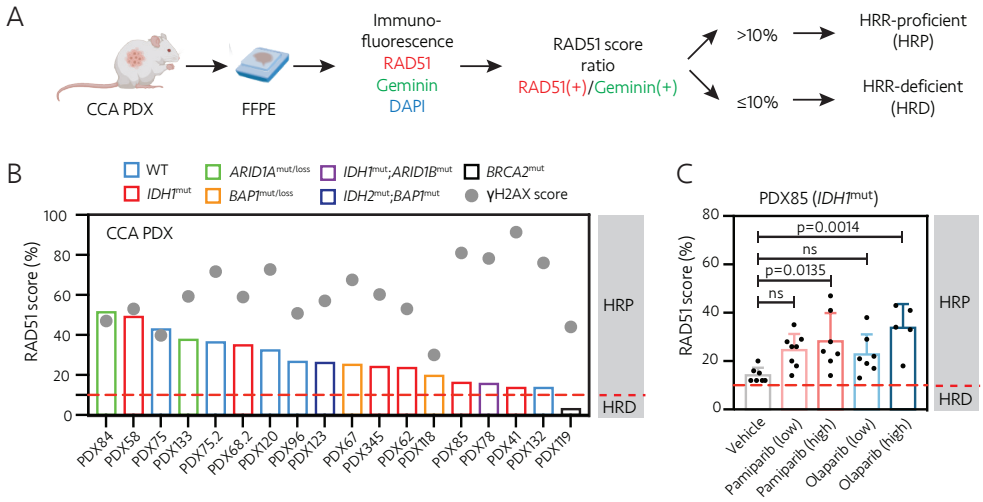

Figure R12. RAD51 assay in CCA_PDXs. (A) Schematic illustration of the RAD51 assay and criteria used to define the proficiency or deficiency of HR repair in FFPE samples. **(B)** RAD51 scores (bars) and γH2AX scores (dots) evaluated in a panel of 18 CCA_PDXs. **(C)** RAD51 scores evaluated at the endpoint (day 20) in PDX85 (*IDH1*^{mut}) treated as in Figure R8. Data are presented as mean ± s.d. and were analyzed by one-way ANOVA multiple comparisons with Dunnett correction. $P < 0.05$ compared to vehicle.

Moreover, we also confirmed that the original CCA biopsy specimens scored concordantly with their matched CCA_PDXs (**Fig R13**), suggesting that the HR repair status observed was not due to the PDX setting but instead was representative of the patient sample of origin. These results demonstrated that in this panel of CCA_PDXs, mutations of *IDH1/2*, *ARID1A/B*, or *BAP1* were not associated with an HRD profile, which would explain the absence of a PARPi treatment sensitivity in these CCA_PDXs.

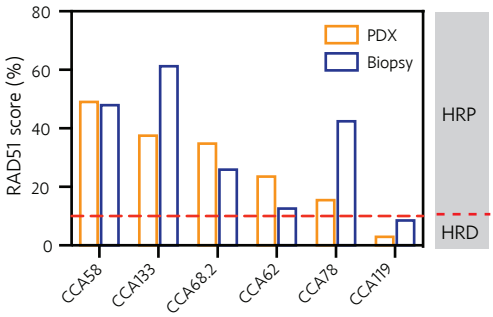

Figure R13. The RAD51 scores of CCA_PDXs concord with those from the original patient biopsy samples.

To further strengthen our findings, we also analyzed an independent cohort of metastatic CCA patients using the RAD51 assay (**Fig R14A**). This analysis confirmed the HRD profiles in CCA patients with pathogenic mutations of *BRCA2* (n=2) (**Fig R14B**). In contrast, CCA patients with pathogenic mutations of *IDH1/2* (n=10), *ARID1A* (n=3), or *BAP* (n=7) showed HRP profiles (**Fig R14B**).

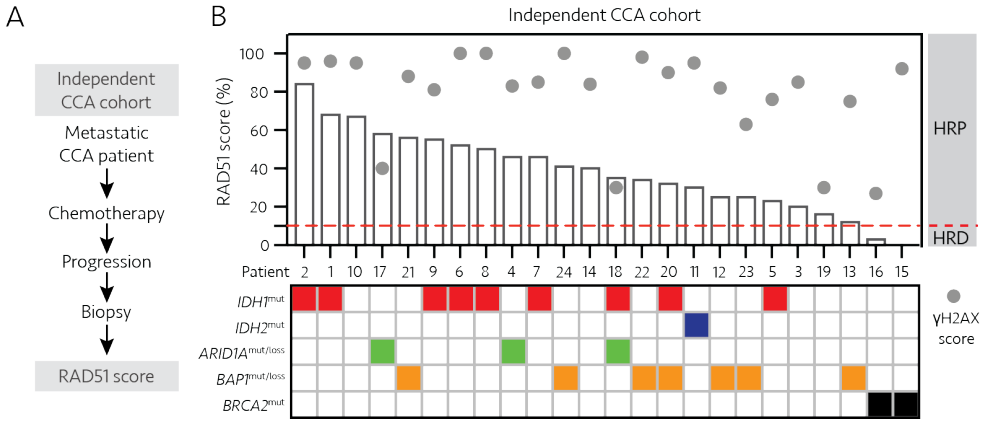

Figure R14. RAD51 assay in CCA patients. (A) Schematic illustration of the RAD51 assay performed in an independent CCA cohort (biopsy samples from advanced CCA patients refractory to chemotherapy). **(B)** RAD51 scores (bars) and γH2AX scores (dots) evaluated in an independent CCA cohort. Pathogenic mutations of *IDH1, IDH2, ARID1A, BAP1*, and *BRCA2* were indicated.

We concluded that pathogenic mutations of *BRCA2*, but not those of *IDH1/2*, *ARID1A*, and *BAP1*, are associated with the HR deficiency profile, at least in metastatic CCA that has progressed following chemotherapy. Importantly, these data also suggest that metastatic CCA patients with *BRCA2* mutations, but not those with *IDH1/2*, *ARID1A* or *BAP1*, are likely to benefit from PARPi treatment.

3. Study of the role of *IDH1* mutation in CCA by an in-depth transcriptomic and DNA methylation characterization of *IDH1*^{mut} CCA_PDXs

We demonstrated that *IDH1*^{mut} CCAs are not associated with HRD, at least not in the advanced metastatic CCA setting that has progressed to platinum-based chemotherapy. To uncover the vulnerabilities of *IDH1*^{mut} CCAs that could be useful for designing new therapeutic strategies, we sought to further characterize the *IDH1*^{mut} CCA tumors. To understand the unique molecular features of *IDH1*^{mut} CCA_PDXs as compared to *IDH1*^{wt} ones, we collected samples from six *IDH1*^{mut} and six *IDH1*^{wt} CCA_PDXs and performed a) genome-wide RNA sequencing (RNA-seq) and b) bisulfite conversion followed by Infinium MethylationEPIC array (**Fig R15**). In the following section, we will present the transcriptomic study results and the DNA methylation characterizations.

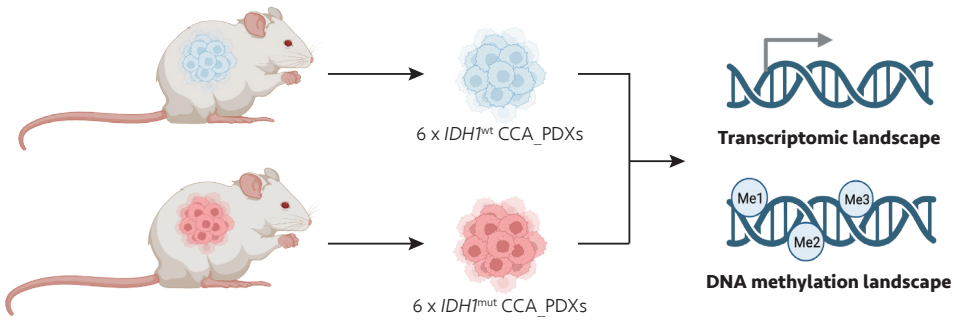

Figure R15. The experimental strategy used to study the role of *IDH1* mutation in CCA_PDXs. Schematic representation of the experimental design followed to approach the research question. In-depth transcriptomic and DNA methylation analyses were conducted with six each of *IDH1*^{wt} and *IDH1*^{mut} CCA_PDXs to understand better the role of the *IDH1* mutation in CCA pathogenesis.

3.1. Transcriptomic profiling of CCA_PDXs

3.1.1. Unsupervised hierarchical clustering separated CCA_PDX samples into two distinct clusters.

With RNA-seq data, we first performed a dimensionality reduction by principal component analysis (PCA) and unsupervised hierarchical clustering. This analysis revealed that CCA_PDX samples could be separated into two clusters (**Fig R16A**). Notably, the two clusters are enriched with *IDH1*^{mut} or *IDH1*^{wt} CCA_PDXs, respectively, suggesting that

the mutation status of *IDH1* is a significant factor associated with the cluster separation. Moreover, we also analyzed the group of genes that contributes the most to the cluster separation (namely "metagene") (**Fig R16B**). We found that Cluster number 1, including all *IDH1*^{mut} tumors and the outlier *IDH1*^{wt} PDX133, was enriched in metabolic processes, such as fatty acid metabolism or the biosynthesis of bile acids (metagene 1). *IDH1*^{wt} tumors, which were specified with metagene 2, are mainly enriched in developmental pathways, such as WNT-β-catenin and Notch, immune-related pathways, and epithelial-to-mesenchymal transition (EMT) factors.

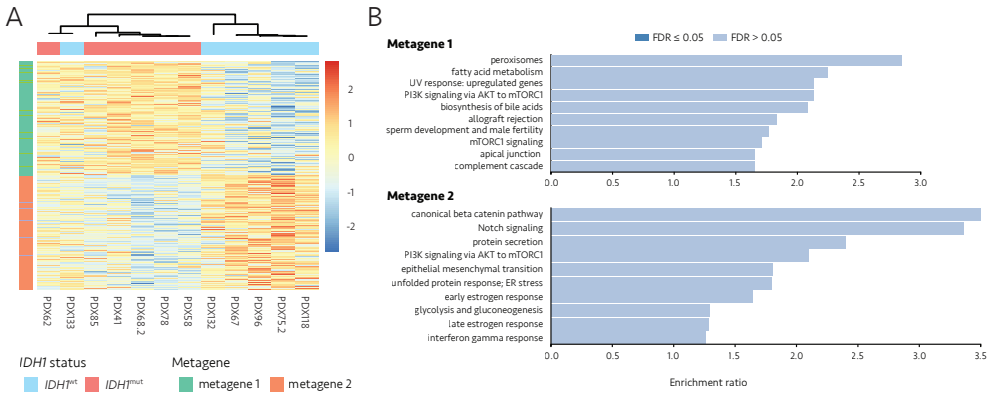

Figure R16. Unsupervised clustering of RNA-seq data separated CCA_PDX samples according to *IDH1* mutation status. After removing mouse read contamination, low-expressed genes were filtered out, and RNA expression data were analyzed by dimensionality reduction (PCA) and unsupervised hierarchical clustering. Two groups of genes contributing the most to cluster separation (metagenes) were identified. **(A)** Unsupervised clustering of CCA_PDXs based on RNA-seq data. **(B)** Gene set enrichment of the two metagenes. FDR, False Discovery Rate.

3.1.2. Differential expression analysis revealed a significant downregulation of gene expression in *IDH1*^{mut} CCA_PDXs as compared to *IDH1*^{wt}.

Next, we performed differential expression (DE) analysis by comparing *IDH1*^{mut} and *IDH1*^{wt} CCA_PDXs. This analysis revealed that 575 genes were significantly dysregulated in *IDH1*^{mut} CCA_PDXs as compared to *IDH1*^{wt} ones. Interestingly, 447 genes were downregulated in *IDH1*^{mut} tumors (**Fig R17A**). Furthermore, Gene Set Enrichment Analysis (GSEA) using the Hallmark database also identified different biological processes enriched in *IDH1*^{mut} and *IDH1*^{wt} CCA_PDXs (**Fig R17B**). Of note, pathways related to hypoxia, estrogen response, EMT, and the immune system (Inflammatory response and

Tumor Necrosis Factor (TNF) signaling via Nuclear Factor-κB (NFκB) appeared to be downregulated in *IDH1*^{mut} CCA_PDXs.

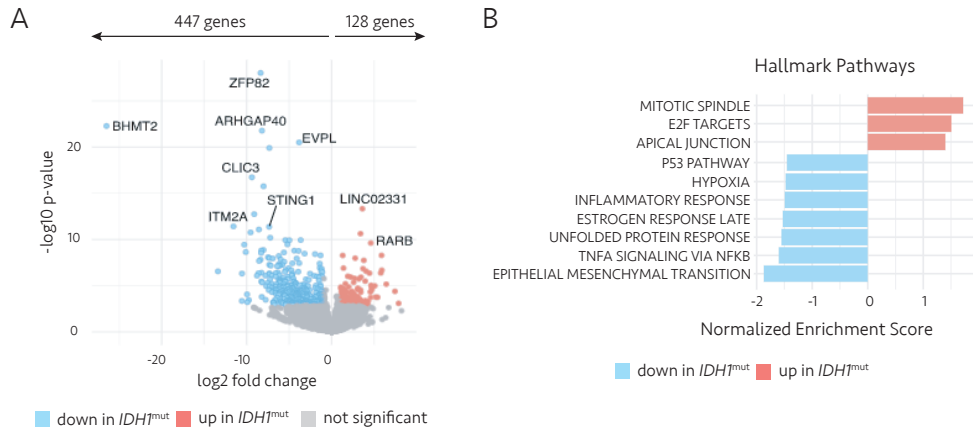

Figure R17. Differential expression analysis between *IDH1*^{mut} and *IDH1*^{wt} CCA_PDXs. Differential expression analysis was performed using DESeq2, and only genes with adjusted p < 0.05 were considered significant. **(A)** Volcano plot showing the distribution of the most differentially expressed genes between groups. The genes of the most down- and up-regulated hits are indicated. **(B)** Hallmark pathways enriched in *IDH1*^{mut} compared with *IDH1*^{wt} CCA_PDXs. Only statistically significant gene sets (p < 0.05) are shown.

3.1.3. DE genes significantly overlap with metagenes.

We compared the genes found in the two analyses to understand the relationship between the DE genes (**Fig R17**) and the metagene sets described previously in the unsupervised clustering analysis (**Fig R16**). Strikingly, we observed that there is a significant overlap between metagenes and DE genes (p < 2.2e-16) (**Fig R18**), suggesting an essential contribution of *IDH1* mutational status-related differentially expressed genes to the sample clustering and highlighting the robustness of the analysis.

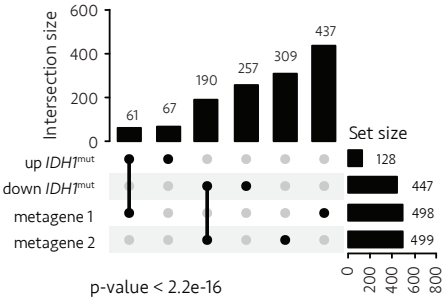

Figure R18. Metagenes obtained by unsupervised clustering significantly overlap with DE genes.

Intersection analysis between metagenes and DE genes. Intersection size defines the number of genes shared by indicated groups. Set size corresponds to the number of genes belonging to each defined group. Fisher's exact test was performed to assess the significance of the overlap.

3.1.4. The expression of the immune-related genes is downregulated in *IDH1*^{mut} CCA_PDXs.

From metagene and DE analysis, we noticed that the immune-related genes are enriched in those genes downregulated in *IDH1*^{mut} CCA_PDXs (**Fig R16** and **R17**). Of note, in a pan-cancer transcriptomic analysis, the *IDH1* mutation correlated with gene signatures of low leukocyte levels across all cancers [286]. Moreover, primary *IDH1*^{mut} grade II/III gliomas showed decreased intratumoral infiltration of $CD8^+$ T cells and reduced expression of interferon-gamma signaling compared to *IDH1*^{wt} counterparts [12, 171, 182, 183, 290, 291, 293-295]. Nonetheless, whether there is an immune dysfunction in *IDH1*^{mut} CCAs has not been fully explored [280, 284, 287, 289]. Therefore, we focused our analysis on comparing the expression of immune-related genes and pathways in our *IDH1*^{mut} and *IDH1*^{wt} CCA_PDXs.

We analyzed the pre-defined immune-related gene sets in the Hallmark database to determine whether their expression is dysregulated in *IDH1*^{mut} CCA_PDXs. We found that "Inflammatory response", "interferon-alpha (IFNα)", and "interferon-gamma (IFNγ)" signatures showed trends to be negatively enriched in our *IDH1*^{mut} CCA_PDXs (**Fig R19A**). In addition, the comparison we performed between *IDH1*^{mut} and *IDH1*^{wt} CCA_PDXs showed a noticeable decrease in the expression of genes related to various immune pathways, including chemokines, cytokines, and interleukins (**Fig R19B**). Among the downregulated genes in *IDH1*^{mut} CCA_PDXs, some examples were particularly striking, such as the stimulator of interferon genes (*STING1*), previously identified as one of the most significantly downregulated genes. It has been found that STING1 plays a crucial role in regulating the transcription of various host defense genes, including type I interferons (IFNs) and pro-inflammatory cytokines, following the recognition of abnormal DNA species [325]. The production of cytokines dependent on STING leads to the recruitment of immune cells to the tumor site. It is worth noting that STING is increasingly being recognized as having a significant role in enhancing immune responses against tumors [326-329].

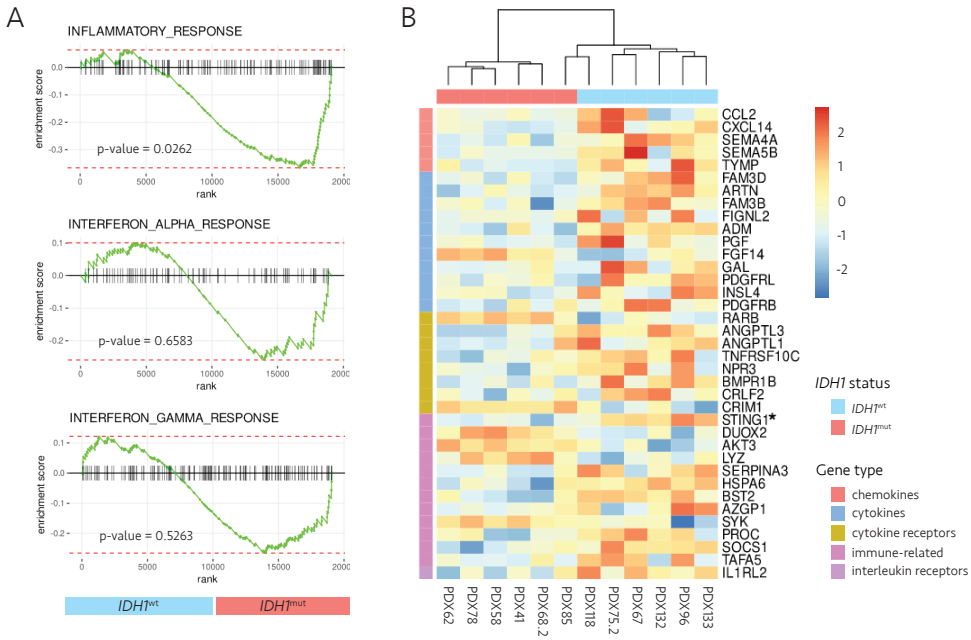

Figure R19. Immune-related gene signatures are downregulated in *IDH1*^{mut} CCA_PDXs. (A) Inflammatory response, IFNα, and IFNβ response GSEA signatures in *IDH1*^{mut} CCA_PDXs compared to *IDH1*^{wt} ones. The p-value corresponds to the NOM p-value obtained by GSEA in the Hallmark database. **(B)** Heatmap showing the difference of immune-related gene expression in *IDH1*^{mut} and *IDH1*^{wt} CCA_PDXs. The immune gene list is from the ImmPort database.

We then evaluated our samples using a 47-gene Interferon signature (IFNsign), which was meticulously crafted by combining genes from both the IFNα and IFNγ response Hallmark gene sets [330]. It is worth noting that high expression of the defined IFN signature (IFNsign^{high}) has been strongly linked to a surge in immune infiltration and a proinflammatory microenvironment in the pancreatic ductal adenocarcinoma (PDAC) [330]. Intriguingly, unsupervised clustering of samples utilizing IFNsign genes successfully segregated the samples into two groups, which were enriched by *IDH1*^{wt} and *IDH1*^{mut} samples respectably (**Fig R20A**). We next calculated the IFNsign scores of our samples and found that *IDH1*^{wt} CCA_PDXs presented a trend of higher IFNsign scores than *IDH1*^{mut} ones (**Fig R20B**).

To ensure the accuracy of our findings, we took steps to confirm that the results we obtained from the RNA-seq analysis were indeed representative of the entire CCA_PDX collection. We selected eight interferon pathway-related genes previously identified as differentially expressed between groups and used RT-qPCR to validate their expression in all of the PDXs in our bank (**Fig R20C**). We found that the differences in gene expression that

we observed were consistently maintained in the expanded sample cohort, providing further evidence of the robustness of our findings. Together, our data demonstrated a decreased immune gene expression in *IDH1*^{mut} CCA_PDXs.

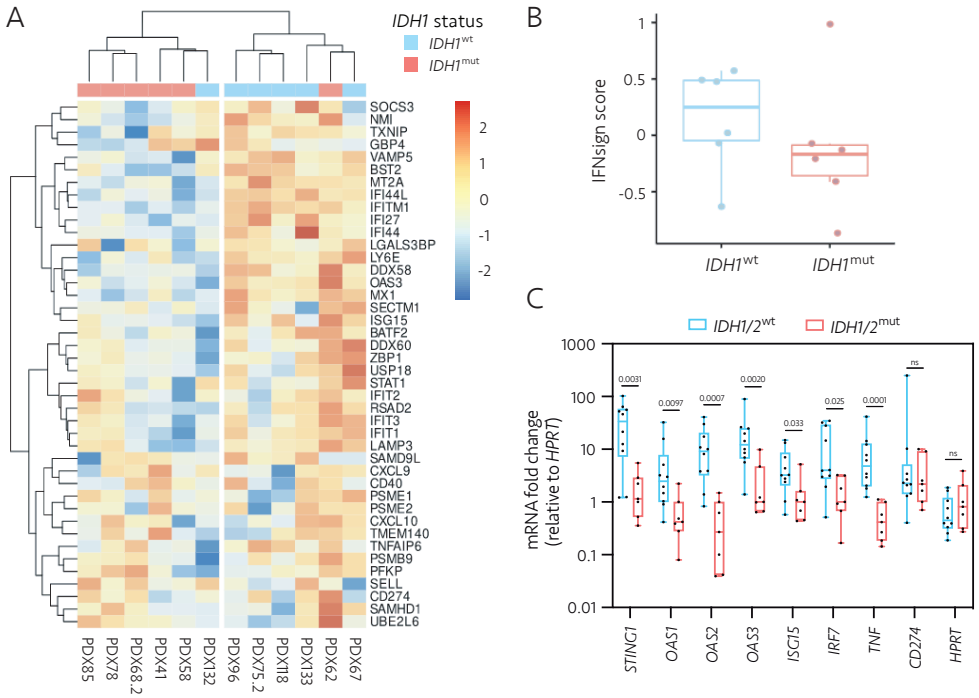

Figure R20. Genes involved in the Interferon signaling are downregulated in *IDH1*^{mut} CCA_PDXs. (A) Heatmap showing the unsupervised clustering of CCA_PDXs based on the differential expression of IFNsign genes. **(B)** IFNsign score in *IDH1*^{wt} and *IDH1*^{mut} CCA_PDXs. **(C)** RT-qPCR analysis of interferon-related gene expression in our CCA_PDXs collection. Genes evaluated were: Stimulator of Interferon Response cGAMP Interactor 1 (*STING1*), 2'-5'-Oligoadenylate Synthetase 1-3 (*OAS1-3*), Interferon Stimulated gene 15 (*ISG15*), Interferon Regulatory Factor 7 (*IRF7*), Tumor Necrosis Factor (*TNF*) and *CD274* (well-known as Programmed Cell Death 1 Ligand 1, PDL1). *HPRT* expression was used as a housekeeping gene for normalization. mRNA data are presented as mean ± s.d. and analyzed by multiple t-tests and the Wilcoxon Mann-Whitney test.

3.2. DNA methylation profiling of CCA_PDXs

Previous studies have demonstrated that mutant IDH1 generates 2-HG, resulting in increased DNA methylation in glioma [170, 171]. To delve deeper into this phenomenon in CCA, we analyzed DNA methylation in our CCA_PDX collection using the Illumina Human MethylationEPIC beadChip.

3.2.1. Unsupervised hierarchical clustering of DNA methylation data separated CCA_PDXs into two groups.

To analyze the variation between *IDH1*^{wt} and *IDH1*^{mut} CCA_PDXs, we first used Nonnegative Matrix Factorization (NMF) deconvolution to perform dimension reduction on the top 20000 variables CpG sites. Interestingly, consistent with the findings from the RNA-seq analysis, we could also identify two major clusters enriched with *IDH1*^{wt} and *IDH1*^{mut} samples, respectively (**Fig R21**). We examined a specific group of CpGs, called metaCpGs, that significantly differentiated the clusters. MetaCpG 1 had over 2000 CpGs that were hypermethylated in the *IDH1*^{mut} CCA_PDXs, while MetaCpG 2 had only 149 CpGs that showed the reverse pattern. As a result, it was evident that *IDH1*^{mut} CCA_PDXs had a hypermethylation phenotype in contrast to *IDH1*^{wt} samples.

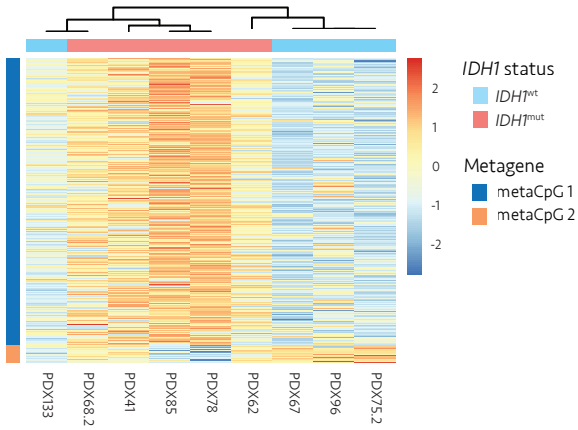

Figure R21. Unsupervised DNA methylation analysis of CCA_PDXs revealed that *IDH1*^{mut} CCA_PDX is associated with DNA hypermethylation phenotype. The methylation value of CpGs was extracted using the limma package, and CpGs with p > 0.01 were filtered out. Unsupervised clustering of the top 20000 most variable CpG sites after dimension reduction used NMF deconvolution.

3.2.2. *IDH1*^{mut} CCA_PDXs show a hypermethylation phenotype.

Examining the differences in DNA methylation of individual CpG sites between *IDH1*^{wt} and *IDH1*^{mut} CCA_PDXs revealed that most changes were gains of methylation in *IDH1*^{mut} CCA_PDXs (**Fig R22A**). After sorting the CpGs based on their locations (e.g., enhancer, gene body, or promoter), we then found that the methylation of enhancer elements and, to a lesser degree, promoter elements were hypermethylated in *IDH1*^{mut} CCA_PDXs (**Fig R22B**).

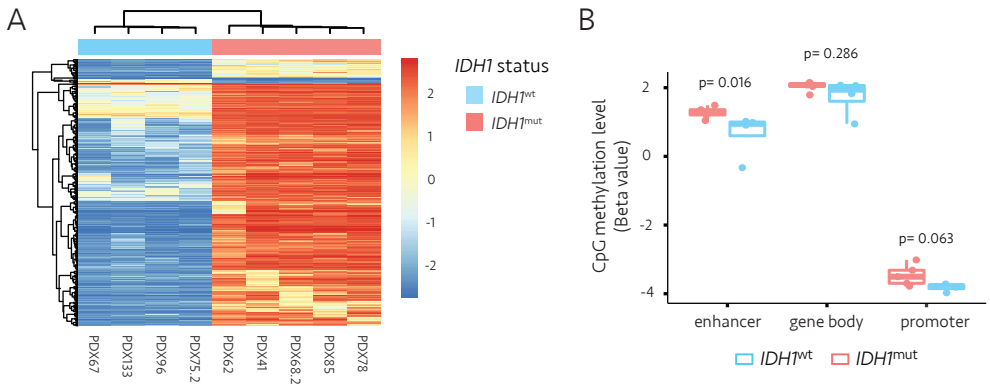

Figure R22. Differential DNA methylation analysis of CCA_PDXs demonstrated a hypermethylation phenotype of *IDH1*^{mut} CCA_PDXs. (A) Comparison of CpG DNA methylation between *IDH1*^{wt} and *IDH1*^{mut} CCA_PDXs. **(B)** Comparison of methylation levels of CpG localized in enhancer, gene body, and promoter region between *IDH1*^{wt} and *IDH1*^{mut} CCA_PDXs. Data are presented as mean ± s.d. and analyzed by a two-sided Wilcoxon Mann-Whitney test.

3.2.3. Differentially methylated CpGs are associated with immune-related genes.

Through GSEA analysis of differentially methylated CpGs using the Hallmark database, we found that there is a significant overlap with findings from the RNA-seq transcriptomic analysis. Notably, CpG associated with genes that are involved in pathways such as "EMT," "hypoxia," and "estrogen response" appeared differentially methylated between *IDH1*^{wt} and *IDH1*^{mut} CCA_PDXs (**Fig R23A**). Importantly, when we focused on promoter methylation, we found that CpGs involved in "IFNγ response" appeared to be differentially methylated between the two groups (**Fig R23B**).

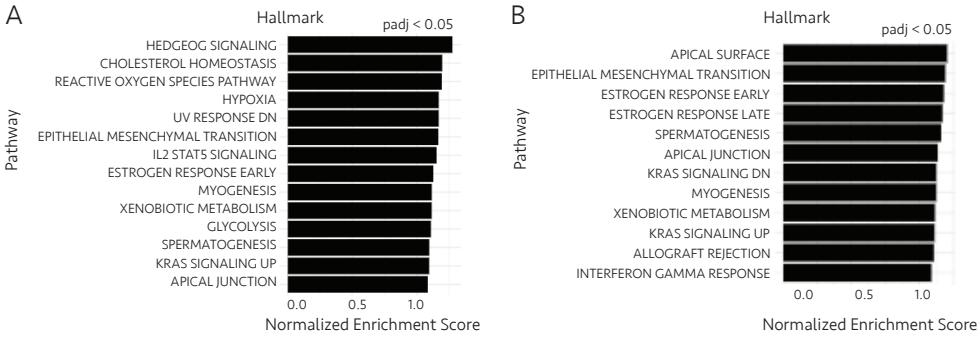

Figure R23. GSEA analysis of differentially methylated CpGs between *IDH1*^{mut} and *IDH1*^{wt} CCA_PDXs with the Hallmark database. (A) Analysis for all CpGs and **(B)** for those restricted to promoter regions. Only gene sets with statistical significance ($p < 0.05$) are shown.

3.2.4. Differentially methylated CpGs are associated with immune-related genes.

We conducted a thorough analysis of immune-related genes in both *IDH1*^{wt} and *IDH1*^{mut} groups, with a particular focus on the CpG methylation level on promoters of genes associated with chemokines, cytokines, cytokine receptors, and TNF signaling (**Fig R24**). Of note, the classification of genes was identical to that used in RNA-seq analysis (**Fig R19B**). Our findings unequivocally demonstrate that these CpGs are significantly more methylated in *IDH1*^{mut} CCA_PDXs, suggesting that hypermethylation of immune-related gene promoters is linked to the downregulation of these genes in these PDXs.

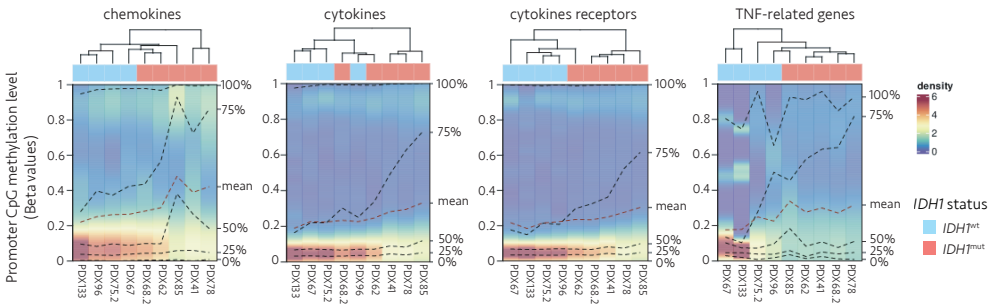

Figure R24. Promoters CpGs of immune-related genes are hypermethylated in *IDH1*^{mut} CCA_PDXs, compared to *IDH1*^{wt}. Density heatmaps showing the promoter CpG methylation levels found in CCA_PDXs. Categorized immune-related gene lists were identical to Fig R19B.

Taken together, these results suggest that immune-related genes or pathways may be downregulated in *IDH1*^{mut} CCA_PDXs due to DNA promoter hypermethylation.

3.3. Mapping of the tumor immune microenvironment (TIME) of CCA_PDXs by multiplexing immunohistochemistry (mIHC)

Based on our transcriptomic and DNA methylation studies on CCA_PDXs, we hypothesized that in *IDH1*^{mut} CCA_PDXs, 2-HG produced by the mutant IDH1 enzyme could be leading to a DNA hypermethylation of specific immune-related gene promoters. This, in turn, could lead to a downregulation of cancer cell-intrinsic immune response pathways (**Fig R25**). However, whether this cancer-cell intrinsic modulation could have an impact on the tumor immune microenvironment (TIME) is still unknown. Of note, our PDX models were generated and maintained in immunodeficient mice. Therefore, these models are not suitable for studying the TIME.

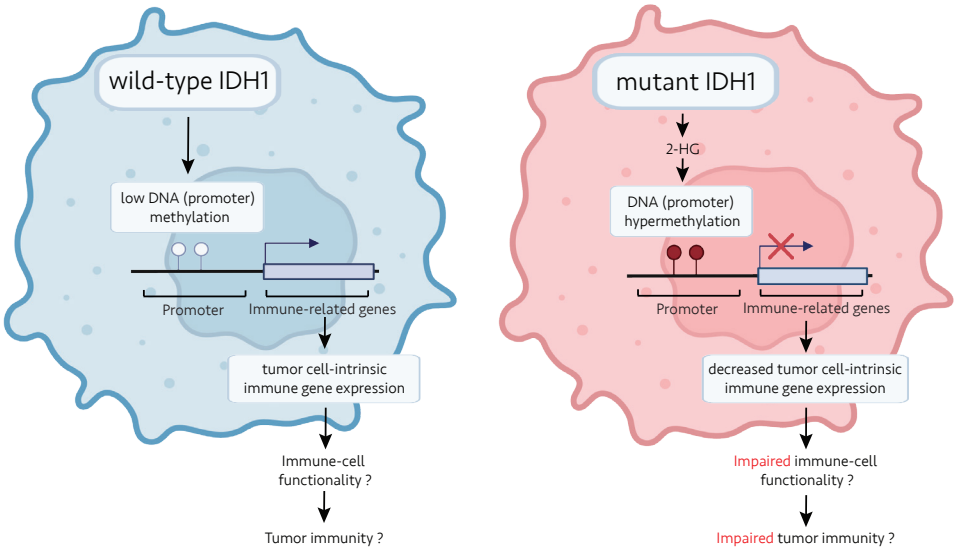

Figure R25. Schematic illustration of the hypothesis drawn based on the results obtained from the genome-wide transcriptomic and DNA methylation studies on CCA_PDXs. The proposed hypothesis entails 2-HG-driven DNA hypermethylation of specific immune-related gene promoters, resulting in a downregulation of related genes in *IDH1*^{mut} CCA (right panel). In addition, these cancer-cell intrinsic defects may impact tumor immunity.

Alternatively, we conducted multiplexing immunohistochemistry (mIHC) on biopsy samples from 8 patients with advanced CCA. Four of these samples were *IDH1*^{mut,} and others were *IDH1*^{wt}. Our mIHC panel includes CD3 (T cell marker), CD8 (cytotoxic T cell marker), CD4 (helper T cell marker), CD163 (monocyte and M2 macrophage marker), and FOXP3 (a marker of suppressive CD4 T cells, Treg cells). Cells positive for these markers were quantified and normalized by area to assess infiltration of the respective immune cell populations. Moreover, pan Cytokeratin (PanCK) staining was used to localize tumor cells and divided the analysis into three different regions: tumoral, proximal to the tumor, and distal to the tumor area (see Materials and Methods). In addition, the cell proliferation marker Ki67 was also included in the panel.

The results showed that as compared to *IDH1*^{wt} patient samples, *IDH1*^{mut} samples exhibit a slightly elevated immune cell infiltration, and this trend was observed across all analyzed populations and in all areas examined (**Fig R26A**). In the area within the tumor, samples show a higher concentration of CD163^{+} cells compared to CD3^{+} cells, irrespective of *IDH1* mutation status. This finding is consistent with previous reports that demonstrate an immunosuppressive tumor microenvironment in CCA, characterized by an abundance

of M2-like suppressive macrophages [44, 277]. Moreover, we observed that *IDH1*^{mut} CCAs exhibited a higher density of CD163^{+} cells as compared to *IDH1*^{wt} samples, in agreement with several recent reports [284, 296]. Intriguingly, despite the higher infiltration, all types of immune cells analyzed showed lower levels of proliferation in the *IDH1*^{mut} samples, as evidenced by lower percentages of Ki67 positivity, particularly in CD8^{+} effector and CD4^{+} helper cells (**Fig R26B** and **C**).

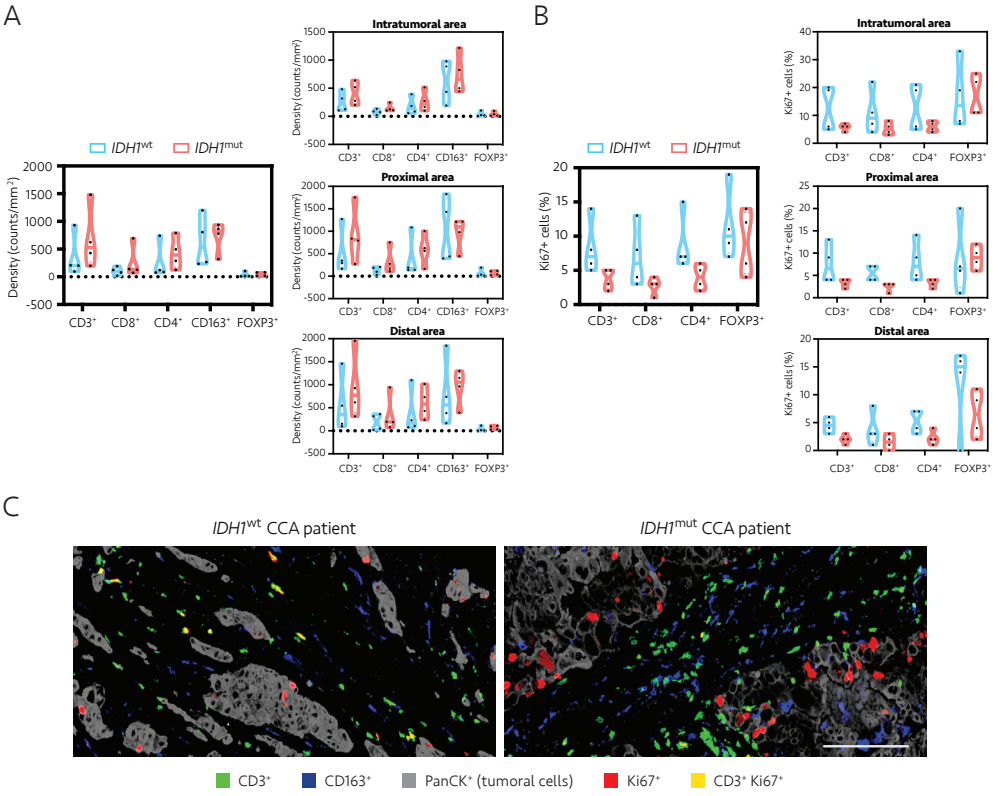

Figure R26. Immune cell infiltrations in *IDH1*^{wt} and *IDH1*^{mut} CCA patients. (A) To determine the infiltration of each immune cell type, we evaluated the density of positive cells normalized by mm^2 in the total tumoral area (left) and in specific regions within the tumoral area (right, including intratumoral, proximal, and distal areas). **(B)** The percentage of Ki67 positive cells was calculated for each T cell population by counting positive Ki67 cells and normalizing the number by the total amount of parent cells in the specific studied area: total tumoral area (left) and each specific region within the tumoral area (right, from top to bottom: intratumoral, proximal or distal areas) **(C)** Representative images of one *IDH1*^{wt} and one *IDH1*^{mut} CCA patient. Scale bar, 50 µm (A and B) Data are presented as violin plots with median (big dashes) and interquartile ranges (small dashes) and analyzed by multiple t-tests and the Wilcoxon Mann-Whitney test. *p < 0.05 comparing the two groups.

Taken together, these results indicate that patients with *IDH1*^{mut} CCA might experience problems with T cell activation rather than T cell infiltration. Despite the ability of T cells to infiltrate the TME, their complete activation and expansion remain a challenge, resulting in an inadequate cytotoxic effect. It is noteworthy, however, that a relatively small sample size limited our investigation, and further inquiry with a larger cohort is imperative to establish conclusive statistical significance.

4. Therapeutical strategies to boost the immunogenicity of *IDH1*^{mut} CCAs

Our findings indicate that reduced expression of immune-related genes, possibly due to excessive DNA methylation of their promoter regions, could be associated with an altered tumor immune microenvironment of *IDH1*^{mut} CCAs (**Fig R27A**). This may negatively affect the effectiveness of T cell tumor infiltrates. We propose that inhibiting either the mutant IDH1 enzyme or DNA methyltransferases (DNMT) - responsible for DNA methylation - could potentially reverse this immunosuppressed phenotype and make *IDH1*^{mut} CCAs more responsive to immuno-oncology therapies **(Fig R27B).**

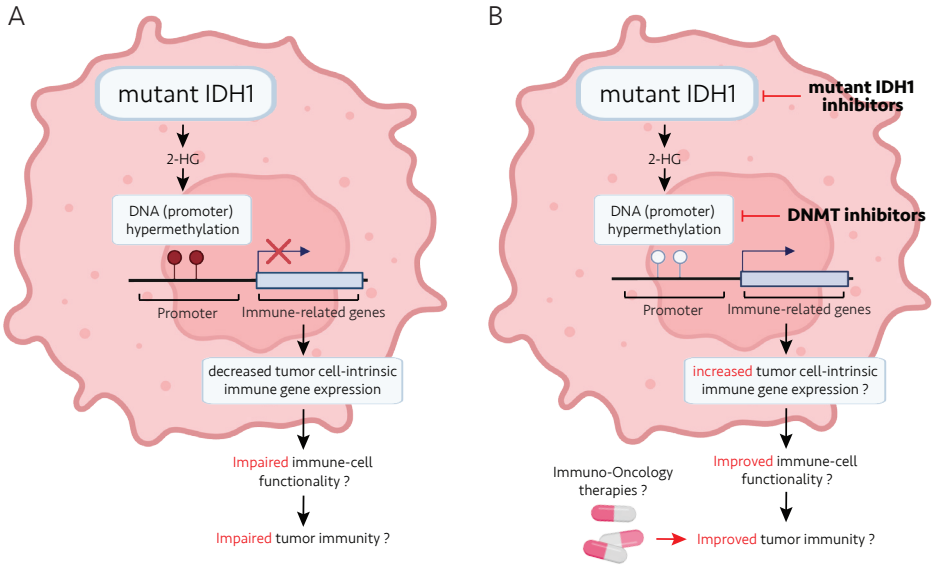

Figure R27. Working hypothesis scheme for the therapeutic intervention of *IDH1*^{mut} CCA. (A) 2-HG produced by mutant IDH1 enzyme may lead to promoter hypermethylation of specific immune-related genes. This can lead to the downregulation of cancer cell-intrinsic immune-related genes and affect the immune microenvironment of *IDH1*^{mut} CCA tumors. **(B)** Inhibiting mutant IDH1 enzyme or DNMTs with pharmaceuticals may enhance the expression of immune-related genes by demethylating their promoters. This process can ultimately increase the immunogenicity of *IDH1*^{mut} CCA tumors.

4.1. CCA cell lines recapitulate the phenotype observed in CCA_PDXs

Our previous studies have demonstrated that PDX models accurately reflect the tumor's characteristics, including its histopathology, genomic landscape, and therapeutic response. However, due to their limited applicability for large-scale, long-time *in vitro* studies, we first conducted preliminary experiments using four CCA cell line models, namely HuCCT1, HuH28, Snu1079, and RBE. HuCCT1 and HuH28 have wild-type *IDH1*, whereas Snu1079 and RBE carry heterozygous *IDH1* R132C and R132S mutations, respectively (**Fig R28A**).

First, we verified whether these cell models recapitulate the phenotype previously observed in our CCA_PDX models. As expected, both *IDH1*^{mut} cell lines showed higher 2-HG levels than the *IDH1*^{wt} cells (**Fig R28B**). Accordingly, higher levels of the DNA methylation mark 5-methylcytosine (5mC) were found in *IDH1*^{mut} Snu1079 and RBE cells (**Fig R28C**). Importantly, we also found that one of the top downregulated genes identified in the *IDH1*^{mut} CCA_PDXs, *STING1*, was downregulated in *IDH1*^{mut} Snu1079 and RBE cell lines compared to *IDH1*^{wt}, both at the mRNA (**Fig R28D**) and the protein (**Fig R28E**) level. Thus, CCA cell lines recapitulate the phenotype observed in CCA_PDXs. We acknowledge that *STING1* is just one of the downregulated genes found in our previous study with CCA_PDXs. Further genome-wide analyses are currently being conducted.

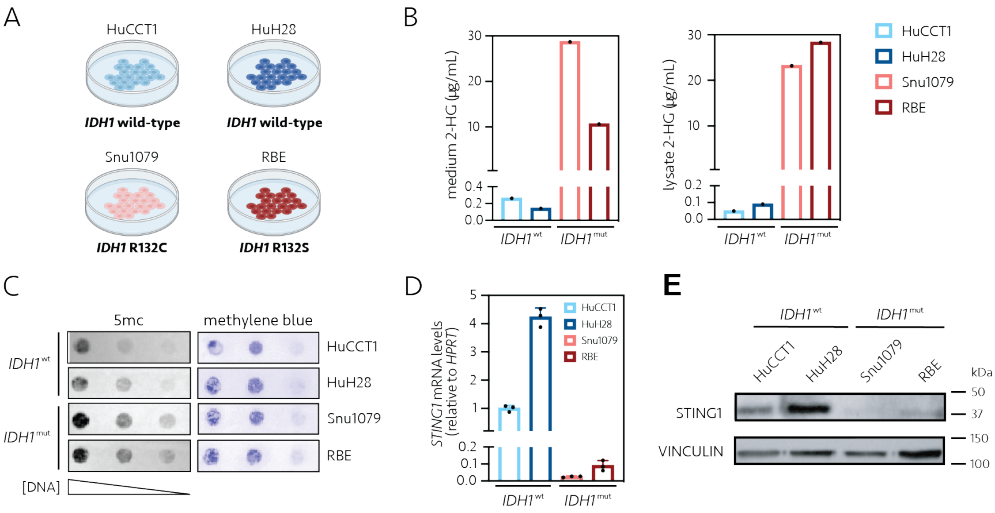

Figure R28. Characterization of the four CCA cell line models. (A) *IDH1* mutation status of four CCA cell line models. **(B)** Quantification of 2-HG by LS-MS. **(C)** 5mC levels evaluation by Dot Blot. Methylene blue was used as the loading control. **(D)** RT-qPCR analysis of *STING1*. *HPRT* expression was used as a housekeeping gene for normalization. mRNA data are presented as mean ± s.d. **(E)** Determination of STING1 protein levels by Western Blot. VINCULIN was used as the loading control.

4.2. Treatment of DNA demethylating agent increases STING expression in *IDH1*^{mut} CCA cell lines

To investigate the potential effects of inhibiting DNA methylation on immune-related gene expression in *IDH1*^{mut} CCA cell lines, we treated CCA cells with a clinically-tested DNA demethylating agent, decitabine. As expected, the application of decitabine decreased 5mC in both *IDH1*^{wt} and *IDH1*^{mut} cell lines (**Fig R29A**). Nevertheless, the upregulation of the immune-related gene *STING1* was observed solely in *IDH1*^{mut} CCA cell lines and not in *IDH1*^{wt} cells (**Fig R29B** and **C**). Similar results were obtained from treating CCA cell lines with another DNA demethylating agent, 5-azacytidine (5-aza) (not shown). Thus, the treatment of DNA demethylating agents can increase STING1 expression in *IDH1*^{mut} CCA cell lines.

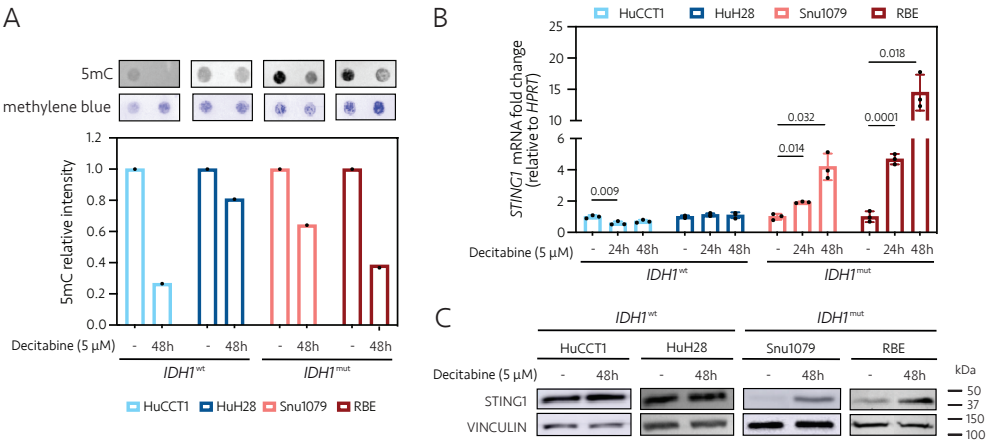

Figure R29. DNA-demethylating agent decitabine treatment increased STING1 expression in *IDH1*^{mut} CCA cell lines. CCA cell lines were treated with 5 µM decitabine and collected for further analysis at indicated time points. **(A)** 5mC levels measured by Dot Blot. Methylene blue was used as a loading control and to normalize 5mC intensity. Quantification was performed using ImageJ. **(B)** RT-qPCR analysis of *STING1*. *HPRT* expression was used for normalization. mRNA data are presented as mean ± s.d., n=3 replicates, and were analyzed by multiple paired Student´s t-tests. **(C)** Evaluation of STING1 protein levels by Western Blot. VINCULIN was used as a loading control.

4.3. Treatment of mutant IDH1 inhibitor increases STING expression in *IDH1*^{mut} CCA cell lines

To verify whether the inhibition of mutant IDH1 could lead to an increase of immune-related genes, we treated *IDH1*^{mut} cell lines Snu10790 and RBE with the mutant IDH1 inhibitor, ivosidenib. Upon treatment, we observed a dose-dependent decrease in the levels

of 2-HG in both the culture medium and cell lysate (**Fig R30A**). Accordingly, reduced 5mC levels were also found in *IDH1*^{mut} cell lines treated with ivosidenib for 120 hours (**Fig R30B**). Nevertheless, there were only slight changes in the STING1 expression, as observed in both mRNA and protein levels (**Fig R30C** and **D**, respectively). A possible explanation of these results is that mutant IDH1 inhibition indirectly affects DNA methylation, in contrast to the impact of DNA demethylating agents (**Fig R27**). To achieve a more powerful effect, it may be necessary to undergo a more extended treatment that produces stronger methylation modifications [168, 172]. Therefore, we have treated Snu1079 and RBE constantly with ivosidenib (5 µM), and these new lines were used for further functional studies.

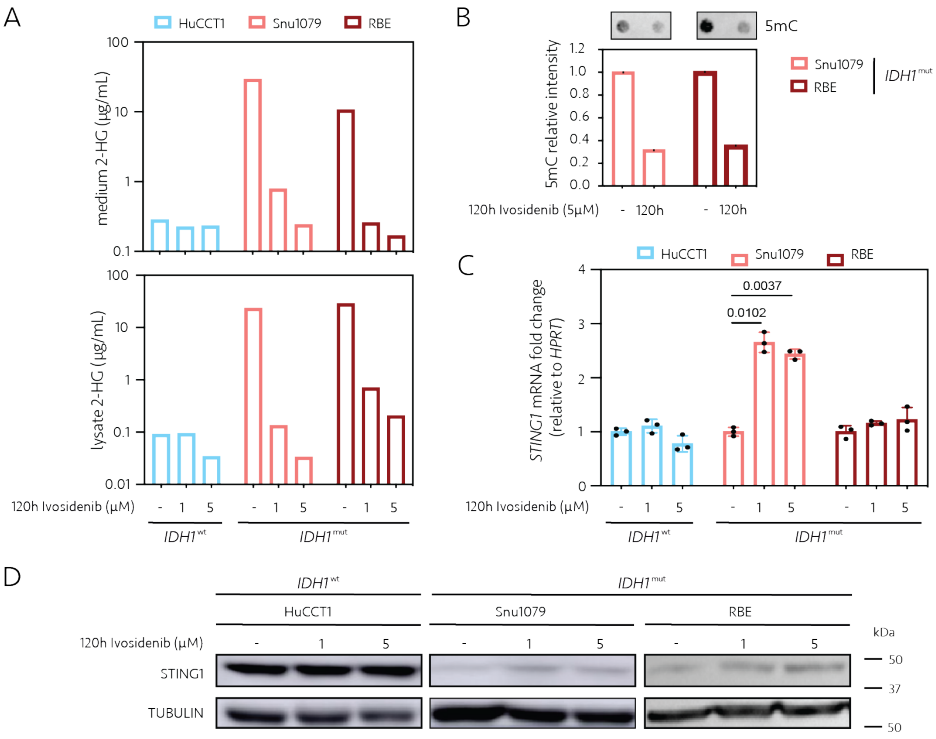

Figure R30. Mutant IDH1 inhibitor ivosidenib treatment can slightly increase STING1 expression in *IDH1*^{mut} CCA cell lines. *IDH1*^{wt} cell line HuCCT1 (as negative control) and *IDH1*^{mut} Snu1079 and RBE were treated with increasing concentrations of ivosidenib for 120 hours and collected for further analysis. **(A)** Quantification of 2-HG by LS-MS. **(B)** 5mC levels measured by Dot Blot. Methylene blue was used as a loading control. **(C)** RT-qPCR analysis of *STING1*. *HPRT* expression was used for normalization. mRNA data are presented as mean ± s.d., n=3 replicates, and were analyzed by multiple paired t-student tests. **(D)** Determination of STING1 protein levels by Western Blot. TUBULIN was used as a loading control.

It is important to note that both DNA demethylating agent and mutant IDH1 inhibitor treatments were shown to decrease 5mC levels and increase STING expression. However, we remain committed to assessing their efficacy in an unbiased manner. We are currently performing genome-wide transcriptomics and DNA methylation studies to verify whether the two potential strategies can enhance immune gene expression.

4.4. HER2-T cell bispecific antibody can be used to study the T cell activation.

Our data shows that *IDH1*^{mut} CCA cells exhibit reduced expression of immune-related genes. Treatment with DNA demethylating agents and mutant IDH1 inhibitors can enhance their expression. However, it remains unclear if these cell-intrinsic characteristics affect the tumor immune microenvironment, particularly T cell activation. Indeed, an impaired T cell activation phenotype was found in our mIHC studies (**Fig R26**). Therefore, we conducted further research to determine if giving decitabine and ivosidenib to *IDH1*^{mut} CCA cells would affect the activation of T cells.

As a T cell model, we opted for peripheral blood mononuclear cells (PBMCs) obtained from healthy donors, which consist of 70% T cells. The activation of T cells hinges on their ability to identify target cells selectively. This process is mediated by the T cell receptor (TCR), which can only recognize and bind to tumor antigens that are appropriately presented on the cell surface by a matched major histocompatibility complex (MHC) molecule [253]. However, the PBMCs were from different donors, and these cells lacked the TCRs that could recognize our CCA cell models. To overcome this difficulty, we took advantage of T cell bispecific antibodies (TCBs), which can elicit anti-tumor responses by cross-linking T cells to tumor cells, and mediate polyclonal T cell expansion that is independent of TCR specificity [331].

Human epidermal growth factor receptor 2 (HER2), also known as receptor tyrosine-protein kinase erbB-2 (ERBB2), is a protein that is overexpressed in many types of cancers, including breast, gastric, and CCA [332, 333]. Several studies have shown that HER2 overexpression is associated with poor prognosis and aggressive tumor behavior in CCA [334]. Interestingly, a therapeutic HER2-T cell bispecific antibody (HER2-TCB) has been reported [335, 336]. This TCB consists of an asymmetric two-

armed immunoglobulin G1 (IgG1) that binds to 1) the CD3ε subunit of the TCR of T cells and 2) the HER2 on the membrane of the tumor cell (**Fig R31** and **33A**). This structure allows the antibody to bring T cells in close proximity to the tumor cells, leading to the destruction of tumor cells [336].

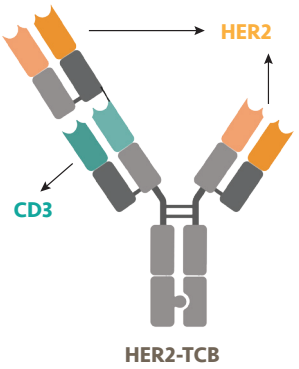

Figure R31. Schematic illustration of HER2-TCB.

We conducted a flow cytometry test to confirm the expression of HER2 in our CCA cell lines, under basal conditions and upon indicated treatments (**Fig R32A** and **B**). The results showed that all four CCA cell lines expressed HER2 (**Fig R32C** and **D**). It is worth noting that administering decitabine or ivosidenib did not significantly change the levels of HER2 expression (less than 2-fold) in these cells (**Fig R32E**). Therefore, the variation in HER2 expression upon decitabine or ivosidenib treatments does not play a significant role in the results of T cell activation.

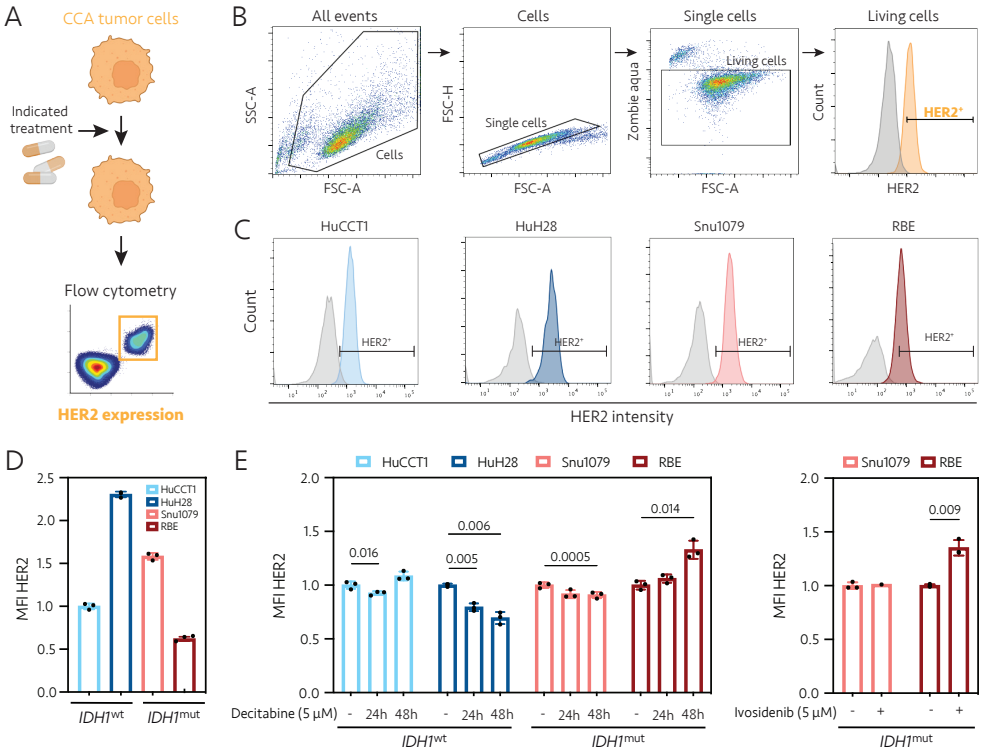

Figure R32. HER2 expression in CCA cells was not affected by decitabine or ivosidenib treatments. CCA cell lines were treated with indicated treatments, stained with anti-HER2, and analyzed by flow cytometry. As a control, all cell lines were stained with only secondary antibodies. **(A)** Schematic showing HER2 expression evaluation by flow cytometry. **(B)** The gating strategy to measure HER2 expression. **(C** and **D)** Mean fluorescence intensity (MFI) of HER2 in the indicated CCA cell lines under untreated basal conditions. Results are shown as histogram plots **(C)** and MFI quantification **(D)**. In grey, the negative control stained with only secondary antibodies for each CCA cell line. **(E)** MFI of HER2 in the indicated CCA cell lines under indicated treatments. Results were normalized to each untreated control for each cell line. Data are presented as mean ± s.d. and were analyzed by multiple paired Student's t-tests.

4.5. T cell activation is significantly improved with HER2-TCB treatment when *IDH1*^{mut} CCA cells had been previously decitabine-treated

We exposed CCA cell lines to 5 µM decitabine for 24 or 48 hours and then refreshed the culture medium to remove any drug left. We then co-cultured the decitabine-treated CCA cells with PBMCs from healthy donors for an additional 72 hours with the presence of 100 pM HER2-TCB. We measured T cell activation and cytotoxicity using the late activation marker CD25 and the cytotoxic marker Granzyme B (GZMB) (**Fig R33**). Of note, CCA cells and PBMC co-culture conditions without the presence of HER2-TCB were used as negative controls. In these experimental conditions, no significant T cell activation is expected.

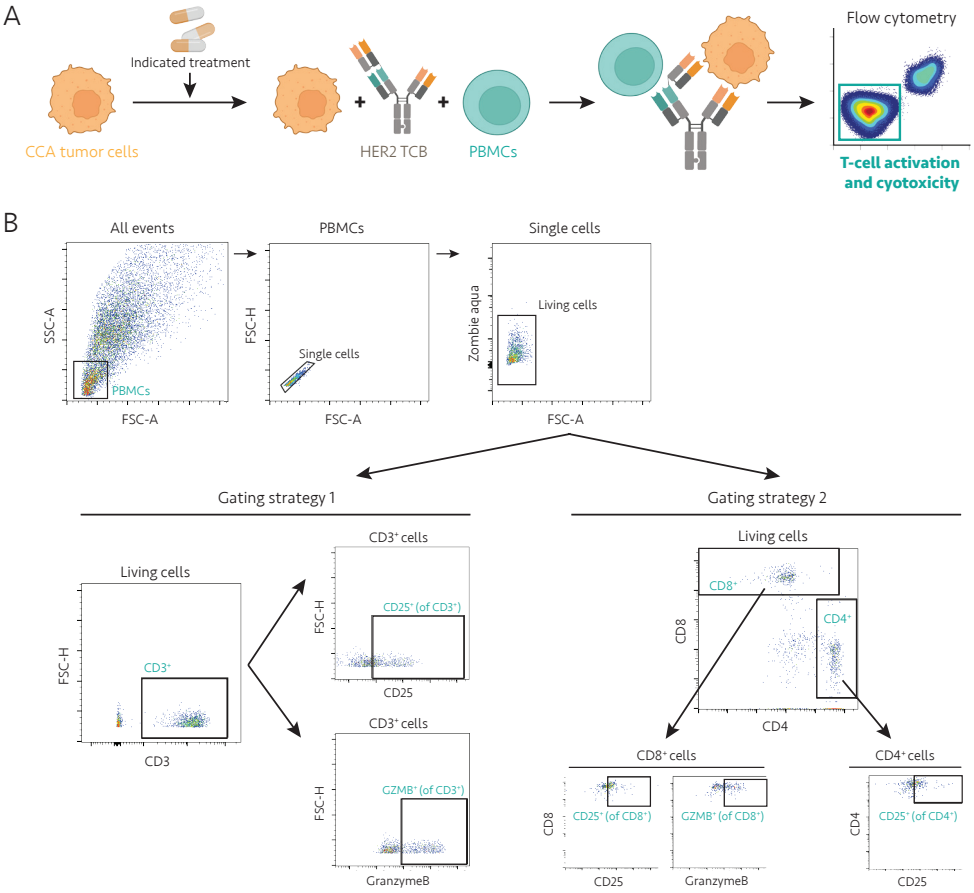

Figure R33. T cell activation and cytotoxicity assessment in co-culture between pretreated CCA cells and PBMCs. (A) Schematic illustration of experimental procedures. CCA tumor cells were treated as previously explained (Fig R29 and 30) and co-cultured with PBMCs for 72 h with 100 pM HER2-TCB. T cell activation and cytotoxicity were evaluated at the endpoint by flow cytometry analysis of the late activation marker CD25 and the cytotoxic activity marker, granzyme B (GZMB)**. (B)** The gating strategy for T cell activation and cytotoxicity evaluation. To examine CD25 and GZMB in $CD3^+$ T cells, we utilized gating strategy 1, and for $CD4^+$ and $CD8^+$ populations, gating strategy 2.

The results of the study showed that when HER2-TCB treatment was not administered, there was little activation of T cells (%$CD25^+$ (of $CD3^+$ cells)) and cytotoxicity (%$GZMB^+$ (of $CD3^+$ cells)) (**Fig 34A** and **B**). However, when HER-TCB was present (at a concentration of 100 pM), co-culturing decitabine-pretreated *IDH1*^{mut} Snu1079 and RBE cells with PBMCs led to a significant increase in the activation of T cells and cytotoxic GZMB expression. In contrast, when decitabine-pretreated *IDH1*^{wt} HuCCT1 and HuH28 cells were co-cultured with PBMCs, the activation of T cells and cytotoxicity were minimal.

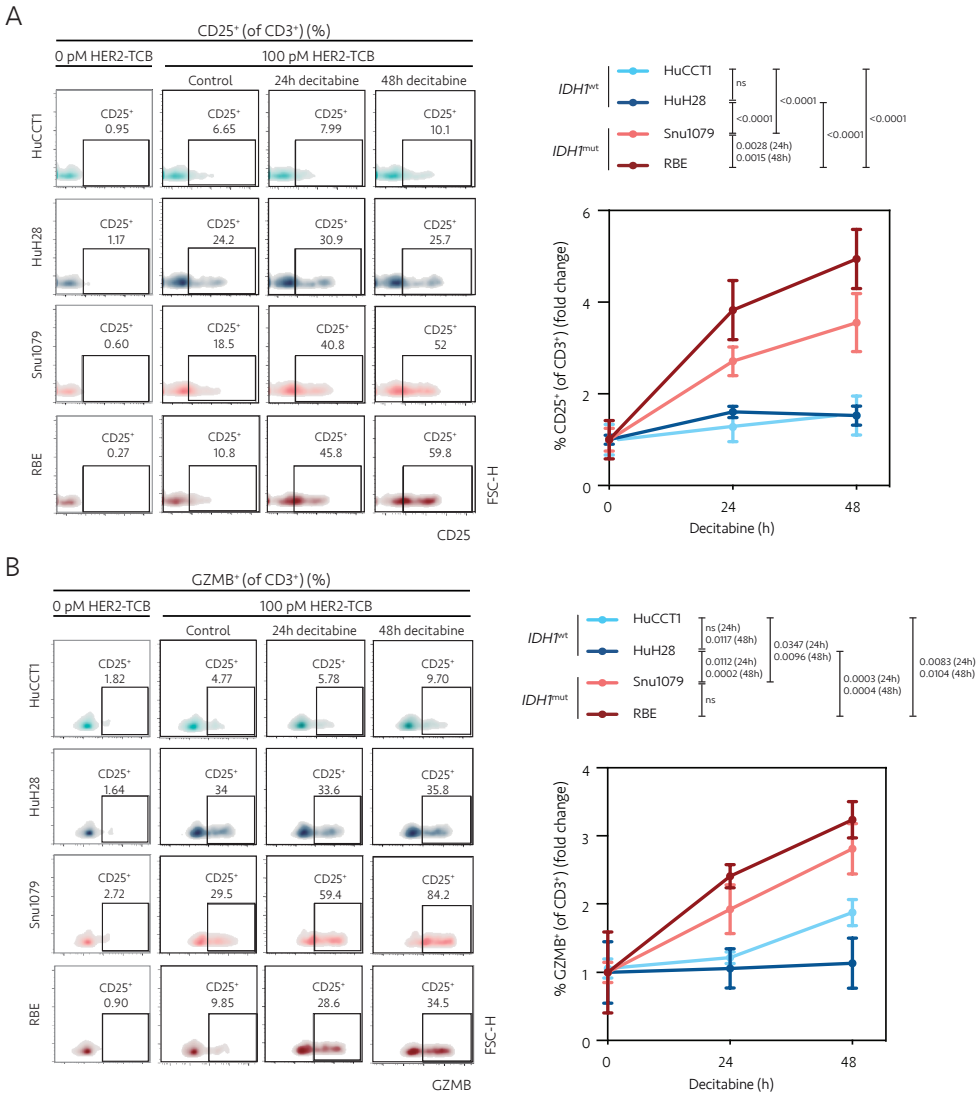

Figure R34. Treatment with decitabine increases T cell activation and cytotoxicity only in co-cultures with *IDH1*^{mut} CCA cells. CCA cells were treated with 5 μM decitabine, then co-cultured with PBMCs with 100 pM of HER2-TCB for 72 h prior to marker evaluation. **(A)** Flow cytometry analysis of CD25, a late activation marker, in CD3$^+$ T cells. Representative density plots (left) and quantification (right). **(B)** Flow cytometry analysis of Granzyme B (GZMB), a cytotoxicity marker, in CD3$^+$ T cells. Representative density plots (left) and quantification (right). The percentage of positivity is represented as the fold change compared to the untreated control for each cell line. Data are presented as mean ± s.d., n=3 independent biological replicates, and were analyzed by two-way ANOVA multiple comparisons with Tukey's correction.

Moreover, we examined the T cell activation and cytotoxicity markers in the CD8$^+$ population, as well as the T cell activation in the CD4$^+$ population. We found that, as compared to decitabine pretreated *IDH1*^{wt} cells (HuCCT1 and HuH28), *IDH1*^{mut} cells (Snu1079 and

RBE) treated with decitabine increased the activation and the cytotoxicity of $CD8^+$ T cells under the presence of HER2-TCB more significantly (**Fig R35A**). In addition, *IDH1*^{mut} cells pretreated with decitabine also increased the activation of $CD4^+$ T cells under the presence of HER2-TCB (**Fig R35B**). Notably, $CD4^+$ helper T cells play a critical role in supporting effector $CD8^+$ functions and directing a sustained immune response against tumors [337].

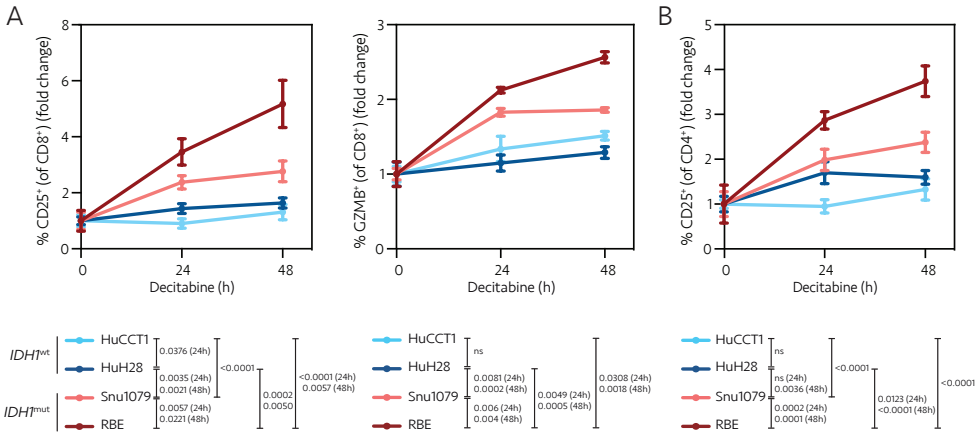

Figure R35. Treatment with decitabine increases cytotoxic $CD8^+$ and helper $CD4^+$ T cell activation only in co-cultures with *IDH1*^{mut} CCA cells. CCA cells previously treated with 5 μM decitabine were co-cultured with PBMCs at a 1:1 ratio and 100 pM of HER2-TCB for 72h prior to marker evaluation. **(A)** Flow cytometry analysis of CD25 late activation marker (left) and Granzyme B (GZMB) cytotoxicity marker (right) in $CD8^+$ T cells. **(B)** Flow cytometry analysis of CD25 late activation marker in $CD4^+$ T cells. The percentage of positivity is represented as the fold change compared to the untreated control for each cell line. Data are presented as mean ± s.d., n=3 independent replicates, and were analyzed by two-way ANOVA multiple comparisons with Tukey correction.

4.6. T cell activation is not improved by HER2-TCB treatment if *IDH1*^{mut} CCA cells were previously ivosidenib-treated

Next, we evaluated whether mutant IDH1 inhibitor ivosidenib treatment of *IDH1*^{mut} cells could increase T cell activation and cytotoxicity with the presence of HER2-TCB. We found that even *IDH1*^{mut} cells treated with ivosidenib for 4 weeks (long-term culture with ivosidenib) did not induce any significant changes in T cell activation (**Fig R36A**) and toxicity (**Fig R36B**). This is unsurprising, as ivosidenib treatment only caused minor changes in the 5mC level and STING expression (**Fig R30**). Moreover, multiple publications have already described the absence of effects of ivosidenib when tested in *in vitro* setting [160, 168, 338].

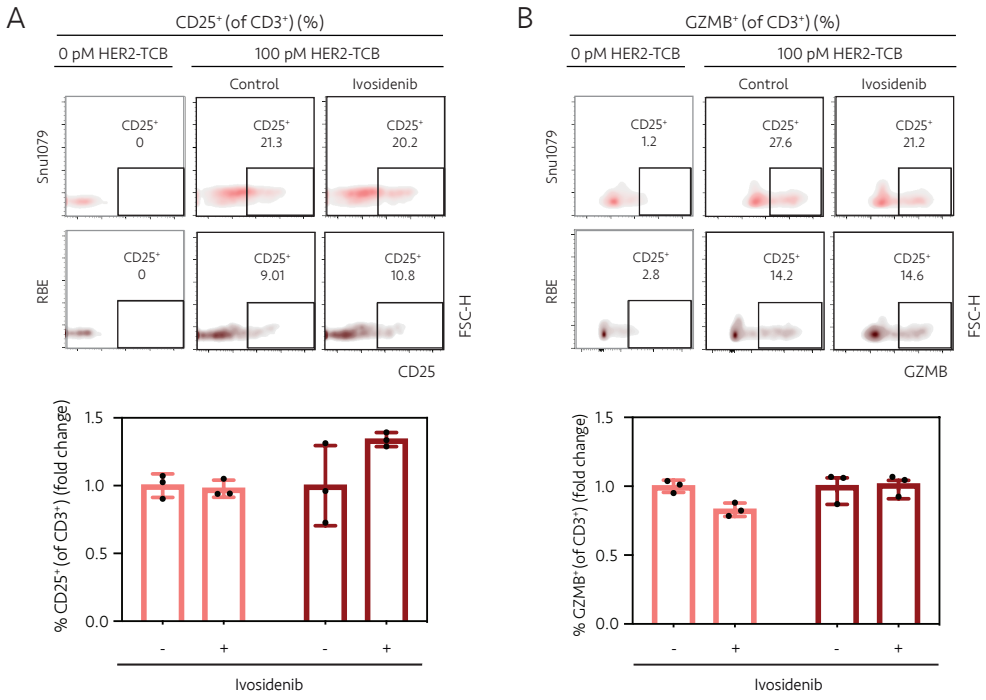

Figure R36. Ivosidenib treatment of *IDH1*^{mut} CCA cells has minimal impact on T cell activation and cytotoxicity with the presence of HER2-TCB. CCA cells were constantly treated with 5µM ivosidenib and then were co-cultured with PBMCs and 100 pM of HER2-TCB for 72h prior to marker evaluation. **(A)** Flow cytometry analysis of CD25, a late activation marker, in CD3$^+$ T cells. Representative density plots (left top) and quantification (left bottom). **(B)** Flow cytometry analysis of Granzyme B (GZMB), a cytotoxicity marker, in CD3$^+$ T cells. The percentage of positivity is represented as the fold change compared to the untreated control for each cell line. Data are presented as mean ± s.d., n=3 independent replicates, and were analyzed by two-way ANOVA multiple comparisons with Tukey´s correction.

Discussion

A new collection of patient-derived xenografts (PDXs) to study advanced metastatic CCA

PDXs have become an essential tool for understanding the mechanisms underlying cancer development and progression, and they are also being used for discovering cancer biomarkers and treatment [339, 340]. While PDXs of CCA have been reported previously, they have mainly been established with surgically resected primary tumor tissues [101-106, 110] (Table I4). Notably, only approximately 25% of patients with CCA are diagnosed early and eligible for surgical resection [7]. In contrast, the remaining 75% of the CCA cases are frequently diagnosed at advanced stages with locoregional involvement or/and distant metastatic lesions, currently without long-lasting or effective therapeutic strategies [7]. Despite this clear unmet clinical need, large collections of PDX models focused on unresectable advanced CCA were missing. We report here a unique collection of CCA_PDXs, of which the majority (18 of 19 CCA_PDXs) was established with biopsy samples of metastatic lesions from patients with confirmed advanced CCA disease.

This collection of CCA_PDX models faithfully recapitulates the histopathologic and genetic characteristics of the corresponding original CCA samples (Fig R2; Fig R3). Of note, the genomic profiles of the CCA_PDX collection compile a list of mutations that have been previously reported to be associated with cholangiocarcinoma pathogenesis, such as mutations in genes *TP53, KRAS, ARID1A, BAP1, CDKN2A/B, BRCA2*, or *PIK3CA* [12, 14, 15, 298]. Moreover, as they are established mainly from patients with metastatic intrahepatic CCA, our CCA_PDX showed a high prevalence of mutations in *IDH1/2* and fusions of *FGFR2*, which is in agreement with reported molecular traits of the intrahepatic CCA [14, 15, 20, 21, 298] (Fig I2).

Moreover, tumor cells derived from CCA_PDXs can grow as tumoroids using optimized *ex vivo* 3D culture conditions. Importantly, as previously reported in breast cancer [100], castration-resistant prostate cancer [13], and osteosarcoma models [302], the drug responses observed in tumoroids derived from CCA_PDXs were in agreement with those observed with CCA_PDX and patients with CCA (Fig R5), thus providing a new potentially valuable platform for rapid, cheap, and high-throughput screening of drug sensitivity and resistance in CCA.

It is important to point out that our CCA_PDX models were developed using tissues from patients who had already received and progressed at least one line of platinum-based

chemotherapy, neoadjuvant chemotherapy, and/or targeted therapy and had progressed (Fig R1). In the clinic, these patients are in desperate need of effective treatment [341]. Our models provide thus an opportunity to deepen the knowledge and test novel therapeutic options for this specific disease stage.

It is worth mentioning that our collection lacks models from treatment-naive metastatic CCA samples. However, we are currently collecting samples to fill this gap.

CCA tumors with *BRCA2* mutations, but not those with *IDH1, ARID1A* or *BAP1* alterations, respond to PARP inhibition.

Tumor cells that lack functional BRCA1/2, key HR proteins, have been shown to be exquisitely sensitive to PARPi [314, 315]. Clinical evidence demonstrated that patients with *BRCA2*^{mut} breast, prostate, and ovarian cancers could benefit from PARPi treatment [318-320]. We found that CCA-derived preclinical models with *BRCA2* mutations respond to PARPi, indicating the potential application of PARPi in advanced CCA (Fig R7; Fig R10). Moreover, a metastatic CCA patient with a pathogenic *BRCA2* mutation (D2723H) showed regressions of several target lesions when compassionately treated with olaparib after progression to several lines of treatment (Fig R11). In line with that, several recent case reports have independently documented the effectiveness of olaparib in patients with CCA with pathogenic deleterious mutations of *BRCA2* [342-344]. As *BRCA2* mutations were reported in approximately 3% of patients with CCA [345], which is non-negligible, further large-scale studies are warranted to systematically evaluate the effectiveness of PARPi in these patients.

Strikingly, our *IDH1*^{mut}, *ARID1A*^{mut}, and *BAP1*^{mut} CCA patient-derived preclinical models did not respond to PARPi treatment (Fig R7; Fig R8; Fig R9). The absence of PARPi effectiveness in these preclinical models is in contrast to what would be expected according to the previously published data [177-179, 228, 229, 238, 241, 242, 316] (Table I6; Table I7). Interestingly, several other preclinical studies also showed a highly variable response of *IDH1/2*^{mut} cancer cells to PARPis [180, 247, 248, 346] (Table I8). In agreement, published preliminary data of the Olaparib Combination trial (OLAPCO) showed no clinical benefit among four *IDH*^{mut} CCA patients treated with olaparib as a monotherapy [347]. In contrast, among five *IDH*^{mut} chondrosarcomas patients included in this trial, one patient exhibited a partial response, while two patients had stable disease lasting over 7 months [347]. Thus,

the variation in PARPi responses among different *IDH*^{mut} tumor types may indicate a tumor-specific influence of *IDH* mutations on DNA Damage repair (DDR). Moreover, a retrospective study suggested that ARID1A loss may confer PARPi resistance in patients with ovarian cancer [230] and a recent phase II also reported that olaparib had limited activity in patients with previously treated mesothelioma with *BAP1* mutations [348]. Taken together, these results suggest that *IDH1*, *ARID1A*, and *BAP1* mutations should not be used as a pan-cancer biomarker to predict PARPi response and that patients with advanced CCA with these mutations are unlikely to benefit from PARPi monotherapy. Further studies are needed to investigate in which cancer type and/or subtype these mutations are associated with sensitivity to PARPi.

CCA tumors with *BRCA2* mutations, but not those with *IDH, ARID1A,* or *BAP1* alterations, display Homologous Recombination deficient phenotypes.

To understand why our *IDH1*^{mut}, *ARID1A*^{mut}, and *BAP1*^{mut} CCA patient-derived preclinical models did not respond to PARPi treatment, we also examined their HR status using the RAD51 assay [225, 226]. Of note, this assay has been applied in several clinical trials, and tumor sample RAD51 scores can predict clinical benefits from PARPi treatment with high sensitivity and specificity [321-324]. Our data showed that RAD51 scores of *IDH1*^{mut}, *ARID1A*^{mut}, and *BAP1*^{mut} CCA_PDX, as well as those of patients with advanced CCA harboring these mutations, are compatible with an HRP profile; PDX119 and patient sample with pathogenic alterations in *BRCA2* were, as expected, scored as HRD (Fig R12; Fig R14). We acknowledge that our study had a small sample size of CCA patients analyzed. To confirm our findings and determine which patients would benefit from PARPi, further studies with RAD51 assay in larger CCA cohorts are needed.

Possible factors linked to the absence of PARPi effectiveness and HRP phenotype observed in CCA with alterations in *IDH, ARID1A*, or *BAP1*

The absence of PARPi effectiveness and HRP phenotype observed in *IDH1*^{mut}, *ARID1A*^{mut} and *BAP1*^{mut} CCA_PDXs are in contrast to previously published data [177-179, 228, 229, 238, 241, 242, 316]. However, several factors could explain these discrepancies. As most of our CCA_PDXs were generated from patients with advanced CCA refractory to

chemotherapy, we could not exclude the possible scenario that *IDH1*^{mut}, *ARID1A*^{mut}, and *BAP1*^{mut} CCA cells were originally deficient in HR, and that the capacity for HR was restored over the disease progression and/or course of treatment. A comparison between primary and metastatic CCA biopsy before and after the treatment could address this. Moreover, the experimental models used by the authors differed greatly from the ones used in the herein study. Following, we are going to discuss in detail these possible factors.

Disease progression

A comparative analysis was conducted to explore the difference in complex HRD estimates between *IDH*^{mut} and *IDH*^{wt} tumors from The Cancer Genome Atlas Program (TCGA) [349]. The HRD parameters included in this study were Loss-Of-Heterozygosity (LOH), Large-Scale Transitions (LST), Telomeric Allele Imbalance (TAI), and Repair Proficiency Scoring (RPS). The study encompassed various tumor types, including 36 primary CCAs. Among these tumor types, *IDH*^{mut} primary CCA tumors did not exhibit a higher HRD profile when compared to wild-type cases across the different HRD estimates evaluated. However, primary glioblastoma (GBM) and low-grade glioma (LGG) tumors presented differences in TAI, LOH (LGG), and LST (GBM) between *IDH*^{wt} and *IDH*^{mut} groups, supporting the possible tumor-type related effects of *IDH* mutations.

Previous treatments

HR restoration over treatment pressure is a mechanism that has been previously reported [350] [351]. Indeed, it has been reported that HRD tumors' response to PARPi is lower if given as monotherapy after progression to platinum exposure due to HR complete or partial function reestablishment [352] [353].

Following the 2-HG-induced HRD profile hypothesis, *IDH* mutations have also been associated with increased sensitivity to DNA damaging agents, such as chemotherapy and radiation [177-179, 241, 246] (Table I7, Fig I13). A multicentre study was conducted on 120 patients with iCCA treated with platinum-based chemotherapy [349]. The study aimed to investigate the impact of *IDH* mutations on progression-free survival (PFS), overall response rate (ORR), and disease control rate (DCR). Results showed no differences between *IDH*^{wt} and *IDH*^{mut} iCCA patients in terms of PFS (7.7 vs. 7.3 months, $p = 0.970$), DCR (66.1% vs. 74.1%, $p = 0.361$), and ORR (27.8% vs. 25.0%, $p = 0.741$), indicating an absence of

increased sensitivity to platinum-based chemotherapy in *IDH*^{mut} iCCA patients. Interestingly, we also compared platinum-based chemotherapy response in our CCA cohort at the Vall d'Hebron University Hospital. We could not find any significant difference, between *IDH*^{wt} and *IDH*^{mut} CCA patient groups, in terms of PFS and OR. (**Fig D1**). Therefore, patient chemotherapy outcomes were aligned with our observed PARPi responses in CCA_PDXs.

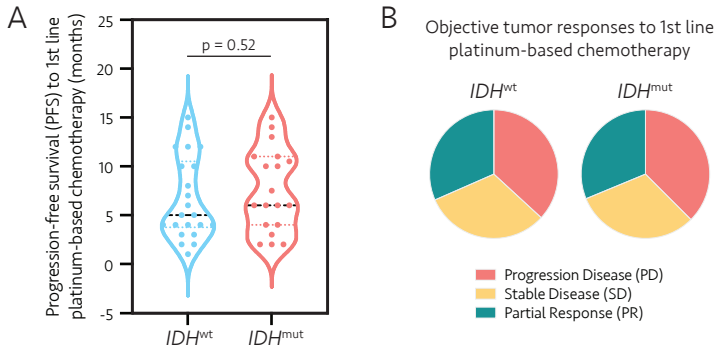

Figure D1. Our CCA cohort showed no differences for platinum-based PFS and objective tumor response between *IDH*^{wt} and *IDH*^{mut} patients. (A) 1st line platinum-based progression-free survival (PFS) of the CCA patients included in this study cohort, given in months and classified as *IDH*^{wt} or *IDH*^{mut}. Data are presented as violin plots with median (big dashes) and interquartile ranges (small dashes) and analyzed by multiple t-tests and the Wilcoxon Mann-Whitney test. *p < 0.05 comparing the two groups. **(B)** Pie charts depicting the distribution of the objective responses of CCA patients to 1st line platinum-based chemotherapy, according to Response Evaluation Criteria in Solid Tumors (RECIST), in *IDH*^{wt} and *IDH*^{mut} patients.

Experimental models

The preclinical evidence substantiating the utility of *IDH, ARID1A,* and *BAP1* mutations as viable surrogate biomarkers for HRD and subsequent PARPi response primarily relies on *in vitro* cell lines and genetically modified mouse models that alter the expression or function of these genes [178, 179, 228, 229, 235, 241] (TableI6 and I7). Gain-of-function (GOF) and loss-of-function (LOF) research models help to establish causal relationships between specific genes and their biological effects while ruling out confounding factors. However, these models do not fully represent the physiological context due to the extreme manipulation of gene expression (complete loss, or overexpression), which differs from the pathophysiological condition. Therefore, we questioned whether the divergent results could be attributed to the different research models used.

Indeed, in a study by Garrett et al. [354], opposite effects of *IDH* mutations on DDR were observed depending on the cellular background. When a mutant IDH1 overexpression

model was used, Garrett and colleagues observed increased DNA damage and a reduced capacity for DNA repair, similar to the findings of Sulkowski or Wang et al. [178, 179, 241, 354]. On the other hand, cells with endogenous *IDH1* mutation showed enhanced DNA repair capacity following radiation. These contrasting results could be interpreted as an adaptation of *IDH1*^{mut} cells over time to high levels of 2-HG, with the activation of compensatory mechanisms to overcome vulnerabilities associated with 2-HG. *IDH* mutations are known to occur early in tumorigenesis and persist during tumor evolution and progression, allowing tumor cells to adapt and survive metabolic changes caused by this genetic condition. Throughout this process, tumor cells acquire a phenotype that likely represents their adaptive response rather than the immediate effects of the mutation [355-357].

Gene promoter hypermethylation is associated with the down-regulation of immune-related genes in *IDH1*^{mut} cells, which could potentially impact TIME.

Observation in our CCA_PDX models

Our study on *IDH1*^{mut} CCA_PDXs revealed a predominantly DNA hypermethylation phenotype (Fig R21; Fig R22), accompanied by transcription repression (Fig R17). These results align with previously reported results in *IDH*^{mut} CCA patients and cell lines [15, 91, 174]. Of note, genes related to "hypoxia," "estrogen response," or "the immune system" exhibit downregulation in *IDH1*^{mut} CCA_PDXs (Fig R17B). Interestingly, differential methylation patterns in these pathways are observed between *IDH1*^{mut} and *IDH1*^{wt} CCA_PDXs (Fig R23; Fig R24).

We observed that multiple cytokines and chemokines were down-regulated in *IDH1*^{mut} CCA_PDXs. One of the most strikingly down-regulated genes in *IDH1*^{mut} CCA_PDXs was the stimulator of interferon genes (*STING1*), together with several of the components involved in the STING1 pathway, such as *OAS1-3, ISG15,* and *IRF7* (Fig R17A; Fig R19B; Fig R20C). Notably, the *STING1* gene promoter in our *IDH1*^{mut} CCA_PDXs exhibited significantly higher CpG methylation levels, specifically in the three CpG positions that are known to be crucial for *STING1* expression [329] (not shown). The STING1 pathway has been identified as a critical regulator of the transcription of various host defense genes, including

type I interferons (IFNs) and pro-inflammatory cytokines, which are essential for effective immune responses against tumors [325-329, 358]. The downregulation of the STING1 pathway due to *IDH* mutations can have an impact on the first line of immune defense, aligning with the observed silencing of NK-related immunity in *IDH1*^{mut} glioma [182]. Furthermore, several studies have suggested a direct association between the epigenetic silencing of tumor cell-intrinsic STING1 through promoter hypermethylation and tumor immunogenicity, as well as subsequent engagement of T cells [329, 359].

Mutant IDH enzymes impact on tumor immune microenvironment in other types of tumors

The association of mutant IDH with immunologically "cold" tumors has been observed in other types of tumors [284, 360, 361]. Notably, a comprehensive analysis of bulk transcriptomics data across multiple cancer types demonstrated a correlation between *IDH1* mutations and gene signatures associated with decreased infiltration of T cells, B cells, and natural killer cells [286]. In glioma, *IDH1*^{mut} tumors were characterized as immunologically "cold" tumors compared to *IDH1*^{wt} tumors [183]. It has been proposed that DNA hypermethylation in *IDH1*^{mut} glioma could lead to epigenetic downregulation of the immune checkpoint co-inhibitory molecule PD-L1 [181, 291]. This phenotype was found to be reversible with the treatment of a mutant IDH1 inhibitor, AGI-5198, in a mouse model of *IDH1*^{mut} glioma [295]. Remarkably, when this inhibitor was combined with standard-of-care chemotherapy and an anti-PD-L1 antibody, complete tumor regression was observed in 60% of the mice. Moreover, the epigenetic silencing of genes encoding natural killer group 2D (NKG2D) ligands in glioma cells made them resistant to NK cell-mediated lysis, which is typically the first line of defense against neoplasia [182]. However, treatment with the DNA demethylating agent decitabine re-sensitized tumor cells to NK-mediated killing, highlighting the role of DNA methylation in *IDH*^{mut} gliomas.

Based on these findings, DNA hypermethylation can be proposed as a plausible mechanism for the silencing of immune-related genes and subsequent immune-evasion in *IDH1*^{mut} tumors.

Mutant IDH enzymes impact on tumor immune microenvironment in the CCA model

One recent study provided direct evidence that mutant IDH1 is responsible for the immunosuppressive phenotype observed in *IDH1*^{mut} CCA. Using a genetically engineered mouse model of *IDH1*^{mut} iCCA and syngeneic allografts, researchers found that the treatment with the mutant IDH1 inhibitor ivosidenib provoked a decrease of R-2HG accumulation in tumors, accompanied by a rapid influx of infiltrating $CD8^+$ T cells, resulting in the suppression of tumor growth [160]. Notably, the antitumor effect of ivosidenib was abolished entirely when $CD8^+$ T cells were depleted. Moreover, upon treatment, the tumor cells exhibited a significant induction of gene expression related to IFNγ signaling. This was attributed to the derepression of the αKG-dependent TET2 demethylase mediated by ivosidenib. However, the underlying mechanism behind the initial promotion of $CD8^+$ T cell infiltration and effector function upon mutant IDH1 inhibition remains unclear.

It's worth noting that the model used in this study required the presence of a *KRAS* mutation for the development of CCA tumors in the *IDH1*^{R132C} background. Previous studies have suggested that these two mutations are mutually exclusive in a large number of cases [17, 22], which raises the possibility that the observed phenotype may result from the cooperation of these two genetic events and may not accurately represent the pathogenesis of CCA.

In our study, we used mIHC to analyze four *IDH1*^{wt} CCA patients and four *IDH1*^{mut} CCA patients (Fig R26). Surprisingly, *IDH1*^{mut} samples showed slightly higher immune cell infiltration but lower proliferation in T cells compared to *IDH1*^{wt} samples (Fig R26). This suggests an immunosuppressed phenotype characterized by impaired T cell activation rather than infiltration (Fig I14; Fig I15; Fig I16). Similar findings of compromised cytotoxicity in T cells have been reported in other *IDH1*^{mut} tumors [287, 290]. We also observed higher levels of $CD163^+$ cells (M2-like macrophages) in *IDH1*^{mut} CCAs, consistent with recent studies [284, 296]. These suppressive M2-macrophages can contribute to the immunologically "colder" phenotype of *IDH1*^{mut} CCAs. However, larger studies are needed to establish statistical significance, and investigating other immune cell types is important given the potential involvement of innate immunity pathways in *IDH1*^{mut} CCA_PDX.

Overall, our results revealed an intrinsic DNA methylation and transcriptional landscape

of *IDH1*^{mut} CCAs that are indicative of an immunosuppressive phenotype (Fig R25). These results align with previous studies conducted on other types of tumors. In the next section, we will discuss whether these tumor-intrinsic features affect the functionality of immune cells.

How does epigenetic silencing of *IDH*^{mut} CCA intrinsic immune signaling impact immune cells?

Based on the results obtained in the mIHC study, we speculated that T cell activation, a crucial step in the immunity cycle, may be impaired in *IDH*^{mut} CCA tumors (Fig I14; Fig I15). T cell activation relies on three essential signals, antigen presentation (signal 1), co-inhibitory molecule signaling (signal 2), and cytokine-mediated stimulation (signal 3).

Firstly, we investigated antigen presentation machinery, which is crucial for signal 1. Our transcriptomic analysis of CCA_PDXs revealed no significant dysregulation of antigen presentation-related genes in *IDH1*^{mut} samples, in contrast to a previous study in glioma [362]. In addition, the HER2-TCB system that we used for T cell activation studies (Fig R33) functions in an MHC-TCR (signal 1) independent manner; thereby, recorded changes in T cell activation in *IDH1*^{mut} cells upon decitabine treatment (Fig R34; Fig R35) require from differential signal 2 or 3 in *IDH1*^{mut} cells compared to *IDH1*^{wt}. Secondly, we examined the expression of co-inhibitory molecules, including PD-L1, associated with signal 2 of T cell activation. Interestingly, we observed similar expression levels of CD274 (PD-L1) and other co-inhibitory molecules between *IDH1*^{mut} and *IDH1*^{wt} CCA_PDXs (Fig R20C). This implies that signal 2 may not be a major contributor to the observed phenotype in *IDH1*^{mut} CCA. In light of the downregulation, concordant with promoter hypermethylation, of genes involved in cytokines, chemokines, and cytokine receptors (Fig R19; Fig R24), we postulate that signal 3 may play a pivotal role in the immunogenicity of *IDH1*^{mut} tumors.

While our primary focus has been on T cell activation and although our preliminary results of the mIHC analysis did not point towards it, it is important to acknowledge the potential presence of a T cell infiltration barrier. The downregulation of gene sets associated with cytokines and chemokines suggests that impaired expression of these molecules could hinder T cell homing to the tumor microenvironment [363]. Further investigation is required to elucidate the extent of T cell infiltration in *IDH1*^{mut} CCA.

DNA hypermethylation represents a promising target for enhancing the immunogenicity of *IDH1*^{mut} CCAs

Our research indicates a possible connection between the decrease in immune-related genes, which could be affected by excessive DNA methylation in their promoter regions, and a changed tumor immune environment in CCAs with *IDH1* mutations. Based on these findings, we propose that therapeutic strategies targeting the mutant IDH1 enzyme or DNA methylation could potentially reverse this immunosuppressed phenotype observed in *IDH1*^{mut} CCAs. By doing so, these tumors may become more responsive to Immune-Oncology (IO) therapies (Fig R27).

Two strategies to decrease DNA methylation in *IDH1*^{mut} CCA cells.

In our initial experiments, we treated *IDH1*^{mut} CCA cell lines with DNA demethylating agents (decitabine and 5-azacytidine) and a mutant IDH1 inhibitor (ivosidenib). The results showed that the DNA demethylating agents caused a decrease in DNA methylation levels (5mC) and an increase in STING1 expression. However, the mutant IDH1 inhibitor had more subtle effects (Fig R29; Fig R30). While these findings suggest that direct targeting of DNA methylation can have a greater impact on immune gene expression, we need further investigation to fully evaluate the changes caused by these treatments. Ongoing studies using genome-wide transcriptomics and DNA methylation analysis aim to confirm the potential of both strategies in enhancing immune gene expression.

Consistent with the observed treatment-related effects on immune gene expression, our results demonstrated a significant improvement in T cell activation when coculturing T cells with *IDH1*^{mut} CCA cells that were pretreated with decitabine. However, the effect on T cell activation was not substantial when using the mutant IDH1 inhibitor. These findings suggest that the DNA demethylation approach, specifically through decitabine treatment, has a greater impact on enhancing T cell activation in the context of *IDH1*^{mut} CCA (Fig R34; Fig R35; Fig R36). The precise mechanisms underlying this differential effect require further investigation; the results of the aforementioned genome-wide analysis might aid at guiding such upcoming research.

DNA demethylating agents in IO

Epigenetic modulation of anti-tumor immunity using DNA demethylating agents

(DNA methyltransferase inhibitors, DNMTi) has been successfully demonstrated in preclinical models of *IDH1*^{mut} glioma [182, 294, 295]. These studies have shown that enhancing the expression of immune-related genes within the tumor is responsible for improving immune responses. While the specific gene sets affected by treatment may vary, all reported mechanisms involve DNA demethylation of the target genes. Importantly, these drugs enhance the tumor's ability to induce an immune response and improve the efficacy of widely used immune-oncology therapies, such as immune checkpoint inhibitors or vaccine immunotherapy [294, 295].

DNMTis have been shown to increase the immune attractiveness of cancer cells by reshaping the tumor's transcriptomic profile [364-366]. This includes the reactivation of cytokine, chemokine, and interferon signaling gene expression, upregulation of antigen presentation machinery, and re-expression of tumor-associated antigens (TAAs) [367-369]. Another mechanism involves the induction of a type I interferon response by increasing the expression of DNA hypermethylated endogenous retroviruses (ERVs) [370-372]. In *IDH*^{mut} tumors, which exhibit a DNA hypermethylation phenotype, treatment with DNMTis has a profound impact on the tumor's transcriptome, as supported by our preliminary data.

The most well-known DNMTis, such as 5-aza and decitabine, are FDA-approved for treating hematological malignancies, including myelodysplastic syndromes (MDS) and certain types of acute leukemia [373-376]. These drugs are highly effective in globally demethylating genomic DNA [377]. However, they also have limitations, including lack of selectivity, potential toxicity due to their integration throughout the genome, and a short half-life under physiological conditions [378]. The demethylation function of DNMTi is widespread, affecting not only target tumor cells but also healthy cells in the body, and may lead to the re-expression of undesired targets within the tumor itself [379, 380]. To mitigate these concerns, we propose intermittent administration of DNMTi as periodic boosts of tumor immunogenicity, potentially enhancing the effects of combination immunotherapies. Our preliminary data indicate persistent effects of DNMTis even after drug exposure is removed (transcriptional changes have been observed to be maintained for ~2 weeks, data not shown), suggesting a potential advantage of intermittent treatment schedules.

Decreased DNA methylation through the inhibition of mutant IDH1 enzyme

In contrast to DNA demethylating agents, the treatment with mutant IDH1 inhibitor ivosidenib showed more subtle results. Here, we outline several possible explanations.

- The experimental setting: previous publications have reported the lack of *in vitro* effects of ivosidenib [160, 168, 338]. To address this, further investigations should be conducted using *in vivo* models, such as implanted CCA cell lines or CCA_PDXs, to evaluate the drug's efficacy in a more physiologically relevant context.
- The indirect effect on hypermethylation: ivosidenib inhibits the mutant IDH1 enzyme, disrupting its metabolic activity. This means that the cells need to adapt to a different type of metabolite availability, which helps to restore the activity of the αKG-dependent demethylases. This process may require longer treatment periods. Prolonged exposure to ivosidenib may be necessary to observe a clear phenotype, as reported in previous studies [168, 172].
- The irreversibility of *IDH* mutation-induced changes: not all epigenetic changes induced by *IDH* mutations may be equally reversible, and the potential for reversibility probably varies across different tissue types. Certain IDH^{mut} tumors might be less responsive to epigenetic changes after normalizing 2-HG levels through the mutant IDH inhibition [168, 172]. For instance, inhibition of mutant IDH1 in glioma cell lines resulted in minimal DNA methylation changes [381].

Further investigation and experimentation are needed to validate these potential explanations and provide a comprehensive understanding of the observed effects.

A single study has investigated the combination strategy of using ivosidenib, an inhibitor of the mutant IDH1 enzyme, with immune-checkpoint inhibitors in CCA. The study suggests that ivosidenib treatment promotes the activation of TET2 demethylase, leading to increased IFNγ signaling and recruitment of $CD8^+$ T cells [160]. Although ivosidenib treatment resulted in the accumulation of $CD8^+$ T cells and elevated tumor PD-L1 expression, the combination with anti-PD-1 antibodies did not lead to the expected reduction in tumor volume. However, blocking CTLA-4 was able to overcome the immunosuppressive effects mediated by other immune cell populations recruited during treatment, resulting in therapeutic synergy. It is important to note that the study used a model with both *IDH1* and *KRAS* mutations. *KRAS*

alterations have been reported to significantly impact the anti-tumor immunity [382], making it challenging to attribute the observed immune-related effects solely to the *IDH1* mutation. Further research is needed to clarify the immune-related effects and therapeutic potential of combining mutant IDH1 inhibition with immune-checkpoint inhibitors in CCA.

Finally, and as a general remark, it is important to note that the current research models used in the experimental studies described in this thesis (both cell lines and CCA_PDXs) lack a compatible and physiologically relevant immune system. Therefore, further validation is required using models incorporating a functional immune compartment. To comprehensively study the role of *IDH* mutation in immune system functionality and evaluate the proposed therapeutic strategies, it is crucial to utilize syngeneic mouse models with introduced *IDH* mutations or humanized mice implanted with CCA_PDX models. Furthermore, access to patient samples treated with mutant IDH1 inhibitors would be invaluable in providing insights and answers to the research questions raised in this context.

Conclusions

The successful development of the first collection of unresectable metastatic CCA_PDXs has allowed us to identify predictive biomarkers of PARP inhibition response in advanced CCA. Strikingly, this revealed a potential role of *IDH1* mutations in the modeling of the immune tumor microenvironment of CCA patients. Altogether, the results of this study open new therapeutic opportunities for treating metastatic CCA.

1. We have generated and characterized an advanced CCA_PDX model collection that can be used both *ex vivo* and *in vivo* for drug efficacy studies.

2. PARP inhibitor treatment inhibited the growth of *BRCA2*^{mut} CCA_PDX, as expected, but it did not impede the growth of *IDH1/2*^{mut}, *ARID1A*^{mut}, or *BAP1*^{mut} CCA_PDXs, neither in tumoroids *ex vivo* nor *in vivo*.

3. Both CCA_PDXs and advanced CCA patient biopsy samples with *IDH1/2*^{mut}, *ARID1A*^{mut}, or *BAP1*^{mut} showed RAD51 scores compatible with homologous recombination (HR) proficiency profiles, explaining the absence of response to PARP inhibition. Importantly, both *BRCA2*^{mut} CCA_PDX and extended *BRCA2*^{mut} patient data confirmed an HR deficient profile associated with this mutation in CCA, in agreement with the recorded positive PARPi responses.

4. Our results suggest that patients with advanced metastatic CCA with *BRCA2* mutations, but not those with *IDH1/2*, *ARID1A* or *BAP1* alterations, will likely benefit from PARP inhibitor treatment. Thus, clinical trials should be prioritized, and alternative vulnerabilities must be identified for patients with mutations of *IDH1/2*, *ARID1A* or *BAP1*.

5. The *IDH1* mutation was the main contributing factor to the clustering of CCA_PDXs, when either transcriptomic or DNA methylation profiles were used for assessment, highlighting the importance of its role in tumor identity.

6. *IDH1*^{mut} CCA_PDXs displayed a downregulation of immune-related response signatures, such as inflammation, interferon-alpha, and interferon-gamma.

7. Promoters of immune-related genes containing CpGs were significantly more methylated in *IDH1*^{mut} CCA_PDXs, suggesting a direct correlation between the reduced expression of these genes and their promoter hypermethylation.

8. *IDH1*^{mut} CCA patients showed a slightly higher but less proliferative tumor T cell infiltration, indicating a potential impairment in T cell activation rather than T cell

infiltration. This data can advocate a potential impact of the transcriptional and epigenetic architectures on the shaping of the immune microenvironment of *IDH1*^{mut} CCA patients.

9. Treatment of *IDH1*^{mut} CCA cell lines with the DNA demethylating agent decitabine, and to a lesser extent, the mutant IDH1 inhibitor ivosidenib, potentially rescues the expression of STING1, a crucial factor involved in initiating an immune response against tumors.

10. Pre-treatment of cancer cells with decitabine could reinvigorate T cell activation and cytotoxic activity in co-cultures of peripheral blood mononuclear cells (PBMCs) with *IDH1*^{mut} CCA cells, but not in those with *IDH1*^{wt} CCA cells. In contrast, ivosidenib treatment had no impact on immune activation.

References

1. Zamani, Z. and S. Fatima, Biliary Tract Cancer, in StatPearls. 2023, StatPearls Publishing

2. Hundt, M., H. Basit, and S. John, Physiology, Bile Secretion, in StatPearls. 2023, StatPearls Publishing

3. Banales, J.M., et al., Expert consensus document: Cholangiocarcinoma: current knowledge and future perspectives consensus statement from the European Network for the Study of Cholangiocarcinoma (ENS-CCA). Nat Rev Gastroenterol Hepatol, 2016. **13**(5): p. 261-80.

4. Valle, J.W., et al., Biliary tract cancer. Lancet, 2021. **397**(10272): p. 428-444.

5. Brindley, P.J., et al., Cholangiocarcinoma. Nat Rev Dis Primers, 2021. **7**(1): p. 65.

6. WHO, W.H.O. ICD-11, International Classification of Diseases 11th Revision. April 2023]; The global standard for diagnostic health information].

7. Banales, J.M., et al., Cholangiocarcinoma 2020: the next horizon in mechanisms and management. Nat Rev Gastroenterol Hepatol, 2020. **17**(9): p. 557-588.

8. Vij, M., et al., Pathological, molecular, and clinical characteristics of cholangiocarcinoma: A comprehensive review. World J Gastrointest Oncol, 2022. **14**(3): p. 607-627.

9. Vithayathil, M. and S.A. Khan, Current epidemiology of cholangiocarcinoma in Western countries. J Hepatol, 2022. **77**(6): p. 1690-1698.

10. Howlader N, N.A., Krapcho M, Miller D, Brest A, Yu M, Ruhl J, Tatalovich Z, Mariotto A, Lewis DR, Chen HS, Feuer EJ, Cronin KA (eds). SEER Cancer Statistics Review, 1975-2018, https://seer.cancer.gov/csr/1975_2018/, based on November 2020 SEER data submission. April 2021 April 2023].

11. Rizvi, S., et al., Cholangiocarcinoma - evolving concepts and therapeutic strategies. Nat Rev Clin Oncol, 2018. **15**(2): p. 95-111.

12. Farshidfar, F., et al., Integrative Genomic Analysis of Cholangiocarcinoma Identifies Distinct IDH-Mutant Molecular Profiles. Cell Rep, 2017. **18**(11): p. 2780-2794.

13. Lawrence, M.S., et al., Mutational heterogeneity in cancer and the search for new cancer-associated genes. Nature, 2013. **499**(7457): p. 214-218.

14. Nakamura, H., et al., Genomic spectra of biliary tract cancer. Nat Genet, 2015. **47**(9): p. 1003-10.

15. Jusakul, A., et al., Whole-Genome and Epigenomic Landscapes of Etiologically Distinct Subtypes of Cholangiocarcinoma. Cancer Discov, 2017. **7**(10): p. 1116-1135.

16. Chan-On, W., et al., Exome sequencing identifies distinct mutational patterns in liver fluke-related and non-infection-related bile duct cancers. Nat Genet, 2013. **45**(12): p. 1474-8.

17. Lowery, M.A., et al., Comprehensive Molecular Profiling of Intrahepatic and Extrahepatic Cholangiocarcinomas: Potential Targets for Intervention. Clin Cancer Res, 2018. **24**(17): p. 4154-4161.

18. Montal, R., et al., Molecular classification and therapeutic targets in extrahepatic cholangiocarcinoma. J Hepatol, 2020. **73**(2): p. 315-327.

19. Verdaguer, H., et al., ESMO Scale for Clinical Actionability of Molecular Targets Driving Targeted Treatment in Patients with Cholangiocarcinoma. Clin Cancer Res, 2022. **28**(8): p. 1662-1671.

20. Valle, J.W., et al., New Horizons for Precision Medicine in Biliary Tract Cancers. Cancer Discov, 2017. **7**(9): p. 943-962.

21. Lamarca, A., et al., Molecular targeted therapies: Ready for "prime time" in biliary tract cancer. J Hepatol, 2020. **73**(1): p. 170-185.

22. Wang, X.Y., et al., Driver mutations of intrahepatic cholangiocarcinoma shape clinically relevant genomic clusters with distinct molecular features and therapeutic vulnerabilities. Theranostics, 2022. **12**(1): p. 260-276.

23. Boscoe, A.N., C. Rolland, and R.K. Kelley, Frequency and prognostic significance of isocitrate dehydrogenase 1 mutations in cholangiocarcinoma: a systematic literature review. J Gastrointest Oncol, 2019. **10**(4): p. 751-765.

24. Isomoto, H., et al., Interleukin 6 upregulates myeloid cell leukemia-1 expression through a STAT3 pathway in cholangiocarcinoma cells. Hepatology, 2005. **42**(6): p. 1329-38.

25. Brivio, S., et al., Tumor reactive stroma in cholangiocarcinoma: The fuel behind

cancer aggressiveness. World J Hepatol, 2017. **9**(9): p. 455-468.

26. Xue, T.C., et al., Differentially expressed gene profiles of intrahepatic cholangiocarcinoma, hepatocellular carcinoma, and combined hepatocellular-cholangiocarcinoma by integrated microarray analysis. Tumour Biol, 2015. **36**(8): p. 5891-9.

27. Zong, Y., et al., Notch signaling controls liver development by regulating biliary differentiation. Development, 2009. **136**(10): p. 1727-39.

28. Zender, S., et al., A critical role for notch signaling in the formation of cholangiocellular carcinomas. Cancer Cell, 2013. **23**(6): p. 784-95.

29. Guest, R.V., et al., Notch3 drives development and progression of cholangiocarcinoma. Proc Natl Acad Sci U S A, 2016. **113**(43): p. 12250-12255.

30. Tian, L., Y. Wang, and Y.Y. Jang, Wnt signaling in biliary development, proliferation, and fibrosis. Exp Biol Med (Maywood), 2022. **247**(4): p. 360-367.

31. Loilome, W., et al., Activated macrophages promote Wnt/β-catenin signaling in cholangiocarcinoma cells. Tumour Biol, 2014. **35**(6): p. 5357-67.

32. Perugorria, M.J., et al., Wnt-β-catenin signalling in liver development, health and disease. Nat Rev Gastroenterol Hepatol, 2019. **16**(2): p. 121-136.

33. Cigliano, A., et al., Role of the Notch signaling in cholangiocarcinoma. Expert Opin Ther Targets, 2017. **21**(5): p. 471-483.

34. Boulter, L., et al., WNT signaling drives cholangiocarcinoma growth and can be pharmacologically inhibited. J Clin Invest, 2015. **125**(3): p. 1269-85.

35. Sugihara, T., et al., YAP and the Hippo pathway in cholangiocarcinoma. J Gastroenterol, 2019. **54**(6): p. 485-491.

36. Carloni, R., et al., Targeting tumor microenvironment for cholangiocarcinoma: Opportunities for precision medicine. Transl Oncol, 2022. **25**: p. 101514.

37. Fabris, L., et al., The Tumor Microenvironment in Cholangiocarcinoma Progression. Hepatology, 2021. **73 Suppl 1**(Suppl 1): p. 75-85.

38. Sirica, A.E. and G.J. Gores, Desmoplastic stroma and cholangiocarcinoma: clinical implications and therapeutic targeting. Hepatology, 2014. **59**(6): p. 2397-402.

39. Høgdall, D., M. Lewinska, and J.B. Andersen, Desmoplastic Tumor Microenviron-

ment and Immunotherapy in Cholangiocarcinoma. Trends Cancer, 2018. **4**(3): p. 239-255.

40. Tamma, R., et al., Inflammatory cells infiltrate and angiogenesis in locally advanced and metastatic cholangiocarcinoma. Eur J Clin Invest, 2019. **49**(5): p. e13087.

41. Greten, T.F., et al., Immunology and immunotherapy of cholangiocarcinoma. Nat Rev Gastroenterol Hepatol, 2023.

42. Affo, S., L.X. Yu, and R.F. Schwabe, The Role of Cancer-Associated Fibroblasts and Fibrosis in Liver Cancer. Annu Rev Pathol, 2017. **12**: p. 153-186.

43. Affo, S., et al., Promotion of cholangiocarcinoma growth by diverse cancer-associated fibroblast subpopulations. Cancer Cell, 2021. **39**(6): p. 866-882.e11.

44. Ma, C., Q. Zhang, and T.F. Greten, MDSCs in liver cancer: A critical tumor-promoting player and a potential therapeutic target. Cell Immunol, 2021. **361**: p. 104295.

45. Zimmer, C.L., et al., Mucosal-associated invariant T-cell tumor infiltration predicts long-term survival in cholangiocarcinoma. Hepatology, 2022. **75**(5): p. 1154-1168.

46. Liang, B., et al., Diagnostic Accuracy of Serum CA19-9 in Patients with Cholangiocarcinoma: A Systematic Review and Meta-Analysis. Med Sci Monit, 2015. **21**: p. 3555-63.

47. Izquierdo-Sanchez, L., et al., Cholangiocarcinoma landscape in Europe: Diagnostic, prognostic and therapeutic insights from the ENSCCA Registry. J Hepatol, 2022. **76**(5): p. 1109-1121.

48. Primrose, J.N., et al., Capecitabine compared with observation in resected biliary tract cancer (BILCAP): a randomised, controlled, multicentre, phase 3 study. Lancet Oncol, 2019. **20**(5): p. 663-673.

49. Park, S.Y., et al., Transarterial chemoembolization versus supportive therapy in the palliative treatment of unresectable intrahepatic cholangiocarcinoma. Clin Radiol, 2011. **66**(4): p. 322-8.

50. Rafi, S., et al., Yttrium-90 radioembolization for unresectable standard-chemorefractory intrahepatic cholangiocarcinoma: survival, efficacy, and safety study. Cardiovasc Intervent Radiol, 2013. **36**(2): p. 440-8.

51. Valle, J., et al., Cisplatin plus gemcitabine versus gemcitabine for biliary tract cancer. N Engl J Med, 2010. **362**(14): p. 1273-81.

52. Shroff, R.T., et al., Gemcitabine, Cisplatin, and nab-Paclitaxel for the Treatment of Advanced Biliary Tract Cancers: A Phase 2 Clinical Trial. JAMA Oncol, 2019. **5**(6): p. 824-830.

53. Oh, D.-Y., et al., Durvalumab plus Gemcitabine and Cisplatin in Advanced Biliary Tract Cancer. NEJM Evidence, 2022. **1**(8): p. EVIDoa2200015.

54. Kelley, R.K., et al., Pembrolizumab in combination with gemcitabine and cisplatin compared with gemcitabine and cisplatin alone for patients with advanced biliary tract cancer (KEYNOTE-966): a randomised, double-blind, placebo-controlled, phase 3 trial. Lancet, 2023.

55. Harding, J.J., et al., Rational development of combination therapies for biliary tract cancers. J Hepatol, 2023. **78**(1): p. 217-228.

56. Kendre, G., et al., Charting co-mutation patterns associated with actionable drivers in intrahepatic cholangiocarcinoma. J Hepatol, 2023. **78**(3): p. 614-626.

57. Abou-Alfa, G.K., et al., Pemigatinib for previously treated, locally advanced or metastatic cholangiocarcinoma: a multicentre, open-label, phase 2 study. Lancet Oncol, 2020. **21**(5): p. 671-684.

58. Goyal, L., et al., Futibatinib for FGFR2-Rearranged Intrahepatic Cholangiocarcinoma. N Engl J Med, 2023. **388**(3): p. 228-239.

59. Abou-Alfa, G.K., et al., Ivosidenib in IDH1-mutant, chemotherapy-refractory cholangiocarcinoma (ClarIDHy): a multicentre, randomised, double-blind, placebo-controlled, phase 3 study. Lancet Oncol, 2020. **21**(6): p. 796-807.

60. Drilon, A., et al., Efficacy of Larotrectinib in TRK Fusion-Positive Cancers in Adults and Children. N Engl J Med, 2018. **378**(8): p. 731-739.

61. Doebele, R.C., et al., Entrectinib in patients with advanced or metastatic NTRK fusion-positive solid tumours: integrated analysis of three phase 1-2 trials. Lancet Oncol, 2020. **21**(2): p. 271-282.

62. Subbiah, V., et al., Dabrafenib plus trametinib in patients with BRAF(V600E)-mutated biliary tract cancer (ROAR): a phase 2, open-label, single-arm, multicentre

basket trial. Lancet Oncol, 2020. **21**(9): p. 1234-1243.

63. Marabelle, A., et al., Efficacy of Pembrolizumab in Patients With Noncolorectal High Microsatellite Instability/Mismatch Repair-Deficient Cancer: Results From the Phase II KEYNOTE-158 Study. J Clin Oncol, 2020. **38**(1): p. 1-10.

64. Meric-Bernstam, F., et al., Zanidatamab, a novel bispecific antibody, for the treatment of locally advanced or metastatic HER2-expressing or HER2-amplified cancers: a phase 1, dose-escalation and expansion study. Lancet Oncol, 2022. **23**(12): p. 1558-1570.

65. Philip, P.A., et al., Phase II study of erlotinib in patients with advanced biliary cancer. J Clin Oncol, 2006. **24**(19): p. 3069-74.

66. Malka, D., et al., Gemcitabine and oxaliplatin with or without cetuximab in advanced biliary-tract cancer (BINGO): a randomised, open-label, non-comparative phase 2 trial. Lancet Oncol, 2014. **15**(8): p. 819-28.

67. Lamarca, A., et al., Second-line FOLFOX chemotherapy versus active symptom control for advanced biliary tract cancer (ABC-06): a phase 3, open-label, randomised, controlled trial. Lancet Oncol, 2021. **22**(5): p. 690-701.

68. Calvisi, D.F., et al., Criteria for preclinical models of cholangiocarcinoma: scientific and medical relevance. Nat Rev Gastroenterol Hepatol, 2023.

69. Tepsiri, N., et al., Drug sensitivity and drug resistance profiles of human intrahepatic cholangiocarcinoma cell lines. World J Gastroenterol, 2005. **11**(18): p. 2748-53.

70. Domcke, S., et al., Evaluating cell lines as tumour models by comparison of genomic profiles. Nat Commun, 2013. **4**: p. 2126.

71. Saha, S.K., et al., Isocitrate Dehydrogenase Mutations Confer Dasatinib Hypersensitivity and SRC Dependence in Intrahepatic Cholangiocarcinoma. Cancer Discov, 2016. **6**(7): p. 727-39.

72. Ben-David, U., et al., Genetic and transcriptional evolution alters cancer cell line drug response. Nature, 2018. **560**(7718): p. 325-330.

73. Massani, M., et al., Isolation and characterization of biliary epithelial and stromal cells from resected human cholangiocarcinoma: a novel in vitro model to study tumor-stroma interactions. Oncol Rep, 2013. **30**(3): p. 1143-8.

74. Miserocchi, G., et al., Management and potentialities of primary cancer cultures in preclinical and translational studies. J Transl Med, 2017. **15**(1): p. 229.

75. Friedrich, J., et al., Spheroid-based drug screen: considerations and practical approach. Nat Protoc, 2009. **4**(3): p. 309-24.

76. Broutier, L., et al., Human primary liver cancer-derived organoid cultures for disease modeling and drug screening. Nat Med, 2017. **23**(12): p. 1424-1435.

77. Nuciforo, S., et al., Organoid Models of Human Liver Cancers Derived from Tumor Needle Biopsies. Cell Rep, 2018. **24**(5): p. 1363-1376.

78. Lau, H.C.H., et al., Organoid models of gastrointestinal cancers in basic and translational research. Nat Rev Gastroenterol Hepatol, 2020. **17**(4): p. 203-222.

79. Cadamuro, M., et al., Animal models of cholangiocarcinoma: What they teach us about the human disease. Clin Res Hepatol Gastroenterol, 2018. **42**(5): p. 403-415.

80. Loeuillard, E., et al., Animal models of cholangiocarcinoma. Biochim Biophys Acta Mol Basis Dis, 2019. **1865**(5): p. 982-992.

81. Tolba, R., et al., Diethylnitrosamine (DEN)-induced carcinogenic liver injury in mice. Lab Anim, 2015. **49**(1 Suppl): p. 59-69.

82. Dill, M.T., et al., Constitutive Notch2 signaling induces hepatic tumors in mice. Hepatology, 2013. **57**(4): p. 1607-19.

83. Elmore, L.W. and A.E. Sirica, Phenotypic characterization of metaplastic intestinal glands and ductular hepatocytes in cholangiofibrotic lesions rapidly induced in the caudate liver lobe of rats treated with furan. Cancer Res, 1991. **51**(20): p. 5752-9.

84. Yeh, C.N., et al., Thioacetamide-induced intestinal-type cholangiocarcinoma in rat: an animal model recapitulating the multi-stage progression of human cholangiocarcinoma. Carcinogenesis, 2004. **25**(4): p. 631-6.

85. Al-Bader, A., et al., Cholangiocarcinoma and liver cirrhosis in relation to changes due to thioacetamide. Mol Cell Biochem, 2000. **208**(1-2): p. 1-10.

86. Thamavit, W., et al., Effects of dimethylnitrosamine on induction of cholangiocarcinoma in Opisthorchis viverrini-infected Syrian golden hamsters. Cancer Res, 1978. **38**(12): p. 4634-9.

87. Thamavit, W., et al., Strong promoting effect of Opisthorchis viverrini infection on dimethylnitrosamine-initiated hamster liver. Cancer Lett, 1994. **78**(1-3): p. 121-5.

88. Massa, A., et al., Evolution of the Experimental Models of Cholangiocarcinoma. Cancers (Basel), 2020. **12**(8).

89. Xu, X., et al., Induction of intrahepatic cholangiocellular carcinoma by liver-specific disruption of Smad4 and Pten in mice. J Clin Invest, 2006. **116**(7): p. 1843-52.

90. Ikenoue, T., et al., A novel mouse model of intrahepatic cholangiocarcinoma induced by liver-specific Kras activation and Pten deletion. Sci Rep, 2016. **6**: p. 23899.

91. Saha, S.K., et al., Mutant IDH inhibits HNF-4α to block hepatocyte differentiation and promote biliary cancer. Nature, 2014. **513**(7516): p. 110-4.

92. Tschaharganeh, D.F., et al., p53-dependent Nestin regulation links tumor suppression to cellular plasticity in liver cancer. Cell, 2014. **158**(3): p. 579-92.

93. El Khatib, M., et al., Activation of Notch signaling is required for cholangiocarcinoma progression and is enhanced by inactivation of p53 in vivo. PLoS One, 2013. **8**(10): p. e77433.

94. O'Dell, M.R., et al., Kras(G12D) and p53 mutation cause primary intrahepatic cholangiocarcinoma. Cancer Res, 2012. **72**(6): p. 1557-67.

95. Hill, M.A., et al., Kras and Tp53 Mutations Cause Cholangiocyte- and Hepatocyte-Derived Cholangiocarcinoma. Cancer Res, 2018. **78**(16): p. 4445-4451.

96. Falcomatà, C., et al., Genetic Screens Identify a Context-Specific PI3K/p27Kip1 Node Driving Extrahepatic Biliary Cancer. Cancer Discov, 2021. **11**(12): p. 3158-3177.

97. Abdolahi, S., et al., Patient-derived xenograft (PDX) models, applications and challenges in cancer research. J Transl Med, 2022. **20**(1): p. 206.

98. Rizvi, S., et al., YAP-associated chromosomal instability and cholangiocarcinoma in mice. Oncotarget, 2018. **9**(5): p. 5892-5905.

99. Yamada, D., et al., IL-33 facilitates oncogene-induced cholangiocarcinoma in mice by an interleukin-6-sensitive mechanism. Hepatology, 2015. **61**(5): p. 1627-42.

100. Bruna, A., et al., A Biobank of Breast Cancer Explants with Preserved Intra-tumor

Heterogeneity to Screen Anticancer Compounds. Cell, 2016. **167**(1): p. 260-274.e22.

101. Leiting, J.L., et al., Biliary tract cancer patient-derived xenografts: Surgeon impact on individualized medicine. JHEP Rep, 2020. **2**(2): p. 100068.

102. Jiang, T.Y., et al., PTEN status determines chemosensitivity to proteasome inhibition in cholangiocarcinoma. Sci Transl Med, 2020. **12**(562).

103. Ojima, H., et al., Establishment of six new human biliary tract carcinoma cell lines and identification of MAGEH1 as a candidate biomarker for predicting the efficacy of gemcitabine treatment. Cancer Science, 2010. **101**(4): p. 882-888.

104. Cavalloni, G., et al., Establishment and characterization of a human intrahepatic cholangiocarcinoma cell line derived from an Italian patient. Tumour Biol, 2016. **37**(3): p. 4041-52.

105. Vaeteewoottacharn, K., et al., Establishment of Highly Transplantable Cholangiocarcinoma Cell Lines from a Patient-Derived Xenograft Mouse Model. Cells, 2019. **8**(5).

106. Wang, Y., et al., Plasmalemma vesicle-associated protein promotes angiogenesis in cholangiocarcinoma via the DKK1/CKAP4/PI3K signaling pathway. Oncogene, 2021. **40**(25): p. 4324-4337.

107. Gao, H., et al., High-throughput screening using patient-derived tumor xenografts to predict clinical trial drug response. Nat Med, 2015. **21**(11): p. 1318-25.

108. Bertotti, A., et al., A molecularly annotated platform of patient-derived xenografts ("xenopatients") identifies HER2 as an effective therapeutic target in cetuximab-resistant colorectal cancer. Cancer Discov, 2011. **1**(6): p. 508-23.

109. Sun, H., et al., Author Correction: Comprehensive characterization of 536 patient-derived xenograft models prioritizes candidates for targeted treatment. Nat Commun, 2022. **13**(1): p. 294.

110. Garcia, P.L., et al., JQ1 Induces DNA Damage and Apoptosis, and Inhibits Tumor Growth in a Patient-Derived Xenograft Model of Cholangiocarcinoma. Mol Cancer Ther, 2018. **17**(1): p. 107-118.

111. Oermann, E.K., et al., Alterations of metabolic genes and metabolites in cancer. Semin Cell Dev Biol, 2012. **23**(4): p. 370-80.

112. Anderson, N.M., et al., The emerging role and targetability of the TCA cycle in cancer metabolism. Protein Cell, 2018. **9**(2): p. 216-237.

113. Parsons, D.W., et al., An integrated genomic analysis of human glioblastoma multiforme. Science, 2008. **321**(5897): p. 1807-12.

114. Pirozzi, C.J. and H. Yan, The implications of IDH mutations for cancer development and therapy. Nat Rev Clin Oncol, 2021. **18**(10): p. 645-661.

115. Liu, S., T. Cadoux-Hudson, and C.J. Schofield, Isocitrate dehydrogenase variants in cancer - Cellular consequences and therapeutic opportunities. Curr Opin Chem Biol, 2020. **57**: p. 122-134.

116. Al-Khallaf, H., Isocitrate dehydrogenases in physiology and cancer: biochemical and molecular insight. Cell Biosci, 2017. **7**: p. 37.

117. Mardis, E.R., et al., Recurring mutations found by sequencing an acute myeloid leukemia genome. N Engl J Med, 2009. **361**(11): p. 1058-66.

118. Yan, H., et al., IDH1 and IDH2 mutations in gliomas. N Engl J Med, 2009. **360**(8): p. 765-73.

119. Ley, T.J., et al., Genomic and epigenomic landscapes of adult de novo acute myeloid leukemia. N Engl J Med, 2013. **368**(22): p. 2059-74.

120. Gross, S., et al., Cancer-associated metabolite 2-hydroxyglutarate accumulates in acute myelogenous leukemia with isocitrate dehydrogenase 1 and 2 mutations. J Exp Med, 2010. **207**(2): p. 339-44.

121. Amary, M.F., et al., IDH1 and IDH2 mutations are frequent events in central chondrosarcoma and central and periosteal chondromas but not in other mesenchymal tumours. J Pathol, 2011. **224**(3): p. 334-43.

122. Dogan, S., et al., Frequent IDH2 R172 mutations in undifferentiated and poorly-differentiated sinonasal carcinomas. J Pathol, 2017. **242**(4): p. 400-408.

123. Mito, J.K., et al., Immunohistochemical Detection and Molecular Characterization of IDH-mutant Sinonasal Undifferentiated Carcinomas. Am J Surg Pathol, 2018. **42**(8): p. 1067-1075.

124. Cairns, R.A., et al., IDH2 mutations are frequent in angioimmunoblastic T-cell lym-

phoma. Blood, 2012. **119**(8): p. 1901-3.

125. Sanson, M., et al., Isocitrate dehydrogenase 1 codon 132 mutation is an important prognostic biomarker in gliomas. J Clin Oncol, 2009. **27**(25): p. 4150-4.

126. Cohen, A.L., S.L. Holmen, and H. Colman, IDH1 and IDH2 mutations in gliomas. Curr Neurol Neurosci Rep, 2013. **13**(5): p. 345.

127. Xu, Q., et al., Correlation Between Isocitrate Dehydrogenase Gene Aberrations and Prognosis of Patients with Acute Myeloid Leukemia: A Systematic Review and Meta-Analysis. Clin Cancer Res, 2017. **23**(15): p. 4511-4522.

128. Shen, Y., et al., Gene mutation patterns and their prognostic impact in a cohort of 1185 patients with acute myeloid leukemia. Blood, 2011. **118**(20): p. 5593-603.

129. DiNardo, C.D., et al., Characteristics, clinical outcome, and prognostic significance of IDH mutations in AML. Am J Hematol, 2015. **90**(8): p. 732-6.

130. Nicolle, R., et al., Integrated molecular characterization of chondrosarcoma reveals critical determinants of disease progression. Nat Commun, 2019. **10**(1): p. 4622.

131. Prensner, J.R. and A.M. Chinnaiyan, Metabolism unhinged: IDH mutations in cancer. Nat Med, 2011. **17**(3): p. 291-3.

132. Mehrjardi, N.Z., D. Hänggi, and U.D. Kahlert, Current biomarker-associated procedures of cancer modeling-a reference in the context of IDH1 mutant glioma. Cell Death Dis, 2020. **11**(11): p. 998.

133. David L.Nelson, M.M.C., Lehninger principles of biochemistry, 4th edition. 2012.

134. Tommasini-Ghelfi, S., et al., Cancer-associated mutation and beyond: The emerging biology of isocitrate dehydrogenases in human disease. Sci Adv, 2019. **5**(5): p. eaaw4543.

135. Han, S., et al., IDH mutation in glioma: molecular mechanisms and potential therapeutic targets. Br J Cancer, 2020. **122**(11): p. 1580-1589.

136. Markolovic, S., S.E. Wilkins, and C.J. Schofield, Protein Hydroxylation Catalyzed by 2-Oxoglutarate-dependent Oxygenases. J Biol Chem, 2015. **290**(34): p. 20712-20722.

137. Herr, C.Q. and R.P. Hausinger, Amazing Diversity in Biochemical Roles of

Fe(II)/2-Oxoglutarate Oxygenases. Trends Biochem Sci, 2018. **43**(7): p. 517-532.

138. Alzial, G., et al., Wild-type isocitrate dehydrogenase under the spotlight in glioblastoma. Oncogene, 2022. **41**(5): p. 613-621.

139. Cloos, P.A., et al., Erasing the methyl mark: histone demethylases at the center of cellular differentiation and disease. Genes Dev, 2008. **22**(9): p. 1115-40.

140. Ito, S., et al., Tet proteins can convert 5-methylcytosine to 5-formylcytosine and 5-carboxylcytosine. Science, 2011. **333**(6047): p. 1300-3.

141. Sullivan, B.A. and G.H. Karpen, Centromeric chromatin exhibits a histone modification pattern that is distinct from both euchromatin and heterochromatin. Nat Struct Mol Biol, 2004. **11**(11): p. 1076-83.

142. Greer, E.L. and Y. Shi, Histone methylation: a dynamic mark in health, disease and inheritance. Nature Reviews Genetics, 2012. **13**(5): p. 343-357.

143. Al Aboud, N.M., C. Tupper, and I. Jialal, Genetics, Epigenetic Mechanism, in StatPearls. 2023, StatPearls Publishing

144. Moore, L.D., T. Le, and G. Fan, DNA methylation and its basic function. Neuropsychopharmacology, 2013. **38**(1): p. 23-38.

145. Parry, A., S. Rulands, and W. Reik, Active turnover of DNA methylation during cell fate decisions. Nat Rev Genet, 2021. **22**(1): p. 59-66.

146. Molenaar, R.J., et al., Wild-type and mutated IDH1/2 enzymes and therapy responses. Oncogene, 2018. **37**(15): p. 1949-1960.

147. Dang, L., et al., Cancer-associated IDH1 mutations produce 2-hydroxyglutarate. Nature, 2009. **462**(7274): p. 739-44.

148. Xu, X., et al., Structures of human cytosolic NADP-dependent isocitrate dehydrogenase reveal a novel self-regulatory mechanism of activity. J Biol Chem, 2004. **279**(32): p. 33946-57.

149. Struys, E.A., et al., Mutations in the D-2-hydroxyglutarate dehydrogenase gene cause D-2-hydroxyglutaric aciduria. Am J Hum Genet, 2005. **76**(2): p. 358-60.

150. Losman, J.A. and W.G. Kaelin, Jr., What a difference a hydroxyl makes: mutant IDH, (R)-2-hydroxyglutarate, and cancer. Genes Dev, 2013. **27**(8): p. 836-52.

151. Yang, H., et al., IDH1 and IDH2 mutations in tumorigenesis: mechanistic insights and clinical perspectives. Clin Cancer Res, 2012. **18**(20): p. 5562-71.

152. Koivunen, P., et al., Transformation by the (R)-enantiomer of 2-hydroxyglutarate linked to EGLN activation. Nature, 2012. **483**(7390): p. 484-8.

153. Avsar, T., et al., IDH1 mutation activates mTOR signaling pathway, promotes cell proliferation and invasion in glioma cells. Mol Biol Rep, 2022. **49**(10): p. 9241-9249.

154. Bralten, L.B., et al., IDH1 R132H decreases proliferation of glioma cell lines in vitro and in vivo. Ann Neurol, 2011. **69**(3): p. 455-63.

155. Shi, J., et al., An IDH1 mutation inhibits growth of glioma cells via GSH depletion and ROS generation. Neurol Sci, 2014. **35**(6): p. 839-45.

156. Lu, C., et al., IDH mutation impairs histone demethylation and results in a block to cell differentiation. Nature, 2012. **483**(7390): p. 474-8.

157. Figueroa, M.E., et al., Leukemic IDH1 and IDH2 mutations result in a hypermethylation phenotype, disrupt TET2 function, and impair hematopoietic differentiation. Cancer Cell, 2010. **18**(6): p. 553-67.

158. Modrek, A.S., et al., Low-Grade Astrocytoma Mutations in IDH1, P53, and ATRX Cooperate to Block Differentiation of Human Neural Stem Cells via Repression of SOX2. Cell Rep, 2017. **21**(5): p. 1267-1280.

159. Ding, N., et al., Oncogenic potential of IDH1R132C mutant in cholangiocarcinoma development in mice. World J Gastroenterol, 2016. **22**(6): p. 2071-80.

160. Wu, M.J., et al., Mutant IDH Inhibits IFNγ-TET2 Signaling to Promote Immunoevasion and Tumor Maintenance in Cholangiocarcinoma. Cancer Discov, 2022. **12**(3): p. 812-835.

161. Reitman, Z.J., et al., Profiling the effects of isocitrate dehydrogenase 1 and 2 mutations on the cellular metabolome. Proc Natl Acad Sci U S A, 2011. **108**(8): p. 3270-5.

162. McBrayer, S.K., et al., Transaminase Inhibition by 2-Hydroxyglutarate Impairs Glutamate Biosynthesis and Redox Homeostasis in Glioma. Cell, 2018. **175**(1): p. 101-116.e25.

163. Raffel, S., et al., BCAT1 restricts αKG levels in AML stem cells leading to IDHmut-

like DNA hypermethylation. Nature, 2017. **551**(7680): p. 384-388.

164. Tang, X., et al., Blockade of Glutathione Metabolism in IDH1-Mutated Glioma. Mol Cancer Ther, 2020. **19**(1): p. 221-230.

165. Liu, Y., et al., Targeting IDH1-Mutated Malignancies with NRF2 Blockade. J Natl Cancer Inst, 2019. **111**(10): p. 1033-1041.

166. Navis, A.C., et al., Increased mitochondrial activity in a novel IDH1-R132H mutant human oligodendroglioma xenograft model: in situ detection of 2-HG and α-KG. Acta Neuropathol Commun, 2013. **1**: p. 18.

167. Ohka, F., et al., Quantitative metabolome analysis profiles activation of glutaminolysis in glioma with IDH1 mutation. Tumour Biol, 2014. **35**(6): p. 5911-20.

168. Tateishi, K., et al., Extreme Vulnerability of IDH1 Mutant Cancers to NAD+ Depletion. Cancer Cell, 2015. **28**(6): p. 773-784.

169. Nepal, C., et al., Genomic perturbations reveal distinct regulatory networks in intrahepatic cholangiocarcinoma. Hepatology, 2018. **68**(3): p. 949-963.

170. Noushmehr, H., et al., Identification of a CpG island methylator phenotype that defines a distinct subgroup of glioma. Cancer Cell, 2010. **17**(5): p. 510-22.

171. Unruh, D., et al., Methylation and transcription patterns are distinct in IDH mutant gliomas compared to other IDH mutant cancers. Sci Rep, 2019. **9**(1): p. 8946.

172. Turcan, S., et al., Mutant-IDH1-dependent chromatin state reprogramming, reversibility, and persistence. Nat Genet, 2018. **50**(1): p. 62-72.

173. Lyu, C., et al., Rare and misincorporated DNA N(6)-methyladenine is a hallmark of cytotoxic stresses for selectively stimulating the stemness and proliferation of glioblastoma cells. Cell Discov, 2022. **8**(1): p. 39.

174. Wang, P., et al., Mutations in isocitrate dehydrogenase 1 and 2 occur frequently in intrahepatic cholangiocarcinomas and share hypermethylation targets with glioblastomas. Oncogene, 2013. **32**(25): p. 3091-100.

175. Cairns, R.A. and T.W. Mak, Oncogenic Isocitrate Dehydrogenase Mutations: Mechanisms, Models, and Clinical Opportunities. Cancer Discovery, 2013. **3**(7): p. 730-741.

176. Fujiwara, H., et al., Mutant IDH1 confers resistance to energy stress in normal biliary cells through PFKP-induced aerobic glycolysis and AMPK activation. Sci Rep, 2019. **9**(1): p. 18859.

177. Inoue, S., et al., Mutant IDH1 Downregulates ATM and Alters DNA Repair and Sensitivity to DNA Damage Independent of TET2. Cancer Cell, 2016. **30**(2): p. 337-348.

178. Sulkowski, P.L., et al., 2-Hydroxyglutarate produced by neomorphic IDH mutations suppresses homologous recombination and induces PARP inhibitor sensitivity. Sci Transl Med, 2017. **9**(375).

179. Sulkowski, P.L., et al., Oncometabolites suppress DNA repair by disrupting local chromatin signalling. Nature, 2020. **582**(7813): p. 586-591.

180. Núñez, F.J., et al., IDH1-R132H acts as a tumor suppressor in glioma via epigenetic up-regulation of the DNA damage response. Sci Transl Med, 2019. **11**(479).

181. Mu, L., et al., The IDH1 Mutation-Induced Oncometabolite, 2-Hydroxyglutarate, May Affect DNA Methylation and Expression of PD-L1 in Gliomas. Front Mol Neurosci, 2018. **11**: p. 82.

182. Zhang, X., et al., IDH mutant gliomas escape natural killer cell immune surveillance by downregulation of NKG2D ligand expression. Neuro Oncol, 2016. **18**(10): p. 1402-12.

183. Amankulor, N.M., et al., Mutant IDH1 regulates the tumor-associated immune system in gliomas. Genes Dev, 2017. **31**(8): p. 774-786.

184. Flavahan, W.A., et al., Insulator dysfunction and oncogene activation in IDH mutant gliomas. Nature, 2016. **529**(7584): p. 110-4.

185. Ward, P.S., et al., The potential for isocitrate dehydrogenase mutations to produce 2-hydroxyglutarate depends on allele specificity and subcellular compartmentalization. J Biol Chem, 2013. **288**(6): p. 3804-15.

186. Urban, D.J., et al., Assessing inhibitors of mutant isocitrate dehydrogenase using a suite of pre-clinical discovery assays. Sci Rep, 2017. **7**(1): p. 12758.

187. Stein, E.M., et al., Enasidenib in patients with mutant IDH2 myelodysplastic syndromes: a phase 1 subgroup analysis of the multicentre, AG221-C-001 trial. Lancet

Haematol, 2020. **7**(4): p. e309-e319.

188. Mellinghoff, I.K., et al., Vorasidenib, a Dual Inhibitor of Mutant IDH1/2, in Recurrent or Progressive Glioma; Results of a First-in-Human Phase I Trial. Clin Cancer Res, 2021. **27**(16): p. 4491-4499.

189. Dang, L. and S.M. Su, Isocitrate Dehydrogenase Mutation and (R)-2-Hydroxyglutarate: From Basic Discovery to Therapeutics Development. Annu Rev Biochem, 2017. **86**: p. 305-331.

190. Stein, E.M., et al., Enasidenib in mutant IDH2 relapsed or refractory acute myeloid leukemia. Blood, 2017. **130**(6): p. 722-731.

191. DiNardo, C.D., et al., Durable Remissions with Ivosidenib in IDH1-Mutated Relapsed or Refractory AML. N Engl J Med, 2018. **378**(25): p. 2386-2398.

192. Pusch, S., et al., Pan-mutant IDH1 inhibitor BAY 1436032 for effective treatment of IDH1 mutant astrocytoma in vivo. Acta Neuropathol, 2017. **133**(4): p. 629-644.

193. Kopinja, J., et al., A Brain Penetrant Mutant IDH1 Inhibitor Provides In Vivo Survival Benefit. Sci Rep, 2017. **7**(1): p. 13853.

194. Natsume, A., et al., The first-in-human phase I study of a brain-penetrant mutant IDH1 inhibitor DS-1001 in patients with recurrent or progressive IDH1-mutant gliomas. Neuro Oncol, 2023. **25**(2): p. 326-336.

195. Nakagawa, M., et al., Selective inhibition of mutant IDH1 by DS-1001b ameliorates aberrant histone modifications and impairs tumor activity in chondrosarcoma. Oncogene, 2019. **38**(42): p. 6835-6849.

196. Popovici-Muller, J., et al., Discovery of AG-120 (Ivosidenib): A First-in-Class Mutant IDH1 Inhibitor for the Treatment of IDH1 Mutant Cancers. ACS Med Chem Lett, 2018. **9**(4): p. 300-305.

197. DiNardo, C.D., et al., Mutant Isocitrate Dehydrogenase 1 Inhibitor Ivosidenib in Combination With Azacitidine for Newly Diagnosed Acute Myeloid Leukemia. J Clin Oncol, 2021. **39**(1): p. 57-65.

198. Tap, W.D., et al., Phase I Study of the Mutant IDH1 Inhibitor Ivosidenib: Safety and Clinical Activity in Patients With Advanced Chondrosarcoma. J Clin Oncol, 2020. **38**(15): p. 1693-1701.

199. Mellinghoff, I.K., et al., Ivosidenib in Isocitrate Dehydrogenase 1-Mutated Advanced Glioma. J Clin Oncol, 2020. **38**(29): p. 3398-3406.

200. Yen, K., et al., AG-221, a First-in-Class Therapy Targeting Acute Myeloid Leukemia Harboring Oncogenic IDH2 Mutations. Cancer Discov, 2017. **7**(5): p. 478-493.

201. Konteatis, Z., et al., Vorasidenib (AG-881): A First-in-Class, Brain-Penetrant Dual Inhibitor of Mutant IDH1 and 2 for Treatment of Glioma. ACS Med Chem Lett, 2020. **11**(2): p. 101-107.

202. Heuser, M., et al., Safety and efficacy of BAY1436032 in IDH1-mutant AML: phase I study results. Leukemia, 2020. **34**(11): p. 2903-2913.

203. Chaturvedi, A., et al., Pan-mutant-IDH1 inhibitor BAY1436032 is highly effective against human IDH1 mutant acute myeloid leukemia in vivo. Leukemia, 2017. **31**(10): p. 2020-2028.

204. DiNardo, C.D., et al., A phase 1 study of IDH305 in patients with IDH1(R132)-mutant acute myeloid leukemia or myelodysplastic syndrome. J Cancer Res Clin Oncol, 2023. **149**(3): p. 1145-1158.

205. Cho, Y.S., et al., Discovery and Evaluation of Clinical Candidate IDH305, a Brain Penetrant Mutant IDH1 Inhibitor. ACS Med Chem Lett, 2017. **8**(10): p. 1116-1121.

206. Machida, Y., et al., A Potent Blood-Brain Barrier-Permeable Mutant IDH1 Inhibitor Suppresses the Growth of Glioblastoma with IDH1 Mutation in a Patient-Derived Orthotopic Xenograft Model. Mol Cancer Ther, 2020. **19**(2): p. 375-383.

207. Watts, J.M., et al., Olutasidenib alone or with azacitidine in IDH1-mutated acute myeloid leukaemia and myelodysplastic syndrome: phase 1 results of a phase 1/2 trial. Lancet Haematol, 2023. **10**(1): p. e46-e58.

208. Caravella, J.A., et al., Structure-Based Design and Identification of FT-2102 (Olutasidenib), a Potent Mutant-Selective IDH1 Inhibitor. J Med Chem, 2020. **63**(4): p. 1612-1623.

209. de Botton, S., et al., Olutasidenib (FT-2102) induces durable complete remissions in patients with relapsed or refractory IDH1-mutated AML. Blood Adv, 2023.

210. Cleary, J.M., et al., Secondary IDH1 resistance mutations and oncogenic IDH2 mutations cause acquired resistance to ivosidenib in cholangiocarcinoma. NPJ Precis

Oncol, 2022. **6**(1): p. 61.

211. Pauff, J.M., et al., A phase I study of LY3410738, a first-in-class covalent inhibitor of mutant IDH1 in cholangiocarcinoma and other advanced solid tumors. Journal of Clinical Oncology, 2021. **39**(3_suppl): p. TPS350-TPS350.

212. Stein, E., et al., A Phase 1 Study of LY3410738, a First-in-Class Covalent Inhibitor of Mutant IDH in Advanced Myeloid Malignancies (Trial in Progress). Blood, 2020. **136**: p. 26-26.

213. Jackson, S.P. and J. Bartek, The DNA-damage response in human biology and disease. Nature, 2009. **461**(7267): p. 1071-8.

214. Pilié, P.G., et al., State-of-the-art strategies for targeting the DNA damage response in cancer. Nat Rev Clin Oncol, 2019. **16**(2): p. 81-104.

215. Groelly, F.J., et al., Targeting DNA damage response pathways in cancer. Nat Rev Cancer, 2023. **23**(2): p. 78-94.

216. Taylor, A.M.R., et al., Chromosome instability syndromes. Nature Reviews Disease Primers, 2019. **5**(1): p. 64.

217. Hanahan, D. and R.A. Weinberg, Hallmarks of cancer: the next generation. Cell, 2011. **144**(5): p. 646-74.

218. Yin, C., et al., Homologous Recombination Repair in Biliary Tract Cancers: A Prime Target for PARP Inhibition? Cancers (Basel), 2022. **14**(10).

219. Sachdev, E., et al., PARP Inhibition in Cancer: An Update on Clinical Development. Target Oncol, 2019. **14**(6): p. 657-679.

220. Zhou, P., et al., Recent advancements in PARP inhibitors-based targeted cancer therapy. Precis Clin Med, 2020. **3**(3): p. 187-201.

221. Chi, J., et al., The role of PARP inhibitors in BRCA mutated pancreatic cancer. Therap Adv Gastroenterol, 2021. **14**: p. 17562848211014818.

222. Sonnenblick, A., et al., An update on PARP inhibitors--moving to the adjuvant setting. Nat Rev Clin Oncol, 2015. **12**(1): p. 27-41.

223. Mirza, M.R., et al., Niraparib Maintenance Therapy in Platinum-Sensitive, Recurrent Ovarian Cancer. N Engl J Med, 2016. **375**(22): p. 2154-2164.

224. Coleman, R.L., et al., Rucaparib maintenance treatment for recurrent ovarian carcinoma after response to platinum therapy (ARIEL3): a randomised, double-blind, placebo-controlled, phase 3 trial. Lancet, 2017. **390**(10106): p. 1949-1961.

225. Castroviejo-Bermejo, M., et al., A RAD51 assay feasible in routine tumor samples calls PARP inhibitor response beyond BRCA mutation. EMBO Mol Med, 2018. **10**(12).

226. Cruz, C., et al., RAD51 foci as a functional biomarker of homologous recombination repair and PARP inhibitor resistance in germline BRCA-mutated breast cancer. Ann Oncol, 2018. **29**(5): p. 1203-1210.

227. Bezrookove, V., et al., Niraparib Suppresses Cholangiocarcinoma Tumor Growth by Inducing Oxidative and Replication Stress. Cancers (Basel), 2021. **13**(17).

228. Shen, J., et al., ARID1A Deficiency Impairs the DNA Damage Checkpoint and Sensitizes Cells to PARP Inhibitors. Cancer Discov, 2015. **5**(7): p. 752-67.

229. Park, Y., et al., Loss of ARID1A in Tumor Cells Renders Selective Vulnerability to Combined Ionizing Radiation and PARP Inhibitor Therapy. Clin Cancer Res, 2019. **25**(18): p. 5584-5594.

230. Hu, H.M., et al., A Quantitative Chemotherapy Genetic Interaction Map Reveals Factors Associated with PARP Inhibitor Resistance. Cell Rep, 2018. **23**(3): p. 918-929.

231. Wang, C., et al., ATM-Deficient Colorectal Cancer Cells Are Sensitive to the PARP Inhibitor Olaparib. Transl Oncol, 2017. **10**(2): p. 190-196.

232. Neeb, A., et al., Advanced Prostate Cancer with ATM Loss: PARP and ATR Inhibitors. Eur Urol, 2021. **79**(2): p. 200-211.

233. Gout, J., et al., Synergistic targeting and resistance to PARP inhibition in DNA damage repair-deficient pancreatic cancer. Gut, 2021. **70**(4): p. 743-760.

234. Bang, Y.J., et al., Olaparib in combination with paclitaxel in patients with advanced gastric cancer who have progressed following first-line therapy (GOLD): a double-blind, randomised, placebo-controlled, phase 3 trial. Lancet Oncol, 2017. **18**(12): p. 1637-1651.

235. Perkail, S., et al., BAP1 is a haploinsufficient tumor suppressor linking chronic pan-

creatitis to pancreatic cancer in mice. Nat Commun, 2020. **11**(1): p. 3018.

236. Sabbatino, F., et al., Case Report: BAP1 Mutation and RAD21 Amplification as Predictive Biomarkers to PARP Inhibitor in Metastatic Intrahepatic Cholangiocarcinoma. Front Oncol, 2020. **10**: p. 567289.

237. Fennell, D.A., et al., Rucaparib in patients with BAP1-deficient or BRCA1-deficient mesothelioma (MiST1): an open-label, single-arm, phase 2a clinical trial. Lancet Respir Med, 2021. **9**(6): p. 593-600.

238. Yang, H., et al., The Association of BAP1 Loss-of-Function With the Defect in Homologous Recombination Repair and Sensitivity to PARP-Targeted Therapy. J Thorac Oncol, 2020. **15**(6): p. e88-e90.

239. Golan, T., et al., Overall Survival and Clinical Characteristics of BRCA-Associated Cholangiocarcinoma: A Multicenter Retrospective Study. Oncologist, 2017. **22**(7): p. 804-810.

240. Molenaar, R.J., et al., IDH1/2 Mutations Sensitize Acute Myeloid Leukemia to PARP Inhibition and This Is Reversed by IDH1/2-Mutant Inhibitors. Clin Cancer Res, 2018. **24**(7): p. 1705-1715.

241. Wang, Y., et al., Targeting therapeutic vulnerabilities with PARP inhibition and radiation in IDH-mutant gliomas and cholangiocarcinomas. Sci Adv, 2020. **6**(17): p. eaaz3221.

242. Gbyli, R., et al., In vivo anti-tumor effect of PARP inhibition in IDH1/2 mutant MDS/AML resistant to targeted inhibitors of mutant IDH1/2. Leukemia, 2022. **36**(5): p. 1313-1323.

243. Wang, P., et al., Oncometabolite D-2-Hydroxyglutarate Inhibits ALKBH DNA Repair Enzymes and Sensitizes IDH Mutant Cells to Alkylating Agents. Cell Rep, 2015. **13**(11): p. 2353-2361.

244. Chen, F., et al., Oncometabolites d- and l-2-Hydroxyglutarate Inhibit the AlkB Family DNA Repair Enzymes under Physiological Conditions. Chem Res Toxicol, 2017. **30**(4): p. 1102-1110.

245. Nagashima, H., et al., Poly(ADP-ribose) Glycohydrolase Inhibition Sequesters NAD(+) to Potentiate the Metabolic Lethality of Alkylating Chemotherapy in

IDH-Mutant Tumor Cells. Cancer Discov, 2020. **10**(11): p. 1672-1689.

246. Lu, Y., et al., Chemosensitivity of IDH1-Mutated Gliomas Due to an Impairment in PARP1-Mediated DNA Repair. Cancer Res, 2017. **77**(7): p. 1709-1718.

247. Ohba, S., et al., Mutant IDH1-driven cellular transformation increases RAD51-mediated homologous recombination and temozolomide resistance. Cancer Res, 2014. **74**(17): p. 4836-44.

248. Venneker, S., et al., Inhibition of PARP Sensitizes Chondrosarcoma Cell Lines to Chemo- and Radiotherapy Irrespective of the IDH1 or IDH2 Mutation Status. Cancers (Basel), 2019. **11**(12).

249. NIH.

250. Manjili, M.H., Revisiting cancer immunoediting by understanding cancer immune complexity. J Pathol, 2011. **224**(1): p. 5-9.

251. Huang, P.W. and J.W. Chang, Immune checkpoint inhibitors win the 2018 Nobel Prize. Biomed J, 2019. **42**(5): p. 299-306.

252. Oh, D.Y., et al., Toward a better understanding of T cells in cancer. Cancer Cell, 2021. **39**(12): p. 1549-1552.

253. Strominger, J.L., Human histocompatibility proteins. Immunol Rev, 2002. **185**: p. 69-77.

254. Alberts, B., Molecular Biology of the Cell. 6th Edition, ed. T.a.F.G. Garland Science, New York. 2015.

255. Chen, D.S. and I. Mellman, Oncology meets immunology: the cancer-immunity cycle. Immunity, 2013. **39**(1): p. 1-10.

256. Cruz, F.M., et al., The Biology and Underlying Mechanisms of Cross-Presentation of Exogenous Antigens on MHC-I Molecules. Annu Rev Immunol, 2017. **35**: p. 149-176.

257. Curtsinger, J.M., D.C. Lins, and M.F. Mescher, Signal 3 determines tolerance versus full activation of naive CD8 T cells: dissociating proliferation and development of effector function. J Exp Med, 2003. **197**(9): p. 1141-51.

258. Sckisel, G.D., et al., Out-of-Sequence Signal 3 Paralyzes Primary CD4(+) T-Cell-De-

pendent Immunity. Immunity, 2015. **43**(2): p. 240-50.

259. Motz, Greg T. and G. Coukos, Deciphering and Reversing Tumor Immune Suppression. Immunity, 2013. **39**(1): p. 61-73.

260. Angell, H. and J. Galon, From the immune contexture to the Immunoscore: the role of prognostic and predictive immune markers in cancer. Curr Opin Immunol, 2013. **25**(2): p. 261-7.

261. Galon, J., et al., Towards the introduction of the 'Immunoscore' in the classification of malignant tumours. J Pathol, 2014. **232**(2): p. 199-209.

262. Pagès, F., et al., International validation of the consensus Immunoscore for the classification of colon cancer: a prognostic and accuracy study. Lancet, 2018. **391**(10135): p. 2128-2139.

263. Galon, J. and D. Bruni, Approaches to treat immune hot, altered and cold tumours with combination immunotherapies. Nat Rev Drug Discov, 2019. **18**(3): p. 197-218.

264. Pardoll, D.M., The blockade of immune checkpoints in cancer immunotherapy. Nat Rev Cancer, 2012. **12**(4): p. 252-64.

265. Waldman, A.D., J.M. Fritz, and M.J. Lenardo, A guide to cancer immunotherapy: from T cell basic science to clinical practice. Nat Rev Immunol, 2020. **20**(11): p. 651-668.

266. Wherry, E.J. and M. Kurachi, Molecular and cellular insights into T cell exhaustion. Nat Rev Immunol, 2015. **15**(8): p. 486-99.

267. Rohaan, M.W., S. Wilgenhof, and J. Haanen, Adoptive cellular therapies: the current landscape. Virchows Arch, 2019. **474**(4): p. 449-461.

268. Arina, A., et al., Adoptively transferred immune T cells eradicate established tumors despite cancer-induced immune suppression. J Immunol, 2014. **192**(3): p. 1286-93.

269. Labrijn, A.F., et al., Bispecific antibodies: a mechanistic review of the pipeline. Nature Reviews Drug Discovery, 2019. **18**(8): p. 585-608.

270. Rader, C., Bispecific antibodies in cancer immunotherapy. Curr Opin Biotechnol, 2020. **65**: p. 9-16.

271. Marcus, L., et al., FDA Approval Summary: Pembrolizumab for the Treatment

of Microsatellite Instability-High Solid Tumors. Clinical Cancer Research, 2019. **25**(13): p. 3753-3758.

272. Le, D.T., et al., Mismatch repair deficiency predicts response of solid tumors to PD-1 blockade. Science, 2017. **357**(6349): p. 409-413.

273. Goeppert, B., et al., Mismatch repair deficiency is a rare but putative therapeutically relevant finding in non-liver fluke associated cholangiocarcinoma. Br J Cancer, 2019. **120**(1): p. 109-114.

274. Jain, A., et al., Tumor mutational burden (TMB) and co-existing actionable mutations in biliary tract cancers (BTC). Journal of Clinical Oncology, 2017. **35**(15_suppl): p. 4086-4086.

275. Zhou, G., et al., Reduction of immunosuppressive tumor microenvironment in cholangiocarcinoma by ex vivo targeting immune checkpoint molecules. J Hepatol, 2019. **71**(4): p. 753-762.

276. Fabris, L., et al., The tumour microenvironment and immune milieu of cholangiocarcinoma. Liver Int, 2019. **39 Suppl 1**: p. 63-78.

277. Loeuillard, E., et al., Targeting tumor-associated macrophages and granulocytic myeloid-derived suppressor cells augments PD-1 blockade in cholangiocarcinoma. J Clin Invest, 2020. **130**(10): p. 5380-5396.

278. Kitano, Y., et al., Tumour-infiltrating inflammatory and immune cells in patients with extrahepatic cholangiocarcinoma. Br J Cancer, 2018. **118**(2): p. 171-180.

279. Konishi, D., et al., Regulatory T cells induce a suppressive immune milieu and promote lymph node metastasis in intrahepatic cholangiocarcinoma. Br J Cancer, 2022. **127**(4): p. 757-765.

280. Job, S., et al., Identification of Four Immune Subtypes Characterized by Distinct Composition and Functions of Tumor Microenvironment in Intrahepatic Cholangiocarcinoma. Hepatology, 2020. **72**(3): p. 965-981.

281. Zhang, M., et al., Single-cell transcriptomic architecture and intercellular crosstalk of human intrahepatic cholangiocarcinoma. J Hepatol, 2020. **73**(5): p. 1118-1130.

282. Bao, X., et al., Molecular Subgroups of Intrahepatic Cholangiocarcinoma Discovered by Single-Cell RNA Sequencing-Assisted Multiomics Analysis. Cancer Immu-

nol Res, 2022. **10**(7): p. 811-828.

283. Dong, L., et al., Proteogenomic characterization identifies clinically relevant subgroups of intrahepatic cholangiocarcinoma. Cancer Cell, 2022. **40**(1): p. 70-87.e15.

284. Martin-Serrano, M.A., et al., Novel microenvironment-based classification of intrahepatic cholangiocarcinoma with therapeutic implications. Gut, 2023. **72**(4): p. 736-748.

285. Chen, S., et al., Multiomic Analysis Reveals Comprehensive Tumor Heterogeneity and Distinct Immune Subtypes in Multifocal Intrahepatic Cholangiocarcinoma. Clin Cancer Res, 2022. **28**(9): p. 1896-1910.

286. Thorsson, V., et al., The Immune Landscape of Cancer. Immunity, 2018. **48**(4): p. 812-830.e14.

287. Xiang, X., et al., IDH Mutation Subgroup Status Associates with Intratumor Heterogeneity and the Tumor Microenvironment in Intrahepatic Cholangiocarcinoma. Adv Sci (Weinh), 2021. **8**(17): p. e2101230.

288. Saatcioglu, H.D., et al., 552 Characteristics of the tumor microenvironment in IDH1-mutated cholangiocarcinoma patients from ClarIDHy trial. Journal for ImmunoTherapy of Cancer, 2022. **10**(Suppl 2): p. A576-A577.

289. Carapeto, F., et al., The immunogenomic landscape of resected intrahepatic cholangiocarcinoma. Hepatology, 2022. **75**(2): p. 297-308.

290. Mathewson, N.D., et al., Inhibitory CD161 receptor identified in glioma-infiltrating T cells by single-cell analysis. Cell, 2021. **184**(5): p. 1281-1298.e26.

291. Berghoff, A.S., et al., Correlation of immune phenotype with IDH mutation in diffuse glioma. Neuro Oncol, 2017. **19**(11): p. 1460-1468.

292. Klemm, F., et al., Interrogation of the Microenvironmental Landscape in Brain Tumors Reveals Disease-Specific Alterations of Immune Cells. Cell, 2020. **181**(7): p. 1643-1660.e17.

293. Bunse, L., et al., Suppression of antitumor T cell immunity by the oncometabolite (R)-2-hydroxyglutarate. Nat Med, 2018. **24**(8): p. 1192-1203.

294. Kohanbash, G., et al., Isocitrate dehydrogenase mutations suppress STAT1 and

CD8+ T cell accumulation in gliomas. The Journal of clinical investigation, 2017. **127**(4): p. 1425-1437.

295. Kadiyala, P., et al., Inhibition of 2-hydroxyglutarate elicits metabolic reprogramming and mutant IDH1 glioma immunity in mice. J Clin Invest, 2021. **131**(4).

296. Friedrich, M., et al., Tryptophan metabolism drives dynamic immunosuppressive myeloid states in IDH-mutant gliomas. Nat Cancer, 2021. **2**(7): p. 723-740.

297. Lau, S.K., et al., Comparative immunohistochemical profile of hepatocellular carcinoma, cholangiocarcinoma, and metastatic adenocarcinoma. Hum Pathol, 2002. **33**(12): p. 1175-81.

298. Wardell, C.P., et al., Genomic characterization of biliary tract cancers identifies driver genes and predisposing mutations. J Hepatol, 2018. **68**(5): p. 959-969.

299. Silverman, I.M., et al., Clinicogenomic Analysis of FGFR2-Rearranged Cholangiocarcinoma Identifies Correlates of Response and Mechanisms of Resistance to Pemigatinib. Cancer Discov, 2021. **11**(2): p. 326-339.

300. Hribar, K.C., et al., A Simple Three-dimensional Hydrogel Platform Enables Ex Vivo Cell Culture of Patient and PDX Tumors for Assaying Their Response to Clinically Relevant Therapies. Mol Cancer Ther, 2019. **18**(3): p. 718-725.

301. Lawrence, M.G., et al., Patient-derived Models of Abiraterone- and Enzalutamide-resistant Prostate Cancer Reveal Sensitivity to Ribosome-directed Therapy. Eur Urol, 2018. **74**(5): p. 562-572.

302. Nomura, M., et al., Tegavivint and the β-Catenin/ALDH Axis in Chemotherapy-Resistant and Metastatic Osteosarcoma. J Natl Cancer Inst, 2019. **111**(11): p. 1216-1227.

303. Fujisawa, T. and P. Filippakopoulos, Functions of bromodomain-containing proteins and their roles in homeostasis and cancer. Nat Rev Mol Cell Biol, 2017. **18**(4): p. 246-262.

304. Fujiwara, H., et al., Isocitrate dehydrogenase 1 mutation sensitizes intrahepatic cholangiocarcinoma to the BET inhibitor JQ1. Cancer Sci, 2018. **109**(11): p. 3602-3610.

305. Lu, Q., et al., BRD4 degrader ARV-825 produces long-lasting loss of BRD4 pro-

tein and exhibits potent efficacy against cholangiocarcinoma cells. Am J Transl Res, 2019. **11**(9): p. 5728-5739.

306. Shorstova, T., W.D. Foulkes, and M. Witcher, Achieving clinical success with BET inhibitors as anti-cancer agents. Br J Cancer, 2021. **124**(9): p. 1478-1490.

307. Morrison-Smith, C.D., et al., Combined Targeting of the BRD4-NUT-p300 Axis in NUT Midline Carcinoma by Dual Selective Bromodomain Inhibitor, NEO2734. Mol Cancer Ther, 2020. **19**(7): p. 1406-1414.

308. Spriano, F., et al., Antitumor activity of the dual BET and CBP/EP300 inhibitor NEO2734. Blood Adv, 2020. **4**(17): p. 4124-4135.

309. Ryan, K.R., F. Giles, and G.J. Morgan, Targeting both BET and CBP/EP300 proteins with the novel dual inhibitors NEO2734 and NEO1132 leads to anti-tumor activity in multiple myeloma. Eur J Haematol, 2021. **106**(1): p. 90-99.

310. Goyal, L., et al., Polyclonal Secondary FGFR2 Mutations Drive Acquired Resistance to FGFR Inhibition in Patients with FGFR2 Fusion-Positive Cholangiocarcinoma. Cancer Discov, 2017. **7**(3): p. 252-263.

311. Goyal, L., et al., TAS-120 Overcomes Resistance to ATP-Competitive FGFR Inhibitors in Patients with FGFR2 Fusion-Positive Intrahepatic Cholangiocarcinoma. Cancer Discov, 2019. **9**(8): p. 1064-1079.

312. Varghese, A.M., et al., Noninvasive Detection of Polyclonal Acquired Resistance to FGFR Inhibition in Patients With Cholangiocarcinoma Harboring FGFR2 Alterations. JCO Precis Oncol, 2021. **5**.

313. Heeke, A.L., et al., Prevalence of Homologous Recombination-Related Gene Mutations Across Multiple Cancer Types. JCO Precis Oncol, 2018. **2018**.

314. Bryant, H.E., et al., Specific killing of BRCA2-deficient tumours with inhibitors of poly(ADP-ribose) polymerase. Nature, 2005. **434**(7035): p. 913-7.

315. Farmer, H., et al., Targeting the DNA repair defect in BRCA mutant cells as a therapeutic strategy. Nature, 2005. **434**(7035): p. 917-21.

316. Mateo, J., et al., A decade of clinical development of PARP inhibitors in perspective. Ann Oncol, 2019. **30**(9): p. 1437-1447.

317. Spiegel, J.O., B. Van Houten, and J.D. Durrant, PARP1: Structural insights and pharmacological targets for inhibition. DNA Repair (Amst), 2021. **103**: p. 103125.

318. Robson, M., et al., Olaparib for Metastatic Breast Cancer in Patients with a Germline BRCA Mutation. N Engl J Med, 2017. **377**(6): p. 523-533.

319. Moore, K., et al., Maintenance Olaparib in Patients with Newly Diagnosed Advanced Ovarian Cancer. N Engl J Med, 2018. **379**(26): p. 2495-2505.

320. de Bono, J., et al., Olaparib for Metastatic Castration-Resistant Prostate Cancer. N Engl J Med, 2020. **382**(22): p. 2091-2102.

321. Llop-Guevara, A., et al., Association of RAD51 with homologous recombination deficiency (HRD) and clinical outcomes in untreated triple-negative breast cancer (TNBC): analysis of the GeparSixto randomized clinical trial. Ann Oncol, 2021. **32**(12): p. 1590-1596.

322. Carreira, S., et al., Biomarkers Associating with PARP Inhibitor Benefit in Prostate Cancer in the TOPARP-B Trial. Cancer Discov, 2021. **11**(11): p. 2812-2827.

323. Guffanti, F., et al., Basal expression of RAD51 foci predicts olaparib response in patient-derived ovarian cancer xenografts. Br J Cancer, 2022. **126**(1): p. 120-128.

324. Blanc-Durand, F., et al., A RAD51 functional assay as a candidate test for homologous recombination deficiency in ovarian cancer. Gynecol Oncol, 2023. **171**: p. 106-113.

325. Ishikawa, H. and G.N. Barber, STING is an endoplasmic reticulum adaptor that facilitates innate immune signalling. Nature, 2008. **455**(7213): p. 674-8.

326. Lee, K.M., et al., Epigenetic Repression of STING by MYC Promotes Immune Evasion and Resistance to Immune Checkpoint Inhibitors in Triple-Negative Breast Cancer. Cancer Immunol Res, 2022. **10**(7): p. 829-843.

327. Zhu, Y., et al., STING: a master regulator in the cancer-immunity cycle. Mol Cancer, 2019. **18**(1): p. 152.

328. Reisländer, T., F.J. Groelly, and M. Tarsounas, DNA Damage and Cancer Immunotherapy: A STING in the Tale. Mol Cell, 2020. **80**(1): p. 21-28.

329. Falahat, R., et al., Epigenetic reprogramming of tumor cell-intrinsic STING func-

tion sculpts antigenicity and T cell recognition of melanoma. Proc Natl Acad Sci U S A, 2021. **118**(15).

330. Espinet, E., et al., Aggressive PDACs Show Hypomethylation of Repetitive Elements and the Execution of an Intrinsic IFN Program Linked to a Ductal Cell of Origin. Cancer Discov, 2021. **11**(3): p. 638-659.

331. Kamakura, D., R. Asano, and M. Yasunaga, T Cell Bispecific Antibodies: An Antibody-Based Delivery System for Inducing Antitumor Immunity. Pharmaceuticals (Basel), 2021. **14**(11).

332. Iqbal, N. and N. Iqbal, Human Epidermal Growth Factor Receptor 2 (HER2) in Cancers: Overexpression and Therapeutic Implications. Mol Biol Int, 2014. **2014**: p. 852748.

333. Harder, J., et al., EGFR and HER2 expression in advanced biliary tract cancer. World J Gastroenterol, 2009. **15**(36): p. 4511-7.

334. Vivaldi, C., et al., HER2 Overexpression as a Poor Prognostic Determinant in Resected Biliary Tract Cancer. Oncologist, 2020. **25**(10): p. 886-893.

335. Arenas, E.J., et al., Acquired cancer cell resistance to T cell bispecific antibodies and CAR T targeting HER2 through JAK2 down-modulation. Nat Commun, 2021. **12**(1): p. 1237.

336. Rius Ruiz, I., et al., p95HER2–T cell bispecific antibody for breast cancer treatment. Science Translational Medicine, 2018. **10**(461): p. eaat1445.

337. Tay, R.E., E.K. Richardson, and H.C. Toh, Revisiting the role of CD4(+) T cells in cancer immunotherapy-new insights into old paradigms. Cancer Gene Ther, 2021. **28**(1-2): p. 5-17.

338. Lau, D.K., et al., Genomic Profiling of Biliary Tract Cancer Cell Lines Reveals Molecular Subtypes and Actionable Drug Targets. iScience, 2019. **21**: p. 624-637.

339. Byrne, A.T., et al., Interrogating open issues in cancer precision medicine with patient-derived xenografts. Nat Rev Cancer, 2017. **17**(4): p. 254-268.

340. Conte, N., et al., PDX Finder: A portal for patient-derived tumor xenograft model discovery. Nucleic Acids Res, 2019. **47**(D1): p. D1073-d1079.

341. Alqahtani, S.A. and M. Colombo, Systemic therapy for advanced cholangiocarcinoma: new options on the horizon. Hepatoma Research, 2020. **6**: p. 70.

342. Cheng, Y., et al., Treatment with olaparib monotherapy for BRCA2-mutated refractory intrahepatic cholangiocarcinoma: a case report. Onco Targets Ther, 2018. **11**: p. 5957-5962.

343. Lin, J., et al., Alterations in DNA Damage Repair Genes in Primary Liver Cancer. Clin Cancer Res, 2019. **25**(15): p. 4701-4711.

344. Su, Y.L., et al., Remarkable Response to Olaparib in a Patient with Combined Hepatocellular-Cholangiocarcinoma Harboring a Biallelic BRCA2 Mutation. Onco Targets Ther, 2021. **14**: p. 3895-3901.

345. Spizzo, G., et al., Molecular profile of BRCA-mutated biliary tract cancers. ESMO Open, 2020. **5**(3): p. e000682.

346. Higuchi, F., et al., Restoration of Temozolomide Sensitivity by PARP Inhibitors in Mismatch Repair Deficient Glioblastoma is Independent of Base Excision Repair. Clin Cancer Res, 2020. **26**(7): p. 1690-1699.

347. Eder, J.P., et al., Clinical Efficacy of Olaparib in IDH1/IDH2-Mutant Mesenchymal Sarcomas. JCO Precis Oncol, 2021. **5**: p. 466-472.

348. Ghafoor, A., et al., Phase 2 Study of Olaparib in Malignant Mesothelioma and Correlation of Efficacy With Germline or Somatic Mutations in BAP1 Gene. JTO Clin Res Rep, 2021. **2**(10): p. 100231.

349. Niger, M., et al., Platinum sensitivity in patients with IDH1/2 mutated vs wild-type intrahepatic cholangiocarcinoma: A propensity score-based study. Int J Cancer, 2022. **151**(8): p. 1310-1320.

350. Patch, A.M., et al., Whole-genome characterization of chemoresistant ovarian cancer. Nature, 2015. **521**(7553): p. 489-94.

351. Kubelac, P., et al., Changes in DNA Damage Response Markers with Treatment in Advanced Ovarian Cancer. Cancers (Basel), 2020. **12**(3).

352. Desnoyers, A., et al., Associations with response to Poly(ADP-ribose) Polymerase (PARP) inhibitors in patients with metastatic breast cancer. NPJ Breast Cancer, 2022. **8**(1): p. 43.

353. Fong, P.C., et al., Poly(ADP)-ribose polymerase inhibition: frequent durable responses in BRCA carrier ovarian cancer correlating with platinum-free interval. J Clin Oncol, 2010. **28**(15): p. 2512-9.

354. Garrett, M., et al., Metabolic characterization of isocitrate dehydrogenase (IDH) mutant and IDH wildtype gliomaspheres uncovers cell type-specific vulnerabilities. Cancer & Metabolism, 2018. **6**(1): p. 4.

355. Watanabe, T., et al., IDH1 mutations are early events in the development of astrocytomas and oligodendrogliomas. Am J Pathol, 2009. **174**(4): p. 1149-53.

356. Johnson, B.E., et al., Mutational analysis reveals the origin and therapy-driven evolution of recurrent glioma. Science, 2014. **343**(6167): p. 189-193.

357. Garrett, M., et al., Emerging Roles of Wild-type and Mutant IDH1 in Growth, Metabolism and Therapeutics of Glioma, in Gliomas, W. Debinski, Editor. 2021, Exon Publications

358. Hu, J., et al., STING inhibits the reactivation of dormant metastasis in lung adenocarcinoma. Nature, 2023. **616**(7958): p. 806-813.

359. Konno, H., et al., Suppression of STING signaling through epigenetic silencing and missense mutation impedes DNA damage mediated cytokine production. Oncogene, 2018. **37**(15): p. 2037-2051.

360. Gao, Y., et al., R-2HG downregulates ERα to inhibit cholangiocarcinoma via the FTO/m6A-methylated ERα/miR16-5p/YAP1 signal pathway. Mol Ther Oncolytics, 2021. **23**: p. 65-81.

361. Kickingereder, P., et al., IDH mutation status is associated with a distinct hypoxia/angiogenesis transcriptome signature which is non-invasively predictable with rCBV imaging in human glioma. Sci Rep, 2015. **5**: p. 16238.

362. Berens, M.E., et al., Multiscale, multimodal analysis of tumor heterogeneity in IDH1 mutant vs wild-type diffuse gliomas. PLoS One, 2019. **14**(12): p. e0219724.

363. Ozga, A.J., M.T. Chow, and A.D. Luster, Chemokines and the immune response to cancer. Immunity, 2021. **54**(5): p. 859-874.

364. Tsai, H.C., et al., Transient low doses of DNA-demethylating agents exert durable antitumor effects on hematological and epithelial tumor cells. Cancer Cell, 2012.

21(3): p. 430-46.

365. Li, X., et al., Increased IFNγ(+) T Cells Are Responsible for the Clinical Responses of Low-Dose DNA-Demethylating Agent Decitabine Antitumor Therapy. Clin Cancer Res, 2017. **23**(20): p. 6031-6043.

366. Chiappinelli, K.B. and S.B. Baylin, Inhibiting DNA methylation improves antitumor immunity in ovarian cancer. J Clin Invest, 2022. **132**(14).

367. Peng, D., et al., Epigenetic silencing of TH1-type chemokines shapes tumour immunity and immunotherapy. Nature, 2015. **527**(7577): p. 249-53.

368. de Charette, M., A. Marabelle, and R. Houot, Turning tumour cells into antigen presenting cells: The next step to improve cancer immunotherapy? Eur J Cancer, 2016. **68**: p. 134-147.

369. Natsume, A., et al., The DNA demethylating agent 5-aza-2'-deoxycytidine activates NY-ESO-1 antigenicity in orthotopic human glioma. Int J Cancer, 2008. **122**(11): p. 2542-53.

370. Chiappinelli, K.B., et al., Inhibiting DNA Methylation Causes an Interferon Response in Cancer via dsRNA Including Endogenous Retroviruses. Cell, 2015. **162**(5): p. 974-86.

371. Strissel, P.L., et al., Reactivation of codogenic endogenous retroviral (ERV) envelope genes in human endometrial carcinoma and prestages: Emergence of new molecular targets. Oncotarget, 2012. **3**(10): p. 1204-19.

372. Stengel, S., et al., Regulation of human endogenous retrovirus-K expression in melanomas by CpG methylation. Genes Chromosomes Cancer, 2010. **49**(5): p. 401-11.

373. Kantarjian, H., et al., Decitabine improves patient outcomes in myelodysplastic syndromes: results of a phase III randomized study. Cancer, 2006. **106**(8): p. 1794-803.

374. Lübbert, M., et al., Low-dose decitabine versus best supportive care in elderly patients with intermediate- or high-risk myelodysplastic syndrome (MDS) ineligible for intensive chemotherapy: final results of the randomized phase III study of the European Organisation for Research and Treatment of Cancer Leukemia Group and the German MDS Study Group. J Clin Oncol, 2011. **29**(15): p. 1987-96.

375. Steensma, D.P., et al., Multicenter study of decitabine administered daily for 5 days

every 4 weeks to adults with myelodysplastic syndromes: the alternative dosing for outpatient treatment (ADOPT) trial. J Clin Oncol, 2009. **27**(23): p. 3842-8.

376. Dombret, H., et al., International phase 3 study of azacitidine vs conventional care regimens in older patients with newly diagnosed AML with >30% blasts. Blood, 2015. **126**(3): p. 291-9.

377. Boumber, Y. and J.P. Issa, Epigenetics in cancer: what's the future? Oncology (Williston Park), 2011. **25**(3): p. 220-6, 228.

378. Stresemann, C. and F. Lyko, Modes of action of the DNA methyltransferase inhibitors azacytidine and decitabine. Int J Cancer, 2008. **123**(1): p. 8-13.

379. Liu, S. and J. Tan, Chapter 2 - DNA methyltransferase inhibitors (DNMTis) as sensitizing agents to overcome chemoresistance, in Epigenetic Regulation in Overcoming Chemoresistance, C. Wu and L. Wang, Editors. 2021, Academic Press. p. 9-23.

380. Erdmann, A., P.B. Arimondo, and D. Guianvarc'h, Chapter 3 - Structure-Guided Optimization of DNA Methyltransferase Inhibitors, in Epi-Informatics, J.L. Medina-Franco, Editor. 2016, Academic Press: Boston. p. 53-73.

381. Rohle, D., et al., An inhibitor of mutant IDH1 delays growth and promotes differentiation of glioma cells. Science, 2013. **340**(6132): p. 626-30.

382. Hamarsheh, S.a., et al., Immune modulatory effects of oncogenic KRAS in cancer. Nature Communications, 2020. **11**(1): p. 5439.

383. Bankhead, P., et al., QuPath: Open source software for digital pathology image analysis. Sci Rep, 2017. **7**(1): p. 16878.

384. Gomez-Gomez, A., et al., Targeted metabolomics in formalin-fixed paraffin-embedded tissue specimens: Liquid chromatography-tandem mass spectrometry determination of acidic metabolites in cancer research. Talanta, 2021. **223**(Pt 2): p. 121740.

385. Serna, G., et al., Sequential immunohistochemistry and virtual image reconstruction using a single slide for quantitative KI67 measurement in breast cancer. Breast, 2020. **53**: p. 102-110.

Appendix

Research article resulting from this thesis:

Serra-Camprubí Q, Verdaguer H, Oliveros W, Lupión-Garcia N, Llop-Guevara A, Molina C, Vila-Casadesús M, Turpin A, Neuzillet C, Frigola J, Querol J, Yáñez-Bartolomé M, Castet F, Fabregat-Franco C, Escudero-Iriarte C, Escorihuela M, Arenas EJ, Bernadó-Morales C, Haro N, Giles FJ, Pozo ÓJ, Miquel JM, Nuciforo PG, Vivancos A, Melé M, Serra V, Arribas J, Tabernero J, Peiró S, Macarulla T, Tian TV. Human Metastatic Cholangiocarcinoma Patient-Derived Xenografts and Tumoroids for Preclinical Drug Evaluation. Clin Cancer Res. 2023 Jan 17;29(2):432-445. doi: 10.1158/1078-0432.CCR-22-2551. PMID: 36374558; PMCID: PMC9873249.

Collaboration with other projects:

Verdaguer H, Saurí T, Acosta DA, Guardiola M, Sierra A, Hernando J, Nuciforo P, Miquel JM, Molero C, Peiró S, **Serra-Camprubí Q**, Villacampa G, Aguilar S, Vivancos A, Tabernero J, Dienstmann R, Macarulla T. ESMO Scale for Clinical Actionability of Molecular Targets Driving Targeted Treatment in Patients with Cholangiocarcinoma. Clin Cancer Res. 2022 Apr 14;28(8):1662-1671. doi: 10.1158/1078-0432.CCR-21-2384. PMID: 35042699.